

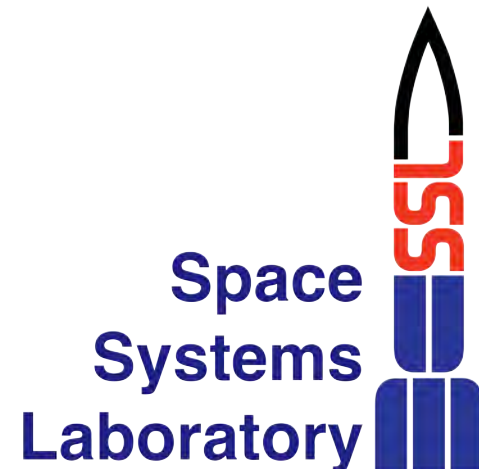
# Logistics Transfer on the Lunar Surface

Moon to Mars Exploration Systems and  
Habitat (M2M X-hab) 2023 Academic  
Innovation Challenge

Final Report  
University of Maryland

Dr. David L. Akin  
June 20, 2023

UNIVERSITY OF  
MARYLAND



# SHELL

## System for Heavy-Lift End-To-End Lunar Logistics

**Theme: Lunar Surface Transporter Vehicle**  
**University of Maryland**



**Undergraduate Aerospace Engineering Team Members**

Brian Amaya	Pranav Ampani	Edwin Arevalo	Adithya Arun
Joshua Batstone	Nicholas Delafuente	Justin DeVito	Joey Fluehr
Seth Gussow	Jack Molter	Adebayo Odusami	Jeet Patel
Anish Sankla	Darian Sawycky	Yida Shen	Cameron Storey
Matthew Thomas	Ayush Varaiya	Matthew Visnich	

**Faculty Advisor: Dr. David Akin**

1. Project Description - Pranav .....	8
RASC-AL Competition – Pranav.....	8
NASA X-HAB - Pranav .....	8
Mission Statement - Pranav.....	8
Logo – Justin DeVito.....	8
2. Team Organization - Darian .....	9
3. Requirements .....	10
3.1 - L1 Requirements – Anish, Matthew, Adithya, Jack.....	10
3.2 - L2 Requirements - Pranav .....	10
3.2.1 - General .....	10
3.2.2 - Lunar Logistics Transportation Vehicle (LLTV).....	10
3.2.3 - Cargo Manipulator (CM) .....	11
3.2.4 - Pressurized Logistics Module (PLM) .....	12
3.3 - L3 Requirements - Pranav .....	12
3.3.1 - LLTV.....	12
3.3.2 - CM.....	14
3.3.3 - PLM.....	16
4. System Outline.....	17
4.1 - System Architecture - Darian.....	17
4.2 - CONOPs – Darian.....	17
4.3 - Block Diagrams - Darian .....	18
4.4 - WBS - Darian.....	19
4.5 - Mission Planning – Seth Gussow .....	21
4.6 - Site Selection – Seth Gussow .....	21
4.6.1 - Haworth 1-2 Characteristics – Seth Gussow .....	25
4.7 - <i>Communication Overview – Seth Gussow</i> .....	26
4.8 - <i>Applicable Landers – Ayush Varaiya</i> .....	27
4.8.1 - Offloading- Darian .....	29
4.9 - Mission Tasking – Seth Gussow.....	29
4.10 - Daily Mission Availability – Seth Gussow.....	30
<b>4.11 - LLV Path Planning- Ayush Varaiya</b> .....	34
4.12 - Inter-site Travelling- <i>Ayush Varaiya</i> .....	35

<b>4.13 - Mission Maintenance- Ayush Varaiya</b> .....	36
<b>4.14 - Extra Activities – Ayush Varaiya</b> .....	38
5. Lunar Logistics Vehicle.....	40
5.1 – Baseline System Architecture – Anish Sankla.....	40
5.2 - Mobility System – Anish Sankla .....	41
5.2a - Wheels .....	42
5.2b - Steering.....	47
5.2c - Suspension.....	48
5.3 - Actuator Design Philosophy – Anish Sankla.....	51
5.4 - Analysis.....	54
5.4a - Accel/Decel – <b>Anish Sankla</b> .....	54
5.4b - Structural Load Cases – <b>Anish Sankla</b> .....	57
5.4c - Hand Beam Calcs – <b>Anish Sankla</b> .....	59
5.4d - FEA – <b>Matthew Thomas</b> .....	60
5.4e - Hertzian Contact Stress – <b>Yida Shen</b> .....	60
5.4f - Wheel FEA – <b>Yida Shen</b> .....	63
5.5 - Standard Payload Interface (SPI) – Matthew Thomas.....	65
5.6 - RASC-AL <i>Hardware Development</i> Jack Molter.....	66
5.7 - Latching Mechanism Design (2) – Edwin Arevalo .....	68
5.8 - Power/Data Transfer – Matthew Thomas .....	71
5.9 - Power Requirements .....	72
5.9.1 - Mobility Power Requirements – Joshua Batstone.....	72
5.9.2 - Avionics Power Requirements – Joshua Batstone .....	74
5.9.3 - Thermal Power Requirements – Joshua Batstone .....	75
5.9.4 - Active Dust Mitigation Power Requirements – Nicholas Delafuente.....	75
5.10 - Power Budget.....	75
5.10.1 - Power Modes – Joshua Batstone .....	75
5.10.2 - Battery Sizing – Joshua Batstone .....	76
5.10.3 - Power System Capabilities – Joshua Batstone.....	77
5.11 - Battery.....	78
5.11.1 - Battery Cell Selection – Adebayo Odusami.....	78
5.11.2 - Secondary vs Primary Cells – Adebayo Odusami .....	78

5.11.3 - Cell Chemistry – Adebayo Odusami.....	78
5.11.4 - Lithium-Ion Battery Trade Study – Adebayo Odusami.....	80
5.11.4 - Cell Geometry – Adebayo Odusami .....	82
5.11.5 - Battery Layout – Adebayo Odusami.....	83
5.11.6 – Battery Box Mass Estimate – Adebayo Odusami .....	86
5.12 – Power Generation.....	87
5.12.1 – Power Generation Trade – Nicholas Delafuente.....	87
5.12.2 - Solar Array Selection – Nicholas Delafuente .....	89
5.13 - Thermal Management.....	90
5.13.1 - Temperature Intervals – Adebayo Odusami.....	90
5.13.2 - Lunar Thermal Environment & Management – Joshua Batstone.....	91
5.13.3 - Motor Thermal Control – Joshua Batstone .....	94
5.13.3 - Warm Electronics Box – Joshua Batstone .....	98
5.13.4 - Battery Thermal Control – Adebayo Odusami .....	101
5.13.5 - Rover Body Thermal Control – Joshua Batstone.....	102
5.13.6 - Solar Array Thermal Control – Nicholas Delafuente.....	105
5.14 - Dust Mitigation.....	106
5.14.1 - Dust Mitigation – Nicholas Delafuente.....	106
5.15 - Avionics Block Diagram – Matthew Visnich.....	109
5.16 - Communications Architecture – Edwin Arevalo.....	114
5.17 - Data Budget -Brian Amaya.....	118
5.17.1 - Antenna link budgets.....	119
5.18 - Avionics Components – Justin DeVito / Matthew Visnich.....	124
5.18.1 - Avionics Components Overview – Justin DeVito .....	124
5.18.4 - Redundancy – Justin DeVito.....	127
5.18.5 - Cameras – Justin DeVito.....	127
5.18.6 - Image Processing – Justin DeVito .....	128
5.18.7 - Navigation – Brian Amaya.....	129
6. Pressurized Logistics Module.....	132
6.1 - Introduction – Adithya Arun.....	132
6.2 - Initial Sizing – Joey Fluehr.....	132
6.3 - Initial Internal Config – Adithya Arun .....	135

6.4 - Initial Crew Assistance – Joey Fluehr .....	137
6.5 - Initial Offloading and Lander Selection – Adithya Arun .....	138
6.6 - Initial Structural Analysis – Joey Fluehr .....	138
6.7 - 45-Day Sizing – Joey Fluehr.....	139
Table 6.7.6: 45-Day Launch Cadence Containers.....	142
6.8 - 45-Day Internal Configuration – Adithya Arun.....	142
6.9 - 45-Day Structural Analysis – Adithya Arun.....	143
6.10 - 45-Day Cadence Launch and Lander Trade/Verification -- Adithya Arun .....	145
6.11 - Final PLM Design Internal Configuration – Adithya Arun.....	147
6.12 - Final PLM Structural Analysis – Adithya Arun .....	147
6.13 - Final PLM Launch and Lander Verification – Adithya Arun.....	148
6.14 - Environmental Control System – Edwin Arevalo .....	150
6.14.1 - Pressure .....	150
6.14.2 - Thermal .....	151
6.14.3 - Humidity.....	151
6.14.4 - Fire Control .....	152
6.14.5 - Thermal Control System – Joshua Batstone .....	153
6.14.6 - PLM Battery – Adebayo Odusami.....	155
6.15 - PLM Docking interface Jack Molter.....	156
6.15.2 - X-HAB Hardware Development Jack Molter.....	157
7. Cargo Manipulator .....	165
7.1 - Mission Context – Matthew Thomas.....	165
7.2 - Concept of Operations – Matthew Thomas .....	165
7.3 - Design Philosophy – Matthew Thomas .....	166
7.4 - Arm vs. Crane Trade – Yida Shen .....	167
7.5 - LSMS Overview – Matthew Thomas .....	167
7.6 - Static Force Model – Matthew Thomas.....	168
7.7 - Load Configurations – Matthew Thomas .....	169
7.8 - Cross-section Design – Matthew Thomas .....	171
7.8.1 - Material Selection .....	171
7.8.2 - Shape Selection .....	172
7.8.3 - Sizing.....	172

7.9 - Stability – Matthew Thomas .....	174
7.10 - Offloading & Deployment – Matthew Thomas .....	176
7.11 - Payload-Manipulator Interface – Matthew Thomas .....	176
7.12 - Thermal Management .....	177
7.12.1 - Cargo Manipulator Thermal Control – Nicholas Delafuente .....	177
7.13 - Power System.....	179
7.13.1 - Umbilical Power – Nicholas Delafuente .....	179
8. Budgeting.....	179
8.1 - Initial Cost Estimations- Ayush Varaiya .....	179
8.2 - Refined Cost Estimations – Cameron Storey.....	181
8.2.1 – LLV – Cameron Storey .....	183
8.2.2 – PLM – Cameron Storey .....	183
8.2.3 – CM – Cameron Storey.....	183
8.2.4 - Launch Costs – Jeet Patel, Cameron Storey.....	184
8.2.5 – Overall – Cameron Storey .....	186
9. Risk Analysis .....	187
9.1 - S3001 Risk Breakdown and Analysis – Pranav.....	187
9.2 - Fault Tolerance Stories - Darian.....	187
9.2.1 - LLV – Darian, Cameron.....	187
9.2.3 - PLM – Jeet Patel .....	190
9.2.4 - CM – Pranav.....	191
9.3 - Mitigation Strategies – Pranav, Darian, Cameron, Jeet.....	193
9.4 - FMECA - Pranav .....	197
10. TRL Analysis – Jeet, Pranav, Darian, Cameron .....	197
10.1 - LLV TRL Analysis – Jeet Patel .....	198
10.2 - PLM TRL Analysis – Jeet Patel.....	199
10.3 - CM TRL Analysis - Jeet Patel .....	201
11. Project Timeline – jeet .....	203
12. Appendix.....	205
12.1 - Spoiler Deployment – Matthew Thomas .....	205
12.2 - Radiation Hardening Assurance Research – Matthew Visnich .....	206
12.3 - Phase Change Materials – Nicholas Delafuente .....	206

12.4 - Regolith Heating – Joshua Batstone ..... 207

12.5 - Azimuthal Sun Tracking – Joshua Batstone ..... 208

12.6 - Ideal Charging Zones – Seth Gussow ..... 208

12.7 - Site Selection Decision Matrix – Seth Gussow ..... 211

12.7 - Initial PLM Thermal Calculations – Edwin Arevalo ..... 211

12.8 - Possibility of Solar Panels to Provide Additional Capabilities to PLM – Edwin Arevalo  
..... 213

12.9 - Making The Video That Got Us Into RASC-AL – Edwin Arevalo ..... 214

12.10 - Flexible User Radio – Edwin Arevalo ..... 219

12.11 - References ..... 220

    12.11.1 - AFSS ..... 220

    12.11.2 - LSM ..... 223

    12.11.3 - MPA ..... 226

    12.11.4 - PPT ..... 227

    12.11.5 - SI ..... 230

**Table of Contents**



## **1. Project Description - Pranav**

SHELL, or the System for End-to-End Lunar Logistics, is a design for enabling logistics transportation on the Lunar surface. It is being created to help supplement the NASA Artemis missions and to pave the way for future missions on Mars.

### **RASC-AL Competition – Pranav**

This year, our team participated in the Revolutionary Aerospace Systems Concepts Academic Linkage competition, or RASC-AL. It is a platform for promoting innovation and creativity in the field of Aerospace Engineering. The category we participated in this year for the Lunar Surface Transporter Vehicle. The purpose of this theme is to nurture the future Artemis missions, where there will be a need to land and deploy various large objects on the lunar surface, such as rovers, logistics carriers, and habitats. To facilitate this, RASC-AL has asked student teams to develop a solution to transport logistics elements across the lunar regolith. Our team was fortunate enough to be selected as one of the few finalists in our category, meaning that we would be able to present at a forum in Florida.

### **NASA X-HAB – Pranav**

Our team also participated in the NASA X-HAB program, which is an initiative that encourages university students to design and develop innovative habitat concepts for future human space exploration missions, especially those beyond Earth's orbit. We have had multiple meetings with representatives from NASA to help facilitate the development of SHELL and logistics elements that will advance technologies and efforts in creating habitable environments for long-duration space missions.

### **Mission Statement - Pranav**

We will design, build, and test technological and operational approaches to moving logistics elements from a lunar lander to the vicinity of the habitat, docking pressurized logistics modules, transferring logistics elements across modules, and internal habitat stowage/retrieval to assess suitability for use in lunar gravity and surface conditions.

### **Logo – Justin DeVito**

The SHELL logo depicts a silhouette of a simplified version of lunar logistics vehicle, which can be thought of as the core of the logistics transport system, which is layered on top of a graphic of the moon. Wrapped around the outside is the mission's name: System for Heavy-lift End-to-end Lunar Logistics. The logo was created in Adobe Illustrator and is meant to mimic the design of NASA mission patches. The logo incorporates the color red because it is the primary color of the University of Maryland, College Park.



**Figure X: SHELL Logo**

**2. Team Organization - Darian**

SHELL is comprised of 19 team members. To efficiently manage such a large group, we split into five different subteams. Each subteam had a unique focus and set of responsibilities to best aid the development of our Lunar system. The first subteam is Systems Integration, or SI. SI was responsible for mission architecture and timelines, systems engineering, mass and cost budgeting, risk analysis, and general project management. The second subteam is Mission Planning and Analysis, or MPA. MPA was responsible for the creation of our design reference mission, any orbital mechanics and lander selection, concept of operations, and mission site selection. The third subteam is Loads, Structures, and Mechanisms, or LSM. LSM was responsible for the structural design and analysis of our entire system. The fourth subteam is Power Propulsion and Thermal, or PPT. PPT was responsible for power generation and storage, power management and budgets, thermal modeling, and thermal control. The final subteam is Avionics, Flight Software, and Simulation, or AFSS. AFSS was responsible for sensors, control systems, navigation systems, and communications. Overall, this organizational structure allowed us to effectively meet deadlines and manage workload while taking advantage of each team member’s strengths. Below is a table showing the team members of each subteam.

SI	MPA	LSM	PPT	AFSS
Pranav Ampani	Seth Gussow	Anish Sankla	Adebayo Odusami	Brian Amaya
Darian Sawycky	Ayush Varaiya	Jack Molter	Joshua Batstone	Justin DeVito
Cameron Storey		Matthew Thomas	Nicholas Delfuente	Matthew Visnich
Jeet Patel		Yida Shen		Edwin Arevalo
		Adithya Aruin		
		Joseph Fluehr		

### 3. Requirements

#### 3.1 - L1 Requirements – Anish, Matthew, Adithya, Jack

<i>ID</i>	<i>Functional Requirement</i>	<i>Requirement Link</i>
MIS-1	System shall be capable of carrying and manipulating a maximum payload of 4.6m in diameter, 7.8m in height	<b>MS</b>
MIS-2	System shall be capable of offloading payloads up to 15000kg	<b>MS</b>
MIS-3	System shall be capable of moving payloads at least 1000m from landing site	<b>MS</b>
MIS-4	System shall be capable of self-deployment from existing or in-development lunar landers	<b>MS</b>
MIS-5	System shall be capable of operating without human operators in physical contact with the system	<b>MS</b>
MIS-6	System shall have an initial operating date of 2028, with a lifetime of at least 5 years	<b>MS</b>
MIS-7	The transport phase shall be over lunar terrain suitable for landings (slopes <5°) for less than a kilometer	<b>MS</b>
MIS-8	System shall be able to mate logistics elements with main habitats	<b>MS</b>
MIS-9	System shall minimize crew interaction and effort in logistics element transfer	<b>MS</b>

#### 3.2 - L2 Requirements - Pranav

##### 3.2.1 - General

<i>ID</i>	<i>Functional Requirement</i>	<i>Requirement Link</i>
GEN-1	System shall be able to withstand expected night durations and temperature requirements that are representative of lunar south pole conditions	MIS-6
GEN-2	System shall include dust mitigation measures for logistics elements during transport phase	MIS-3
GEN-3	System shall operate in an Artemis Site on the lunar surface	MIS-7

##### 3.2.2 - Lunar Logistics Transportation Vehicle (LLTV)

<i>ID</i>	<i>Functional Requirement</i>	<i>Requirement Link</i>
LTV-1	System shall maintain communication with Earth ground stations for the initial servicing mission.	MIS-5

LTV-2	System shall be capable of maneuvering payloads with sizes ranging from CTBs to habitats	MIS-1
LTV-3	System shall be able to recharge itself without crew interaction	MIS-5,MIS-6
LTV-4	System shall not preclude the use of multiple cooperative LLTVs to transport logistics elements	MIS-5
LTV-5	System shall be maneuverable in lunar terrain with slopes less than 5° within a 1km radius	MIS-7
LTV-6	System shall have an on board processor to enable operations without crew interaction	MIS-5
LTV-7	Vehicle shall not exceed 5 mt in mass and 5.25x5.25x8 meters in dimensions.	MIS-4

### 3.2.3 - Cargo Manipulator (CM)

<i>ID</i>	<i>Functional Requirement</i>	<i>Requirement Link</i>
CMX-1	System shall be capable of manipulating payloads with 1.5 degrees of accuracy	MIS-8
CMX-2	System shall be able to handle a payload at 15000 kg including lifting down from lander, transporting across surface, and adjusting position	MIS-2
CMX-3	System shall have a stowed configuration for transport and off-loading phase	MIS-7
CMX-4	System shall have a power and communication interface with the LLV	MIS-6
CMX-5	System shall be capable of offloading LLTV from all lunar landers including HLS and CLPS providers	MIS-4
CMX-6	System end effector shall have the means of mating with all logistics element configurations	MIS-1

### 3.2.4 - Pressurized Logistics Module (PLM)

<i>ID</i>	<i>Functional Requirement</i>	<i>Requirement Link</i>
PLM-1	System shall have standard docking interfaces to mate with other logistics modules (i.e. habitats)	MIS-8
PLM-2	System shall be capable of pressurization suitable for sensitive logistics elements	MIS-8
PLM-3	System shall offload lunar weight of the logistics elements from the crew performing transfer out of PLM	MIS-9
PLM-4	System shall comply with NASA Standard 3001 vol. 2 for crew interfaces	MIS-8, MIS-9
PLM-5	System shall be capable of offloading from lunar landers capable of transporting at least 5 mt of payload to the Moon.	MIS-4

### 3.3 - L3 Requirements - Pranav

#### 3.3.1 - LLV

##### 3.3.1a - Mechanical

<i>ID</i>	<i>Functional Requirement</i>	<i>Requirement Link</i>
LME-1	System shall be capable of actively securing the payload and restricting 6 DOF	LLV-2

##### 3.3.1b - Mobility

<i>ID</i>	<i>Functional Requirement</i>	<i>Requirement Link</i>
LMO-1	System shall have a top speed no less than 2 cm/s under full capacity	LLV-5
LMO-2	System shall have the capability of traversing over obstacles no less than 25 cm in height	LLV-5
LMO-3	System shall be able to raise or lower height of chassis by 40 cm	LLV-5
LMO-4	System shall be able to control chassis rotation in roll between -15 and 15 degrees with an accuracy of 0.5 degrees	LLV-2
LMO-5	System shall be able to control chassis rotation in pitch between -15 and -15 degrees with an accuracy of 0.5 degrees	LLV-2
LMO-6	System shall be able to control the height of each mobility linkage independently	LLV-2

## 3.3.1c - Avionics

<i>ID</i>	<i>Functional Requirement</i>	<i>Requirement Link</i>
LAV-1	The system shall have all of its EEEE components adequately shielded of the radiation present on the lunar surface and soil (protons, electrons, galactic cosmic rays, etc.)	GEN-1
LAV-2	The System shall have 4 optical cameras	LTV-5
LAV-3	Each camera shall require less than 10 Watts of power, and be able to operate between -55 and 50 degrees	LTV-5
LAV-4	Each camera shall have a pixel array size of 1920 x 1080	LTV-5
LAV-5	Each camera shall weigh less than 0.425 kg and be 75 x 85 x 55 mm	LTV-5
LAV-6	The system shall use a processor with capabilities similar to the RAD5545 SBC from BAE Systems	LTV-6
LAV-7	The SBC shall weigh less than 2kg and be smaller than 209 x 209 x 15 mm	LTV-6

### 3.3.1d - Power, Propulsion, and Thermal

<i>ID</i>	<i>Functional Requirement</i>	<i>Requirement Link</i>
LPT-1	The rover critical electrical components, including the flight computer, driving electronics, and sensors shall be thermally regulated to within temperature bands of -35 C to 30 C. Batteries shall be regulated to within temperature bands of -20 to 40 C. Solar cells shall be regulated to within temperature bands of -80 to 100 C. Motors shall be regulated to within temperature bands of -50 to 50 C.	GEN-1
LPT-2	Over darkness periods not exceeding 420 hours at ambient temperatures not below 50 K, the logistics rover shall be able to maintain the temperature of components to within their respective survival bands.	GEN-1
LPT-3	Logistics vehicle(s) shall have active and passive dust mitigation on solar panels.	GEN-2
LPT-4	The vehicle shall be capable of generating enough energy to charge full battery capacity over a period not exceeding 96 hours.	LTV-3

### 3.3.1e - Software

<i>ID</i>	<i>Functional Requirement</i>	<i>Requirement Link</i>
LSO-1	System shall be semi-autonomous with onboard GNC processing capabilities	LTV-1, LTV-3

### 3.3.2 - CM

#### 3.3.2a - Mechanical

<i>ID</i>	<i>Functional Requirement</i>	<i>Requirement Link</i>
CME-1	System shall have at least 3 DOF	CMX-1

CME-2	System shall be able to control rotation in yaw between 0 and 360 degrees with an accuracy of 1.5 degrees	CMX-1
CME-3	System shall be able to control rotation in pitch between -85 and 85 degrees with an accuracy of 1.5 degrees	CMX-1
CME-4	System shall be able to be stored in a maximum envelope of 0.75x0.75x2.5 m	CMX-3
CME-5	System shall have 4m reach under full load, with a max operating height of 6m	CMX-2

### 3.3.2b - Avionics

<i>ID</i>	<i>Functional Requirement</i>	<i>Requirement Link</i>
CMA-1	System manipulator shall know its location in its workspace	CMX-1
CMA-2	Cargo Manipulator shall have an onboard camera or equivalent sensor	CMX-1

### 3.3.2c - Power, Propulsion, and Thermal

<i>ID</i>	<i>Functional Requirement</i>	<i>Requirement Link</i>
CPT-1	The motors of the cargo manipulator shall be thermally regulated to within temperature bands of -50-50 C through the use of thermal breaks and a passive thermal control system..	GEN-1
CPT-2	Over darkness periods not exceeding 420 hours, the cargo manipulator shall be able to maintain the temperature of electronics, and motors to within their respective temperature bands.	GEN-1

### 3.3.2d - Software

<i>ID</i>	<i>Functional Requirement</i>	<i>Requirement Link</i>
CMS-1	Cargo Manipulator processing should be handled by the LLV	CMX-1



### 3.3.3 - PLM

#### 3.3.3a - Mechanical

<i>ID</i>	<i>Functional Requirement</i>	<i>Requirement Link</i>
PLE-1	System shall utilize a Stewart platform design interface to orient the docking mechanism.	PLM-1
PLE-2	System shall be capable of maintaining pressurization to 14psi	PLM-2
PLE-3	System shall withstand launch loads	PLM
PLE-4	System shall include a method of relieving payload bearing loads from crew operating within the PLM	PLM-3
PLE-5	System shall not impede hatch operations in a depressurization event (according to NASA-STD-3001)	PLM-1, PLM-4
PLE-6	System shall include a hatch capable of transporting logistics elements to other modules.	PLM-3
PLE-7	System shall be able to deploy from lander autonomously	PLM-5

#### 3.3.3b - Avionics

<i>ID</i>	<i>Functional Requirement</i>	<i>Requirement Link</i>
PLA-1	System shall have onboard sensors capable of monitoring pressurization	PLM-2
PLA-2	System shall have the means to control internal pressurization	PLM-2

#### 3.3.3c - Power, Propulsion, and Thermal

<i>ID</i>	<i>Functional Requirement</i>	<i>Requirement Link</i>
PLT-1	The payload module shall be thermally regulated passively by an exterior coating to maintain a nominal exterior temperature of 50-90 F	GEN-1
PLT-2	The payload module shall have an umbilical power connection through the docking interface to facilitate the transfer of power for autonomous operation to survive for 7 days	PLM-1

#### 3.3.3d - Software

<i>ID</i>	<i>Functional Requirement</i>	<i>Requirement Link</i>
PLS-1	System Shall be capable of regulating internal pressurization	PLM-2

## 4. System Outline

### 4.1 - System Architecture - Darian

Our system can be broken up into three major subsystems: The Lunar Logistics Vehicle, the Pressurized Logistics Module and Habitats, and the Cargo Manipulator. The PLMs and Habitats will be the primary payloads for the LLV and will create a sustained Lunar settlement. The LLV will also utilize the Cargo Manipulator to move smaller payloads. The LLV, Habitat, and PLM are shown to the right.



**Figure x: LLV, Habitat, and PLM on Lunar surface**

### 4.2 - CONOPs – Darian

Upon first landing on the Lunar surface, the LLV must be offloaded from its lander. Habitats and PLMs must also be offloaded. At this point, the LLV will approach the desired payload. It's active suspension will lower the body of the LLV into a crouched position; the LLV will continue to drive forward, surrounding the payload and standard payload interface. Once correctly positioned, the LLV's active suspension will begin to raise the body out of its crouched position and into its nominal drive height. As the body of the LLV rises, it will latch with the standard payload interface, ensuring a secure connection during transportation. After nominal drive height is reached, the LLV will drive to the desired location. Once the LLV and payload have arrived at the desired offloading location, the latching process will occur in reverse: The LLV's active suspension will lower and the LLV will disconnect from the standard payload interface. The LLV is then able to back away from the payload, return to nominal drive height, and begin its next task. A comic strip of this baseline mission is shown below in figure [x].

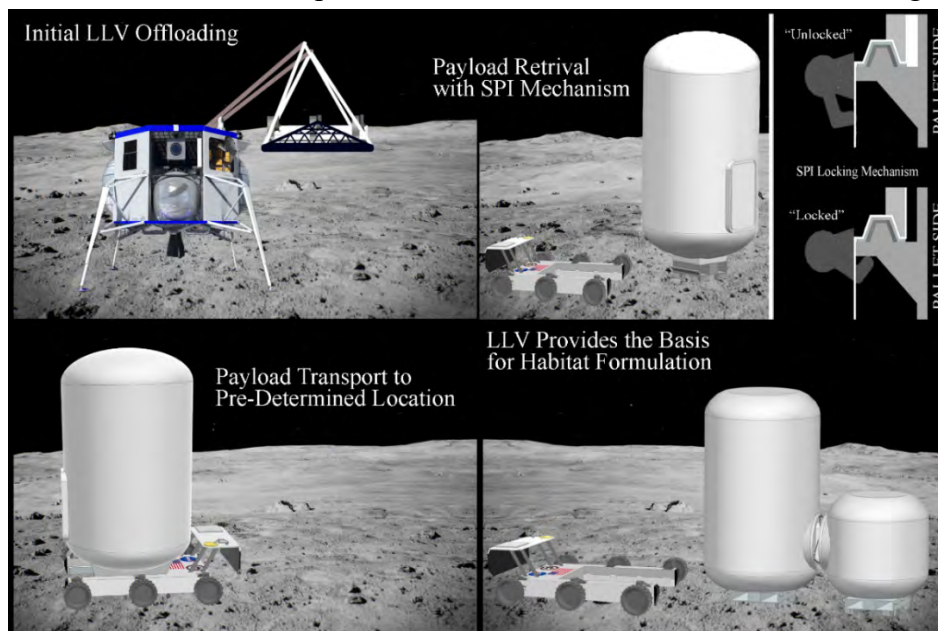


**Figure x: Visual Concept of Operations by Seth Gussow**

If the LLV's payload is a habitat, it will simply be left in the desired location. If the payload is a PLM, it will be maneuvered in such a way that it can dock with an already placed habitat. From this docked position, crew members within the habitat will be able to enter the PLM and offload the supplies and logistics elements contained within.

The LLV is also capable of using a cargo manipulator to move smaller payloads. The cargo manipulator also sits on a standard payload interface, so it is picked up in the same way that the habitats and PLMs are. Once properly connected to the LLV, the cargo manipulator can move and position smaller payloads. These payloads can also be placed onto the same standard payload interface as the cargo manipulator for long distance transportation.

### 4.3 - Block Diagrams - Darian

SHELL can be broken into three major subsystems: the LLV, PLM, and CM. The figures below depict system block diagrams that show how each component to these three major subsystems interface with one another, as well as outlining thermal control.

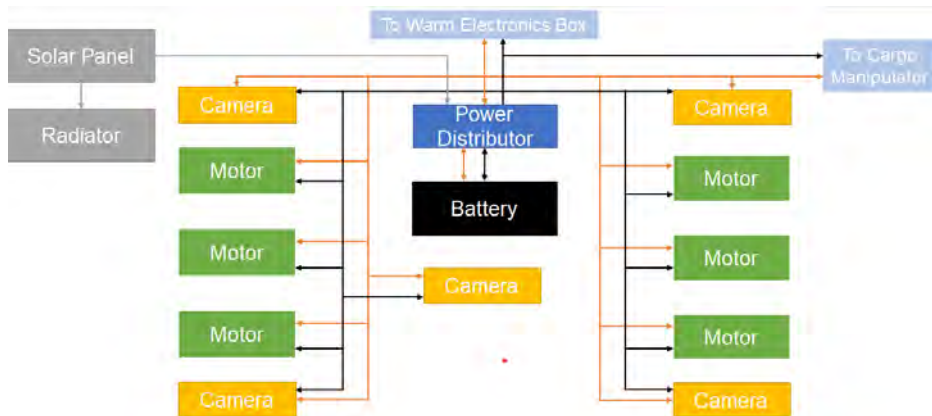
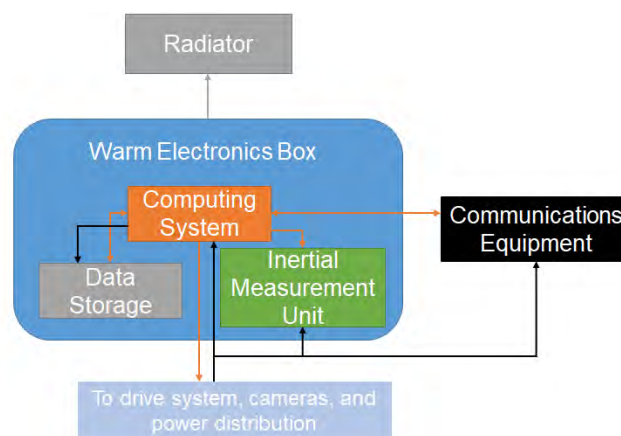


Figure x to the left shows the system block diagram of the LLV, with figure x showing the inside of the warm electronics box. Note that yellow corresponds to sensing, black to power distribution, and gray to power generation.

**Figure x: LLV system block diagram**



**Figure x: Warm electronics box system block diagram**

To the right in figure x is a simple block diagram for the Cargo Manipulator. Since most thermal control and power is part of the LLV, only actuation is shown for the Cargo Manipulator.

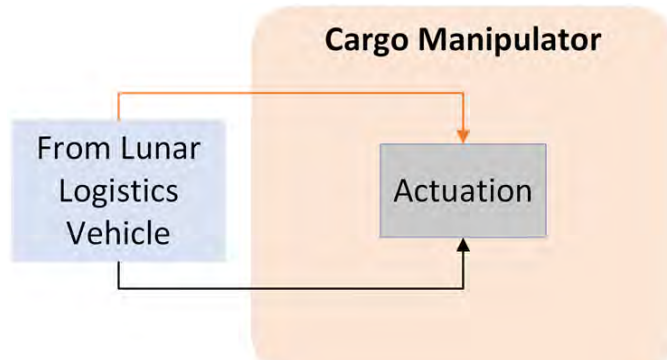


Figure x: Cargo Manipulator system

Finally, figure x to the right shows the system block diagram for the PLM. Similar to the Cargo Manipulator, much of the thermal control and power is supplied externally and is therefore not shown on the block diagram.

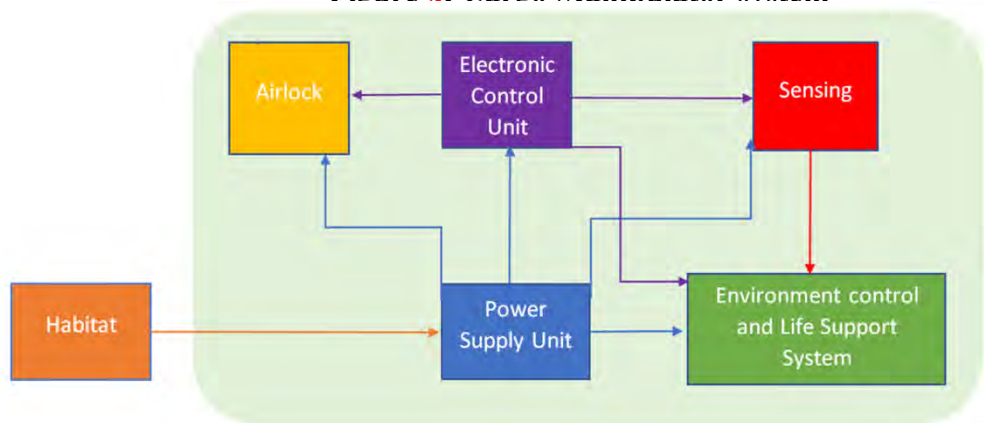


Figure x: PLM system block diagram

#### 4.4 - WBS - Darian

The work breakdown for development of each of the three major systems is shown in the following figures. These figures show which subteam was responsible for each subsystem within our three major systems. Note that project management, risk analysis, and budgeting tasks are not included in these figures as they are not related to the development of one specific system.

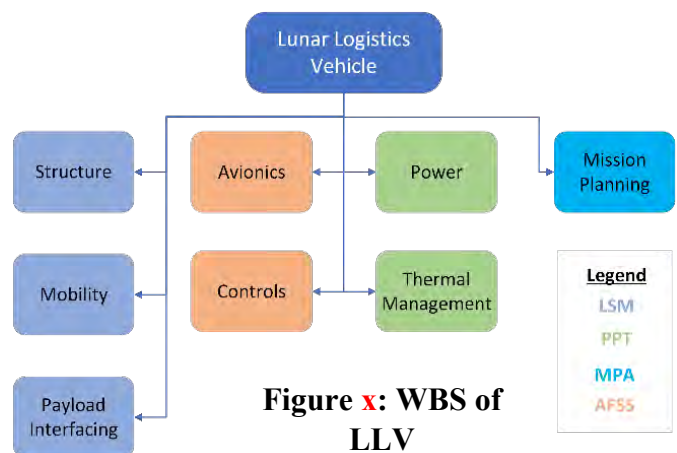
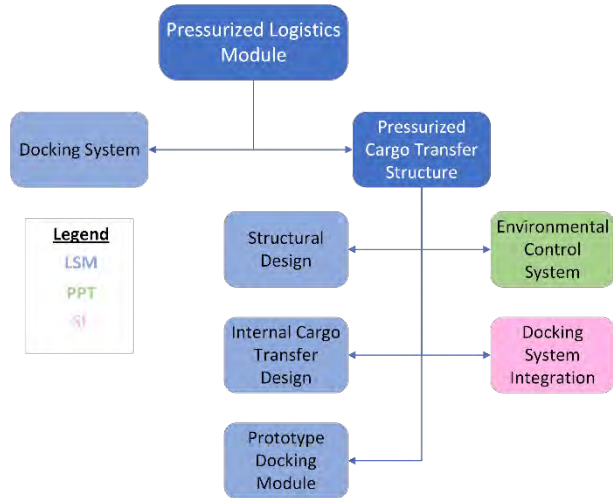
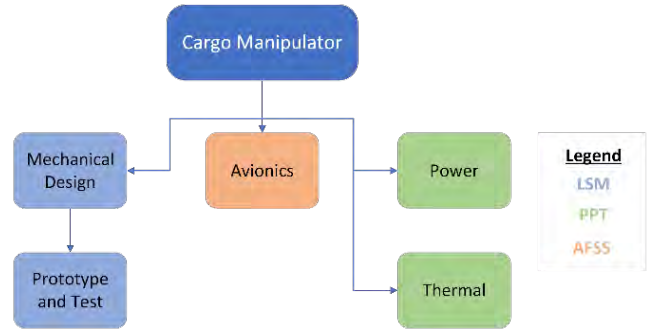


Figure x: WBS of LLV



**Figure x: WBS of PLM**



**Figure x: WBS of CM**

#### 4.5 - Mission Planning – Seth Gussow

Crucial to our mission was developing methods to survive on the lunar surface. We set out to find areas where we could deploy our LLV and provide ample opportunity for NASA to develop a habitat on the lunar surface. In support for NASA’s habitat, we developed methods that aided the science goals while also utilizing our LLV as much as possible to maximize its purpose. The following sections outline our goals for a lunar landing and potential landers for our LLV in addition to offloading concepts. Along with this we develop an understanding of our full mission outlook and what we view as a typical day for our LLV will be.

#### 4.6 - Site Selection – Seth Gussow

The initial driving factor for site selection was to fall within the pre-defined Artemis sites to provide NASA with familiar locations that could be made into a permanent settlement. NASA had already provided 13 sites on the lunar south pole that they indicated would have locations for a permanent settlement and our goal was to set out to find locations where we could operate our LLV.

Our initial criterion was based on MIS-7, a level 1 requirement that dictated that our LLV must operate in areas up to 5 degrees in slope. This led us to examine areas on the lunar south pole that were under 5 degrees in slope and within Artemis sites. Data was mostly viewed through Arizona State University’s QuickMap which compiled the Lunar Reconnaissance Orbiter Camera’s data along with other resource mappers (MPA-1). This allowed us to intuitively see many layers of data such as sunlight, terrain slope, temperature, and many more in an easy to work with resource.

First viewing terrain slope data, we were able to find over 65 subsites within the Artemis regions. This was done by selecting the Applied Coherent Technology (ACT) combined data file of “Terrain Slope” in addition to adding the “Artemis 3: Candidate Landing Sites” layer. The ACT

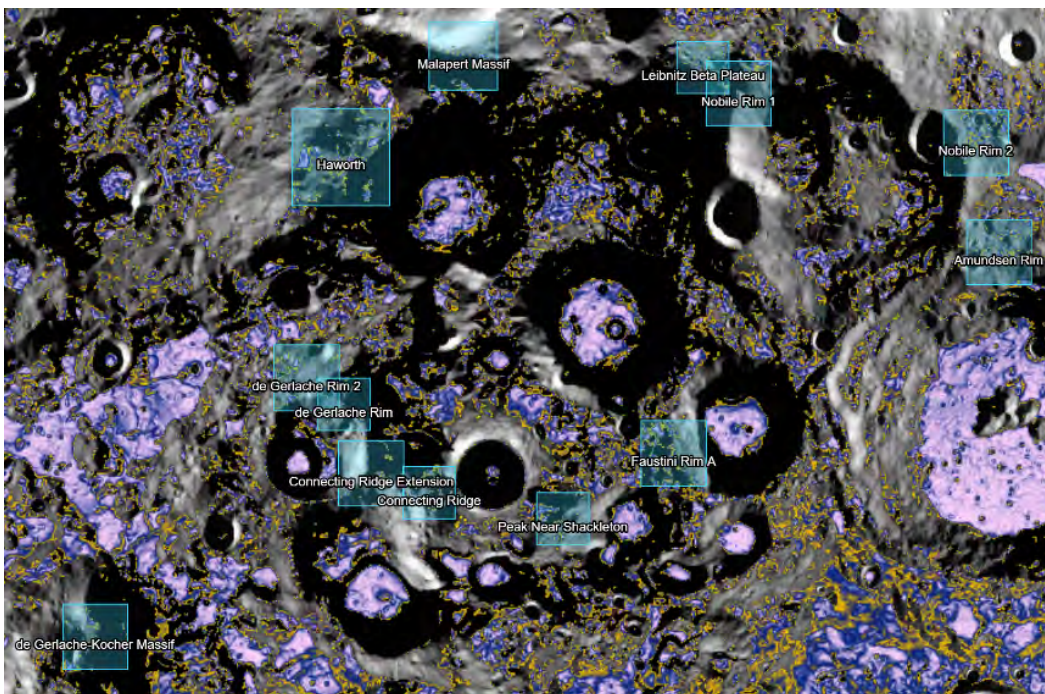


**Figure 4.6.1: ASU QuickMap Application with Slope and Artemis III sites**

combined file considers the Lunar Orbiter Laser Altimeter (LOLA) data and imagery files compiled by ACT. By setting the range of the slope layer and masking the outlier data (any slope above 5-degrees) we can see our usable areas which then became our subsites. The image of what can be seen with these layers active are shown in Figure 4.6.1. The areas that fell within the Artemis candidate sites became our internal subsites which would need to be further broken down (MPA-1).

The next part of site selection became how we would be operating the vehicle and the longevity of the mission. As MIS-6 states, our LLV must remain operational for at least 5 years starting in 2028. To support such a long mission, we intended to look for sites where we could operate our vehicle for extended periods of time that matched the south pole's sunlight schedule in addition to mapping when the Earth would be visible for communication purposes. This led us to look for sites that would have at least 30% sunlight availability stemming from level 2 requirement LPT-2. As our LLV was planned with solar capabilities, we decided against areas on the south pole that had multiple dark lunar days to maintain adherence to this requirement. While a site with extended solar periods would have left us with nearly 4-months of constant sunlight, we felt that needing to hibernate or bring an expensive power source to the surface would not benefit the mission more than a consistent operating schedule.

Earth communications was also a big sticking point in site selection. With communication relay satellites not yet operational around the moon we wanted to find a way that we could be self-reliant if necessary. This would require Earth visibility from our site if we intended to have operations. We decided that as a contingency for any future lack of relay communications arrays that we would require our site to have Earth visibility 30% of the time. While we do not intend to communicate directly back to Earth during operation, the availability to have a window of communication with Earth is viewed as upside for our site selection. When examining sites in ASU QuickMap we were able to quickly see the average Earth visibility of the area. If any site fell below a 30% average, we would discard these sites and look for other options, ending with us having 58 usable subsites that we would further examine (MPA-1).

After having these 58 sites based purely on slope and earth communication, we needed to include the other items required for survival within our site. This led us to research the available sunlight and the elevation of the sunlight within these regions. This was done by utilizing the NASA Jet Propulsion Laboratory (JPL) Horizon's tool, allowing us to view the sun as observed by a point on the lunar surface. From our above 58 sites we had stored the central coordinates of each site as seen in the ASU QuickMap application. To view data using these coordinates certain bounds needed to be set up when running the program. The main bound was time, in which the simulation was run between 2028 and 2033 marking a 5-year period. Using these selenocentric

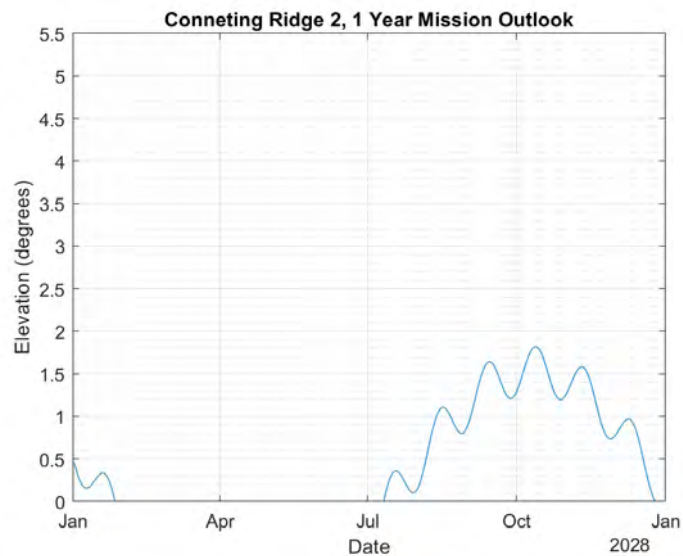


**Figure 4.6.2: Subsite “Cold” Region**

coordinates we could place them into the JPL Horizons tool to quickly compare each site, specifically looking for sun elevation.

After pulling data for each of our 58 subsites a MATLAB script was created to easily plot the data for 1 lunar day, 1 lunar year, and the full 5-year period. Specifically using the 1 lunar year plots the type of solar availability was seen and sorted into three different groups. These three groups were defined as: "Favorable" - Less than 21 days (about 3 weeks) of darkness, "Somewhat Favorable" - Between 21 and 29 days (about 4 weeks) of darkness, and "Cold" - Over 1 full lunar day of darkness. An example of both a "cold" site and a "favorable" site are shown in figures 4.6.2 and 4.6.3 respectively.

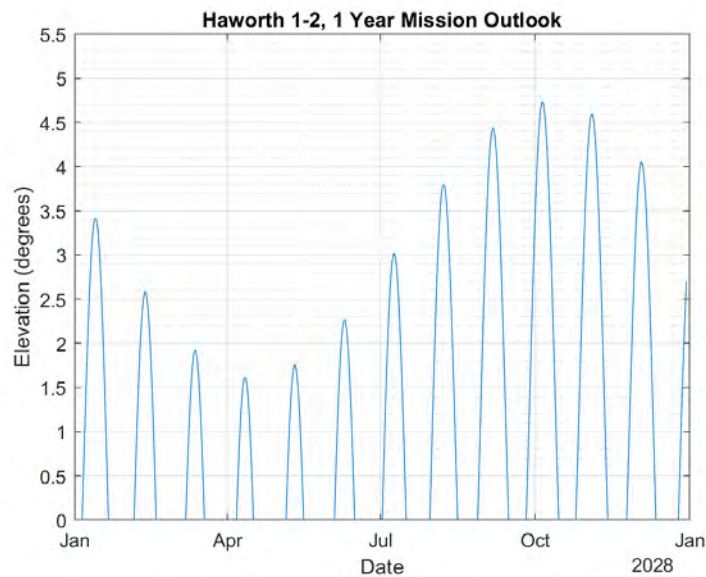


**Figure 4.6.3: Subsite “Favorable” Region**

Following our previous requirements that we would not remain in a site with periods of darkness above 480 hours we continued to study the “favorable” regions selected. Ultimately, we were left with 16 sites that fit the criteria for sunlight availability, Earth visibility, and subsite area. Something that we wanted to continue to investigate was the roughness of the terrain. While the overall rock size of the lunar south pole is relatively unknown, roughness maps are available which give us a basic idea of the lunar terrain. Once again using the ASU QuickMap, we were able to find the average roughness based on the area of our subsites. After pulling this data we created a decision matrix to determine the actual weight of each of the 16 remaining subsites.

When setting out to compare these 16 subsites our goal was to determine the worst possible site available and continue to design our LLV and its operations around this site. This would allow us to lay the blueprint of a “worst-case” scenario for LLV survivability while also allowing NASA the flexibility to choose from a plethora of habitable sites. Our goal with providing 16 usable sites was allowing NASA the option to pick a site to their liking while also proving that we can reasonably survive in any of these sites. From this, our decision matrix was laid out with the following criteria and weights: sunlight availability in days (50%), surface roughness (10%), Earth visibility average (10%), and area in km<sup>2</sup> (30%). These weights were



determined by ranking individual characteristics by data availability and usefulness for mission planning.

As discussed previously sunlight availability was a major concern and dictated many of the options on the LLV and mission planning, thus assigning it the largest weight aligned with the analysis previously done at 50%. The lower weights of Earth visibility average and roughness were mostly dictated by mission planning need. With Earth visibility largely being reliant on not having any relay network we understood that this was an absolute worst-case scenario and is discussed more in depth in the “Communications Planning” section. As mentioned prior, roughness data was available for the lunar south pole and showed relatively consistent measurements in each of the 16 sites. Lastly, we wanted NASA to have the flexibility to travel at extended distances within each site, hence why area represented 30% of the weight. While RASC-AL only requires 1 km of travel, by allowing for more area of the lunar surface to be explored it opens the possibility of what NASA can accomplish with the Artemis missions.

After applying the weights to the data, we had acquired we were able to rank the sites based purely on this matrix. Ultimately, it left our internally named Haworth 1-2 as our “worst case” site that we survive in; a 7.47 km<sup>2</sup> area site with ample opportunities for habitat settlement that fell within the Artemis III Haworth region. This became our site that we intended to plan on designing for and developing the LLV capabilities around, however we believe the capabilities demonstrated can be applied to any of the presented 16 subsites. The full decision matrix is laid out in the appendix and indicated the true values of each of the subsites. As noted below in figure 4.6.4, Haworth 1-2 has a favorable sunlight pattern with extended periods of sunlight in the summer and ample time for mission tasking in the winter and this is further discussed in the “Mission Tasking” section. A visual representation of the bounding area of Haworth 1-2 is shown in figure 4.6.4 and displays the slopes in the area up to 5 degrees (MPA-1).

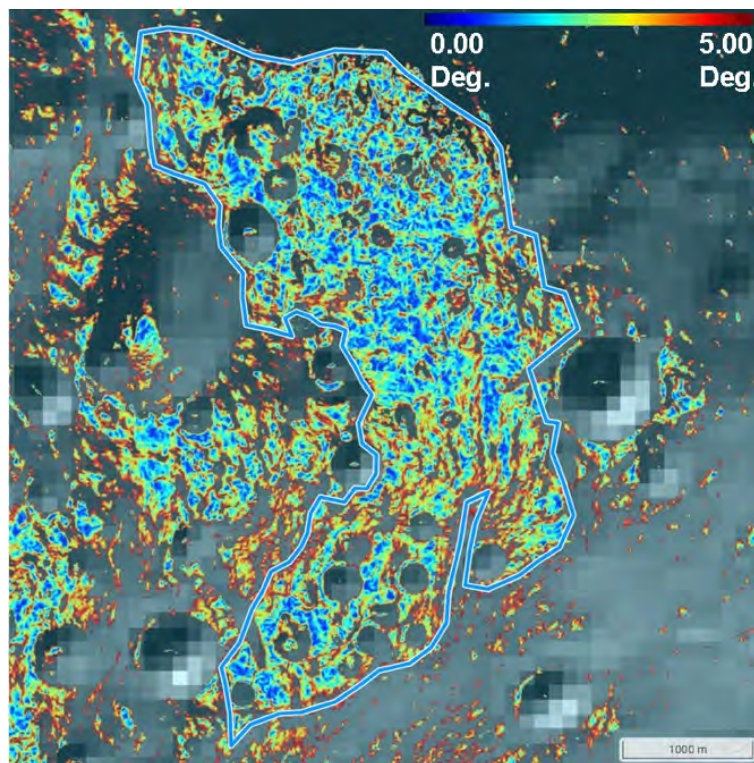


**Figure 4.6.4: Haworth 1-2 Slope Map**

#### 4.6.1 - Haworth 1-2 Characteristics – Seth Gussow

Now that we had a site that we were planning our mission around we could begin to explore the characteristics further. The most important aspects that we were interested in were those that would impact survivability including sunlight hotspots, permanently shadowed regions, and temperature bands. Each of these impacts the mission in different ways, whether it be finding locations that would be safe to charge or access to areas of interest for NASA's scientific goals.

Specifically examining temperature, our internal level 3 requirement LPT-2 dictates that our ambient temperature shall not fall below 50 degrees Kelvin. Using the ASU QuickMap, we can easily see temperature bands on the lunar surface, specifically looking at lunar winter where we would expect to see the lowest temperatures. From this we were able to find that our lowest possible temperature was 43.4 K (represented in figure 4.6.1 as pink, with warm being bright yellow), very close to our minimum but still above our requirement. A temperature map of winter minimums is displayed in figure MPA-5 and shows that our northern area seems to be the coldest location. While we believe that the southern portion of this subsite would be more beneficial for NASA and the Artemis missions, we can survive within the region even if stationed in the north (MPA-1).

A feature that NASA specifically mentioned when selecting the Artemis candidate landing sites was access to a Permanently Shadowed Region (PSR) within their regions. This was something that we examined when initially selecting subsites, however, did not dictate criteria based solely on this. We found that many of the subsites did include areas of PSR's in addition to a nominal sunlight pattern. As shown in figure 4.6.2, Haworth 1-2 includes a few PSR's within the deeper craters of the subsite. While there are some smaller ones in the southern portion of the region, there is access to larger ones in the north which coincides with the colder areas of Haworth 1-2. If

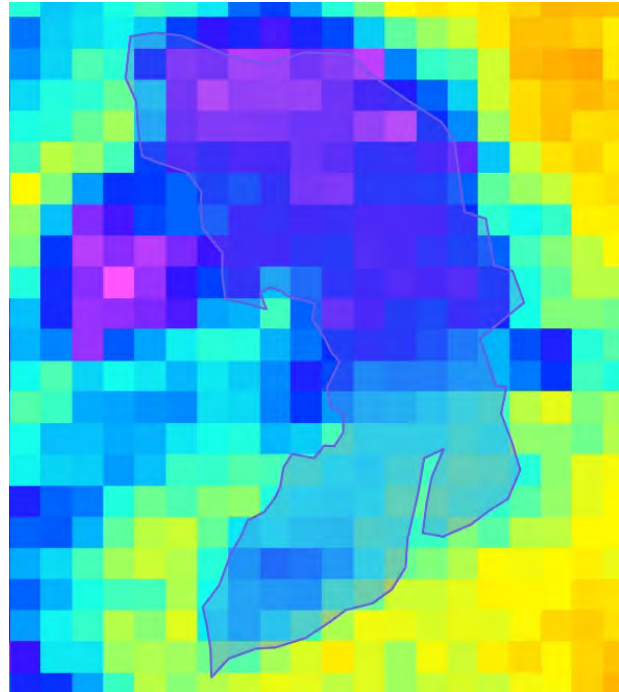


**Figure 4.6.1.1: Haworth 1-2 Winter Temperature Map**

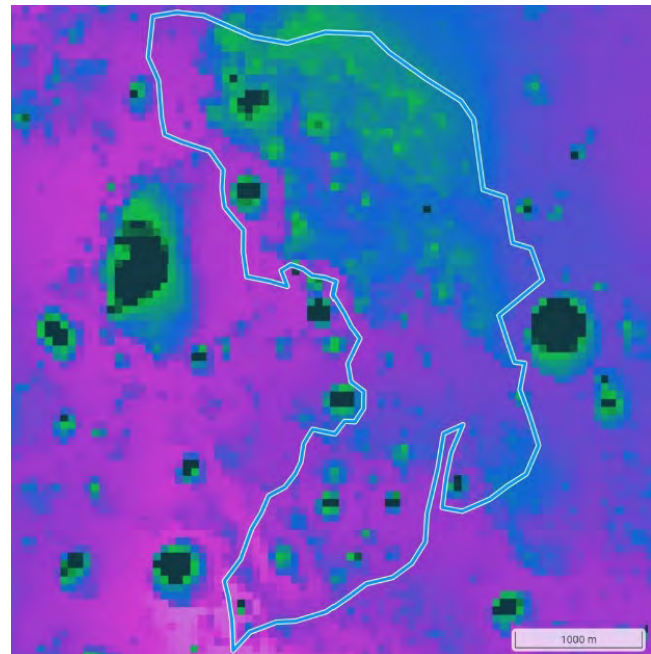


**Figure 4.6.1.2: Haworth 1-2 Sunlight Availability Map**

NASA were to explore PSR's on their Artemis missions Haworth 1-2 would not be a barrier to these scientific goals.

As shown in Figure 4.6.2, there is ample amounts of sunlight on the western side of the region and the southern portion of Haworth 1-2, with higher sunlight represented in pink and the green spots indicated less sunlight available. This is crucial for our LLV's survivability as we intend to charge for extended periods of time if we expend our battery fully. While a nominal charging period for only a 1 km mission is under 15 hours there are use cases that will require longer charging times. This is discussed further in the "Mission Tasking" section. Haworth 1-2 provides excellent coverage for charging and enables us to explore the full subsite without any major solar concerns. Additionally, Haworth 1-2 is relatively flat, and we believe that sunlight obstructions are minimal in the area. Preliminary analysis on sunlight obstructions is discussed further in the appendix and compares the elevation of the sun with the elevation of the terrain around the LLV.

#### 4.7 - Communication Overview – Seth Gussow

A significant concern with mission planning on the lunar surface is the availability of a communications network. With no currently operating lunar relay satellites it is hard to know for certainty what options will be available come 2028. Our goal was to identify areas that were currently in development in addition to creating a system that could help "future proof" our LLV for the 5 years of operation. We chose to explore the planned operations as well as the availability of direct to Earth communications from our LLV.

Our selected site of Haworth 1-2 has an Earth visibility of 37%, considerably less than what would be reasonably required by NASA for a human presence on the moon. While some locations on the lunar south pole do have 100% connectivity Haworth 1-2 does not have this luxury and will need to have another source of connection. While our LLV is designed to operate without constant Earth connectivity, a consistent connection to Earth is favorable for both LLV operations and any planned EVA operations.

Of the planned relay systems, Lunar Gateway appears to be the most fleshed out of the ideas. With a planned initial launch of sections starting in 2024 this aims to put Gateway into operation well before our 2028 operating timeline. However, Gateway only plans on having the capability for two simultaneous links using the HALO Lunar Communication System (HLCS). As our LLV and its missions are not crewed the likelihood of our mission gaining priority for these channels is very slim. While there is a planned third link available in the Power and Propulsion Element there is still not enough availability for Lunar Gateway to be a reliable source of communication forwarding (MPA-14).

Another current project with NASA is the Exploration and Space Communications' (ESC) Lunar Communications Relay and Navigation Systems (LCRNS) which aims to tackle the lunar relay satellite issue. While work on this is preliminary, it is a sign that NASA fully intends on creating and operating a relay network for missions to communicate not only with other lunar assets but also back to Earth. More specifically, it aims to accelerate the creation of assets such as LunaNet, a 2019 initiative to help with "networking; positioning, navigation and timing; detection and information; and science." We believe that NASA's commitment to creating a lunar relay network is a priority and that it is reasonable to assume that NASA would implement the beginnings of such before our mission and any permanent habitation of the lunar south pole.

As there is no active lunar relay network, we wanted to create an onboard communication system that would be reliant on current technology and be able to communicate with future lunar

missions. When setting out to identify bands of interest for our communication availability we looked initially at the International Communication System Interoperability Standards (ICSIS) to remain compliant with these standards. Within these standards there are specifics on Cislunar Space Platforms (CSP) that allow for S and Ka-band link forwarding, which would be the most appropriate for our mission needs. This of course emphasizes the need for a relay system and reduces the burden on the LLV's antenna specification. Our goal was to design our LLV to be compliant with the ICSIS standards to encompass future relay systems that should also follow these standards. This allows our LLV to potentially work with future relay systems without the need for multiple technologies (MPA-14).

In addition to communicating with assets in a lunar network and back on Earth one of our objectives was to be able to communicate with other lunar assets. Specifically, we wanted to communicate with the established habitats on the lunar surface that would be within our specified landing sites. While we can provide power and communications data when transporting a habitat or other payload, having the ability to communicate with assets directly on the surface is a priority. This is accomplished by having a specific antenna for lunar assets in which we can receive commands directly from the astronauts within the habitat or send position and data updates without the need for jumping off a relay satellite. This also adds a layer of redundancy for communications with Earth. If our own antennas are blocked for any reason, we can use a lunar asset such as a habitat to transmit data back to Earth on our behalf.

#### **4.8 - *Applicable Landers – Ayush Varaiya***

One of the key aspects to get started on the mission is the success in transporting all the resources and equipment needed to the moon. This involves the selection of the right lander for the habitat and the LLV as well as creating a method to take the equipment off the lander once the lander reaches the moon.

The first aspect of the mission is the habitat for the astronauts. With a weight of 15 metric tons, the only lunar lander that can carry this weight is the SpaceX Starship. The SpaceX Starship has a maximum capacity of 100 metric tons and a fairing diameter of 9 meters which fits the habitat dimensions as well (MPA-13). In addition, it is the only lander that is currently being funded by NASA to be used on future lunar missions. It was chosen by NASA because it budgeted the lowest development cost at 2.9 billion dollars, compared to the competitor, Blue Moon, which had a development cost of 6 billion dollars (MPA-17). Also, Starship has estimated the lowest launch cost compared to its competitors.

The next aspect of our mission is the logistics vehicle which has a maximum weight of 2000 kilograms. The LLV was designed to fit on lunar landers such as the NASA Orion, Commercial Lunar Payload Services (CLPS), Blue Origin Blue Moon, and other lunar landers with enough payload space for the LLV. Bounded by the weight and size, the vehicle we chose is the Blue Origin Blue Moon lunar lander. The payload capacity of the Blue Moon is 4500 kilograms, and it has a 7-meter diameter fairing which is big enough for the dimensions of the logistics vehicle (MPA-17). In addition to the lander, we also plan on sending any other resources that would be needed with the extra payload space. While this lander is currently privately funded, it is a better choice for the payload since the Starship would be too big for only the vehicle. Also, the cost for this lander would be lower than the Starship since Blue Moon is smaller in size.

Once the landers were selected, we started to calculate the  $\Delta V$  from the Earth to the Moon to find out the speed of the lander. We used a Hohmann transfer to calculate the transfers from Earth to Low Earth Orbit (LEO), LEO to Lunar Transfer Orbit (LTO), LTO to Low Lunar Orbit (LLO), and LLO to landing (MPA-4). Adding all the  $\Delta V$  values from each transfer, the initial estimation for the total  $\Delta V$  to the moon was about 6.9 km/s.

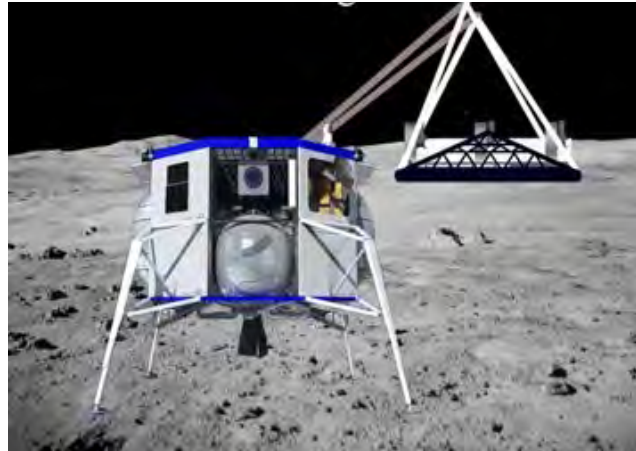


**Figure 4.8.1. Offloading Concept for Blue Origin Blue Moon**

Once the habitat and the lander have landed on the moon, we need to devise a plan to get it to the surface. Upon researching past missions and how the rovers were offloaded, we plan to use a platform lift-style lowering mechanism. At first, we planned to use the elevator on the Starship, but due to no official news about the elevator, we decided to create our own offloading concept. Similar to the concept provided by the Blue Moon lander, the platform lift-style lowering mechanism will use cables attached to a platform and lower to the lunar surface. Also, we did not know the weight limit for the elevator which is another reason we deemed it necessary to have our own concept.

While the weight of the lander is much greater than the payload being loaded off, we made sure tipping was not an issue. We based our tipping calculations on the Blue Moon since that is the lighter choice out of the two landers we plan to use. To start, we researched the dry mass of the Blue Moon which is 3000 kilograms, and we have the weight of the LLV which is 2000 kilograms. We assumed the worst-case scenario which is when the lander lands on a slope of  $5^\circ$ . To calculate the maximum weight of the payload before tipping, we first found the length of the base length of the lander which was 21 meters. Then, we found the length of the base if it was on a  $5^\circ$  incline which was 22.5 meters. Once these calculations were done, we were able to find the moment force of the lander and solved for the maximum weight of the payload. Upon completing the calculations, we found that any payload under 26,000 kilograms could land on the moon without risking the lander to tip over.

#### 4.8.1 - Offloading- Darian

Ideally, we would like to utilize the offloading mechanisms being developed in conjunction with whichever lander we ultimately use. Unfortunately, since many of these offloading concepts are in early states of development, there is no guarantee that they will be operational when we plan to begin operations on the lunar surface, or if they are operational there is no guarantee they will interface with our systems. To ensure we are able to proceed following our timelines, we have designed our own versatile lander offloading concept that, with some modifications, can be used with a variety of landers and payloads depending on what is required for mission success. These modifications will ensure the offloading mechanism properly fits whichever lander is being used, and if it is only required for lighter payloads, is not overdesigned in order to minimize cost.

Our offloading concept is a platform lift style lowering mechanism as shown in figure [x]. It consists of two arms attached to the payload area of our desired lander. Each arm has a cable and winch that attaches to a platform. The payload is loaded onto this platform. When stowed, the arms are vertical. When it is time for the payload to be offloaded, the pair of winches will raise the platform slightly then the arms will pivot, bringing the platform over the edge of the lander. From here the winches will lower the platform to the lunar surface where the payload can be removed. If the payload is the Logistics Vehicle, it will simply drive off the platform, otherwise the Logistics Vehicle will drive onto the platform, attach to the payload, and remove it. The platform will then return to its stowed position.

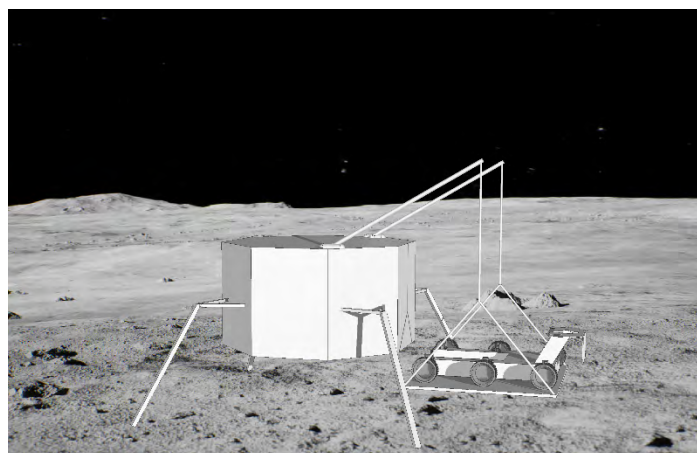


**Figure x: Our offloading concept with the LLV as the payload**

#### 4.9 - Mission Tasking – Seth Gussow

One of the biggest tasks in planning for a five-year operating period was estimating how active our LLV would be and forecasting the utilization of our time on the lunar surface. This includes the servicing of large habitat missions, the inclusion of the planned Artemis missions, the servicing of smaller Commercial Lunar Payload Services (CLPS) missions, and the limiting of downtime for our LLV. This led us to prioritize the maximization of time spent actively to make the most of our LLV's architecture.

The first step in determining how much our LLV would need to move was figuring out the planned lunar missions that would arrive during our planned five-year lifetime. Due to our LLV being designed in part to help the Artemis habitat remain active, we set out first to explore how many planned Artemis missions would be landing during our lifetime. From the NASA Office of Inspector General (NASA OIG) we determined that as of September 2021 there would be 15 launches within 2028-2033. This gave us a baseline for larger scale operations where we would expect these launches to send larger payloads with a cadence of 122 days on average. With this information we were able to begin to build our overall timeline for surviving for 5 years on the lunar surface.

In support of these missions would be resupply missions which we are dubbing Pressurized Logistics Modules (PLM). These were internally designed to support the reference habitat, aiming to bring supplies up to the lunar surface at a regular basis. The proposed cadence of these PLMs is 28 days and is discussed further in the “Pressurized Logistics Module” subsection below. Initially examined using the ISS resupply cadence, we believe our PLM cadence is aptly distributed over our 5-year cycle in addition to minimizing launch costs. By creating a PLM with a shorter cadence, it opens the door to smaller landers that in turn reduce overall mission costs. This 28-day cadence translates to 65 launches over the 5-year period, our largest mission servicing task.

Our last major mission servicing task fell to the CLPS landers, smaller payloads that would support the larger Artemis mission. While these are still in the developmental phase, there are some instances where the NASA OIG points out specific plans for future scheduled landings (MPA-14). From these instances we were able to determine that NASA expected CLPS landers to arrive at the lunar surface every 90 days, landing around 16 for our life cycle. Although we would probably not be required to service all the potential CLPS landings we wanted to design for the capability and be aware of these landings.

There are approximately 96 planned landings that we would need to be available to service over our five-year lifetime and take into consideration when planning. As we plan our daily tasking, we will consider this calculated 96 launches per five years, breaking down further to around 19 per year bringing us to just over 1 per lunar day. With a scheduled arrival of every 20 days, we can fully expect to service at least one launch per lunar day meaning that we must be available for payload retrieval.

Type	Cadence	5-Year Total
Artemis	122 days	15
PLM	28 days	65
CLPS	90 days	16
<b>Total Landings</b>		<b>96</b>

**Table 4.9: 5-Year Launch Cadence Outline**

#### 4.10 - Daily Mission Availability – Seth Gussow

Understanding how frequently our LLV needs to operate is crucial to planning our internal components. We began by studying the site features of our chosen landing site, specifically examining the available sunlight and how long we could expect to operate. As we are a solar powered LLV, sunlight availability is the limiting factor of our motion. While our battery capacity is quite large, we still need to be able to survive the cold lunar nights and ensure we do not exceed our safe depth of discharge.

Starting out with examining our sunlight we look back to our typical lunar day which is 29.5 Earth days. This equates to 708 hours within a lunar day, however within Haworth 1-2 this is of course not all sunlit. In the summer, Haworth 1-2 has 19 days of pure sunlight (456 hours) which is our most usable timeframe. As expected, the winter does not provide nearly as much light with only around 12 days of constant light (288 hours). While there is a 13 lunar day cycle, by using our absolute maximum and minimums we can plan for our best- and worst-case scenario for sunlight availability. With much of our time being spent needing to charge our batteries, having ample sunlight in addition to extended mission tasking will be important.

As described in requirements MIS-2 and MIS-3, we know that our maximum load case is 15000 kg (15 mt), and we must travel 1000 meters. While MIS-3 was the driving factor behind finding a landing site larger than 1 km<sup>2</sup>, we understood that we would probably be traveling more than just 1000 meters in one trip and that this was just a minimum capability. Additionally, we wanted to look for a solid definition of a full mission servicing to which we settled on a full “out-and-back” excursion of our LLV. This meant that a full-service mission would include an empty leg of our LLV with no payload followed directly by a 15 mt payload on our LLV. By using this metric, we were able to investigate total mission servicing time and how long we would expect to need to charge for.

One of the largest challenges was determining how fast we could service a mission. With sunlight being once again the limiting factor, we wanted to be able to service at least one mission per day in a reasonable time frame. As discussed previously in “Mission Tasking,” there would be instances where we would be required to service more than one mission in a lunar day, adding incentive for our LLV to be capable of 2 missions per lunar day. This meant that when picking a speed, we needed to consider the worst-case scenario, 288 hours of sunlight availability, and ensure that we could complete a full charge to survive the extended lunar night in the winter.

In addition to sunlight, we needed to consider what the capability of our batteries was and the threat of overheating the motors. By carrying 15 mt we were putting a lot of stress on our motors and were worried that if we went too fast, we would burn out the motors quickly. Discussed further in our thermals section, we found to offset the stress of the 15 mt payload we would need to reduce our speed during this use case. A side effect of this was that we would reduce the power drawn from the battery making our movement slightly more efficient. As a first

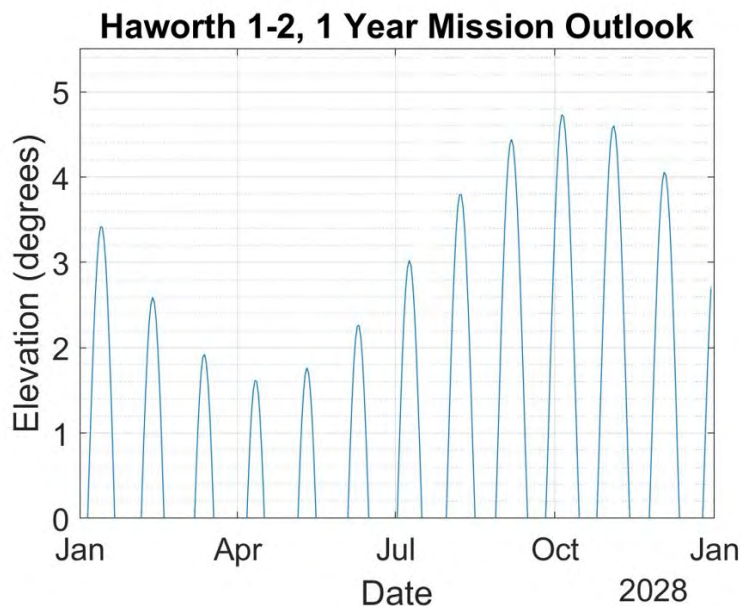


**Figure 4.10.1: Haworth 1-2; 1 Year Mission Outlook**



pass we settled on a speed of 0.02 m/s (2 cm/s, 0.045 mph) when carrying a 15 mt habitat and going 0.2 m/s (20 cm/s, 0.45 mph) when empty or carrying smaller payloads such as a CLPS lander payload. Considering pathfinding error, we estimated that a single leg of the minimum trip would be 1100 meters, or 2200 meters for the entire trip. That meant under our defined speeds we could complete a servicing mission in just 16.81 hours, a small dent in our 288-hour minimum timeframe.

However, we quickly discovered that moving this slow under a full 15 mt load presented a few issues. Specifically, our power draw increased at this speed due to the avionics components needing to be powered on for longer periods of time. Along with this, we understood that moving for extended periods of time logically would increase our mission risk and any problems encountered while moving and potentially causing unnecessary stress on the vehicle. Because of this we chose to examine our speeds once more, specifically aiming to increase our fully loaded speed while minimizing charging time required and battery draw. We chose to minimize these parameters to prioritize the time available once again for the LLV to operate on the lunar surface and maximize use of the sunlight availability.

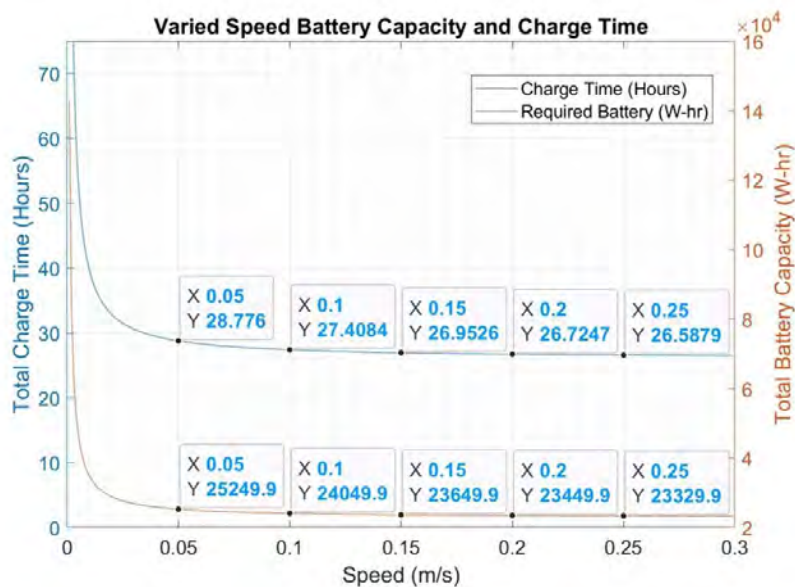


**Figure 4.10.2: LLV Speed Optimization Plot**

We quickly found that the relation between charging time and required battery were very similar, both decreasing logarithmically when we increased the speed of our LLV. As suspected, if we went slower, specifically at 0.02 m/s, we would put far too much stress on the capacity of the batteries and increase our charge time significantly when we did not have to. As such, we decided to increase our speed to a full 15 mt load. As shown above in Figure 4.10.2, we saw diminishing returns in both charging time and battery capacity once we were past the 0.1 m/s mark. As mentioned previously we were also concerned about motor heating under our full 15 mt load condition and decided it would be best to operate at this 0.1 m/s mark. As such, we will require the LLV to only proceed at 0.1 m/s when carrying the full 15 mt habitat while continuing

to move at 0.2 m/s when unloaded or taking on lighter payloads such as a pressurized logistics module.

While we could have increased the speed of our LLV, we felt that it was unnecessary to do so as this would already allow us to fully service a mission in ample time. Specifically, we could service a full 2200-meter mission in under 6 hours including a 30% margin for any significant pathfinding error. With this capability in mind, we knew that we could accomplish large scale retrieval missions and remain comfortable with our battery health. It is important to note that with these time considerations we are not planning on discharging our battery below 80%, the safe and recommended line of our selected battery. This is discussed further in the “Battery” subsection.

Looking farther than just a 1000-meter habitat retrieval we knew our LLV was capable of much more, specifically being able to traverse long distances without any major stoppages. Our LLV can comfortably transport a 15 mt payload up to 12,000 meters (12 km) before requiring a charging stop. Significantly this assumes no active solar charging while moving our vehicle, only counting active charging when stopped on the lunar surface. While a major limitation is slope in the area, Haworth 1-2 boasts relatively flat land and with the bounding area just over 7 km we can comfortably maneuver within the area while hauling a full habitat.

Using this 12 km distance, our total traverse time one way is 33 hours moving at 0.1 m/s and still considering an 80% depth of discharge. A full servicing mission of a habitat payload at this distance must include 16.7 hours of unloaded travel in addition to the 33.3 hours of payload travel. The full breakdown of a mission including a 30% margin is seen in Table 4.10. The day shown is an average lunar day, taking the average hours of sunlight available within the Haworth 1-2 region representing a traditional day for our LLV.

Item	Length (hours)
Unloaded Travel	16.7
Loaded Travel	33.3
Unloaded Charging	11.1
Loaded Charging	71.5
Margin (30%)	39.8
<b>TOTAL</b>	<b>172.4</b>
<b>EXTRA</b>	<b>199.6</b>

**Table 4.10: 12 km Servicing Mission Timing Outline**

Of note is the charging conditions, in which we require 2 charging times to cover the full 24 km trek. This is purely for battery health, as we do not want to over draw from our battery and jeopardize our system. Thus, we require just over 82 hours of sunlight to charge on this extended servicing mission. Additionally, we show that we have around 200 hours of free time that we can spend either on other servicing opportunities or mission tasks. This fits our recommended timeframe of being able to service two missions in one lunar day. Even on a lunar day of only 288 hours, a dark winter day, we can still service a full mission along with charging and have around 115 hours to either service a smaller mission or partake in other mission tasks.

This flexibility is a fantastic part of our mission, as we can not only service a wide variety of payloads but also allow NASA the opportunity to send multiple coinciding missions during one lunar day and fully expect our LLV to be able to service them. Along with this capability, our extended range opens the possibility of extending the bounds of NASA’s Artemis program and enhances the science goals of a permanent lunar habitat.

#### 4.11 - LLV Path Planning- Ayush Varaiya

The pathfinding process started with research on how other missions control their rovers. Some examples we took were the Mars Perseverance Rover and the Curiosity Rover. These rovers use a navigation system, AutoNav, where operation engineers use 3D glasses and direct the rover where to go on Mars. The operation engineers plan the stops on the way to the destination and the rover uses its cameras and images to avoid obstacles and reach these stops (MPA-15). In addition, a new rover, Volatiles Investigating Polar Exploration Rover (VIPER), was taken into consideration since the rover is planned for launch in 2024. VIPER will have operation engineers plan two-week routes for the rover to traverse over and the rover will collect ice samples on the way (MPA-4). It was evident that these rovers were traversing Mars and the Moon to collect scientific data, but we needed path planning that would find the most optimal path from one place on the Moon to another.

With a maximum of 15 tons on the rover, we needed to make sure the shortest path was taken with minimal obstructions to ensure the payload was delivered successfully without any complications. Since there is not too much terrain information on the South Pole of the moon, we needed to account for unknown situations and needed a more active pathfinding process. Also, we can only traverse up to 11° of slope with a maximum payload and 13° of slope without a payload, which bounded the path even more. In addition, the rover would require a lot of power which is why finding the shortest path would conserve the most battery. Taking these complications in mind, we started to research ways that the vehicle can actively follow a path given by engineers, as well as figure out a way to maneuver past obstacles, if there are any, caught by the cameras.

At first, we researched the use of LunaNet. LunaNet is a new method of communication with Earth for any mission on the Moon. The goal for this technology is for missions to be able to use LunaNet and upload and download data at any time compared to the present system which only lets missions communicate at scheduled times. Also, LunaNet will have navigation capabilities that will allow missions to track their crew and robotic missions (MPA-3). While this approach could be used, the technology is still being developed and being created for the Artemis missions. Since we would need direct communication with the vehicle during the start of the missions, it was deemed to be more useful to create software that could be more in line with our goal for the mission.

After conducting further research, we discovered a new NASA technology that helps rovers steer using landmarks. The development and research of artificial intelligence combined with current data of the moon has been conducted by Alvin Yew, a NASA research engineer at Goddard Space Flight Center. Yew started his research with the data of the Lunar Orbiter Laser Altimeter (LOLA) from NASA's Lunar Reconnaissance Orbiter (LRO). Yew used the photographs taken by the LRO, slope maps, and lunar roughness to try and replicate that data with an AI duplicate. If the AI can replicate the information we have already, we can trust the AI to send accurate data back if a rover is traversing over unknown areas (MPA-10). This technology combined with known features of the moon could help engineers on Earth figure out the location of rovers as well.

We decided to create software that could use Yew's technology and combine it with other technologies such as Goddard Image Analysis and Navigation Tool (GIANT), which was developed by Andrew Liounis, a NASA engineer. This tool analyzes pictures and measures the distance to landmarks, such as craters and rocks, within visibility (MPA-15).

The goal of the software created is to be able to take the rover to the location of the payload and deliver it to the destination. To achieve this goal, the software will ask for the coordinates of the landing site, the vehicle's location, and the destination for the payload. From these coordinates, the software will create a path that avoids craters, large rocks, and large slopes. After, the operation engineers review the path to ensure all obstacles are avoided. Once the path is sent to the vehicle, engineers can manually view the cameras to check if any unaccounted-for debris shows up. If an emergency occurs, the software can get overridden and engineers can manually operate the vehicle.

There were a couple of issues that we researched which led us to create this software. First, rocks were a huge issue for us since we cannot traverse over them depending on size. To solve this issue, we will be using optical cameras that show us the view in front of the vehicle to ensure no rocks are in the path. Also, to create a time-optimized path we plan to use GIANT and cameras to ensure the path chosen will have a low slope. In addition to the software helping our mission, we will be able to create a better terrain map by traversing the surface of the moon and capturing data as it drives.

In the future of this mission, we plan to utilize beacons to localize the south pole of the moon and create roadways. By localizing the moon, we can create roadways to make path planning autonomous which will make it easier for the logistics vehicle to get from one place to another. This will help in creating a map of the moon for future south pole missions.

#### **4.12 - Inter-site Travelling- *Ayush Varaiya***

For the Artemis missions, 13 different sites were chosen on the south pole of the moon. These sites were chosen depending on the craters and the scientific significance the sites could have for research. For our purposes, we had to find parts of each site that we were able to traverse over due to the limitations of the LLV. With a maximum traversable slope of about 13° while unloaded, we were able to narrow down the potential sites with the most traversable surface for our limitations. Other factors that were considered are the sunlight and the area of the narrowed regions.

As mentioned previously, we decided to recommend an area within the Haworth Artemis region which we dubbed Haworth 1-2. Below is an image of the entire Haworth Artemis site with our subsite highlighted on the left side of the image in blue. The areas shown in color indicate areas that are traversable by our LLV, opening the door to NASA for a much larger usable area. While we are not required to go this distance, the ability to do so paves the way for extensive NASA science missions in the future.

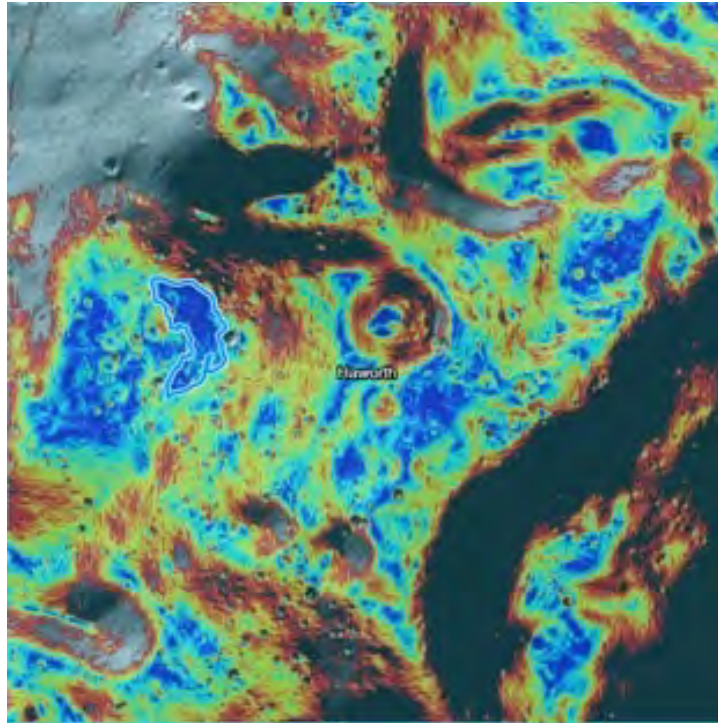


**Figure 4.12.1. Haworth 1 Slope Map**

One of the sites that were chosen for further consideration is Haworth. This site had the largest area for the parameters we were looking at. We would be able to move around this site with an unloaded and loaded LLV. Also, we have the potential of driving 12 kilometers on a single charge with a 15 metric ton payload on the LLV. This gives us the capability to drive within the Haworth 1-2 and outside of the area of Haworth 1-2 but stay in Haworth 1. Haworth 1-2 is an area we marked ourselves that gave us the desired slope map which is part of the original Haworth 1 Artemis site. As our LLV can traverse slopes upwards of 11 degrees when fully loaded with a habitat, we believe the flexibility offered to NASA is invaluable. The ability to traverse such a large area enables NASA to develop more than one settlement or satellite settlement on the lunar surface.

#### **4.13 - Mission Maintenance- Ayush Varaiya**

During the 5-year mission period, it is important to consider potential risks and create solutions for these challenges. We plan to need maintenance throughout the mission duration due to abundant amounts of lunar debris. This debris is made up of many minerals such as silicon, oxygen, titanium, glass beads, and others which stick to surfaces due to electrostatic forces. Lunar dust will stick on the cameras and sensors during lunar landings, driving on the surface, and extra vehicular activities, which could cause damage to the vehicle. This could affect their function and cause the vehicle to become unstable and tip over if the components have limited view. Lunar dust can also get on the solar panels and limit the amount of power solar panels generate. Also, the cargo interface is at risk because if the lunar dust gets on the interface, the payload has the potential to slip off if not latched properly.

To avoid these issues, we started to research methods to limit the effects of lunar dust on the vehicle. The first solution was to use a soft-bristle brush. There was a test by NASA that

compared different material bristles including nylon, PTFE, and Thunderon. To duplicate lunar dust, NASA researchers used NU-LHT-1D lunar simulant and created a moon-like atmosphere. Upon testing, the nylon bristles were able to remove 90% of the simulated dust, while the PTFE was able to remove 80%, and Thunderon was inconclusive. Next, the researchers tested the difference between using long bristles and shorter bristles. The longer bristles were deemed more effective and were longer lasting as well. While there was a discrepancy between brushes depending on the material it was being used on, the nylon brushes did well with the lunar dust in the laboratory conditions (MPA-7). Taking all the different brush types, we made the decision to use nylon long-bristle brush to solve the lunar dust problem.

Upon further research, there was a new spray that was able to blow away lunar dust. Washington State University conducted a study where they used liquid nitrogen spray to get rid of moon dust. They were trying to simulate the lunar dust that gets caught on a spacesuit, so the researchers used barbie dolls and coated them with volcanic ash to represent lunar dust and placed them in a vacuum to simulate the conditions on the moon. They conducted three tests: liquid cryogen spray, liquid nitrogen pour, and compressed air. The cryogen spray was able to remove 91.99% using 50 cm<sup>3</sup> of spray on a 194 cm<sup>2</sup> piece of cloth. Under the same parameters, the compressed air was only able to remove 69.24% of the dust. For the liquid nitrogen pour, about 50 cm<sup>3</sup> was poured out onto the same size of fabric and was able to remove 73.77% of the dust (MPA-18). Upon these results, we decided to use liquid cryogen spray.

In the study with the brushes, it was found that the material of the spacesuit that the researchers tested on had significant effect when brushed against. The nylon bristles caused scratches on the surface of the suit which could cause further damage over time, and it would be harder to remove lunar dust if the dust sticks to the scratches (MPA-11). Since the body of the vehicle is made of aluminum, we do not expect the material to degrade significantly since it is metal. While the lunar dust on the body can be solved by the brush, the other delicate parts of the vehicle will need more care. Since the brush could scratch cameras, sensors, and solar panels, it was important to find a method that could limit damage which is why the liquid nitrogen spray is a viable alternative. We plan to use cryogen spray for the small parts of the vehicle, so we do not have to launch more spray than we need. With the combination of the brush and the liquid cryogen spray, it is possible to remove most, if not all, of the lunar dust.

Another maintenance need for the vehicle is the modular components on board. With the harsh conditions on the moon and unknown terrain track on the south pole, we believed it was important to ensure we were able to complete the missions even if some of the modular components become unresponsive.

One of the modular components will be the mobility module. This module will consist of the wheel on the vehicle and the suspension attached to it. There will be 6 mobility modules for each of the wheels on the vehicle. At first, we planned to keep all the wheels connected, but that meant that if one wheel were unresponsive, the whole vehicle would be immobilized. Upon further research, it was more beneficial to keep each wheel in its own hot-swappable box, so if one of the boxes were to become unresponsive, we could switch it out for a new box during an extravehicular activity (EVAs). The advantage of this is it allows for rapid repair and replacement and helps reduce time for maintenance of the vehicle.

In addition to being replaced during EVAs, the module is equipped with a free-rotation mode for the wheels. This means that if a wheel is damaged or not rotating coordinated with the other wheels, the wheel will be free flowing and will continue to rotate with reduced mobility.

This will put more pressure on the other wheels to carry the load and may not be the ideal process, but it will ensure the mission is not at a halt due to one malfunction.

Another component that might need to be replaced over time is the camera housing. With the goal of making the LLV completely autonomous, we need multiple cameras and sensors to ensure the vehicle knows where it is going and avoiding all obstacles it cannot drive over. To ensure the LLV is functioning to its full potential, each camera housing will be built as a modular unit as well which can make it easier to replace if a component malfunctions.

The maintenance of the LLV is feasible only during extravehicular activities (EVAs) because this is the only time astronauts will be able to get close to the vehicle. First, the lunar dust can be sprayed off or brushed off during an EVA to ensure all parts are working to their intended performance. Also, if any of the mobility modules do break down, they can be replaced during EVAs as well. By creating the mobility modules, it makes the vehicle easy to maintain and reduces the risk of critical failures if we replaced one camera at a time.

#### **4.14 - Extra Activities – Ayush Varaiya**

Picking up and delivering payloads using the vehicle is the main mission, but there will be some time where the vehicle will have down time without any responsibilities. As stated in the mission schedule, there are about 120 hours that are allocated for additional activities that the vehicle can be capable of. Within this time, we must include time to charge the vehicle to ensure we can service the upcoming missions without loss of power since it only used solar energy and battery.

In addition to charging, there were a couple of ideas we had that could utilize the LLV in diverse ways. After the astronauts take all the packages from the PLM into the habitat and put the trash into the PLM, the PLM will not be useful anymore. Instead of creating a dump yard on the moon, we planned to use the PLMs in a positive way. First, we planned to use the PLMs to create walls to limit the spread of dust. We could use the interlocking interface to ensure the PLMs can stay in place and the wall stays intact. These walls could be placed around landing sites since these areas will have the highest rate of lunar dust spread. Since there will be multiple PLM missions, we will have enough PLMs to create a wall large enough to seclude a landing site. Also, we planned to create greenhouse-like tents for storage of any resources that were not able to fit inside the habitat. Another idea was to sinter the lunar surface to settle the lunar dust on the surface. This would help keep the lunar dust from kicking up onto the vehicle. The last idea was to use the pallet-interface and create a pallet that would have seats for astronauts to use as a vehicle. This would help astronauts get from one place to another quicker than walking and would help conserve their energy. While all these ideas were feasible, none would be possible without localizing the moon first.

We believed that localizing the sites we were on would be advantageous to the future of the mission and other missions to the moon as well. Due to the lack of information about the surface on the south pole, we believed that it is important to localize the moon to ensure future missions can use the information to their advantage.

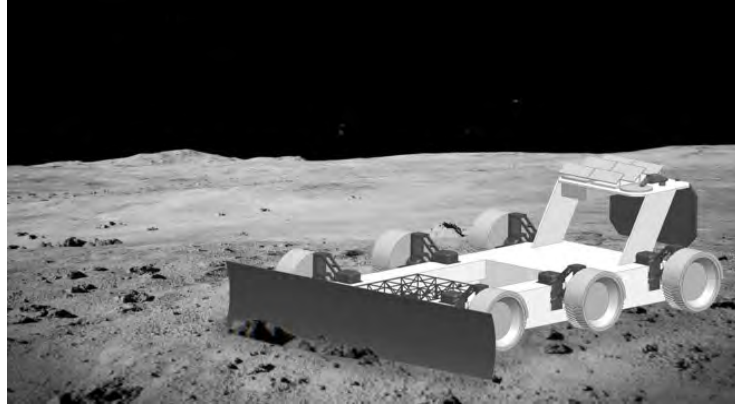


**Figure 4.14.. Plow Attachment on LLV**

To start the localization of the moon, it is important to make travelling on the moon easier for crewed and uncrewed missions. We decided to grade roadways on the moon which can help vehicles travel to the moon without having to worry about obstacles. We will launch a large plow attachment, as shown in the picture above, that can move large boulders out of the way of planned roadways (MPA-6). The plow attachment will be attached just like another payload and can be manipulated in height using the suspension of the wheels. The attachment can also level the moon's surface. In addition to roadways, the plow can create landing sites to help lunar landers select a landing site where they are certain the lunar lander will have no complications such as tipping or sinking. Grading the roadways will result in known slopes of each road and minimal rocks on the path.

To start with the local position system, it was important to create a map of the moon. We decided to use physical beacons that will be placed automatically from the vehicle, as well as image-assisted beacons. The physical beacons will be used to map out landing sites, as well as larger craters that need to be avoided by rovers on the moon. Due to the size of the vehicle, it was impossible to carry enough physical beacons and place them at every intersection or every roadway. Since we cannot use physical beacons at every point, image-assisted beacons will help confirm landmarks, such as craters and larger rocks, by comparing it to satellite-based imagery. By creating multiple known landmarks, future lunar vehicles can use the landmarks to increase mapping accuracy and distance estimations as well. This will also make positioning errors easier to detect and ensure a prompt solution for the next task.

The local positioning system will pair well with the roadways because it will be easier for engineers to direct future rovers on which path to take and will lessen communication between rover and Earth. It will give future missions the freedom to use autonomous driving with the help of the beacons.



## 5. Lunar Logistics Vehicle

### 5.1 – Baseline System Architecture – Anish Sankla

The LLV consists of a core U-shape chassis to intake payloads and a 6-wheel, all steering, active suspension mobility system to provide optimal performance on the lunar terrain. A fixed platform carries the solar panels, radiators, and antennae for the mission. Underslung latches are used to lock payloads into the payload bay during transportation. The payload bay enables the center of mass of the vehicle to be closer to the geometric center of the vehicle. This is highly important for vehicle performance as evenly distributed load on the wheels would result in optimal performance of the vehicle.

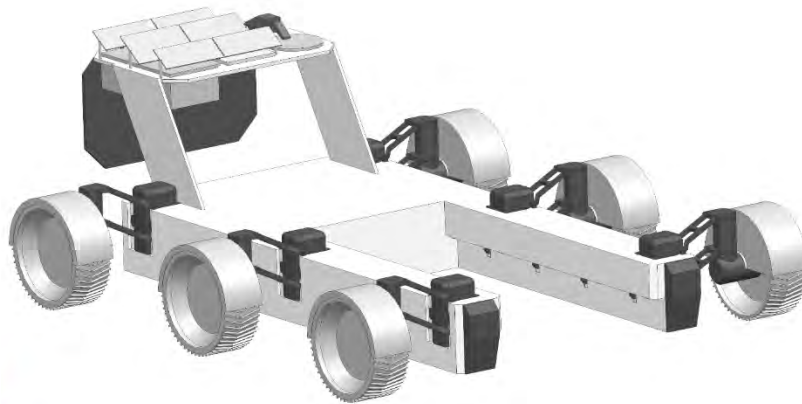


**Figure 5.1.1: Lunar Logistics Vehicle (LLV)**

Figure 5.1.2 shows the preliminary sizing of the vehicle, with wheelbase dimensions at crouch being 4m X 4.3m. The vehicle is capable of fitting within most launch fairings horizontally, with the dotted circle indicating a 7m minimum required fairing diameter. The vehicle also has a deep payload intake bay which allows for multiple payload configurations, from short to long payloads to a combination of both.

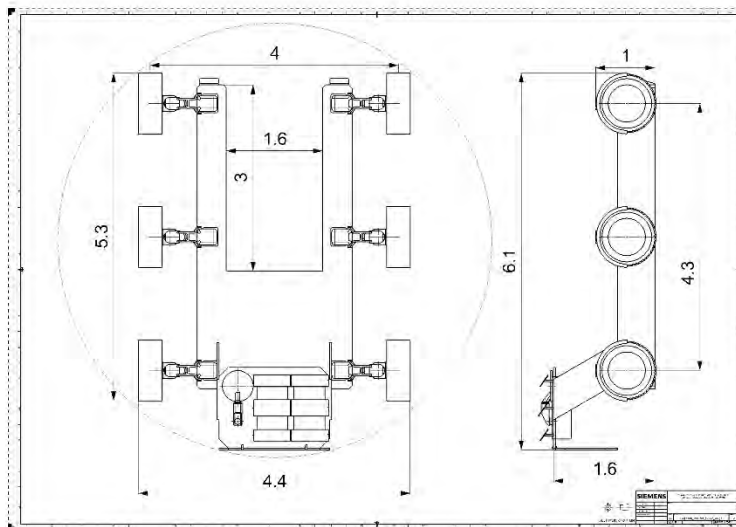


**Figure 5.1.2: LLV Sizing Drawing**

Table 5.1.3 shows the mass breakdown of the LLV. The mobility and chassis estimates are rough from CAD measurements, while the power estimate is from determining preliminary solar panel and battery size. This mass is used for the subsequent mobility analysis to properly size the wheels and actuators in the mobility system.

System	Mass Estimate (kg)	Notes
Chassis	700	Estimate from rough CAD model
Power	680	Initial estimate of ~650kg battery and ~30kg solar panels
Mobility	450	Estimate of 75kg for each wheel-steering-suspension assembly
Thermal	60	Notional allocation for thermal management, warm boxes, radiators, etc.
Mechanical	150	Notional allocation for payload interface, component deployment, etc.
Avionics & Harnessing	150	Notional allocation for all avionics components and harnessing
Total	2190	
30% Margin	<b>2850</b>	

**Table 5.1.3: LLV Mass Breakdown**

## 5.2 - Mobility System – Anish Sankla

The mobility system is the core of the vehicle architecture and mission architecture. It sets payload capabilities as well as vehicle performance in the unforgiving lunar environment. Multiple architecture options were researched to better understand the underlying component decisions to make with respect to steering and suspension. Rovers such as the Lunokhod rover have a passive suspension with skid steering, while others such as the Mars rovers have partial or all-wheel steering with a rocker bogie suspension. NASA's Chariot rover and Venturi Astrolab's FLEX rover take a different approach with all-wheel steering and an active suspension on each mobility module. Each of these architectures has their own benefits and drawbacks, and through definition of system requirements and design drivers, a mobility architecture for this mission can be chosen.

The baseline architecture drivers for this vehicle are derived from system and mission requirements. The vehicle must have the capability of moving both large and small payloads efficiently, which means the mobility system must perform well in the lunar regolith in both heavy and light load cases. Having coordinated degrees of freedom can also improve performance in the lunar environment. Since the mission is at the lunar south pole, the sun will have a low sun angle throughout the lifetime of the vehicle. This will drive solar panel placement, and sun tracking during driving is favorable. Multiple configurations of the vehicle will also simplify the deployment of the vehicle from launch to operation. Finally, the vehicle must be fault-tolerant in order to prevent the loss of mission due to a fault in the mobility system. Table 5.2.1 also lists the driving load cases that the vehicle will see during nominal operation.

These design drivers influence the subsequent architecture selection of the lunar logistics vehicle.

Vehicle Mass [kg]	Payload Mass [kg]	Nominal Speed [m/s]	Design Slope [deg]
2850	0	0.2	5
2850	3300	0.2	5
2850	15000	0.1	5

**Table 5.2.1: Nominal Drive Cases For LLV**

5.2.1 - Wheels

*Terramechanics Model*

To better understand the wheel-soil interaction in lunar regolith, a terramechanics model was built to assist in the completion of mobility trades. An excel calculator was built to produce performance characteristics of a given wheel geometry at a given load in lunar regolith. The calculator uses recorded lunar regolith properties to determine the sinkage of the wheel in regolith, the Terzaghi soil bearing capacity and drawbar pull per slip of the wheel [LSM-3]. Drawbar pull is the net tractive force of the wheel in regolith. It is calculated by determining the tractive force per wheel, then subtracting compression resistance, bulldozing resistance, gravitational resistance, and internal rolling resistance per wheel. Slip is the percentage of tangential velocity of the wheel that is not transferred to the linear velocity of the vehicle.

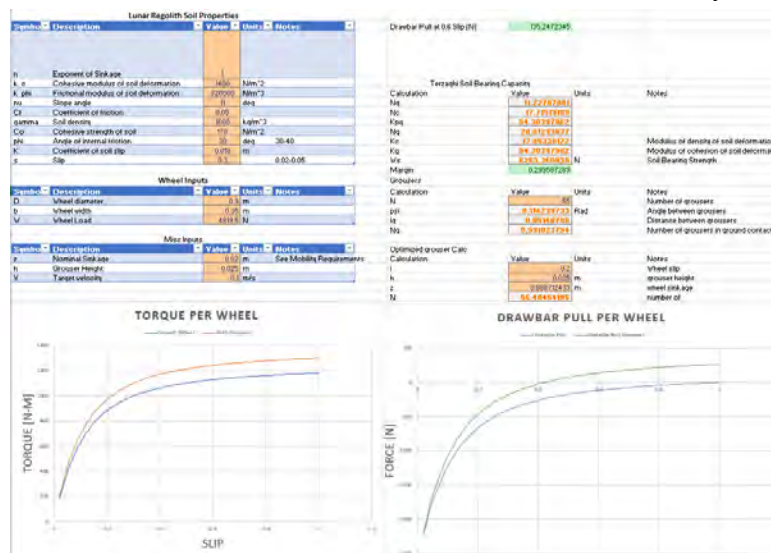


**Figure 5.2.11: Layout of Terramechanics Model**

The drawbar pull per wheel slip plot is the main performance curve used in characterizing wheel geometry. The slip at which the curve crosses zero is the minimum slip that the wheel will have during operation. This number should be as low as possible, however, will always be greater than zero due to the loose regolith.

*Number of Wheels Trade Study*

A trade conducted early on was the number of wheels the vehicle should have. More wheels would reduce individual wheel load, but also increase the mass and complexity of the system. Terzaghi soil bearing capacity was also a major consideration as there must be margin to

breaking the soil surface causing the vehicle to sink. 4 and 6 wheels were traded, and in the end, a 6-wheeled rover was chosen.

When comparing soil bearing capacity between the two wheels, the rover was assumed to be carrying its max 15 metric ton payload and the vehicle weight would be distributed equally between all wheels. Table 5.2.12 shows the margin on soil bearing capacity. 6 wheels has a much larger margin than 4, and the vehicle can be fault tolerant with this configuration as one wheel can be lost from the mobility system and the wheel load would not break the soil surface. A 4-wheel configuration would lead to additional complexities in incorporating fault tolerance into the design.

**Terzaghi Soil Bearing Capacity**

# Wheels	Wheel Load (N)	Capacity (N)	Margin
4	7229	7553	0.04
6	4820	6263	0.30

**Table 5.2.12: Soil Bearing Capacity for 4 and 6-Wheel Configurations**

For wheel sizing, it was important to understand how different wheel geometry variables affected performance characteristics of the wheel. The wheel geometry selection had two main objectives, increase thrust and decrease resistance. To increase thrust generated per wheel, the wheel diameter and width should be increased. To decrease resistance, sinkage should be minimized by increasing wheel surface area, therefore increasing diameter and width, as well as adding grousers to the design. However, it is important to note that an increase in wheel diameter also increases wheel actuator requirements. Table 5.2.13 shows the affects of wheel number as well as addition of grousers to the wheel. Grousers reduce the amount of slip at zero drawbar pull, which is an additional benefit. Between the 4 and 6-wheel configurations, there is a 10%-20% difference in drawbar pull, however, there is a >50% difference in torque required per wheel at 0 drawbar pull. This further supports the decision for a 6-wheel configuration to reduce actuator requirements and wheel size.

# Wheels	DP @ 60% slip (N)	Slip at 0 DP	Torque at 0 DP (N-m)
4, No Grousers	400	29%	1450
6, No Grousers	370	25%	910
4, Grousers	595	23%	1450
6, Grousers	500	21%	900

**Table 5.2.13: Comparison**

### *Wheel Sizing*

Once a 6-wheel configuration was chosen. The wheel geometry was adjusted to fit within vehicle constraints for wheel sizing. Table 5.2.14 lists the finalized wheel parameters chosen for the vehicle design. Figures 5.2.16 and 5.2.17 show the drawbar pull and torque required plots for a wheel at max load and 5 degrees. The minimum slip for the finalized wheel geometry is 21%. Additionally, in using the terramechanics model, the wheels are shown to also allow for traversal of slopes up to 11 degrees with degraded performance at 60% slip, characterized in figure 5.2.18.

Parameter	Design Choice	Justification
Number of Wheels	6	Lower torque reqs
Wheel Load	4820	Load leveled across all wheels
Outer Diameter	0.9 m	Sized around volume/system constraints
Width	0.35 m	Reduce sinkage and increase soil bearing capacity
Grouser Height	0.025 m	Reduce required number of grousers
Number of Grousers	55	Minimum grouser for optimum performance per [LSM-1]
Chevron Angle of Grousers	16 deg	Allows for constant rolling radius on hard ground
Effective Ground Pressure	4.86 kPa	Calculated from [LSM-2]
Soil Bearing Capacity at Max Load	6263 N	Terzaghi bearing capacity [LSM-3]

**Table 5.2.14: Wheel Parameters**

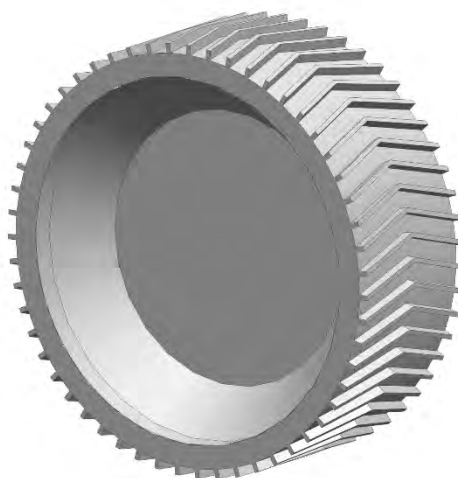


**Figure 5.2.15: Notional Wheel Geometry**

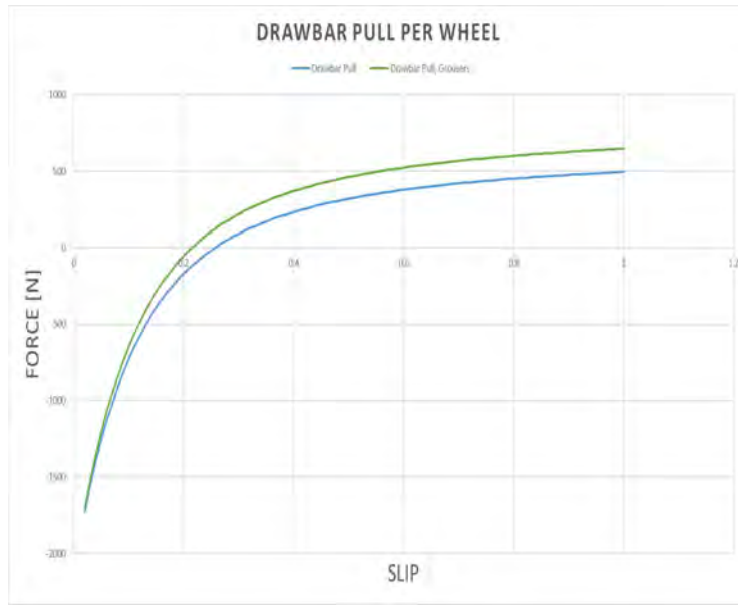


**Figure 5.2.16: Drawbar Pull Per Wheel at Max Load and 5° Slope**

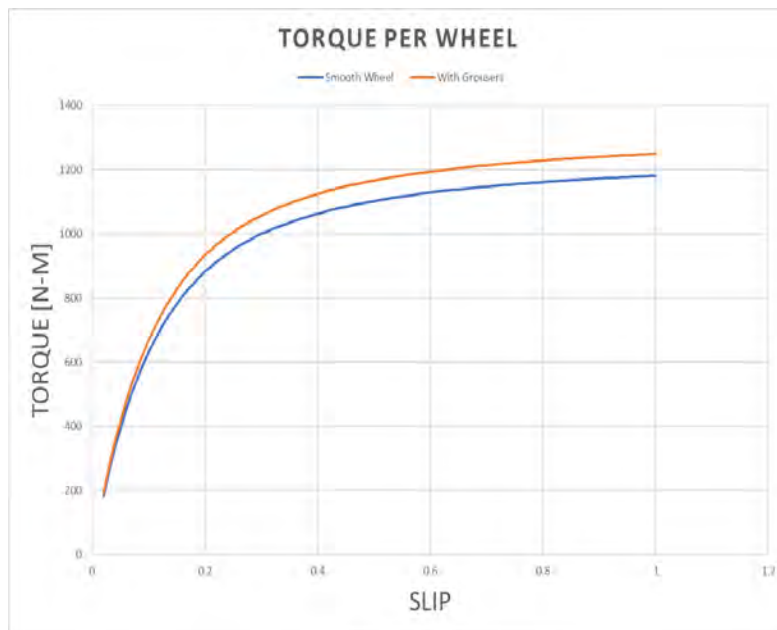


**Figure 5.2.17: Torque Required Per Wheel at Max Load and 5° Slope**

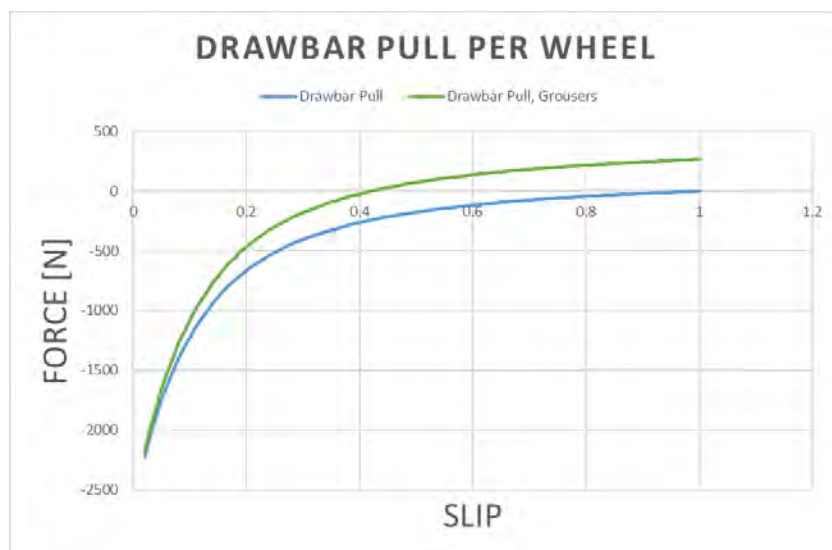


**Figure 5.2.18: Drawbar Pull Per Wheel at Max Load and 11° Slope**

#### *Wheel Actuator Requirements*

To set the actuator requirements that must be met, the plots generated from the terramechanics model of the wheel were used to determine the torques and speeds the actuator would be operating at. Table 5.2.19 lists the wheel actuator requirements that are used during preliminary motor selection and actuator design. A 20% margin was added to the slip percentage for actuator speed requirements, and a peak torque of 1200 N-m was chosen to envelope the max loading torque up to 60% slip. These actuator torques also account for 11° slopes with a max payload.

#### **Wheel Actuator Requirements**

Parameter	Value	Units
Max Continuous Torque	<b>964.8</b>	N-m
RPM @ Max Torque (25% Slip, 0.1 m/s)	<b>2.686</b>	RPM
Max Continuous Power	<b>271.4</b>	W
Peak Torque	<b>1200</b>	N-m
Peak Speed (25% slip, 0.2 m/s)	<b>5.372</b>	RPM

**Table 5.2.19: Wheel Actuator Requirements**

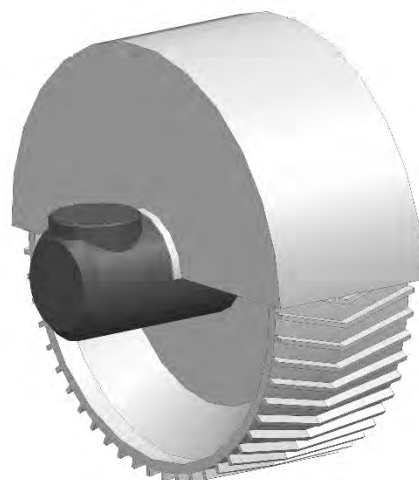


**Figure 5.2.110: Wheel Actuator With Fender on Wheel**

### 5.2.2 - Steering

#### *Active vs Skid Steering Trade*

A trade was conducted early on to determine if skid steering would be sufficient for the vehicle or active steering in some capacity would be required. The power draws for skid steering and active steering configurations were compared for the same 6-wheeled vehicle [LSM-4]. From table 5.2.21, it is apparent that skid steering requires over 50% more power than active steering. Additionally, skid steering would hinder alignment capability as well as solar tracking during transport. Ultimately, 6-wheel active steering was chosen for these capabilities as well as better hazard avoidance and crab-drive, where the wheels can be turned perpendicular to the chassis for lateral movement.

Configuration	Turning Speed	Turning Radius	Turning Velocity	Total Power Required
Turn-In-Place Skid Steer	0.0063 rad/s	-	-	494 W
Turn-In-Place Steered	0.0063 rad/s	-	-	285 W
Skid Steer Around a Turn	-	3 m	0.02 m/s	601 W
Double Ackerman Steer Around a Turn	-	3 m	0.02 m/s	387 W

**Table 5.2.21: Steering Considerations: Skid vs. Active**

#### *Steering Actuator Sizing*

To determine the actuator requirements for the steering actuator, the main resistive force considered was sideways bulldozing force that would be acting on the part of the wheel that has sunk into the regolith. This resistive force would have to be overcome by the torque of the actuator to turn the wheel. Equation 5.2.23 [LSM-5] was used to calculate the bulldozing force and the force was applied conservatively to the part where the wheel enters the regolith.



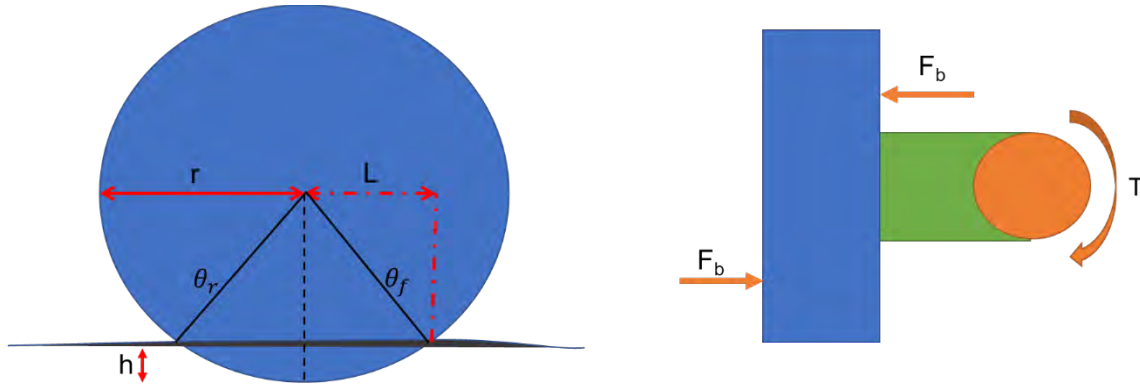


**Figure 5.2.22: FBD of Steering Joint**

$$F_b = [\cot(X_c) + \tan(X_c + \varphi)] \times \int_{\theta_r}^{\theta_f} \left[ h(\theta) + \frac{1}{2} \rho h^2(\theta) \left( \cot(X_c) + \frac{\cot^2(X_c)}{\cot(\varphi)} \right) \right] (r - h(\theta) \cos(\theta)) d\theta \quad (5.2.23)$$

Table 5.2.24 lists the steering actuator requirements used for preliminary motor selection and actuator layout. The nominal actuator speed was determined by finding the angular rate of the wheel at max nominal driving speed about the steering axis. The continuous required actuator torque is 22.61 N-m at an output speed of 6 RPM.

**Steering Actuator Requirements**

Parameter	Description	Value	Units
phi	Ground Swell Angle [LSM-5]	37.2	deg
Xc	Soil Distractive Angle [LSM-5]	26.4	deg
l	Steering actuator axis to wheel center plane	0.32	m
T	Bulldozing Force Torque	<b>22.61</b>	N-m
w	Actuator Speed	<b>5.968</b>	RPM
P	Actuator Power	<b>14.13</b>	W
T_peak	130% Continuous Torque	<b>29.40</b>	N-m

**Table 5.2.24: Steering Actuator Requirements**

### 5.2.3 - Suspension

#### *Suspension Baseline*

When determining the suspension architecture required for this system, mission requirements on payload handling and terrain compliance were considered. The payloads the LLV would have to service would be on uneven terrain, so the vehicle would need the capability of adapting to terrain for payload intake. Additionally, with such a wide range of payload sizes, load leveling will be critical to prevent skewed wheel loads and mitigate uneven wheel wearing. The design would also have to be self-enclosed so that the entire mobility module could be replaced easily.

In the end, the baseline suspension architecture was inspired by the NASA Chariot suspension, which is a low-bandwidth active suspension. This means that an actuator can actively change suspension height while a spring/damper can serve as the passive suspension during traversal. The low-bandwidth means that the actuator is placed in series with the suspension, resulting in 1-10 Hz control capability. This is acceptable for the current LLV design

speeds as they are low. A powered lead screw actuator is used to change the angle of a four-bar linkage that controls wheel height. The lead screw and four-bar linkage are coupled by a spring/damper, which serves as the passive part of the suspension.

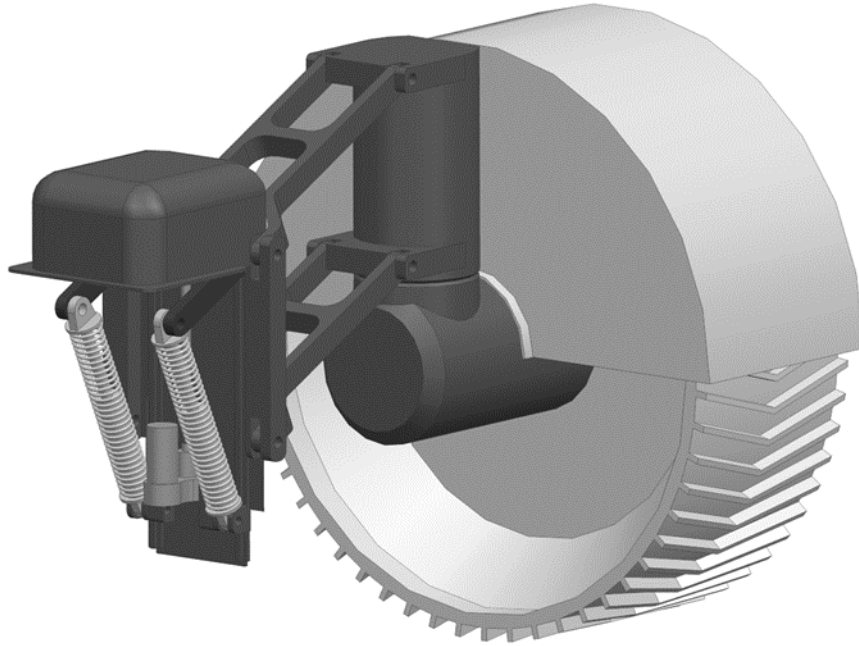


**Figure 5.2.31: Suspension Attached to Wheel Steering Module**

### *Suspension Model*

To understand the forces in the suspension and to size the linkage, an excel model was built of the suspension. The model was simplified for a first pass sizing and would be refined down the road. Figure 5.2.32 shows the critical dimensions used in the suspension model. The spring/damper link (SDL) is treated as a rigid link and the sum of the moments about the top link pivot is used to determine the force required in the SDL for static equilibrium knowing normal force on the wheel. The component of the SDL force in the direction of the lead screw is then the required force that needs to be applied by the lead screw actuator.

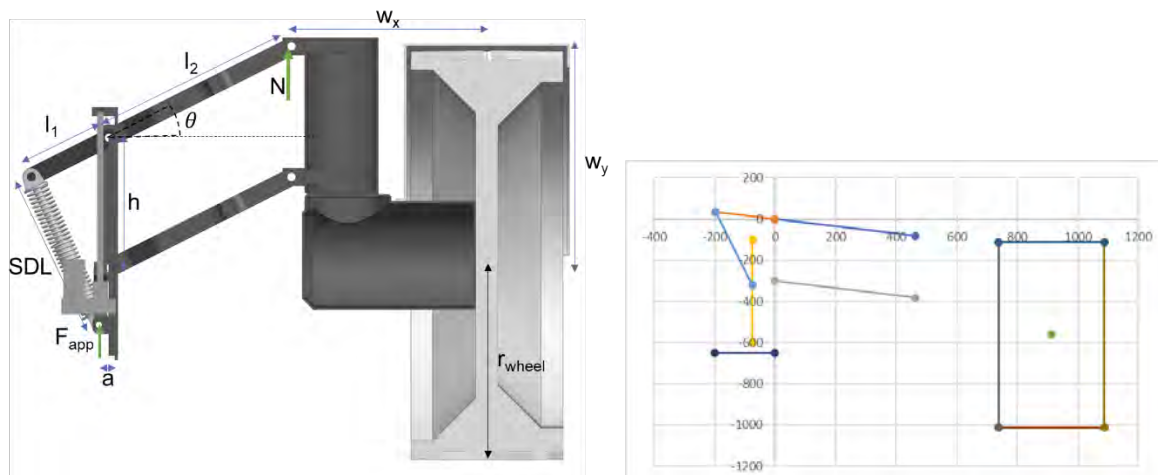


### Figure 5.2.32: Suspension Critical Dimensions and Excel Implementation

#### *Suspension Actuator Sizing*

A nominal ACME screw thread was chosen for first pass sizing of the actuator. Knowing the required linear force and the geometry of the lead screw, the required actuator torque could be calculated for both raising and lowering the suspension linkage. As the suspension angle changes, so does the angle of the force applied from the SDL, so required torque will change through the full motion of the linkage. Figure 5.2.33 shows the change in raising and lowering torque as a function of suspension angle. Most notably, lowering torque is positive, which means the lead screw is self-locking and does not require motor holding torque to keep the suspension linkage in place.

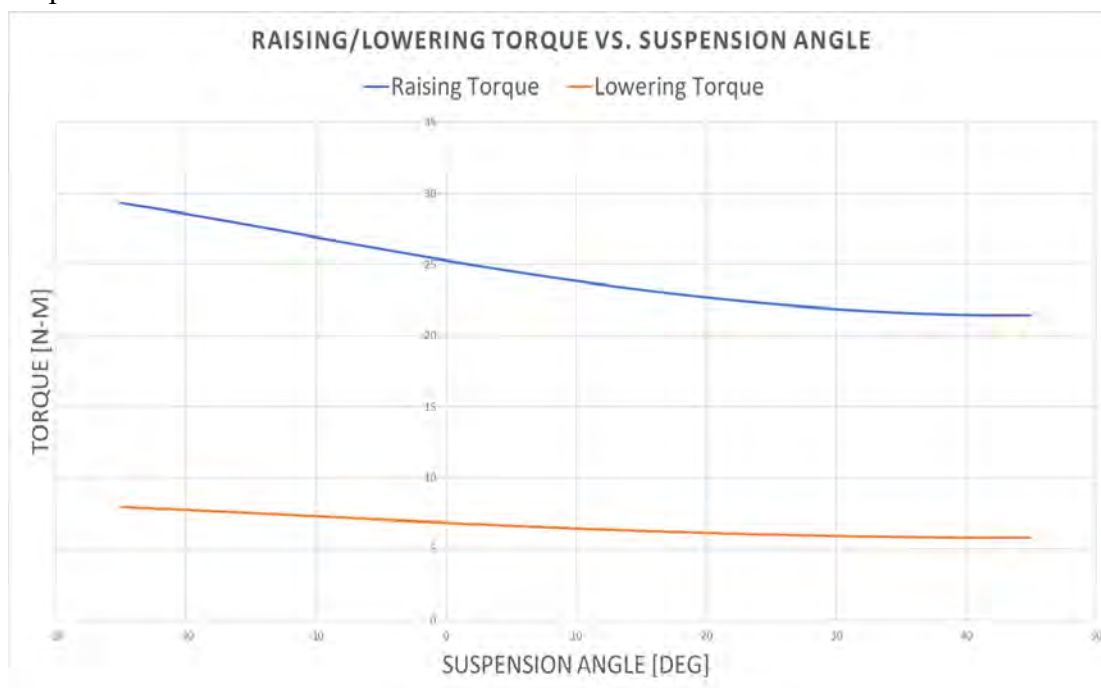


**Figure 5.2.33: Raising and Lowering Torque vs. Suspension Angle**

Table 5.2.34 lists the suspension actuator requirements that are used during preliminary motor selection and actuator design. Continuous required torque was found to be 29.3 N-m to have a 5 mm/s lead screw travel. This number would be refined in the future to account for active control needs for the suspension for constant load leveling in undulating terrain. The von mises stress of the lead screw was also calculated based on power screw geometry, which is below yield strengths of common stainless steels which would most likely be used for the lead screw material.

#### Suspension Actuator Requirements

Parameter	Description	Value	Units
D	Lead Screw Major Diameter [LSM-6 Table 8-1]	20	mm
P	Lead Screw Pitch [LSM-6 Table 8-1]	2.5	mm
n	Number of threads	2	
f	Friction factor (dry steel screw, steel nut) [LSM-6 Table 8-5]	0.15	

Von Mises Stress	Lead screw von mises stress [LSM-6 eqn. 5-14]	256.4	Mpa
e	Lead screw efficiency [LSM-6 eqn. 8-4]	35.68	%
V	Raising speed	5	mm/s
T_Max	Max continuous torque	<b>29.30</b>	N-m
w	Actuator speed	<b>60</b>	RPM
P	Max continuous power	<b>184.1</b>	W
T_peak	130% continuous torque	<b>38.09</b>	N-m

**Table 5.2.34: Suspension Actuator Requirements**

### 5.3 - Actuator Design Philosophy – Anish Sankla

For preliminary motor selection, the Kollmorgen Motioneering design tool was used to streamline the process. The company has flight heritage in space motor design and free to use motor selection tools. Separate analysis was done for each actuator and a preliminary frameless motor was chosen. For the preliminary actuator designs, frameless motors were chosen for mass reduction and thermal considerations. 120V brushless DC motors fit with the current battery sizing. For each specific actuator, there was a selection between harmonic and planetary gearing to reach the outputs needed. Permanent magnet brakes will be used to mitigate the need for continuously powering the motors for braking. Capacitive or magnetic encoders will be used for commutation and position sensing. Table 5.3.1 lists a summary of the actuator selection for each component of the mobility module.

Actuator	Suspension	Steering	Wheel
<b>Motor Type</b>	Brushless DC	Brushless DC	Brushless DC
<b>Motor P/N</b>	KBM-10H01-C	KBM-10H01-C	KBM-25H03-G
<b>Gearbox Type</b>	Harmonic	Harmonic	Planetary
<b>Gearbox Ratio</b>	70:1	70:1	100:1
<b>Gearbox Efficiency [LSM-7,8]</b>	90%	90%	94%
<b>Motor Peak Tq. [N-m]</b>	1.22	1.22	21.71
<b>Max Speed [RPM]</b>	19700	19700	3324
<b>Continuous Torque Margin</b>	3.36%	35.81%	7.62%
<b>Peak Torque Margin</b>	100.9%	161.6%	70.07%

**Table 5.3.1: First Pass Motor Selection**

For the wheel actuator, a two-stage planetary gearbox was chosen as the reduction method, which would give a higher efficiency than a single stage harmonic gearbox. This is especially important for the wheel actuator as it has the highest power requirements so it will generate the most heat due to inefficiencies. Figure 5.3.2 shows the output from the Motioneering tool. With this preliminary selection, it is clear that there are motors that meet the general requirements set by the wheel analysis. Figure 5.3.3 shows a notional layout for the wheel actuator. The output of the frameless motor will be coupled to the planetary gearbox, which will output to the wheel hub. The brake and encoder are placed on the opposite side of the motor.

Sizing: Wheel Actuator  
 System: KBM-25H03-G/ AKD-x02406 (120 V)

PRINTABLE REPORT

SAVE THIS SYSTEM

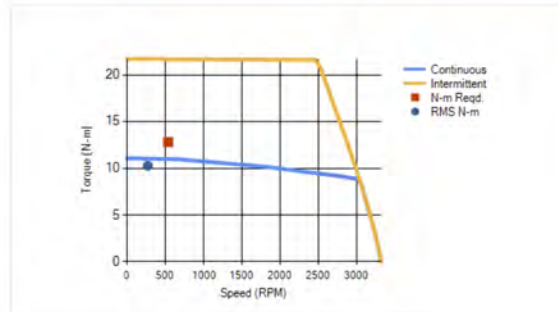
Margins

	Available	Required	% Margin
Cont. Tq. (N-m)	11.05	10.26	7.62
Peak Tq. (N-m)	21.71	12.77	70.07
Max. Speed (RPM)	3324	537.2	518.76
Cont. Power (Watts)	2460	288.7	752.10

RMS Speed (RPM)	268.6		
-----------------	-------	--	--

Inertia

	Load	Motor	Ratio
Inertia (kg-m <sup>2</sup> ):	0.000	7.860E-004	0.00



Show Speed on X-Axis

Inertia (At component)

Total Reflected Inertia	0.000 kg-m <sup>2</sup>		
-------------------------	-------------------------	--	--

Figure 5.3.2: Wheel Actuator Sizing Results [CITE]

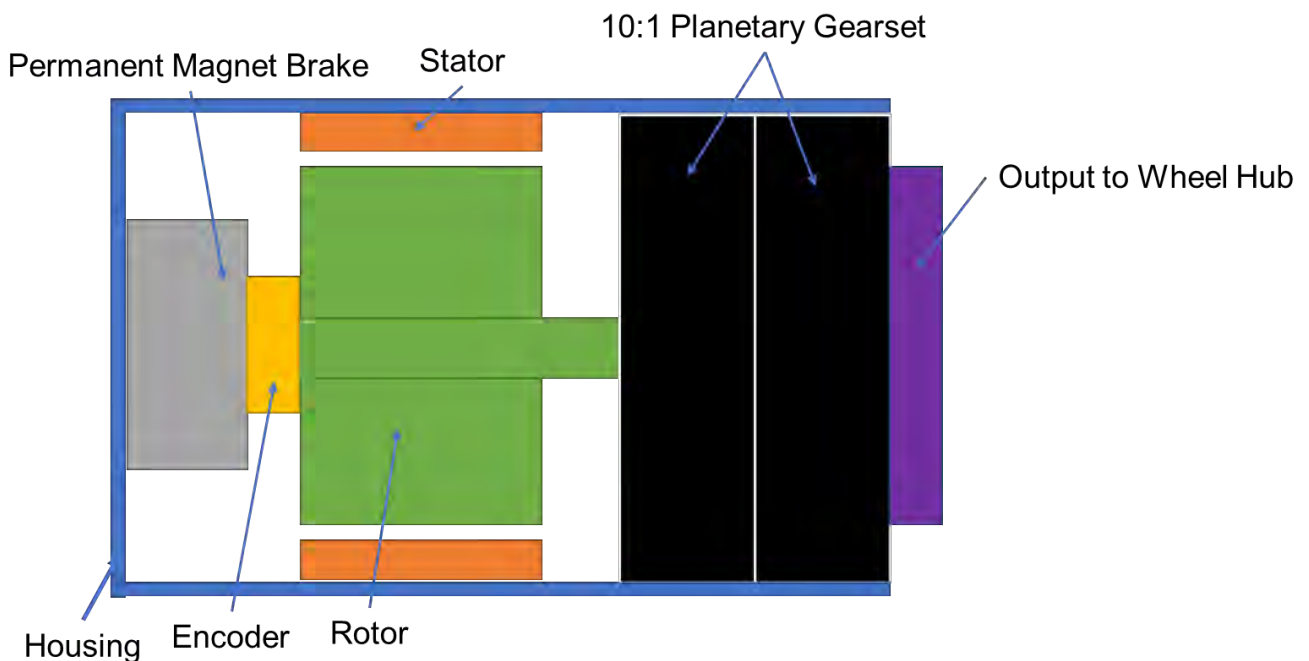


Figure 5.3.3: Notional Wheel Actuator Layout

For the steering actuator, a single stage harmonic gearset was chosen. It is important that the output of this actuator is accurately measured, so a reduction method was chosen that does not have any backlash. After preliminary motor selection, it was found that the same frameless motor could be used for the steering and suspension actuators. This is beneficial as design scope decreases since there is one less motor module to be designed. Figure 5.3.5 shows the notional layout of the steering actuator. A general motor with a brake and encoder will be usable for both actuators. The motor output will mount to a separate gearing which will connect to the harmonic gearset, so the motor axis is off-set from the steering actuator axis. The harmonic output is

coupled to both the actuator output base that mounts to the wheel actuator, as well as an encoder that is fixed to the main housing. This encoder will be used to accurately measure the steering angle.

### Sizing Result Details

[CONTACT US](#)

Sizing: Steering Actuator  
System: KBMS-10H01-C/ AKD-x00606 (120 V)

[PRINTABLE REPORT](#)
[SAVE THIS SYSTEM](#)

#### Margins

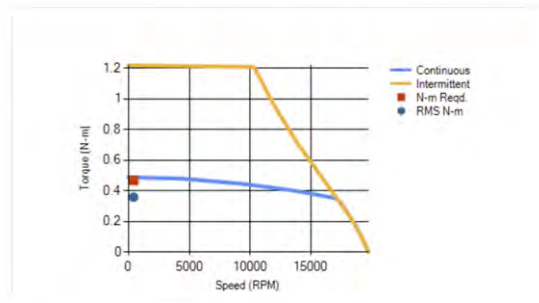
	Available	Required	% Margin
Cont. Tq. (N-m)	0.4874	0.3589	35.81
Peak Tq. (N-m)	1.221	0.4667	161.55
Max. Speed (RPM)	19700	420.0	4590.95
Cont. Power (Watts)	560.0	15.78	3447.73

#### RMS Speed (RPM)

420.0

#### Inertia

	Load	Motor	Ratio
Inertia (kg-m <sup>2</sup> ):	0.000	1.020E-005	0.00


 Show Speed on X-Axis

**Figure 5.3.4: Steering Actuator Sizing Results**

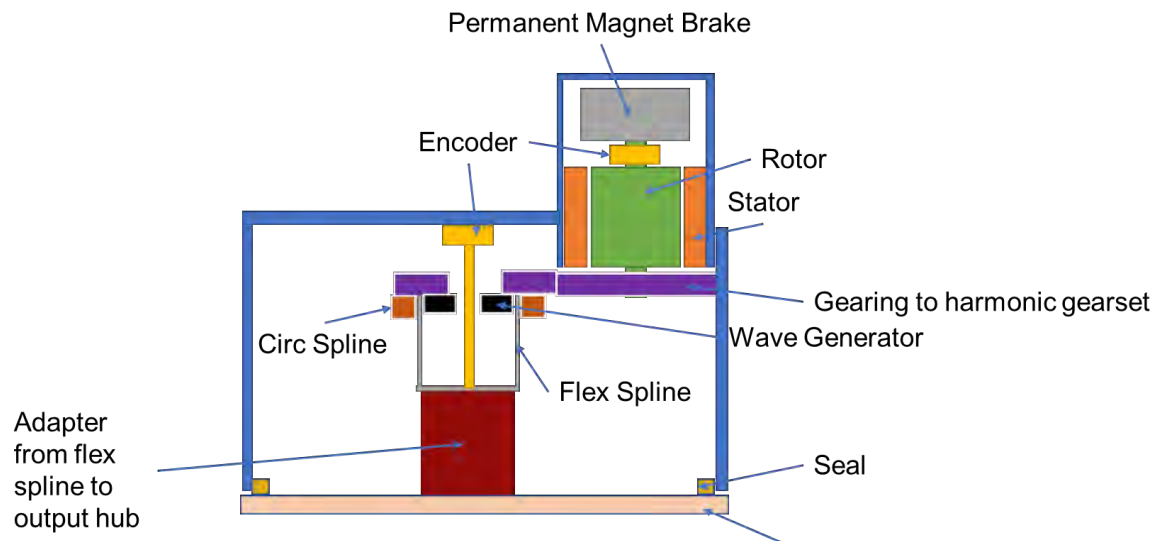


**Figure 5.3.5: Notional Steering Actuator Layout**

The suspension actuator will utilize a harmonic gearset for the same reasons as the steering actuator: reduction of backlash. Figure 5.3.7 shows the notional layout of the suspension actuator. The motor axis is offset from the lead screw axis to reduce actuator length and better mechanism packaging. The harmonic output will couple to a gearing set to couple with the lead screw. There are three encoders needed for this mechanism. The first is coupled to the motor for commutation. The second is measuring output on the leadscrew to measure spring/damper base height. The third measures suspension angle. The combination of suspension angle and spring/damper base height indicates spring compression, and therefore the load on the wheel.

**Sizing Result Details**

[CONTACT US](#)

Sizing: **Suspension Actuator**  
 System: **KBM-10H01-C/ AKD-x00606 (120 V)**

[PRINTABLE REPORT](#)

[SAVE THIS SYSTEM](#)

Margins

	Available	Required	% Margin
Cont. Tq. (N-m)	0.4807	0.4651	3.36
Peak Tq. (N-m)	1.215	0.6046	100.89
Max. Speed (RPM)	19700	4200	369.10
Cont. Power (Watts)	560.0	204.6	173.77
RMS Speed (RPM)			4200

Inertia

	Load	Motor	Ratio
Inertia (kg-m <sup>2</sup> ):	0.000	4.920E-006	0.00

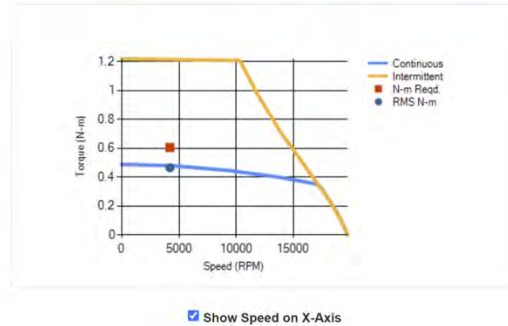


**Figure 5.3.6: Suspension Actuator Sizing Results**

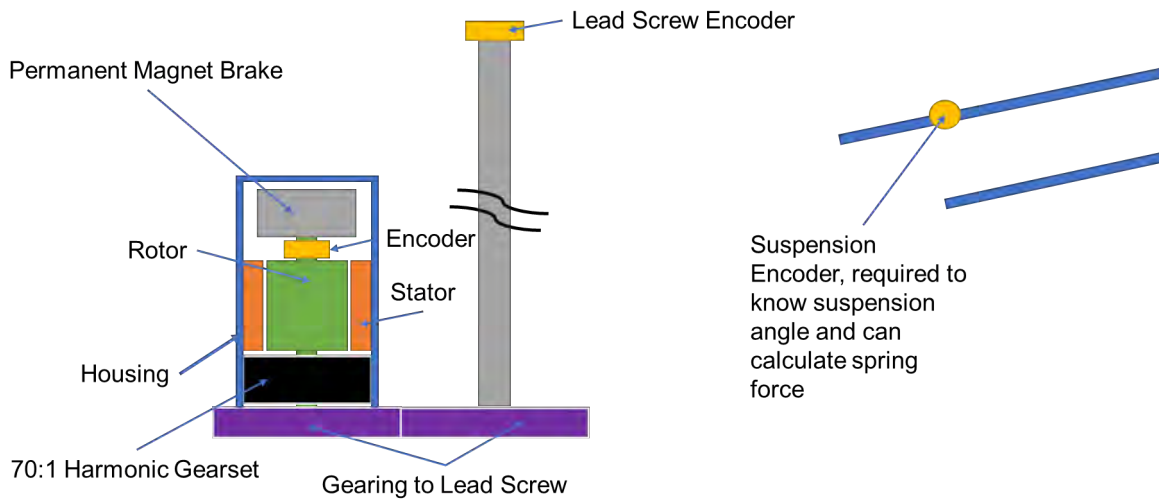


**Figure 5.3.7: Notional Suspension Actuator Layout**

**5.4 - Analysis**

**5.4.1 - Accel/Decel – Anish Sankla**

Considering that the LLV would have to transport a 15 mt vertical habitat at its max load, it was important to make sure that there would be no possibility for tipping the vehicle during the transport phase. To verify that the wheel-base geometry meets stability requirements, a short analysis campaign was conducted for tipping stability during acceleration and deceleration of the vehicle. Figure 5.4.11 shows the necessary dimensions needed to complete the analysis. Essentially, an acceleration or deceleration limit for the vehicle was calculated by finding the acceleration or deceleration value at which the resulting acceleration vector combining acceleration force and gravity would point past the wheel-base. If this acceleration limit was found to be negative or the deceleration limit was found to be positive, this load case would

result in tipping of the vehicle and the design would have to be reevaluated. Table 5.4.12 lists the load cases considered during the analysis.

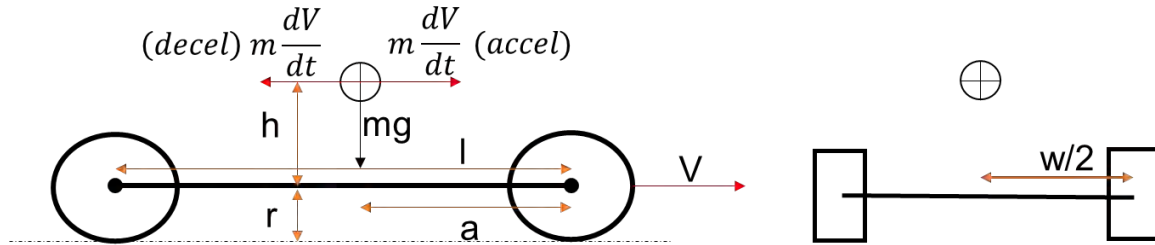


Figure 5.4.11: Accel/Decel Analysis Model Setup

#### Load Cases

Case #	Vehicle Mass	Payload Mass	a	h	V (m/s)	Slope (deg)
1	2000	15000	1.94	3.41	0.1	5
2	2000	15000	1.94	3.41	0.1	0
3	2000	15000	1.94	3.41	0.1	-5
4	2000	3300	2.31	2.28	0.2	5
5	2000	0	2.95	0.3	0.2	5
6	2000	15000	1.94	3.41	0.1	11/-11

Table 5.4.12: Load Cases Considered in Analysis

The acceleration limits for each load case are calculated from equation 5.4.13 [LSM-4] and tabulated in Table 5.4.14. The critical case is having a max payload on an 11° slope, which is expected. This acceleration is feasible which means that the vehicle will be capable of carrying a vertical habitat on an 11° slope without tipping should the proper acceleration limits be held.

$$\frac{dV}{dt} = g \left[ \left( \frac{l-a}{h+r} \right) \cos(\theta) - \sin(\theta) \right] \quad (5.4.13)$$

#### Acceleration Limits

Case	Slope (deg)	Acceleration Limit (m/s <sup>2</sup> )
1	5	0.929
2	0	1.074
3	-5	1.212
4	5	1.153
5	5	3.194
6	11	<b>0.746</b>

Table 5.4.14: Acceleration Limits

The deceleration limits for each load case are calculated from equation 5.4.15 [LSM-4] and tabulated in Table 5.4.16. The critical case is having a max payload on an -11° slope, which is expected. This deceleration is feasible which means that the vehicle will be capable of carrying a vertical habitat on an -11° slope without tipping should the proper deceleration limits be held.

$$\frac{dV}{dt} = -g \left[ \left( \frac{l-a}{h+r} \right) \cos(\theta) + \sin(\theta) \right] \quad (5.4.15)$$



**Deceleration Limits**

Case	Slope (deg)	Deceleration Limit (m/s <sup>2</sup> )
1	5	-0.9523
2	0	-0.8142
3	-5	-0.6699
4	5	-1.5067
5	5	-6.4889
6	-11	<b>-0.4901</b>

**Figure 5.4.16: Deceleration Limits**

Apart from acceleration and deceleration, pitch-over criteria was also considered for an impulsive stop due to an obstacle. The center of gravity of the vehicle is treated as a point mass and the criteria to meet is to keep kinetic energy of the vehicle less than the potential energy of the vehicle. This is to ensure that should all the potential energy be impulsively converted to kinetic energy, the vehicle will not tip. This is a conservative estimate and is mainly used to see if the nominal driving speeds of the vehicle are at risk of tipping. From equation 5.4.17 [LSM-4], impulsive tipping was found to not be an issue for the vehicle as the critical velocity limit, which is at max payload, is 1.29 m/s, well above the nominal operating speeds of the vehicle.

$$V_{limit} = \sqrt{2g(\sqrt{x^2 + h^2} - h)} \quad (5.4.17)$$

**Impulsive Pitch Over Criteria**

Case	V limit (m/s)
1,2,3,6	<b>1.290</b>
4	1.769
5	2.939

**Table 5.4.18 Impulsive Pitch-Over Criteria Analysis**

Additionally, turning stability was also looked at but was found to be a non-issue since for the nominal drive speeds, the minimum turning radius was less than the width of the vehicle. In this analysis, the centripetal acceleration of the vehicle combined with gravity could not point farther than the wheelbase.

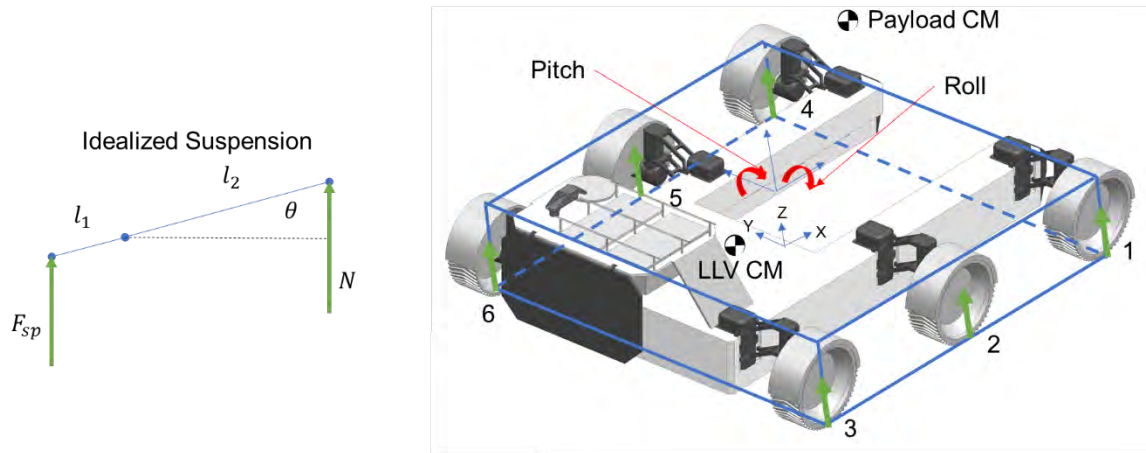
$$r_{min} = \frac{v^2}{g} \left[ \frac{y}{h} \cos(\theta) - \sin(\theta) \right]^{-1} \quad (5.4.19)$$

**Turning Stability**

Case	Slope (deg)	Min Turning Radius (m)
1	5	0.0121
2	0	0.0103
3	-5	0.0090
4	5	0.0305
5	5	0.0037
6	11	0.0155

**Table 5.4.110 Minimum Turning Radii Required****5.4.2 - Structural Load Cases – Anish Sankla**

For a better understanding of wheel loads based on vehicle pose and payload weight, a model was built in excel that would output wheel loads that can be used for structural analysis, suspension sizing, and requirement verification. An idealized vehicle geometry is used in the analysis, where the critical values are the locations of the wheels with respect to the origin, set to the geometric center of the vehicle at the bottom of the chassis, the center of mass of the vehicle, as well as the center of mass of the payload. The suspension is simplified so that the spring force counteracting the wheel is always parallel to the wheel normal force. Suspension angle is also an input that will change the wheel positions automatically. The wheel positions in the vehicle frame are converted into the base frame using a transformation matrix and obstacles can be added to each wheel; either a rock adding height or a crater lowering wheel height [LSM-9]. The excel spreadsheet utilizes the GRG Nonlinear solver to find the pose of the vehicle as well as the wheel forces by solving constraint equations 5.4.22-5.4.26. The constraint equations are force equilibrium in Z as well as moment equilibrium in both pitch and roll.

**Figure 5.4.21: Wheel Force Modeling Setup**

$$\Delta x_{sp} = \frac{l_1}{l_2} (\Delta z_w + z_{obst}) \quad (5.4.22)$$

$$k \Delta x_{sp} \frac{l_1}{l_2} = F_{sp} \frac{l_1}{l_2} = N \quad (5.4.23)$$

$$\sum F_{sp(i)} \frac{l_1}{l_2} = W_v \quad (5.4.24)$$

$$\sum F_{sp(i)} \frac{l_1}{l_2} x_{(i)} - W_v x_{cg} = 0 \quad (5.4.25)$$

$$\sum F_{sp(i)} \frac{l_1}{l_2} y_{(i)} - W_v y_{cg} = 0 \quad (5.4.26)$$

Wheel #	Wheel Base Vector [Xw]v						Global Translation Vector						
	1	2	3	4	5	6	0.999859621	0	0.01675523	0			
	2.15	0	-2.15	2.15	0	-2.15	0.000375701	0.999749	-0.0224197	0			
	-2.05	-2.05	-2.05	2.05	2.05	2.05	-0.016751017	0.022423	0.99960823	0.123817			
	-0.3616146	-0.36161	-0.36161	-0.36161	-0.36161	-0.36161	0	0	0	1			
	1	1	1	1	1	1							
							[X_w]0				[X_cg]0		
Rover Cg	-1						2.143639249	-0.00606	-2.1557571	2.143639	-0.00606	-2.15576	0.315116
Payload Cg	0	0.5					-2.040569514	-2.04138	-2.042185	2.0584	2.057592	2.056784	-0.03929
System Cg [Xcg]v	0	0					-0.319637512	-0.28362	-0.2476081	-0.2277	-0.19169	-0.15567	1.875486
Vehicle Origin	0						1	1	1	1	1	1	1
	0.3	2											
	1	1											
Optimization parameters													
Parameter	Value	Min	Max	Notes									
theta	-1.28484	-10	10	Roll									
phi	-0.96005	-10	10	Pitch									
zc	0.123817	0	2										
Misc Inputs													
Parameter	Value	Units	Notes										
Rover Mass	2500	kg											
Payload Mass	15000	kg											
Suspension Ar	-10												
Spring Consta	150000	N/m											
Spring length	1	m											
Weight	28350	N											
l1	0.2	m											
l2	0.47	m											
Wheel #	Obstacle h	idxspr	Fspr	N	x_w(i)	y_w(i)							
1	0.3	0.14552218	21828.33	9288.65	2.143639	-2.04057							
2	0	0.03318801	4978.201	2118.383	-0.00606	-2.04138							
3	0	0.04851341	7277.011	3096.6	-2.15576	-2.04219							
4	0	0.0569834	8547.51	3637.238	2.143639	2.0584							
5	0	0.0723088	10846.32	4615.455	-0.00606	2.057592							
6	0	0.0876342	13145.13	5593.672	-2.15576	2.056784							
Constraint Eqs													
Sum Left	Expected	Residual											
1	28350	28350	7.4888E-08										
2	-5.69471E-08	0	5.6947E-08										
3	3.00372E-08	0	3.0037E-08										
			1.6187E-07										

Figure 5.4.27: Wheel Force Modeling Excel Sheet Layout

Multiple load cases were checked with the tool and are tabulated in table 5.4.28. Overall, pitch and roll of the vehicle were within +/- 2.5°, which can be leveled with the active suspension. The red highlights wheel loads above Terzaghi bearing capacity, which occurs when obstacles are present. Path planning will assist in avoiding obstacles, but this preliminary analysis shows that the vehicle should be capable of traversal with obstacles. This is an idealized model and would benefit from additional integration of the suspension model and proper sizing of the spring/damper as the spring constant was arbitrarily set to 150 kN/m for the first pass.

Load Case	1	2	3	4	5	6	7	8
<b>Vehicle Mass [kg]</b>	2850	2850	2850	2850	2850	2850	2850	2850
<b>Payload Mass [kg]</b>	0	3300	15000	15000	15000	15000	15000	15000
<b>Suspension Angle [deg]</b>	-10	-10	-10	-10	-10	-10	-10	-10
<b>Obstacle Height</b>	-	-	-	0.3	0.3	0.3	-0.3	-0.3
<b>Wheel #</b>	-	-	-	1	2	3	1	3
<b>Roll [deg]</b>	0	0	0	-1.21	-1.21	-1.21	1.21	1.21
<b>Pitch [deg]</b>	-0.366	-0.061	0.836	-0.806	0.836	2.479	2.479	-0.806
<b>F_w1 [N]</b>	396.0	1599	5671	9617	3142	4815	1726	6527
<b>F_w2 [N]</b>	769.5	1660	4819	2290	10438.4	2290	7349	7349
<b>F_w3 [N]</b>	1143	1722	3968	3112	1438	7913	4824	22.27
<b>F_w4 [N]</b>	396.0	1599	5671	3811	5485	7158	7531	4184
<b>F_w5 [N]</b>	769.5	1660	4819	4633	4633	4633	5006	5006
<b>F_w6 [N]</b>	1143	1722	3968	5455	3781	2108	2481	5828

Table 5.4.28 Wheel Modeling Load Cases and Outputs

### 5.4.3 - Hand Beam Calcs – Anish Sankla

To verify that the chassis structure can withstand the loads during operation, a simplified beam model was used for preliminary analysis of the U-shape arm of the chassis. The arm is modeled as a cantilevered beam with 12150 N applied at the locations of the wheels which was chosen as triple the vehicle weight with a max payload. This is a highly conservative analysis but should be an indicator if the design will not work. A rectangular cross section with a 5mm thickness is used for the beam, however, the actual chassis cross-section will be irregular, increasing moment of inertia while also leading to coupled deflection in Y and Z. A MATLAB script was written to generate a shear moment diagram for the model, as well as the maximum stress at the root of the beam and the maximum deflection at the end of the beam. Figure 5.4.32 shows the output of the script. Maximum deflection was found to be 8.5mm while maximum stress was 28.8 MPa. This is well within the yield strength for any material that would be used for the chassis, such as Al 7075-T73.

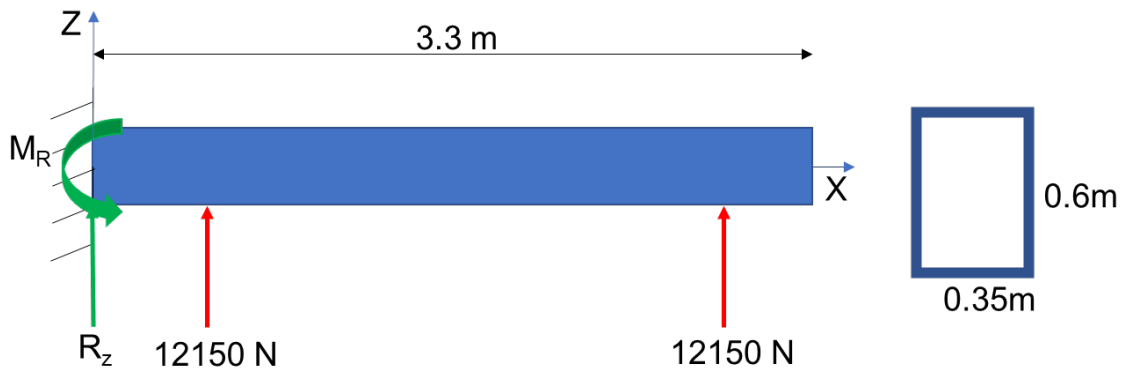


**Figure 5.4.31: Beam Model Setup**

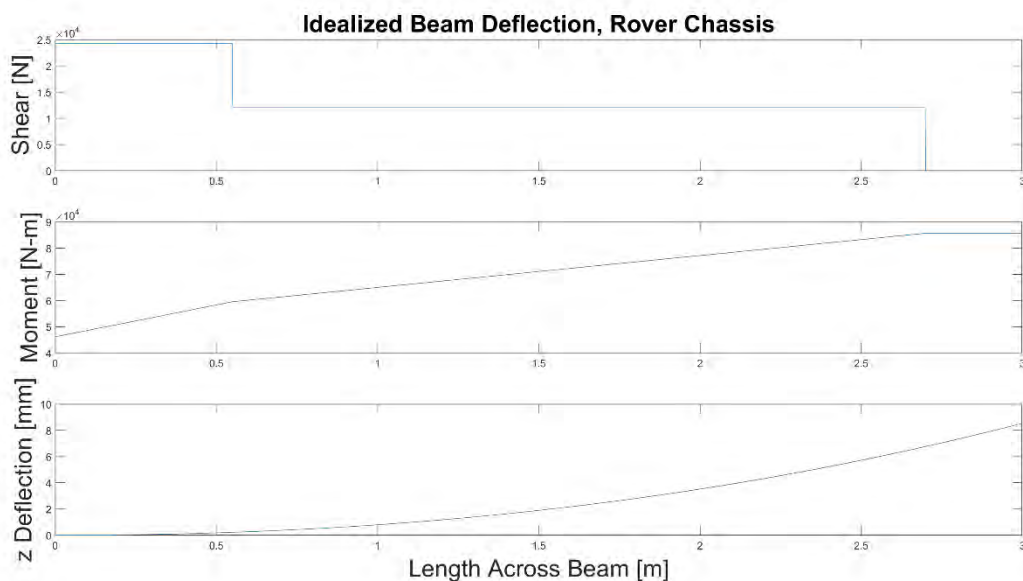


**Figure 5.4.32: Preliminary Beam Model Calculations**

#### 5.4.4 - FEA – Matthew Thomas

To build confidence in the capabilities of the LLV chassis, FEA was also completed to verify the hand calculations for stress within the vehicle. For the FEA set-up, the chassis was fixed at each of the six-wheel housings to model the reaction forces of the auto-leveling wheels. The case tested in FEA assumed flat terrain with a direct downward force from the payload. To model the weight of the payload the force was distributed across four of the latching points with direct downward loading. By loading directly at the latches, this FEA does not account for the torsion created by the payload, so it was decided to set the payload mass at three times the expected mass of 15,000 kg. By oversizing the payload mass, confidence is increased that the LLV chassis will be capable of supporting the normal and torsional load during the mission. After increasing the load, it is 18,225 N per latching point.

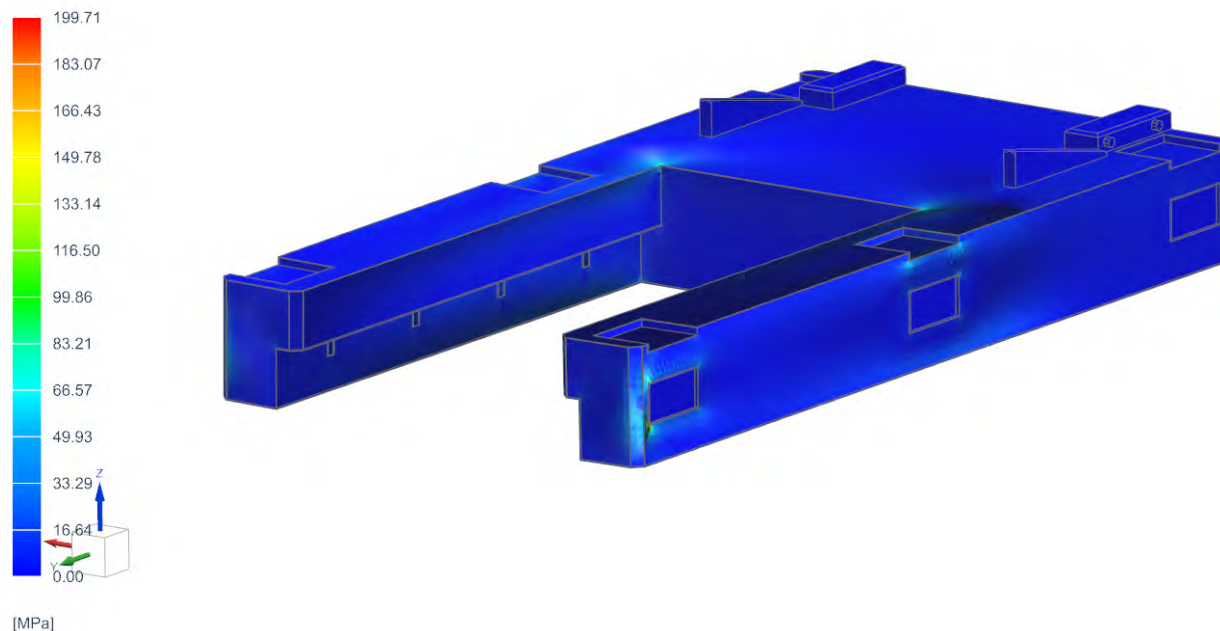


Figure 5.4.41: LLV chassis FEA with downward load of 18,225 N per latch

As seen in the figure, the peak stress at the concentration points reaches 200 MPa, but these are located at the loading points. Given that the loading points are not perfectly represented in this FEA, it can be assumed that the actual peak stress will be lower than 200 MPa. Regardless, this value remains well within the yield strength of the selected chassis material. In addition, the arms of the U-shape chassis remain primarily within the range of 25-30 MPa which aligns well with the hand calculations and is safe from yielding. Considering the load in this FEA is three times the expected value, this FEA builds significant confidence in the LLV's capability to support the payload mass.

#### 5.4.5 - Hertzian Contact Stress – Yida Shen

To understand the contact stress between the wheel of Lunar Logistics Vehicle (LLV) and lunar rocks is integral to the success of any mission on the lunar surface. The contact stress influences the durability, traction, and energy efficiency of the rover [LSM-24]. Hertzian contact stress analysis provides insights into these parameters and informs the design process. The

Hertzian contact stress theory offers a means of analyzing the stress distribution within two bodies in contact, typically at a cylinder or along sphere [LSM- 25].

The input parameters (table 5.4.51) for Hertzian contact stress analysis are derived from the mechanical properties of the materials in contact and the geometric characteristics of the wheel. For this case, Aluminum 6061 wheel was taken into consideration, which in contact with lunar surface which is composed of basaltic rock. The elastic modulus (E) and Poisson's ratio ( $\nu$ ) for the basaltic rock, as the contact material, are approximately 70 GPa and 0.24 respectively [LSM - 24]. These two numbers are not constant, both two changes according to the temperature and air pressure. The diameter size of Lunar Rocks is 0.3m, and it is the baseline for obstacle height.

Parameter	Wheels (Aluminum 6061)	Lunar Rocks (Basalt)	Unit
Object shape	Cylinder	Cylinder	
Poisson's ratio [ $\nu_1, \nu_2$ ]	0.33	0.24	
Elastic modulus [ $E_1, E_2$ ]	69	70	GPa
Diameter of object [ $d_1, d_2$ ]	0.9	0.3	m
Force [N]	4590		N
Line contact length [l]	2.697		M

**Table 5.4.51 Wheel analysis Input**

Upon The Hertzian contact stress analysis between the Aluminum 6061 wheel and the basaltic lunar surface reveals key parameters (Table5.4.52) that provide insights into the interaction between the two bodies under the specified load conditions (Eq5.4.51-Eq5.4.55). The maximum Hertzian contact pressure is found to be approximately 13.5 MPa. This parameter is crucial as it represents the most severe stress the wheel material is subjected to at the contact point. An elevated contact pressure can lead to an increase in wear and tear, thereby affecting the lifespan and the performance of the wheel. The width of the rectangular contact area is determined to be around 0.16 m. Which is essential since it dictates the area over which the wheel load is distributed. A larger contact area may lead to a reduction in contact pressure, potentially decreasing the rate of wheel wear and enhancing traction performance.

Parameter	Wheels	Basalt (Lunar Rocks)	Unit
Maximum Hertzian contact pressure $P_{\max}$	13.5	13.5	MPa
Max shear stress $T_{\max}$	4.1	4	MPa
Depth of max shear stress z	0.063	0.021	mm
Rectangular Contact area width 2b	0.16	0.16	mm

*Table5.4e.2 Hertzian Contact Stress*

$$\rho_{\max} = \frac{2F}{\pi bl} \quad \text{Eq.(5.4.51)}$$

$$\tau_{xz} = \frac{\sigma_x - \sigma_z}{2} \quad \text{Eq. (5.4.52)}$$

$$\sigma_x = -2\vartheta\rho \max \left[ \sqrt{\left(1 + \frac{z^2}{b^2}\right)} - \left|\frac{z}{b}\right| \right] \quad \text{Eq. (5.4.53)}$$

$$\sigma_z = \frac{-\rho_{max}}{\sqrt{\left(1 + \frac{z^2}{b^2}\right)}} \quad \text{Eq. (5.4.54)}$$

$$b = \sqrt{\frac{2F}{\pi l} \frac{\frac{(1-\vartheta_1^2)}{E_1} + \frac{(1-\vartheta_2^2)}{E_2}}{\frac{1}{d_1} + \frac{1}{d_2}}} \quad \text{Eq. (5.4.55)}$$

The resultant image (Figure 5.4.51) of the Hertzian contact stress analysis is a plot of stress versus depth from the contact surface, often called a stress- depth profile. This plot effectively represents the distribution of stress within the wheel material as LLV moves deeper from the point of contact with the lunar surface. The stress-depth profile is characterized by a peak if not located at the surface but rather at some depth within the material, which in the case is approximately 0.052m. This is a critical parameter, as occurrence of the maximum shear stress beneath the surface means that failures due to excessive shear stress (like yielding or fatigue crack initiation) could also begin inside the material, not just surface.

Moving further from the point of contact, the stress gradually tapers off, decreasing with the increase in depth. It implies that the influence of contact stress reduced with depth, and the wheel's interior experiences significantly less stress than the region near the contact surface. The image provides a direct, visual understanding of how stress is distributed within wheel material due to contact with the lunar surface.

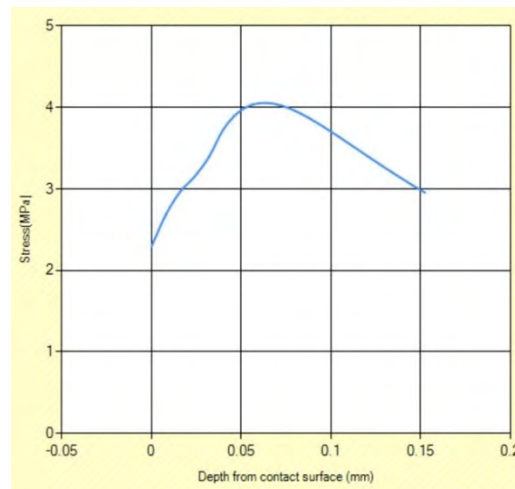


Figure 5.4.51[LSM-18] Stresses vs Depth from contact surface (wheel)

#### 5.4.6 - Wheel FEA – Yida Shen

Finite Element Analysis (FEA) plays a pivotal role in the design and optimization of lunar rover wheels. The lunar environment is highly challenging, marked by extreme temperatures, lack of atmosphere, and a unique regolith surface. Thus, understanding the wheel's response to these conditions is essential [LSM-26]. FEA enables design optimization aiding engineers in balancing between minimizing weight and maximizing strength and durability, crucial factors for lunar missions. [LSM- 27]. FEA also assists in predicting possible failure points, enabling their mitigation in the design phase, a far more cost- effective strategy than addressing these issues post-launch. Performance predictions made possible through FEA provide insights into wheels' behavior on various lunar terrains, from rocks to steep slopes, which can be crucial for mission planning.

The sections of the grid that contribute significantly to computational accuracy should be refined, while those that do not significantly contribute to computational accuracy can be coarsened appropriately. The mesh size of the hub is controlled to be 10mm, culminating in the final finite element mesh division diagram. After the division, the model grid consists of 194,036 nodes and 107,988 elements. Using the boundary conditions module in the Analysis Settings, a Fixed Support is applied to the herringbone tooth surface on the bottom of the hub. A vertical downward surface load of 4820N is applied on the surface of the cylinder protruding from the hub shaft, as shown in Figure 5.4f.1.

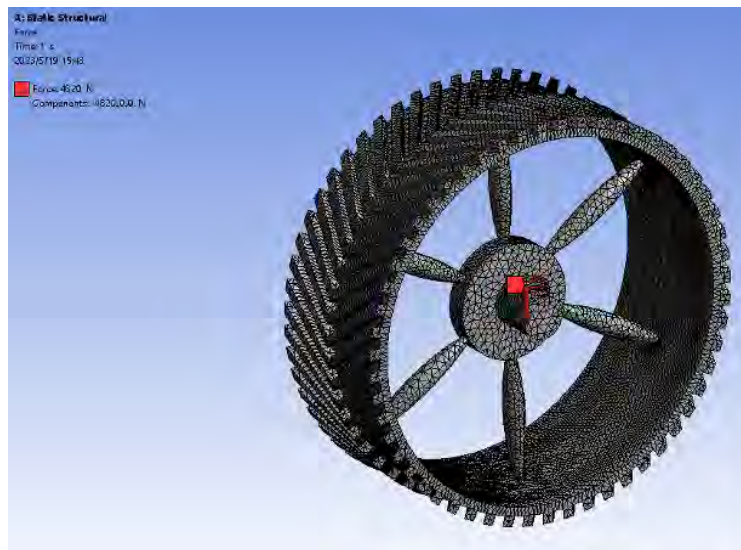


Figure 5.4.61 Determination of Hub Boundary Conditions

In the Solution module, Total Deformation, Equivalent Elastic Strain, and Equivalent Stress are set for extracting the overall deformation, equivalent strain, and equivalent stress of the hub, respectively. The analysis results are shown in Figures 5.4.62, 5.4.63, and 5.4.64. The finite element results reveal that the maximum deformation occurs at the upper spoke, with a deformation of 0.15mm. The maximum stress of the hub is located at the junction of the spoke and the inner wheel, where the maximum stress  $\sigma$  equals 98.89 MPa, a stress value less than the permissible stress of structural steel at 250 MPa. The finite element analysis of the hub, as mentioned above, demonstrates that this hub can meet the requirements for static strength.



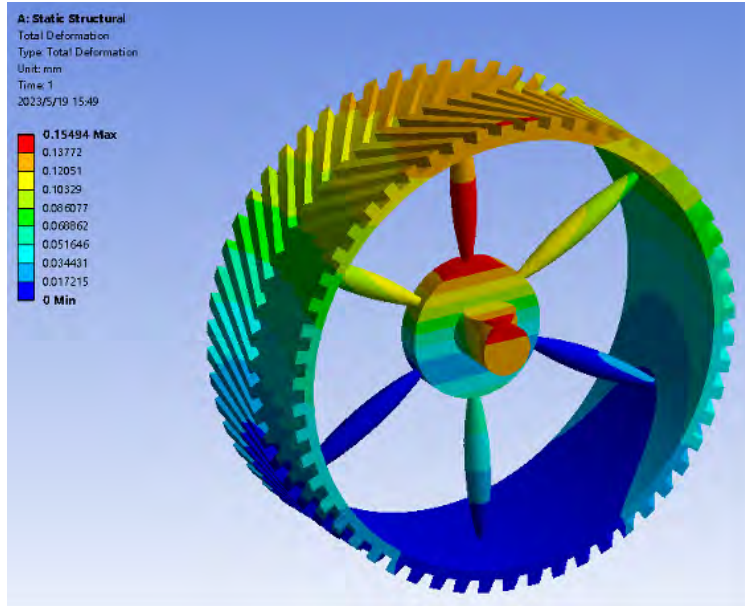


Figure 5.4.62 Overall Deformation of the Wheel

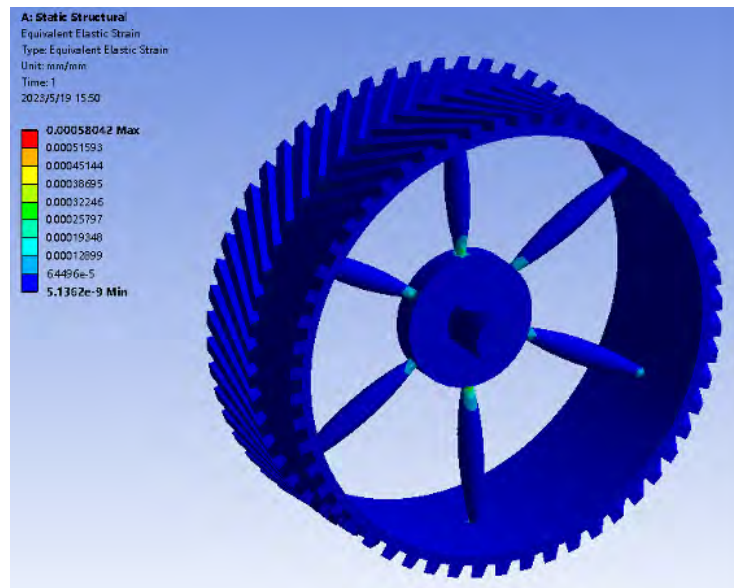


Figure 5.4.63 Equivalent Strain of the Hub

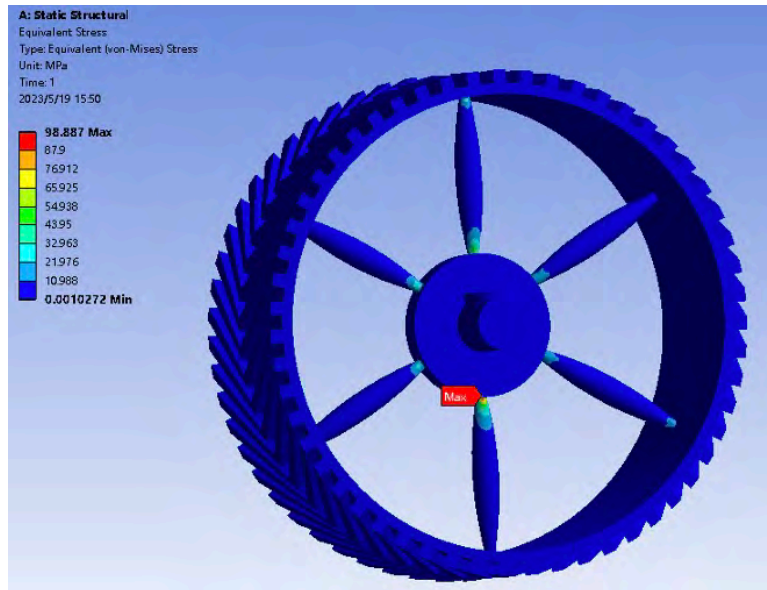


Figure 5.4.64 Equivalent Stress of the Hub

### 5.5 - Standard Payload Interface (SPI) – Matthew Thomas

To transport payloads across the lunar surface, the development of an interface to constrain the payload to the LLV will be crucial. For this purpose, the Standard Payload Interface (SPI) has been developed for LLV to allow payloads to be rigidly constrained during transit. The SPI utilizes two major systems to constrain the payload: the cup-cone interface and an over-center latching mechanism. The full SPI can be seen in fig. 5.5.1.

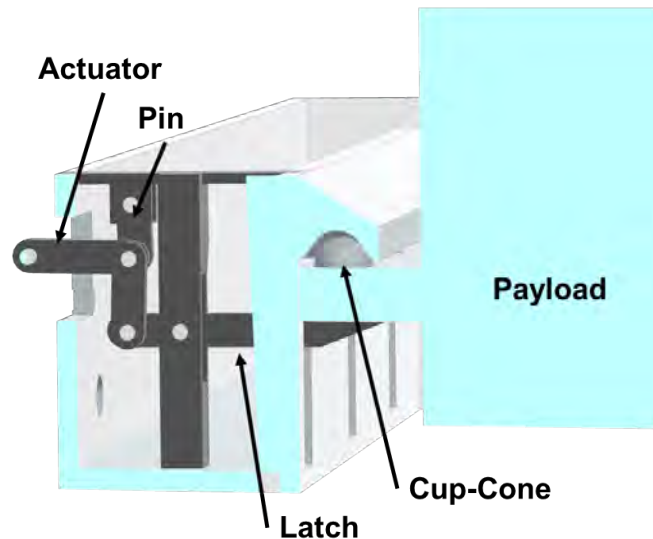


Figure 5.5.1: Standard Payload Interface diagram

The cup-cone interface utilizes cups on the LLV chassis and cones on the payload to constrain the payload as seen above. Utilizing four of these interfaces on each side of the U-shape chassis, the payload is constrained in 5 DOF, only free to translate in the z-axis. To

prevent the system from becoming over-constrained, one side of the chassis (not shown above) will use slots rather than cups to receive the payload cones.

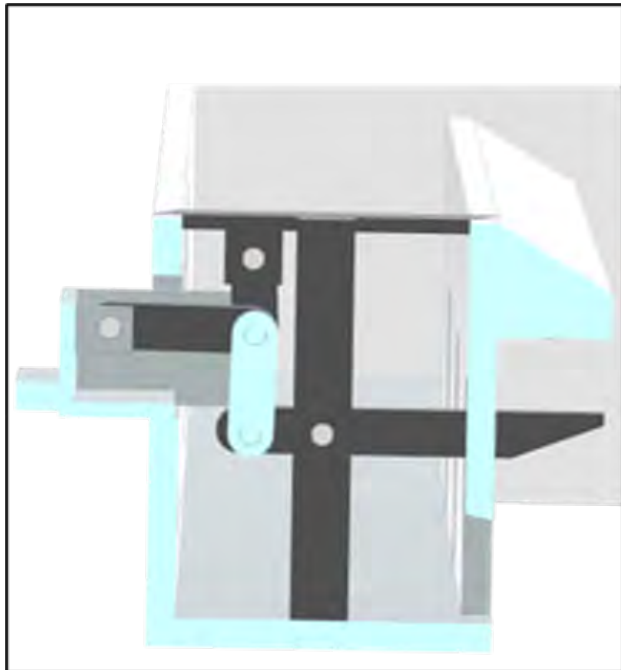
To fully constrain the payload and prevent it from sliding out of the cup-cone interface, an over-center latching mechanism was used. The over-center latch will come from beneath cup-cone interface and provide an upward force to prevent z-axis translation. The advantage of the over-center latching mechanism is that the system does not require the actuators to be under constant torque while carrying a payload. Once the over-center mechanism passes the center position, the downward force of the payload will drive the pin into a support rather than unlocking the system. To unlock the latch, the actuator must be activated, or a significant anomaly must occur.

During the development of the SPI, a static force model was created to determine the required actuator force to lock and unlock the latching mechanism. The model used static force concepts to determine the load in each linkage as the pin moved through its operational envelope. For this use case, the model assumed a payload mass of 15,000 kg distributed across 8 latches. The model also assumed that latch met the payload 5 degrees before center and reached the support 1 degree past center. From these assumptions, the model estimates a max locking force of 531 N and a max unlocking force of 112 N. These outputs can be used for motor sizing and selection during the implementation of this concept.

## 5.6 - RASC-AL Hardware Development -Jack Molter

As of the writing of this final report the RASC-AL hardware development is still in full swing and will add more value and benefit than the current state. This section of the paper will focus on what has been done and only touch on the planned work.

To begin RASC-AL hardware the team and I did a lot of brainstorming, the focus was to highlight the most novel system(s) in our design that would allow the team to showcase what makes our design different from other entries. Some of the initial ideas were 3D printing a full scaled rover for showcase, building a scaled rover chassis and interface system out of aluminum 8020 for moon yard testing, or building a scaled pallet. A big aspect we would like to test is During our PDR presentation the pallet idea received a lot of negative feedback, causing the team to come to a consensus to end the pursuit of this idea to work on coming up with a lighter alternative that also could have some uses after its initial purpose of interfacing. For this reason, the idea of building a pallet was eliminated. Additionally, shortly after PDR the payload interface was



changed to include actuated latches and a cup cone interface, a significant deviation from the proposed trunnion concept at PDR.

Figure 5.6.1: Latching mechanism CAD

With the new interface mechanism being researched and developed I chose to focus on this for aspect of our rover for hardware development and testing. With time being limited and the mechanism unverified, I decided to only print one of the latches for proof of concept. Unfortunately, with only one of these latches the 3D model was not able to actually pick anything up, limiting its value to the overall presentation. Our current rover design uses 8 of these mechanisms, and its active suspension to secure payloads and transport them. This design is different than the current designs of proposed logistics transporters like the NASA Athlete's payload interfacing mechanism. The rovers cup cone interface could also be shown off in this design, increasing its value and making this the most popular choice amongst myself and the team as the direction to go for hardware.

To begin a scale of 1:10 was chosen based off the printer envelopes available and the minimum linkage size required. Using a static force model made by Matt of the over center latching mechanism I scaled this design to fit in an 8" x 9" slice of one rover flange. The linkages were directly scaled from the model to accurately represent the mechanism. A central post was added to the interior of the flange to act as the stop for the over center latch. The link that would bear the weight of the payload was lengthened to emphasize the mechanism, at the expense of it not being fully retractable back into the flange as in the actual design. The CAD model can be seen in Figure 5.6.1. The final design was split into several pieces to allow for the 3D printer to print without using excessive amounts of support material. Additional tolerances that were not present in the image were also added.

Due to time constraints to meet CDR the mechanism was not electrically actuated, and an actuation method had to be chosen that could be applied quickly. For this I used a sliding mechanism that would be attached to the exterior of the flange. The design was split into multiple parts for better print quality and put together. The final design can be seen in Figure 5.6.2.

Figure 5.6.2: Latching mechanism 3D print

The model works decently and being able to visualize, at least to some extent, how the rover would actually pick something up is useful, but there is so much more that should have been done. The model falls short of being able to actually pick something up due to only having one latch. Furthermore, the model has nearly no actual load bearing capacity and even with two of the latches they would only be able to pick up a small payload unrepresentative of what the rover will be carrying.

In the coming weeks the plans are to go back to a scaled rover with actuated latches, wheels will be added in some capacity, and a system for raising and lowering the rover to pick up cargo will be implemented. Initial brainstorming, creating a timeline, and component selection has begun. The preliminary architecture is to have an actuated suspension for raising



and lowering of the rover to pick up cargo, wheel mounted motors for single direction driving capability, and linear actuators on either 4 or 6 latches for securing payloads. To accompany the rover print will be similarly scaled habitat and PLM prints to act as payload and add to the value of the hardware. As a possibility, we are looking into how to test the rover's capability on uneven terrain, and possibly, the Cocoa Beach sand.

To ensure the work gets done the away team has begun meeting regularly virtually and in person to discuss design choices and characteristics. We will also be meeting with Dr. Akin as regularly as possible to complete the LLV mockup before the competition in June.

### 5.7 - Latching Mechanism Design (2) – Edwin Arevalo

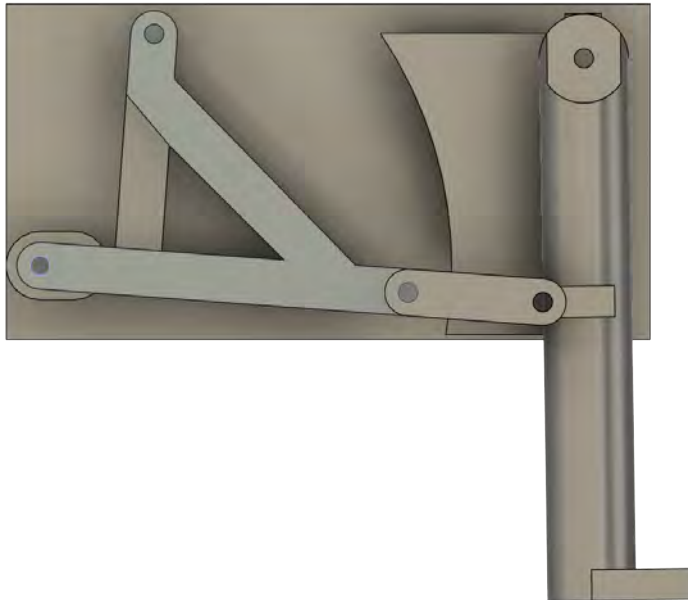


*Figure 5.7.1: Secondary latching concept*

With the guidance of Prof. David Akin, this latching mechanism was heavily inspired by landing gear mechanisms commonly found on airplanes. The main downward strut on the right side of the figure above carries all load since the male Standardized Payload Interface (SPI) would go placed on the lip pictured in the bottom right of the figure. A linear actuator is connected to the top left hole to move the latch between active and stowed positions seen in the two figures below.

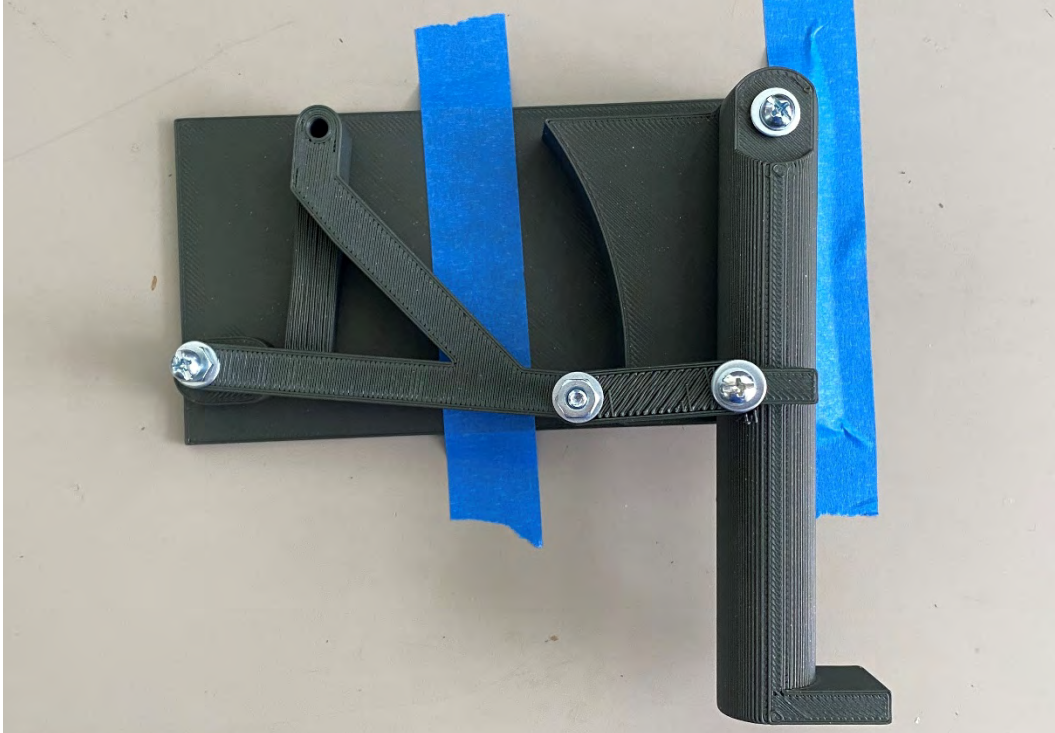


Figure 5.7.2: Active Position



Figure 5.7.3: Stowed Position

The linear actuator would be placed near the center of the entire mechanism and would be at its minimum length while in the active position and its maximum length while in the stowed position. In other words, extending the linear actuator would retract the latch. Ideally, a locking spring would be placed to maintain the over center latching position.

In order to model this latching mechanism for a real world scaled design we took into consideration the dimensions of our available 3D printing beds and airport regulation suitcase sizes and decided a 19.6x10 inch size for the chassis would be acceptable, see figure X

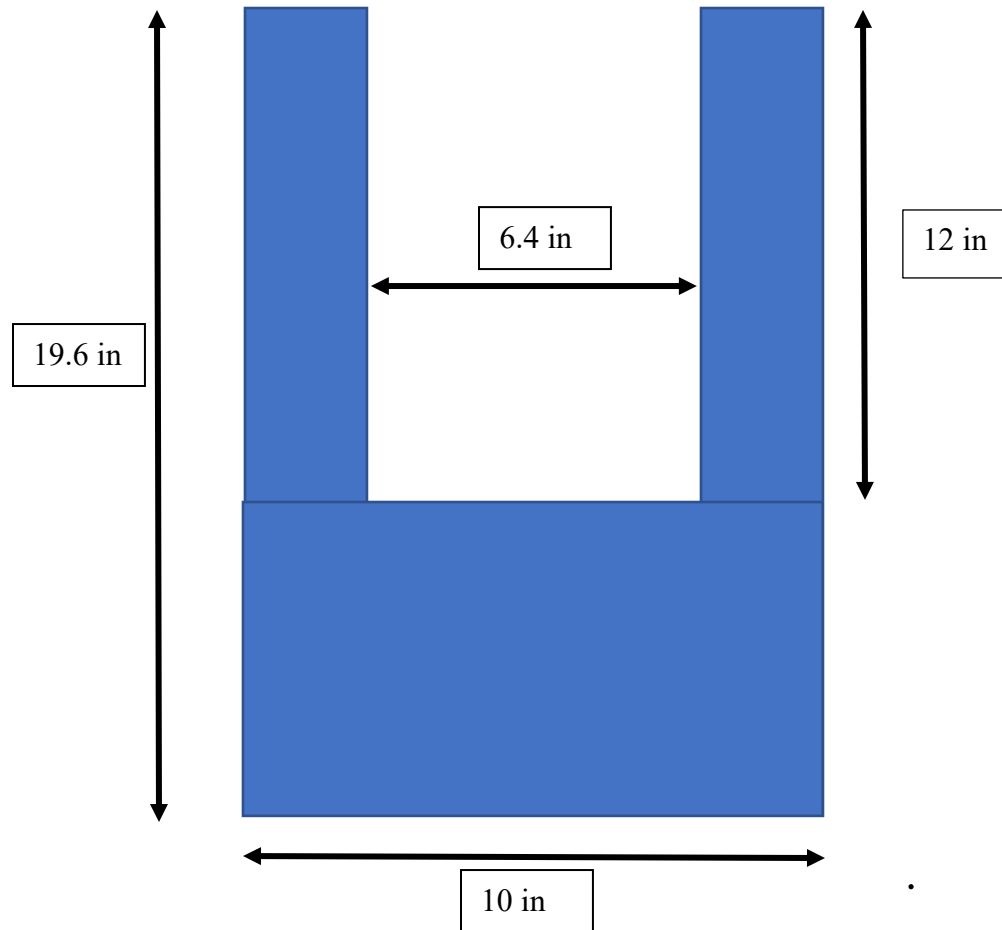


Figure 5.7.4: Scale sizing for chassis

The current scaling size is about 10 times smaller than the projected full-scale model and after accounting for a reasonable wall thickness for the 3D printout, seen in the figure above, and speaking with the rest of the RASC-AL away team, namely Pranav Ampani, Jack Molter, and Brian Amaya, it quickly became evident that we needed to adjust deviate from the actual model size.

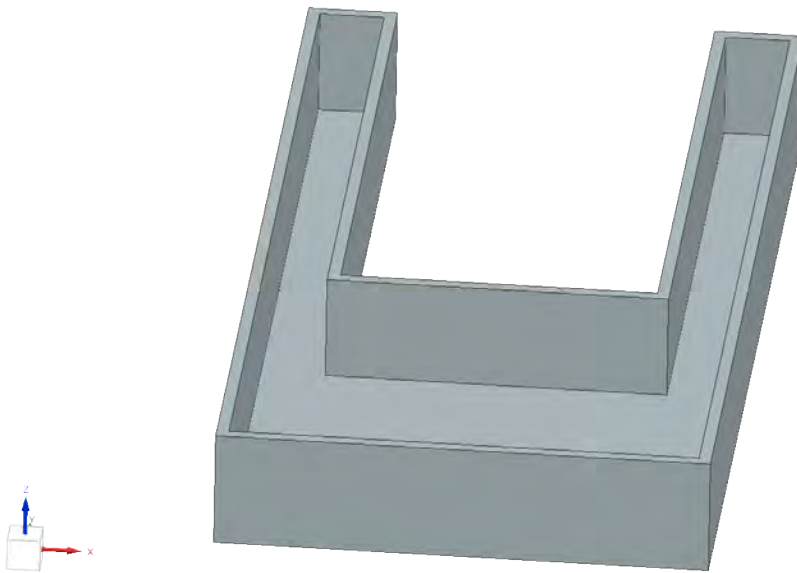


Figure 1.7.5: CAD model including estimated wall thickness. Shows small regions for electronics.

After scaling and accounting for wall thickness, a width of 1.3 inches is left to work with in the space for electrical housing for the latch. Considering that the current micro linear actuator has a stroke length of 1 inch, it is clearly necessary to increase the width of the housing compartments. This will decrease the bed size for potential payloads, but we don't foresee this becoming an issue as payloads can always be scaled as well, it is more important we can demonstrate a working model. Current work is being done using an elegoo mega 2560 project board to create a working scaled prototype of the latching mechanism for the RASC-AL competition.

### 5.8 - Power/Data Transfer – Matthew Thomas

In addition to physically constraining the payload to the LLV, it is also crucial to determine a method for passing data and power between the LLV and the payload. Some of the payloads interfacing with the LLV will need power, such as the PLM, and others may also require commands, such as the cargo manipulator. To address this issue, SHELL will use the Honeybee Robotics dust-tolerant electrical connector [LSM-10]. The electrical connector developed by Honeybee Robotics utilizes dust-tolerant, flexible membranes to reduce contamination by lunar dust. Experiments completed by the Honeybee Robotics team have shown significant reductions in lunar dust within the connector when implementing the membranes [LSM-10]. SHELL's implementation of this concept can be seen in fig. 5.8.1.



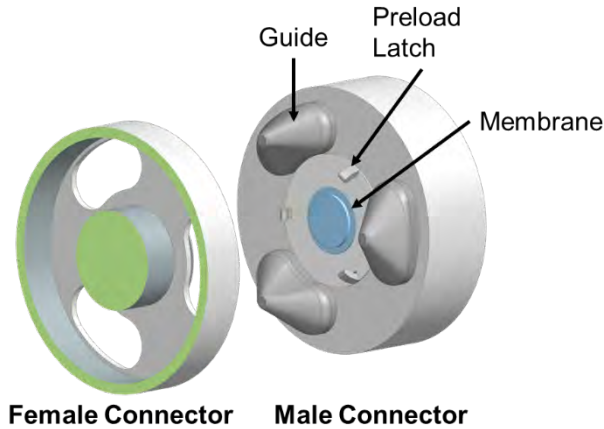


Figure 5.8.1: Dust-tolerant electrical connector

Leveraging Honeybee’s research, SHELL will place the male connector of the interface at the base of the LLV’s U-shape chassis. The female connector will be placed on the adjacent side of the payload. By housing the power and data pins behind dust-tolerant membranes on the male and female connector, they will be protected from the lunar environment. Once the payload has been constrained to the LLV using the SPI, a linear actuator will drive the male connector forward until in contacts the female connector with the assistance of the physical guides. After contact, preload latches will mate the faces and an internal actuator will drive the pins through the membranes to establish power and data transfer.

## 5.9 - Power Requirements

### 5.9.1 - Mobility Power Requirements – Joshua Batstone

The mobility system of the vehicle is comprised of six mobility modules, each of which is equipped with an active suspension system, active steering system, and drive system. The maximum loading case of the vehicle was estimated to be 17,850 kg, considering an estimated rover mass of 2,850 kg and a 15,000 kg payload (the habitat module), and this would need to be transported up a maximum slope of 5°, as per our internal design requirements. Other anticipated loading cases include transporting the pressurized logistics module or PLM (4,700 kg total), CLPS landers (3,350 kg total), and travelling unloaded (2,850 kg total). Using our terra-mechanics model, assuming six wheels of diameter 0.9 m and width 0.35 m, the wheel slip and torque were calculated for each loading case at zero drawbar-pull (the minimum amount of force required to move forwards). From the slip and torque, the total power required to achieve a given target speed can be calculated using the following expression (Eq. 5.9.1).

$$P(v) = N(v \cdot \tau)(1 + SR)/(R \cdot \eta) \quad \text{Eq. (5.9.1)}$$

Where  $N = 6$  is the number of wheels,  $v$  is the target speed of the vehicle in  $m/s$ ,  $\tau$  is the torque per motor in  $N\cdot m$ ,  $SR$  is the slip ratio,  $R$  is the wheel radius in  $m$ , and  $\eta = \eta_{\text{motor}}\eta_{\text{gearbox}}$  is the composite motor and gearbox efficiency. Two metrics of power and energy usage were determined, including the power-per-cm/s of travel speed, and the energy used per kilometer of travel. For this analysis, a composite motor-gearbox efficiency of  $\eta = 0.9$  was used (corresponding to  $\eta_{\text{motor}} = 0.95$ , and  $\eta_{\text{gearbox}} = 0.95$ ) which was determined to be a reasonable

point of estimation based on our preliminary motor and gearbox selection. The terra-mechanics and corresponding total power/energy estimates are tabulated below (Table 5.9.1).

Table 5.9.1: Tabulated Results from Terra-Mechanics Model for Different Loading Cases.

Load Case	Unloaded		+ CLPS		+ PLM		+ Habitat	
Total Mass	2,850 kg		3,350 kg		4,700 kg		17,850 kg	
Slip Ratio   Torque	0.25	129 N-m	0.24	152 N-m	0.21	218 N-m	0.21	965 N-m
Power per cm/s	<b>24 W</b>		<b>28 W</b>		<b>40 W</b>		<b>173 W</b>	
Energy per km	<b>664 W-hr</b>		<b>776 W-hr</b>		<b>1095 W-hr</b>		<b>4810 W-hr</b>	

From our thermal analyses of the drive motors, a maximum speed of 10 *cm/s* was imposed for the maximum loading case (transporting the habitat), which enveloped all other loading cases at speeds of 20 *cm/s*. These speeds were therefore selected as our baselines for power estimation and tasking and are tabulated below (Table 5.9.2).

Table 5.9.2: Tabulated Drive System Power for Different Loading Cases at 5° Slope.

Load Case	Unloaded	+ CLPS	+ PLM	+ Habitat
Travel Speed	20 cm/s	20 cm/s	20 cm/s	10 cm/s
Power	<b>480 W</b>	<b>560 W</b>	<b>800 W</b>	<b>1730 W</b>

Nominal operation for the drive system is set at the maximum loading design point: a load of 17,850 *kg*, traversing a 5° slope at 10 *cm/s*. From tipping calculations and imposing a maximum allowable slip ratio of 60%, maximum traversable slopes for both the habitat and unloaded cases were determined to be 11° and 13°, respectively. In these off-design regimes, the terra-mechanics model was again used to determine the slip and torque and thereby drive system power. Notwithstanding other design considerations, these results are tabulated below (Table 5.9.3).

Table 5.9.3: Tabulated Drive System Power in Off-Design Slope Traversal.

Load Case	Unloaded		+ Habitat	
Traverse Slope	13°		11°	
Travel Speed	20 cm/s		10 cm/s	
Slip Ratio   Torque	0.58	175 N-m	0.55	1181 N-m
Power	<b>831 W</b>		<b>2710 W</b>	

For the steering system, a terra-mechanics model was developed to compute the sideways-bulldozing torque required. Selecting an actuator speed of 6 RPM, and assuming a combined motor and gearbox efficiency of  $\eta = 0.9$ , the steering power for each loading case was calculated and is tabulated below (Table 5.9.4).

Table 5.9.4: Tabulated Steering System Power for Different Loading Cases.

Load Case	Unloaded	+ CLPS	+ PLM	+ Habitat
Bulldozing Torque	2.3 N-m	2.5 N-m	3.2 N-m	22.6 N-m
Power	<b>10 W</b>	<b>11 W</b>	<b>14 W</b>	<b>94 W</b>

For the suspension system, a lead-screw model was developed, taking into account the work required to lift different loads, as well as the friction in the mechanism. Selecting an actuator speed of 60 RPM, and once again assuming an actuator efficiency of  $\eta = 0.9$ , the peak torques and corresponding power were determined for each loading case and are tabulated below (Table 5.9.5).

Table 5.9.5: Tabulated Suspension System Power for Different Loading Cases.

Load Case	Unloaded	+ CLPS	+ PLM	+ Habitat
Peak Torque	6.1 N-m	7.2 N-m	10.0 N-m	38.0 N-m
Power	<b>196 W</b>	<b>230 W</b>	<b>323 W</b>	<b>1230 W</b>

Although the steering and suspension systems draw significant power in the maximum design loading case, these systems will not be used at full capacity continuously while in transit. For purposes of energy usage estimation and battery sizing, a nominal usage of 20% was assumed for the steering system, and a nominal usage of 5% was assumed for the suspension system.

### 5.9.2 - Avionics Power Requirements – Joshua Batstone

To determine the power requirements for the system avionics, reference parts deemed representative of their respective technologies were selected as placeholders and used as a basis for power estimation. Components included as part of this analysis include a primary flight computer, data storage devices, navigation cameras, inertial measurement units, and communications equipment. Redundant systems are assumed to be cold, with minimal power consumption except in the event of a failure. These components, as well as their selected reference parts and power consumption are tabulated below (Table 5.9.6).

Table 5.9.6: Avionics Reference Parts and Power Consumption.

Component	Computer [PPT-1]	SSD × 3 [PPT-2]	Camera × 12 [PPT-3]	IMU [PPT-4]	Comm.
Reference Part	<i>RAD5545</i>	<i>GLS87CR064G3</i>	<i>MER Navcam</i>	<i>LN-200S</i>	-
Power Budget	35 W	5 W	20 W	15 W	25 W

The Mars Exploration Rovers' Navcam was selected as a reference component for the primary pathfinding and navigation cameras. These are rated for nominal operation at 2.15 W, running at the same power level as the MER Hazcams<sup>[PPT-3]</sup>. Three similar cameras will be placed on the front and back surfaces of the LLV, and one will be placed near each mobility module assembly for direct line of sight to each wheel. At any given time, only nine cameras should be operating nominally. An allocation of 25 W has been set aside to power the DTE and

satellite relay communications systems, with only one of these expected to be operational at any given time.

### 5.9.3 - Thermal Power Requirements – Joshua Batstone

To determine the power requirements for the rover thermal control system, steady state thermal balances were performed for each major subsystem, including the mobility modules, warm electronics box (WEB), warm battery box, solar array, and rover body. These analyses should represent overestimates of the thermal control power required and are discussed in-depth in the *Thermal Analysis* section of the report. Tabulated below is a summary of these findings for purposes of motivating the power system design (Table 5.9.7).

Table 5.9.7: Summary of Thermal Control Power Requirements by Subsystem.

Subsystem	Rover Body	Motors	Solar Array	WEB	Battery
Power Budget	47 W	18 W	8 W	13 W	10 W

### 5.9.4 - Active Dust Mitigation Power Requirements – Nicholas Delafuente

To operate electrodynamic dust shields (EDS), the dust displacement current only takes a few milliwatts, which would be a negligible amount. However, there is still power in the current configuration which is from the supply. This means that regardless of the size of the EDS, the power requirement will be approximately 2-4 Watts since the supply will not change very much [PPT-17].

## **5.10 - Power Budget**

### 5.10.1 - Power Modes – Joshua Batstone

While performing different tasks, different subsystems will require varying amounts of power. For purposes of battery and cable sizing, as based on a standard tasking schedule for a reference lunar day, it is important to determine accurate power estimates for these different expected operational modes. Fundamentally, there are two primary operational states of the vehicle: hibernation and transportation. While in hibernation, it is essential to conserve energy as much as is feasible, and so the mobility system is assumed to be turned off completely, and avionics are assumed to be operating at standby levels, primarily being used for thermal control and management purposes. While in transportation, the power required by the mobility system is highly variable, based on the weight of the load, the slope being traversed, and whether or not the suspension and steering systems are being utilized at full capacity. For estimation purposes, at nominal conditions for each loading case the slope traversed is assumed to be a constant 5°, defined as our design point, and the steering and suspension systems are assumed to be operating at their maximum capability for 20% and 5% of the time, respectively. Additionally, avionics and active dust mitigation are assumed to be operating at full power-draw while in transportation, corresponding to 100 W and 4 W, respectively. Tabulated below is a breakdown of the power required for different operational modes of the vehicle, considering several different loading cases (Table 5.10.1).

Table 5.10.1: Total Power Consumption by Operational Mode

Mode	Maximum	Nominal	+ PLM	Unloaded	Hibernation
------	---------	---------	-------	----------	-------------

<b>Power</b>	3160 W	1920 W	925 W	596 W	100 W
--------------	--------	--------	-------	-------	-------

A visual breakdown of each of these operational modes, categorized by major vehicle systems, is shown below (Fig. 5.10.1).

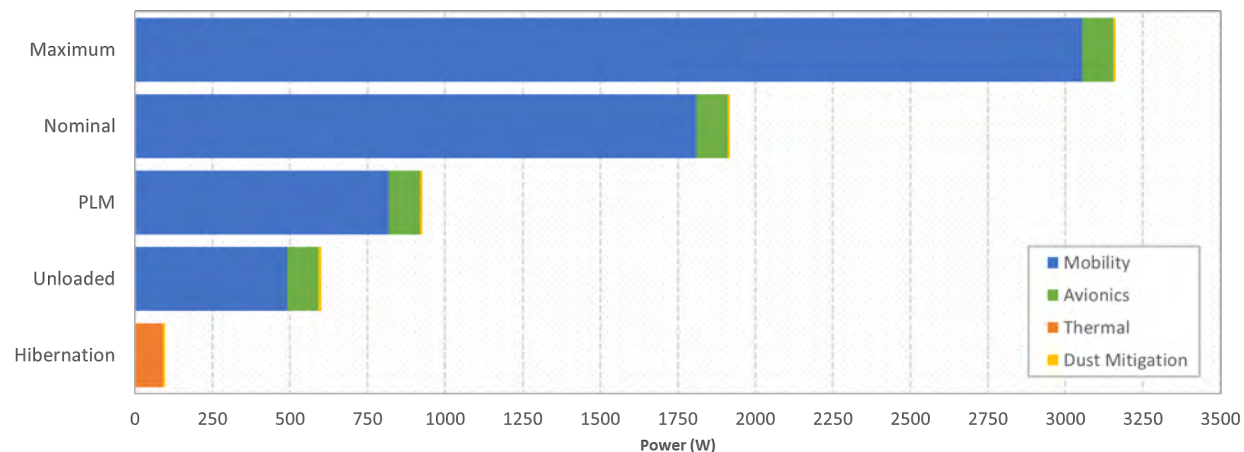


Figure 5.10.1: Visual Breakdown of Different Operational Modes for the LLV.

Although the system is not expected to reach its maximum power level (3200 W) under realistic usage, this should represent an enveloping case for all vehicle operational modes, and as such it is important that the battery and other relevant electronics are rated to withstand such power draw. This power draw is also used as the basis for estimating battery heat generation as part of the battery thermal analysis.

#### 5.10.2 - Battery Sizing – Joshua Batstone

In order to meet the daily energy requirements of the system, it was important to size the battery such that it would have sufficient capacity to both execute tasking and survive the lunar night in only one charge. To these ends, a daily reference tasking day was developed, in which the LLV would be expected to transport a habitat module (nominal design case) over a distance of 4 km, hibernate for 420 hours, and have 20% of its initial capacity remaining, for purposes of battery health and conditioning. From mission planning and analysis, we were able to select a design reference site, designated Haworth 1-2, which should represent the worst-case design scenario for rover operability. This subsite has a mean diameter of approximately 4 km, and experiences lunar nights not exceeding 420 hours during the polar winter. This reference tasking day is summarized below (Table 5.10.2).

Table 5.10.2: Reference Tasking Day Used for Power Estimation.

Reference Tasking Day		
Travel 4 km with Habitat	Hibernate for 420 hr	20% Battery Remaining

Travelling at 10 *cm/s* under nominal conditions for 4 km results in a travel time of 11.1 hours, corresponding to a nominal energy consumption of 21.33 *kW-hr*. Likewise, hibernating for 420 hours corresponds to an energy consumption of 42.04 *kW-hr*, totaling to a combined 63.27 *kW-hr*. Accounting for 20% capacity left results in a required battery capacity of 79.09

*kW-hr*, and as such a capacity of 80 *kW-hr* was selected. As follows is a visual representation of this battery capacity per reference tasking day, broken down by subsystems (Figure 5.10.2).

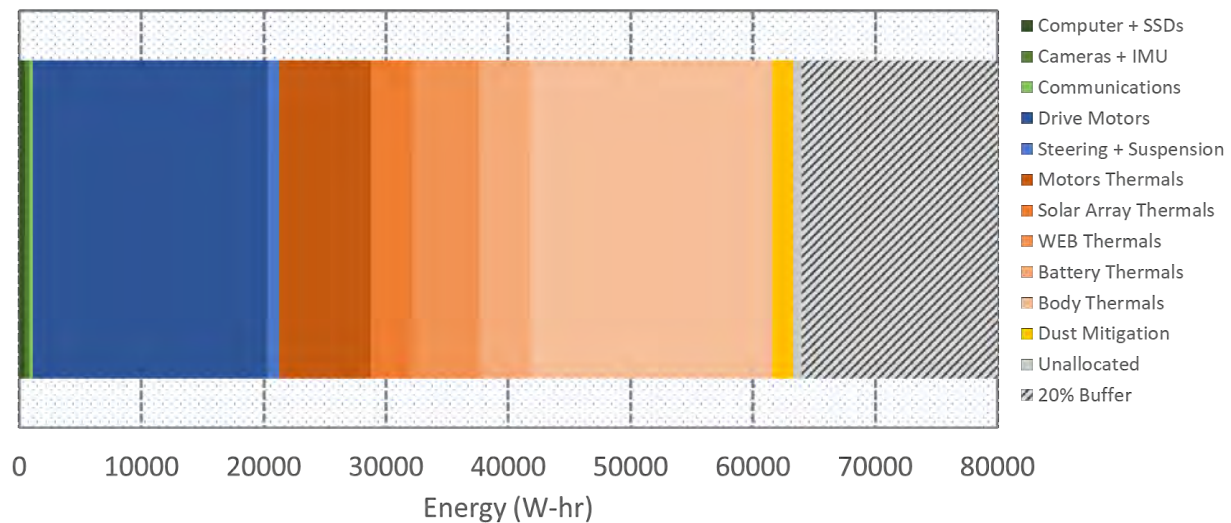


Figure 5.10.2: Battery Capacity Breakdown over Reference Tasking Day.

Although the power consumption during hibernation is significantly smaller (100 W) than nominal operation (1915 W), due to the much longer periods over which the system must hibernate, thermal control becomes the largest consumer of energy on a lunar-day basis.

### 5.10.3 - Power System Capabilities – Joshua Batstone

Based on our preliminary battery sizing, and power consumption estimates by subsystem, we are able to determine the maximum capabilities of the LLV under a variety of different conditions. These include the maximum travel distances for a nominally loaded and unloaded vehicle, at 5° and maximum slope for each case, as well as the maximum period of hibernation. Each of these calculations restricts battery usage to 80% depth of discharge. These results are tabulated below (Table 5.10.3).

Table 5.10.3: Maximum Capabilities of Power System.

Loading Case	Max Distance	Travel Time
Unloaded (5° slope)	76.8 km	107 hr
Unloaded (13° slope)	24.5 km	34.1 hr
Habitat (5° slope)	12.1 km	33.4 hr
Habitat (11° slope)	7.9 km	11.0 hr
<b>Max Hibernation Time</b>		
<b>640 hr</b>		

## 5.11 - Battery

### 5.11.1 - Battery Cell Selection – Adebayo Odusami

After understanding the total power draw requirements for the operation of our Lunar Logistics Vehicle, we were able to calculate the total battery capacity required to meet the mission requirements which came to about 80,000 W-hr. This enabled us to accurately design a battery box for these requirements. The first step in designing our battery box was battery cell selection. This was a crucial step for us because choosing the right battery cell would help lay a solid foundation for the design and assembly of our battery box, whereas picking a less efficient cell could prove very costly and detrimental for our mission. There were a number of trades that were conducted for choosing a cell. The significant trades to mention include a trade on primary battery cells versus secondary battery cells, battery cell chemistries, and battery cell geometry (cylindrical vs pouch vs prismatic), which will all be discussed more in the next paragraphs.

### 5.11.2 - Secondary vs Primary Cells – Adebayo Odusami

The first step for us in selecting our battery cell was deciding between a primary cell and a secondary cell. Primary battery cells, also known as single-use or single-cycle cells, are cells that cannot be recharged once discharged completely. Some examples of primary cells include Zinc-carbon, Alkaline, and Lithium Iron Sulphate cells. Primary cells are popular for their high specific energy, and their high internal resistance, making them a great option for missions where mass conservation is important. A secondary cell on the other hand, is a cell that can be charged and discharged a certain number of times until reaching its end of life. For most secondary cells, this end of life comes after about >500 cycles, and a cycle in simple terms is one discharge and recharge of a battery or battery cell. Some examples of secondary cells are Nickel Cadmium (NiCd), Nickel Metal Hydride (NiMH), and Lithium Ion (Li-ion) cells. Secondary cells are popular for their low internal resistance; however, their energy density is not as high as that of primary cells. They are usually a better option for longer duration missions. The decision between a primary and secondary cell was assessed based on the expected total battery mass, cost, heat dissipation, mission power draw requirements, and mission duration.

We closed this trade with the selection of secondary cells for our mission. Although their lower comparatively lower energy densities, their ability to operate for many cycles makes them a better fit for our 5-year mission window. Now that we have closed the trade on primary vs secondary cells, the next step for us was choosing the best cell chemistry for our mission.

### 5.11.3 - Cell Chemistry – Adebayo Odusami

Conducting a trade on secondary battery cell chemistries was a key step in our battery design process. This is because different chemistries have their respective energy density ranges, temperature ranges, as well as cycle lives. Choosing a cell chemistry with a relatively low energy density, temperature band and cycle life might prove extremely detrimental to our mission. As mentioned earlier, some examples of secondary cell chemistries include Lead acid, NiCd, NiMH, and Li-ion chemistries. We did not include Lead acid cell chemistry in our trade off because it has the lowest specific energy (about 30 - 50Wh/kg), lowest cycle life (about 200 - 300 cycles) and a high charge time (about 8 - 16 hours); making it highly unlikely for adoption for our mission. The table below shows the following figures of merits that were assessed for the comparison between the different secondary battery cell chemistries. It highlights their various characteristics and specifications.

	NiCd	NiMH	Li-ion
<b>Specific Energy (W-hr/Kg)</b>	45-80	60-120	90-250
<b>Internal resistance</b>	Very low	Low	Low
<b>Cycle life (80% DoD)</b>	1000	300-500	500-2000
<b>Charge Temperature (°C )</b>	0 to 45°C		0 to 45°C
<b>Discharge Temperature (°C )</b>	-20 to 65°C		-20°C to 60°C
<b>Overcharge Tolerance</b>	Moderate	Low	Low
<b>Self-discharge / month</b>	20%	30%	<5%
<b>Cell voltage (nominal) (V)</b>	1.2V	1.2V	3.2-3.7V
<b>Maintenance Requirements</b>	Full discharge every 90 days when in full use		Special charge circuit

Table 5.11.1

<https://batteryuniversity.com/article/bu-107-comparison-table-of-secondary-batteries>

The first thing to note from the table is the energy densities of each cell type. The Lithium-ion cell wins in this category with an energy density ranging from 90 to 250 W-hr/Kg, about double those of the NiCd and NiMH cell types. All three cell types have relatively low internal resistances, that is they allow high current density to pass through them, reducing the amount of energy lost to heat. NiCd batteries generally have a cycle life of 1000 cycles, while NiMH batteries range from 300 to 500 cycles. Li-ion batteries offer the highest cycle life, ranging from 500 to 2000 cycles.

The table above provides the temperature range within which each battery type can be charged and discharged safely. Both NiCd and NiMH batteries have a charge temperature range of 0 to 45°C and a discharge temperature range of -20 to 65°C and -20 to 60°C, respectively. Li-ion batteries share almost the same charge and discharge temperature ranges as NiCd and NiMH, Li-ion cells have a slightly thinner temperature range. The overcharge tolerance indicates the ability of a battery to withstand overcharging without significant damage. This is also an important figure of merit for us because we want to be able to account for overcharging wearing on battery cells. NiMH and Li-ion batteries all have a low tolerance for overcharging, with NiCd batteries offering moderate tolerance. Self-discharge/month highlights what percentage of the cell capacity is lost over a time period of one month when not in use. NiCd batteries have the lowest self-discharge rate of <5% per month, while NiMH batteries have a self-discharge rate of



30% per month. Li-ion batteries have the lowest self-discharge rate of 20% per month. We want our batteries to still have enough capacity to power our rover after the rover has been idle for months, so the Li-ion cell is the best choice for this consideration. In summary, the table provides an overview of the key figure of merits for selecting the best cell chemistry for our mission, and it was clear to us that the best cell chemistry was the li-ion cell.

#### 5.11.4 - Lithium-Ion Battery Trade Study – Adebayo Odusami

The Li-ion cell is the general name for any cell that has a lithium element as an anode, and another element as its cathode. There are several types of lithium-ion batteries, and each type has its strengths and weaknesses. This was the start of our next trade in selecting the optimal cell. Common cathode materials are Lithium Manganese Oxide (also known as spinel or Lithium Manganate LMO) , Lithium Nickel Manganese Oxide, Lithium Iron Phosphate (LiFePO<sub>4</sub>), Lithium Nickel Cobalt Aluminum Oxide (or NCA), and Lithium Titanate Oxide (LTO). All these cell types are all good choices of batteries, but it is important to ensure the cell we choose can endure the conditions on the lunar surface. The trade off on lithium-ion cells was conducted by assessing each cell based on their voltage at full charge, their voltage at full discharge, their Energy densities (Specific Energy W-hr/kg), their cycle life, and temperature at which thermal runaway occurs. The table below shows how each cell performs per the listed figure of merits above.

	<b>Lithium Manganese Oxide</b>	<b>Lithium Nickel Manganese Oxide</b>	<b>Lithium Iron Phosphate</b>	<b>Lithium Nickel Cobalt Aluminum Oxide</b>	<b>Lithium Titanate Oxide</b>
<b>Full charge</b>	4.20V	4.20V (or higher)	3.65V	4.20V	2.85V
<b>Full discharge</b>	3.00V	3.00V	2.50V	3.00V	1.80V
<b>Specific Energy (W-hr/kg)</b>	100 - 150	150 - 220	90 - 120	200 - 260	70 - 80
<b>Cycle life (ideal)</b>	300–700	1000–2000	1000–2000	500	3000–7000
<b>Thermal runaway</b>	250°C (higher when empty)	210°C (higher when empty)	270°C (safe at full charge)	150°C (higher when empty)	One of safest

Table 5.11.2

From the table above, we can see the specifications on each cell. We chose our final cell using an elimination method. It was quite a challenge to pick a final cell because where one cell comes first in a category, it comes last in another category. The first cell that was removed from the cell options was Lithium Titanate Oxide. Although it has the highest cycling amongst the cells, it has the lowest energy density of 70 to 80 W-hr/kg. This is a key factor for our mission because efficient mass utilization is one of our goals. The next cell we eliminated was the

Lithium Manganese Oxide. The elimination of the LMO cell was as a result of its low cycling, and not having adequate information on it. From our trade off, our first analysis brought us to the conclusion that either the Lithium Nickel Manganese Oxide, Lithium Iron Phosphate, or Lithium Nickel Cobalt Aluminum Oxide were decent choices.

From the graph below, we can see that these three cells came out top of their class. We decided initially to move forward with the LiFePO<sub>4</sub> cell because it had comparative specifications to that of the NMC and NCA cells, it was the safest, and it was the most innovative. However, this innovation was what led to us not moving forward with the LiFePO<sub>4</sub> cell. We ran into a lot of dead ends during our research, and because of the time constraint we had, we were not able to provide a solid argument as to why the LiFePO<sub>4</sub> cell would be a better option for space mission than NMC cells and NCA cells that are already space proven. Because of this, we then decided to go with the NMC cell which had good cycling, high energy density, and high thermal runaway tolerance, where we ran into another issue.

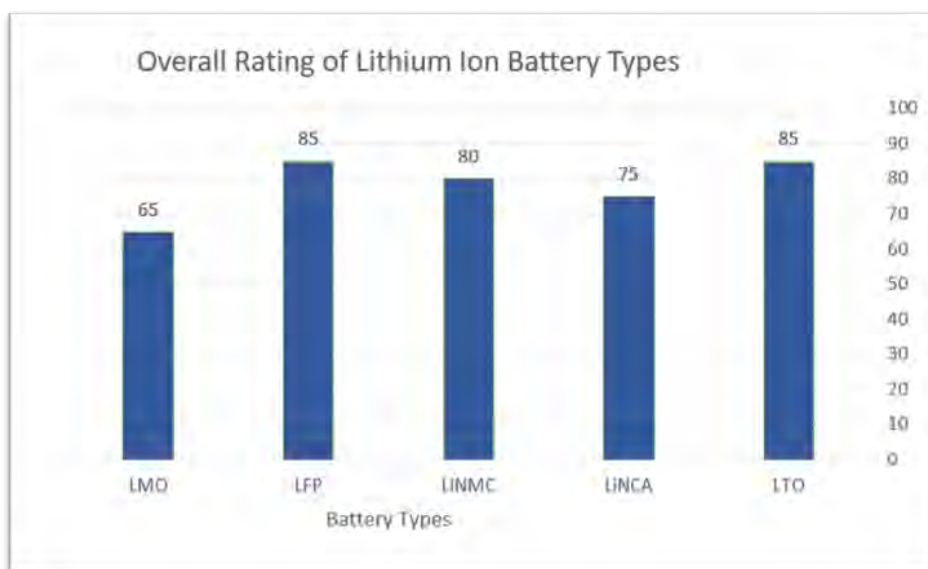


Figure 5.11.1

The issue we faced with the NMC cell was not particularly a mission threatening issue, it was more of a problem with the assembly into the final battery box, and future maintenance. Recall that our battery capacity was about 80,000 W-hr. The typical NMC cell has about 5Ah (Ampere-hours) of capacity with a nominal voltage ranging up to 4V. This brings the typical cell capacity to about 20W-hr. Using these numbers to get an estimate on the number of cells that we would need for our mission, we divided the total capacity needed of 80,000 W-hr by the individual cell capacity of 20 W-hr, and that gave us a total number of about 4000 NMC cells. This means to meet our mission battery box capacity requirements using NMC cells, we would require about

4000 cells or more. We believed that having that many cells in a battery box will make it difficult to assemble. Cell replacement would also be a tedious task in the event that a cell is bad, and a replacement is needed. Another thing that made us close off on the NMC cell type was that having that many cells would mean more connectors, separators, and more wires which would add to the total mass of the battery box. This brought our final selection for our battery cell to the

Lithium Nickel Cobalt Aluminum Oxide cell. We are confident this is a good choice for our mission because of its high energy density and comparable cycling. We also conducted good

research on NCA cells to give us a solid argument and strong foundation for picking this cell. From our research we found that NCA cells have been used in space before. Before we dived into selecting our reference cell, we had to decide between a cylindrical, pouch, and prismatic (rectangular) cell geometry.

#### 5.11.4 - Cell Geometry – Adebayo Odusami



	Prismatic	Cylindrical
Model example picture		
Pros	Higher Energy density	Better thermal safety
Cons	Less efficient thermal management, thermal runaway	Lower packaging density

Table 5.11.2

The table above shows a comparison between prismatic cells and cylindrical cells, listing the pros and cons of each cell geometry. This was a relatively easy trade for us to conduct, and we were able to select the prismatic cell geometry as our final choice. The main reason for this selection is due to the ease of assembly of prismatic cells, and their space utilization. It is also important to note that cylindrical cells have better thermal safety; however, the battery box would be thermally insulated (i.e thermal barriers between cells and modules, Teflon thermal breaks around battery box), and proper thermal analysis would be conducted to prevent thermal runaway. [<https://www.sciencedirect.com/science/article/pii/S254243512030088X>]

We found a great model NCA cell produced by eagle pitcher who are industry giants in the production of batteries and have designed batteries for previous space missions such as in the space shuttle. Additionally, the GPS III, the Mars Exploration Rovers (MER) Spirit, Opportunity, and Perseverance (Exhibit 1), as well as the Juno mission—which traveled the farthest distance from Earth for a lithium-ion system—all used lithium-ion cells and batteries manufactured by EaglePicher. [<https://www.eaglepicher.com/blog/batteries-enabling-planetary-and-deep-space-exploration/>]. The table below contains the specifications of our reference cell.

Cell Specifications (Lithium Nickel Cobalt Aluminum Oxide)		
Parameters	Units	Value
Nominal Voltage	V	3.6
Nominal Capacity	Ah	60.0
Mass	kg	1.6
Energy Density	W-hr/kg	160
Operating Temperature	°C	-20 to 40
L x W x H	cm	13.8 x 3.4 x 15.5
Power	W-hr	216

Table 5.11.3



Figure 5.11.2: Cell CAD Mockup

The reference cell we chose has a good energy density, and an impressive nominal capacity. This high nominal capacity will allow us to reach out total battery capacity requirement with lesser cells than the NMC cells. These cell specifications were used to design our final battery box.

#### 5.11.5 - Battery Layout – Adebayo Odusami

The first step in the designing of our battery box as mentioned earlier was understanding the battery box requirements. This was a total capacity of 80,000 Wh, and a bus voltage of 120V. Then, we were tasked with choosing the cell, or a model cell in which we decided to go with the Eagle Pitcher 3.6V 60Ah Space Cell. Using this reference cell, and the equations listed below, we were able to calculate the total number of cells and the total cell mass in our battery box.

$$N_{cell} = \frac{Capacity_{total}}{V_{cell} * Ah_{cell}} = \frac{80,000 W - hr}{3.6 * 60 W - hr}$$

$$M_{cell,total} = N_{cell} * m_{cell} = \frac{80,000 W - hr}{(3.6 * 60) W - hr} * 1.6 kg$$

This gave us a total of 370 cells, and a total cell mass of about 593 kg. However, due to space optimization, geometry, and establishing redundancy, these numbers were updated to **374 cells** and **600 kg** which will be discussed more in the coming paragraph. Now that we know the total number of cells, the next step for us was figuring out the best method of cell arrangement into modules and into the battery box. To meet the bus voltage of 120V, we would require several cells in series, this is because voltage adds up when cells are connected in series, and capacity adds up when cells are connected in parallel. So, we divided the bus voltage of 120V by the individual cell nominal voltage of 3.6 V to get the number of series cell connections we would

$$N_{cell,parallel} = \frac{N_{cell}}{N_{cell,series}} = \frac{374}{34} = 11 \text{ parallel connections}$$

require. This calculation gave us a total series cell connection number of 34. Now that we have established the number of cells in series needed, we

were able to calculate the number of parallel cell connections needed to meet the current draw requirements by using the formula on the left. This gave us a total of 11 parallel connections

needed. Now all that was left to do was stack the cells and integrate the necessary battery regulating systems.

Our idea for cell stacking was arranging the cells into modules, then arranging these modules into the final box assembly. There were two considerations for arranging our cells into modules; a series arrangement or a parallel arrangement. This brought us to our next trade off. The table below shows a graphic depiction of how we arrived at our conclusion for this trade off. The left column shows what would happen if we adopted a series connection method for the cells in our modules. If one cell in the module goes bad, then the entire module goes bad. Whereas, if we implored a parallel connection method in our modules, if one cell dies in the module, we are still able to draw power from the rest of the cells in the module, as depicted as the green colored cells on the right column. Therefore, for built in redundancy, it was clear the better choice was the parallel cell arrangement into modules, then connecting these modules in series to meet the bus voltage and capacity requirements of our battery. The next issue we were faced with was the arrangement of the cells in the battery box to ensure that it fits into the rover. This was an issue for us because we required 34 module arrangements, and 34 only has 4 factors: 1,2,17, and 34. To go into more detail, this would mean for optimum space and mass, we have to arrange these modules in rows or columns of these factors. For each arrangement tried, we resulted in a length of our battery box larger than our rover width. On the contrary, if we decided to go with 3 or 4 row or column arrangements, yes, the box will fit, but there are two other things to account for; adding extra modules which would increase the mass, or removing the modules not needed and having empty pockets of space. A summary of our results from trying different module arrangements is shown in the table below.

Battery Box	Modules per row	Modules per column	No of cells	Modules removed	Dimensions (cm) (L x W)
Red	2	17	374	0	281 x 90
Blue	5	7	385	1 (11 cells)	225 x 116
Green	4	9	396	2 (22 cells)	180 x 149
Black	3	12	396	2 (22 cells)	135 x 199

*Table 5.11.4: Summary Table for Battery box sizing*

We tried four different module arrangements for our battery box. The box-colored red has the

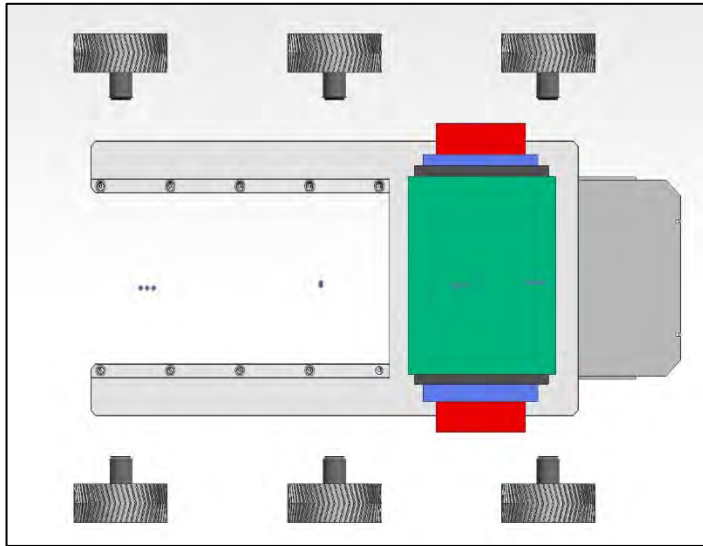


Figure 5.11.3: Different battery box

optimal space and mass utilization with 0 modules being removed; however, its length is more than the width of our rover and as such will not fit. This left us with the three other battery boxes colored blue green and black. We decided to pick our final battery box based off critical visualization of the understanding that we must leave enough room for other components that might go in the rover. Our final choice for the battery box was the black box. The black box's dimensions are in between those of the blue and green battery boxes making it our top choice,

and the design we chose to move forward with. This brought our total battery box dimensions to be 1983mm x 1347mm x 233mm (L x W x H). A computer aided design (CAD) mockup of how we envision the cells will be arranged in our battery box is shown in figure X below.

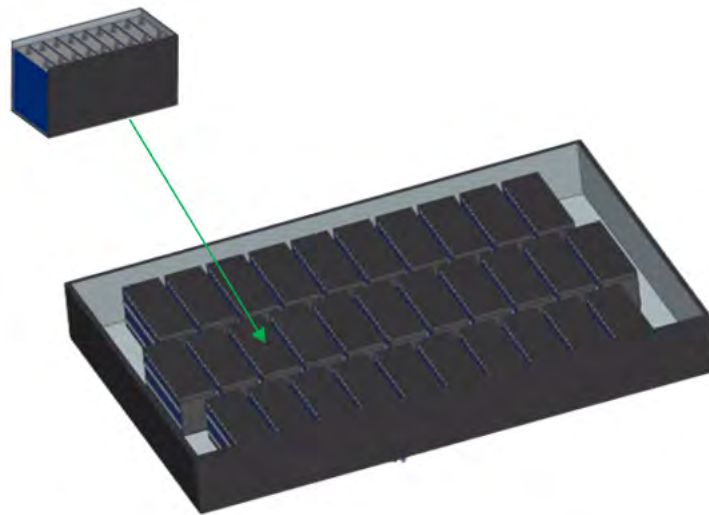


Figure 5.11.4: CAD mockup of module level and box level

Recall that for our battery box selection, we had to remove two modules, one for the top row, and one from the bottom row. This is why our cell arrangement inside the box is not a perfect rectangle. We also left gaps between each module to allow for ventilation and reduce conduction within the battery. The next and final steps for the completion of our battery box were selecting a BMS (Battery Management System), choosing a housing material, calculating the WBB (Warm Battery Box) final mass, and conducting adequate thermal analysis. Installing a BMS is important to monitor the battery's temperature, voltage, and current. The BMS will

protect the battery from overcharging and over-discharging. The BMS would also be able to communicate with the rover's main control system to provide battery status updates.

Our next consideration was integrating a power distribution system for efficient power supply and distribution from our battery to our main components and subsystems.

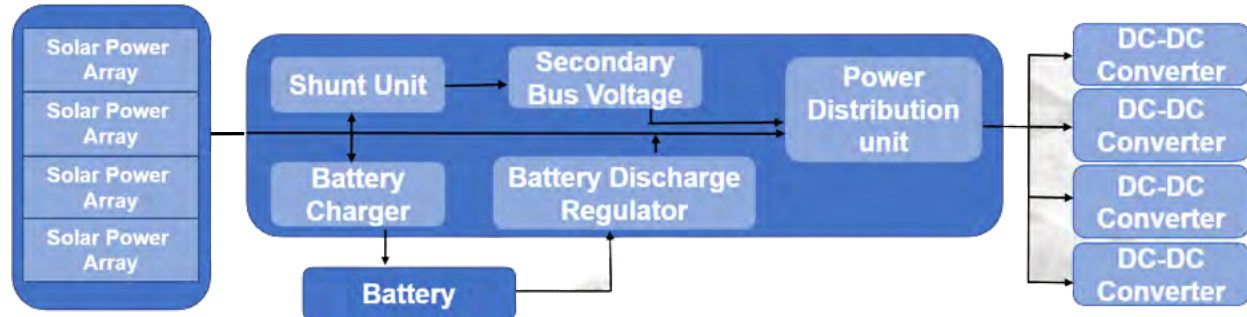


Figure 5.11.5 2: Block diagram for Power Distribution

The figure above shows our schematic for power distribution to subsystems. Our PCDU consists of a battery charger to direct energy to the battery to be stored; a shunt unit to regulate current, a battery discharge regulator to regulate the voltage from the battery, a secondary bus voltage for subsystems that require lesser voltage; and a power distribution unit to distribute power across the rover. Power goes into the PCDU, then into the battery to be stored and released back for usage through the PCDU. Power is then output finally from the PCDU to several subsystems that will have their respective DC-DC buck (step down) converters. We require a secondary bus voltage for our battery because of the difference in voltage requirements per subsystem. For instance, the wheel requires as high as 120V for operation, while some subsystems like the cameras require only about 5V of power.

#### 5.11.6 – Battery Box Mass Estimate – Adebayo Odusami

To arrive at our final battery box mass, we estimated the mass of the battery box housing and components and added that to the total cell mass of 600 kg. For our battery box housing material, we decided to go with carbon fiber-reinforced polymer (CFRP). CFRP has very low weight, high stiffness and strength, and low coefficient of thermal expansion (CTE) [<https://www.mdpi.com/2079-6439/6/4/92>]. CFRP's also have low densities of about 1.5 – 2.0  $g/cm^3$  [Jawaid]. To get the mass of the CFRP battery box housing, we used a thickness of 0.2cm for its sides, and a thickness of 0.3cm for its base and top. Using these thicknesses, we were able to calculate the volume of the battery box to about 300  $cm^3$ , and with a CFRP density of 2.0  $g/cm^3$ , our battery box housing mass was about 40 kg. Sample calculation is shown below.

Recall the battery box dimension is 198.3cm x 134.7cm x 23.3cm (L x W x H).

$$\begin{aligned}
 V1 &= 199 * 135 * 24 = 644760 \text{ cm}^3 \\
 V2 &= (199 - 0.4) * (135 - 0.4) * (24 - 0.6) = 625518 \text{ cm}^3 \\
 \text{Volume of WBB} &= V1 - V2 = 19242 \text{ cm}^3 \\
 \text{Mass of Housing} &= \text{Density} * \text{Volume of WBB} \\
 \text{Mass of Housing} &= 2 \frac{g}{cm^3} * \frac{1kg}{1000g} * 19242 \text{ cm}^3 = 40 \text{ kg}
 \end{aligned}$$

We implored the calculation to get the mass of the WBB housing using CFRP material. We then estimated the mass of all other components (i.e wiring and connectors) to be

about 10 kg. This brought our total battery box mass to **650 kg**; 600 kg cells, 40 kg housing, and 10 kg components.

## 5.12 – Power Generation

### 5.12.1 – Power Generation Trade – Nicholas Delafuente

For missions requiring space-grade equipment, there are only a few options for power generation. In this case, the research was based on past Lunar and Martian rovers. The Perseverance Mars rover uses a multi-mission radioisotope thermal generator (MMRTG), which was the first area of interest for power generation. The MMRTG can generate power the entire time it is on, which is one of the major benefits of using it. Another form of power generation is through solar arrays, as seen on Sojourner from the Mars Pathfinder. For solar arrays, the only power generation is when the Sun is present.

To be able to make the right power generation decision for SHELL, the mission planning requirements must first be considered. A lunar day is 708 hours, and at the chosen landing site, the longest period in one lunar day that the rover will be without sun is 420 hours. For the MMRTG, the rover will be generating power for the entire 708 hours. For the solar array, the rover will be generating power for 288 hours and will then have to be thermally regulated for 420 hours. Now that the power generation hours over each lunar day are known, the characteristics of solar arrays and MMRTG must be considered.

	Solar Array	MMRTG
<b>Mass Required (kg)</b>	30	90
<b>Power Generation (W)</b>	890	220
<b>Cost (\$/W)</b>	20	1,000,000

Table 5.12.1

Based off the power requirements for SHELL, the necessary solar array sizing is 2m<sup>2</sup>, which is what the values in the table above are based on. For the MMRTG, there must be a total of two, also displayed in the table above. The main focus of the power generation trade is to see which system will perform better, but cost is still relevant, so it is included.

Now that the mission requirements and characteristics of each power generation option are known, the final step is to compare how much energy each generates on a lunar day and compare that on a mass basis. First, the MMRTG generates 220 Watts over the course of 708 hours, for a total of 155 kW-hr/day. On a per-mass basis, this is around 1730 (E/day)/kg.

Looking at the solar array, to achieve 80% depth of discharge, the battery is able to be charged twice up to 70 kW-hr/day, for a total of 140 kW-hr/day. Since there are 420 hours where the rover is in the dark and it takes 90 W to thermally, it will take a total of 37 kW-hr/day to thermally regulate over the lunar night. This means the solar array will generate 107 kW-hr/day. On a per-mass basis, this is 3400 (E/day)/kg.



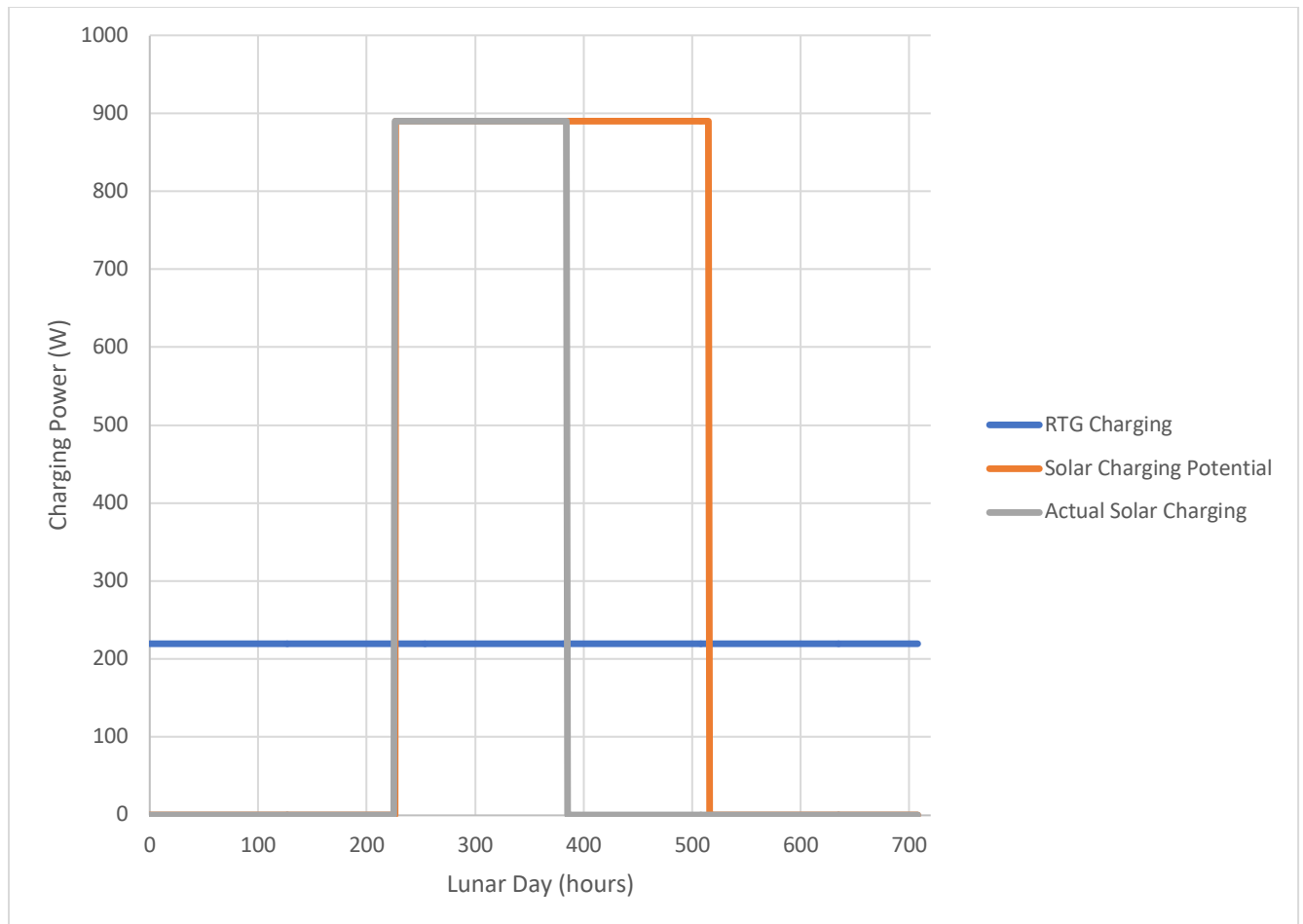


Figure 5.12.1

Solar Array (E/day)/kg	MMRTG (E/day)/kg
3400	1730

Table 5.12.2

The graph above displays the potential charging time for both the solar array and the MMRTG. Since the MMRTG can generate power for the entire lunar day, 80% depth of discharge does not need to be considered. For this, the energy/day is the area beneath the blue line. For the solar array, there is potential to charge for the entire 288 hour light period, but the battery will not be able to store all of the power. The orange line shows the 288 hour sunlight period, where the gray shows the actual charging period done by the solar array. The energy/day of the solar cells is the area beneath the gray curve.

From these results, it was evident that choosing solar cells was the best option for SHELL. Although (energy/day)/kg is more important, it is also worth noting that the cost per Watt of MMRTG was 50,000 times more expensive than the solar array.

Finally, the last thing that was considered for the power generation trade was a combination of MMRTG and solar cells, or hybrid. Once the comparison between the two was

completed, it was clear that there did not need to be a hybrid power generation type. Since solar cells work for the given design, adding the extra mass and cost of the MMRTG just to generate power during the lunar night was not necessary. This solidified the idea that a solar array was the choice for power generation.

#### 5.12.2 - Solar Array Selection – Nicholas Delafuente

To select a solar cell that would work for SHELL, it had to be space grade and be able to withstand extreme temperatures. The typical commercial solar cell can withstand temperatures between -40 C to 65 C, [PPT-18] and are usually single junction with an efficiency between 15-20% [PPT-19]. Solar cells in space must have a higher temperature band and higher efficiency, since at the minimum, the Moon can produce temperatures ranging from minus to plus 100 degrees Celsius. There were certain cells that have been used in space that caught our interest, being multi-junction cells, specifically triple junction cells.

Triple junction cells are made up of three layers: gallium indium phosphide, gallium arsenide, and gallium indium arsenide.

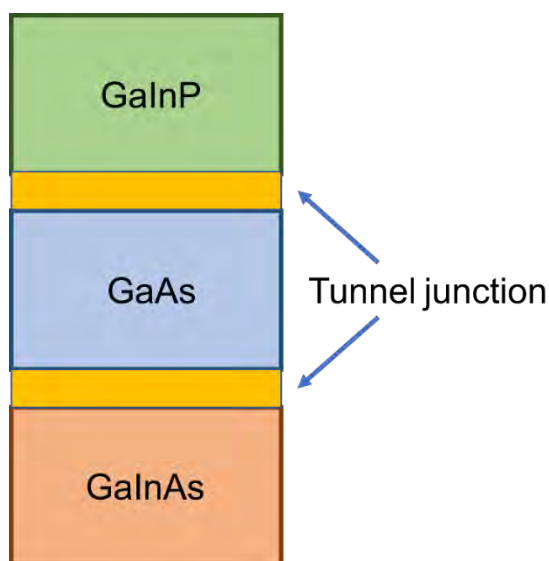


Figure 5.12.2

Triple junction cells not only have a very high efficiency, but they can get to temperatures between -80 C to 100 C and still be operational [PPT- 20]. Attached below is a table of the main factors we considered as well as the cell sizing necessary for this mission.

<b>Cell Type</b>	<b>Area (m<sup>2</sup>)</b>
Triple Junction	2
<b>Mass (kg)</b>	<b>Power Generation (W)</b>
30	890
<b>Space-Grade Efficiency</b>	<b>Degradation per Year of Initial Efficiency</b>
34.2%	2.50%

Table 5.12.3 [PPT-21,22]

From the data presented above, the efficiency is twice as high as typical commercial solar panels, and through other factors like temperature and mass, choosing to go with triple junction solar cells was an easy decision.

There were other solar cells considered like ultrathin-film cells or cells with more junctions than three, but the triple junction cell described above has been tested and used in space.

## 5.13 - Thermal Management

### 5.13.1 - Temperature Intervals – Adebayo Odusami

Operating a lunar rover in the harsh environment of space requires careful consideration of temperature intervals for various subsystems. Extreme temperatures on the Moon can impact the performance and functionality of critical components and subsystems. We selected our temperature intervals for each component based on the allowable operating temperatures from reference parts to allow for optimal operation and longevity. The chart below shows the temperature interval chosen for major components.

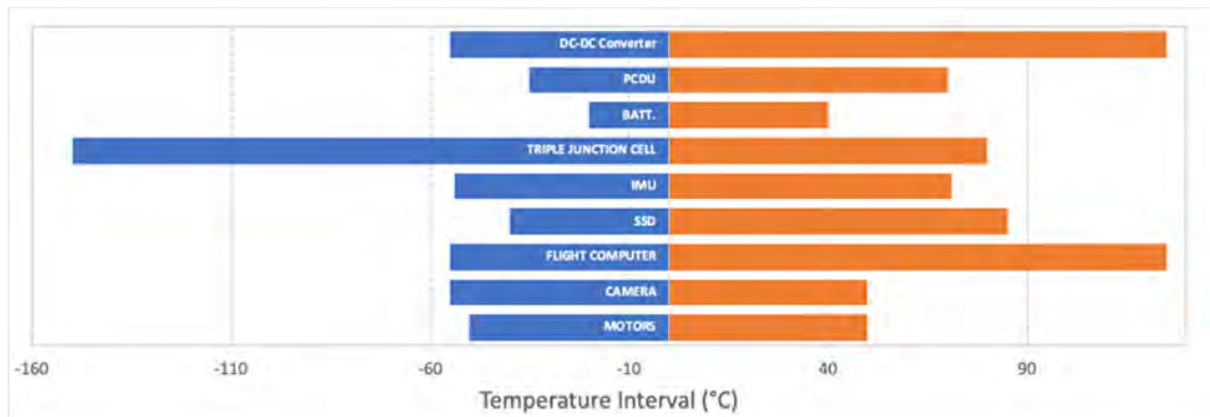


Figure 5.13.1: Temperature intervals by system components.

The DC-DC converter converts the rover's primary power supply to different voltage levels required by various subsystems. The maximum operating temperature band for this component is from  $-55^{\circ}\text{C}$  to  $125^{\circ}\text{C}$  (218K to 398K). Operation within this range will ensure efficient power conversion and prevent issues such as overheating. The PCDU manages the power distribution within the lunar rover, ensuring proper energy allocation to various subsystems. The recommended operating temperature range for the PCDU is from  $-35^{\circ}\text{C}$  to  $70^{\circ}\text{C}$  (238K to 343K) to ensure stability and efficiency in power distribution. The operating temperature range for the battery is from  $-20^{\circ}\text{C}$  to  $40^{\circ}\text{C}$  (253K to 313K). Operating within this range helps maintain battery efficiency, prolongs its lifespan, and prevents issues such as reduced capacity or damage due to extreme temperatures. The Triple Junction cell responsible for generating power from sunlight via solar panels has an operating temperature range of  $-150^{\circ}\text{C}$  to  $80^{\circ}\text{C}$  (123K to 353K). This wide range accommodates the extreme temperature variations experienced on the Moon, allowing for optimal power generation. The IMU measures the rover's motion, orientation, and acceleration, providing crucial data for navigation and control. The recommended operating temperature range for this component is from  $-55^{\circ}\text{C}$  to  $70^{\circ}\text{C}$  (219K to 344K) <sup>[PPT-4]</sup>. Operating within this range ensures accurate measurements and prevents issues such as drift or malfunctioning of the IMU sensors. The SSD is responsible for

storing and retrieving data within the lunar rover's onboard computer system. To ensure data integrity and avoid potential issues such as data corruption or loss, the temperature range we chose for our SSD is from  $-40^{\circ}\text{C}$  to  $85^{\circ}\text{C}$  (233K to 358K) <sup>[PPT-2]</sup>. Operating within this range will help maintain the SSD's reliability and performance. The flight computer which serves as the brain of the lunar rover, controlling its navigation, communication, and decision-making processes will be regulated from  $-55^{\circ}\text{C}$  to  $125^{\circ}\text{C}$  (218K to 398K) <sup>[PPT-1]</sup>. The camera subsystem which is vital for capturing images and providing visual information has a temperature band of  $-55^{\circ}\text{C}$  to  $50^{\circ}\text{C}$  (218K to 323K) to ensure optimal image quality and performance. Operating within this range will prevent issues like sensor damage, reduced image identification, and operational failures. Finally, the motors which are a crucial component will be maintained to an operating temperature range from  $-50^{\circ}\text{C}$  to  $50^{\circ}\text{C}$  (223K to 323K). Operation within this range will help prevent issues such as motor stalling, reduced efficiency, and potential damage due to extreme temperature variations.

#### 5.13.2 - Lunar Thermal Environment & Management – Joshua Batstone

The lunar poles present some of the most extreme thermal environments in the solar system, with ground temperature fluctuations ranging from 40 to 250 K ( $-233$  to  $-23^{\circ}\text{C}$ ) <sup>[PPT-5]</sup>. For regions which are not permanently shadowed, periods of illumination may last for as long as 20 days (during the polar summer), and periods of darkness may exceed 21 days (during the polar winter). From our design reference mission analysis, we selected a subsite of Haworth 1 (designated Haworth 1-2) to serve as our reference site, with periods of darkness not exceeding 420 hours (17.5 days), and periods of illumination not exceeding 456 hours (19 days) <sup>[PPT-5]</sup>. In this subsite, ground temperatures range from 50 to 250 K, though in reasonably level regions (slope  $\leq 5^{\circ}$ ) they typically do not reach above 220 K <sup>[PPT-5]</sup>. Considering these long-duration periods of continuous illumination and darkness, a steady-state handling of the thermal equilibria is an appropriate option for a first-pass analysis. Due to the lack of any significant atmosphere on the moon, the dominant modes of heat transfer between thermal systems and the lunar environment are radiative and conductive. However, due to the low thermal conductivity of the lunar regolith (between 0.0006 and 0.007 W/m-K for fluff and depth regolith layers) <sup>[PPT-6]</sup> conductive losses to the environment typically remain very small ( $< 1$  W for the LLV). For this reason, these losses are not considered as part of our analysis.

To determine the viability of a thermal control system design, a worst case hot and cold scenario must be identified, and steady-state equilibrium temperatures must remain within the system temperature interval. The worst-case hot condition typically occurs when the system is exposed to the maximum incident solar flux, has the lowest radiative view factor to space, the highest ground temperature, and is generating the maximum internal power. The worst-case cold condition occurs during the lunar night (no insolation), when the ground temperature is lowest, the radiative view factor to space is highest, and when the system is generating only enough internal power to remain within its design temperature interval.

When considering heating due to the sun, both primary and secondary sun effects were taken into account. Given the high latitude of our design reference site (approximately  $-86.8^{\circ}$ ), the maximum elevation of the sun above the horizon was determined to be approximately 10 degrees. This low-elevation sun results in the majority of heating occurring on the sides of the rover. For this same reason, the solar arrays used to generate power for the system were mounted

vertically (perpendicular to the ground). The top and bottom surfaces can each experience some direct measure of insolation. Under the worst design conditions (in which the local terrain slope and maximum elevation of the sun are combined) the top surfaces will experience incident sunlight at  $15^\circ$ , whereas in a separate worse-case condition, the bottom surfaces will experience incident sunlight at a maximum of  $5^\circ$ . This is shown visually in Fig. 5.13.2.

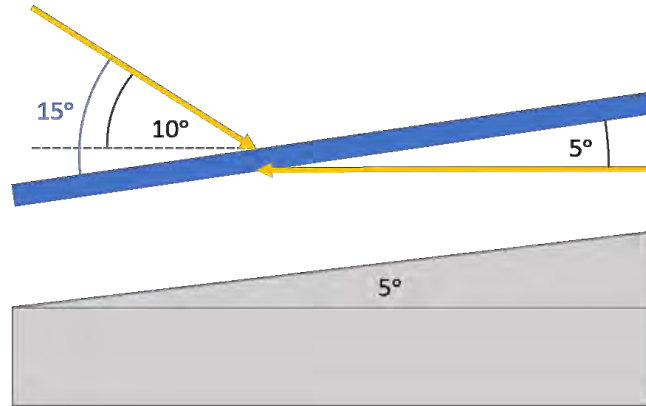


Figure 5.13.2: Direct Insolation of Top and Bottom Surfaces at  $5^\circ$  Design Slope.

Secondary sun effects consider the reflection of sunlight off the lunar surface, onto the body. From previous studies, the albedo factor (i.e., the percentage of light reflected from the surface) is known to be dependent on the angle of incidence. This dependence can be modeled by a relatively simple equation <sup>[PPT-7]</sup>:

$$A(\phi) = A_0 + 0.045 \left( \frac{90^\circ - \phi}{45^\circ} \right)^3 + 0.14 \left( \frac{90^\circ - \phi}{90^\circ} \right)^8 \quad \text{Eq. (5.13.1)}$$

Where  $\phi$  represents the angle (in degrees) between the surface and the incident ray, and  $A_0$  is the albedo factor at normal incidence, which is taken to be  $A_0 = 0.105$  <sup>[PPT-7]</sup>. The albedo model assumes a diffuse reflection of the incident sunlight; in other words, the reflected rays are roughly isotropic above the plane of reflection. In order to compute the surface albedo (power per  $m^2$  parallel to the surface), the incident sunlight is multiplied by the albedo factor, as shown in Eq. 5.13.2.

$$P_{ALBEDO}(\phi) = A(\phi)I_{sol}\sin(\phi) \quad \text{Eq. (5.13.2)}$$

As shown in Fig. 5.13.3, the maximum angle of incidence will be approximately  $\phi = 15^\circ$ , which will correspond to the maximum surface albedo:  $P_{ALBEDO} = 121 W/m^2$ . This value is assumed for all secondary sun heating calculations and should represent an overestimate.

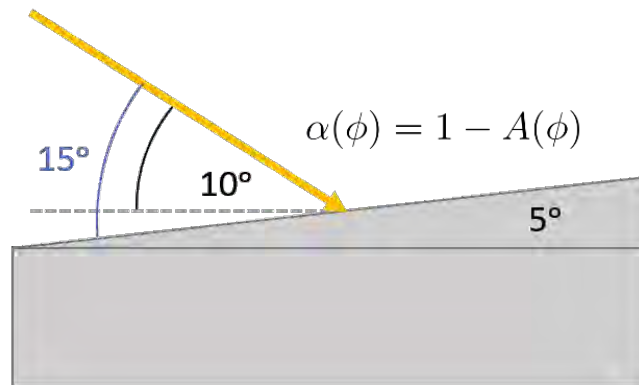


Figure 5.13.3: Surface Albedo of the Moon at 5° Design Slope.

In order to isolate the system from the lunar environment, a radiative insulation must be used, and this is typically some form of multi-layer-insulation (MLI). Although the thermal properties of MLI can be adjusted by modifying the layer materials, number of layers, and spacing material, for the purposes of this first pass analysis, a reference MLI with 25 layers of double-side-aluminized Mylar (6  $\mu\text{m}$  thick) spaced by Dacron web was selected <sup>[PPT-8]</sup>, as this configuration has experimentally measured and validated effective thermal properties (Table 5.13.1). This configuration is used for all internal and external systems that make use of MLI.

Table 5.13.1: Effective Thermal Properties of Reference MLI <sup>[PPT-8]</sup>.

Number of Layers	$\epsilon_{\text{eff}}$	$\alpha_{\text{eff}}$
25	0.016	0.003

If the system exceeds its maximum temperature in the worst-case hot condition, then typically a radiator must be added to dissipate the waste heat, sizing the radiator such that additional heat from incident sunlight on the radiator is also rejected. Similarly, if the system falls below its minimum temperature in the worst-case cold condition, then additional heat must be added, at the same rate as heat is lost radiatively at the minimum control temperature. Despite the simplicity of these approaches, taken together they work against one another. To maintain temperatures in the worst-case cold condition, the system should be radiatively insulated to the maximum possible extent, which does not allow for heat to be dissipated efficiently in the worst-case hot condition. Likewise, radiators are high-emittance surfaces, meaning that in the worst-case cold condition, substantial energy is wasted by them. A solution to this problem can be found in louvers. Louvers are mechanisms that make use of a bimetallic coil to passively open or close a blade (louver blade) such that below a control temperature the radiator will be occluded. This helps to minimize the radiative losses during the lunar night, while also allowing the system to reject heat efficiently during the lunar day at peak operation. In order to quantify the effective thermal properties of louvers, the ATS-6 satellite louvers were used as a reference, given the sparseness of other available data. The effective emissivity of the ATS-6 louvers for the open and closed cases were found from testing to be 0.71 and 0.115, respectively <sup>[PPT-9]</sup>. The effective absorptivity of the louvered panels is heavily dependent on the orientation of the sun with respect to the louver blades. Assuming fully opened louver blades, the effective absorptivity for illumination angles of 5°, 15°, and 90°, are 0.02, 0.10, and 0.12, respectively <sup>[PPT-9]</sup>. These values

all assume a panel surface finish of OSR, with a solar absorptivity of 0.08 and an IR emissivity of 0.77 <sup>[PPT-9]</sup> and should implicitly account for the effects or internal reflections within the louver assembly. These values are tabulated below (Table 5.13.2).

Table 5.13.2: Effective Thermal Properties of ATS-6 Louvers <sup>[PPT-9]</sup>.

Surface Finish	$\epsilon_{\text{eff}}$ (Open)	$\epsilon_{\text{eff}}$ (Closed)	$\alpha_{\text{eff}}$ (90°)	$\alpha_{\text{eff}}$ (15°)	$\alpha_{\text{eff}}$ (5°)
OSR	0.71	0.115	0.12	0.10	0.02

To simplify much of our thermal analyses, and build in some inherent margin to our estimates, radiative view factors of certain surfaces were estimated to be 0 or 1, in such a way as to overestimate the objective. For example, for side-facing surfaces, which share a significant view-factor with the ground ( $F_{\text{view,ground}} \cong 0.5$ ), in the hot case analysis (where radiation to the ground is less efficient than to space) this view factor could be estimated to be 1 (if the surface is relatively low emissivity), resulting in an overestimate for hot-case temperature. Likewise, if we are performing cold case analysis for the same surface, we might assume that this view factor is 0, resulting in an overestimate for the power required to maintain the steady-state temperature. For high-emissivity surfaces, or other cases where this handling might result in an unnecessary degree of overestimation, a view-factor calculator database <sup>[PPT-10]</sup> was used to estimate the view-factors such that a more modest overestimate was achieved.

A last key simplification made over the course of our thermal analysis is the assumption that bodies remain isothermal. Since our thermal design methodology involves local dissipation of heat at the point where it is generated, this assumption should remain reasonably valid, given that temperature gradients across the vehicle should be small. However, for a higher fidelity analysis, as the design resolution is increased and refined, finite element methods would need to be leveraged.

### 5.13.3 - Motor Thermal Control – Joshua Batstone

Thermal control of the mobility modules proved among the most challenging tasks in the thermal design of the LLV. The design temperature interval we based our motor thermal control system on was (-50 °C to 50 °C), which was selected based on the (-55 °C to 55 °C) temperature interval of the brushless DC motors used on the MSL and M2020 rovers <sup>[PPT-11]</sup>, with added margin. Due to the high mechanical power required to transport the habitat module, and inefficiencies inherent in the mechanical and electrical assemblies of the drive motors, large amounts of waste heat are generated under nominal operating conditions. If left unchecked, this heat would quickly cause the motors to exceed their maximum survival temperature. Likewise, in the extreme cold of the lunar night, the motors will require heating in order to remain above their minimum survival temperature, and this can be accomplished by passing a trickle current through the windings for internal resistive heating.

Under the worst-case-hot operating conditions, sky visibility is notably occluded (either heavily or fully) by the habitat module. Because of this, pointing any radiating surfaces upwards was deemed infeasible from a design perspective, and so the decision was made to instead have them face downwards towards the ground. The disadvantage of this is that radiative efficiency is reduced (by about 20%), but the benefit is that the radiative view-factor is unchanging for

different loading cases, direct incident sunlight is limited to  $5^\circ$  (reducing direct sun heating), and dust accumulation on the surface should be reduced due to the adverse gravitational gradient. Under nominal operating conditions, the mechanical power required by each motor is 2595 W per m/s of travel speed, allowing us to perform analysis considering different motor efficiencies. As mentioned before, the surface albedo was assumed to be  $120 \text{ W/m}^2$ , and the surface temperature was assumed to be 250 K, both of which should represent overestimates. This worst-case hot condition is represented visually below in Fig. 5.13.4.

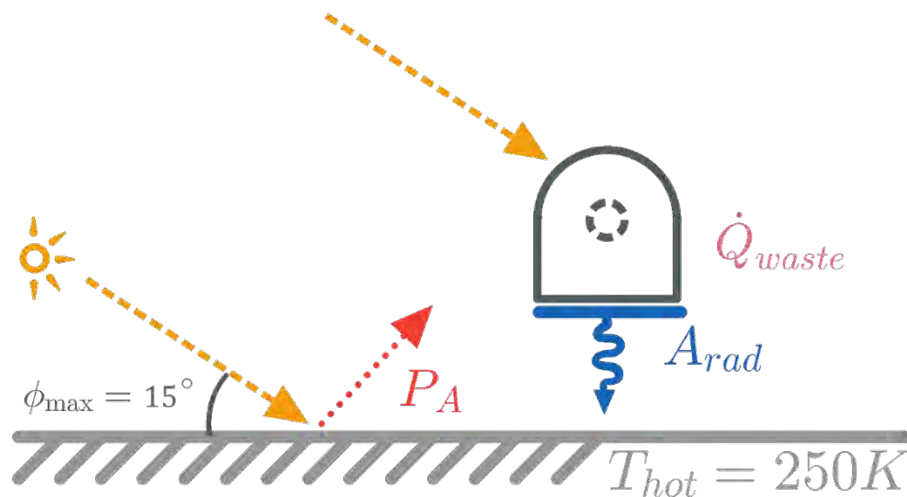


Figure 5.13.4: Hot Case Setup for Motor Thermal Analysis.

Two different approaches to handling this thermal control were considered and analyzed. The first of these was a suspension-coupled radiator cover design, wherein the radiator itself or cover to the radiator would be deployed by a mechanism coupled to the active suspension system. This would be configured in such a way as to cover the radiator whenever the suspension was in the stowed configuration, and to uncover it while in the driving configuration. A design feasibility study was performed to determine, for a given radiator size and efficiency a.) what the maximum speed is for the worst-case hot condition, and b.) whether in the worst-case operating cold condition the temperature of the motors would remain above the minimum control temperature.



A graph representing this design feasibility space is shown below in Fig. 5.13.5.

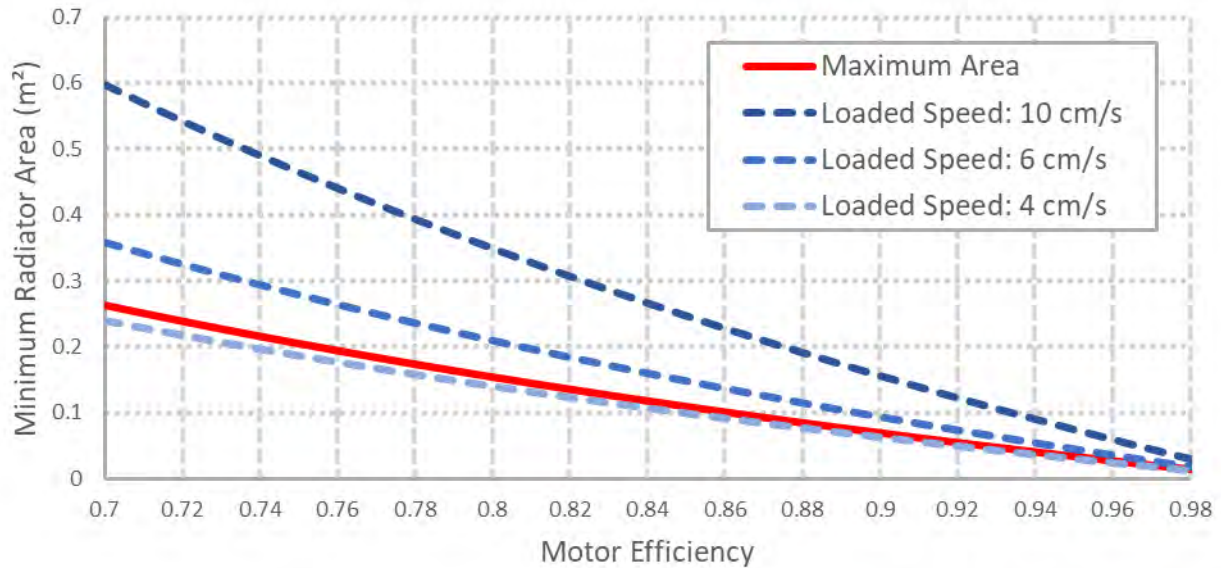


Figure 5.13.5: Suspension-Coupled Radiator Design Feasibility Regions.

In Fig. 5.13.5, the red line represents the maximum area allowable for a given motor efficiency, above which the cold-case minimal operation (which considered an unloaded rover traveling at 20 cm/s just at the start of a period of illuminance) would drop below the minimum control temperature. For fully loaded (transporting habitat) speeds above around 4 cm/s, there exists no design space, whereas below that point the rover begins to move slowly enough to result in a meaningful reduction in tasking ability, as determined by mission planning and analysis. Additionally, to remain above minimum temperatures, the unloaded rover would be required to travel at a minimum of 20 cm/s, otherwise enough waste heat would not be generated. This could be resolved by adding additional resistive heating elements, but this would represent an unnecessary inefficiency, especially given that under these conditions the radiator would be deployed.

We therefore opted to use a louvered radiator control system, wherein the covering and uncovering of the radiative surface is achieved through the use of louvers. This allows for a finer level of thermal control over the operational range of the vehicle, an increased travel speed (since it is no longer constrained by cold-case considerations), and greater flexibility as to the layout and positioning of the radiators. Tabulated below are the worst-case hot and cold conditions for the louver-integrated drive system motors (Table 5.13.3).

Table 5.13.3: Worst Case Hot, Cold Conditions for Louver-Integrated Motors <sup>[PPT-9, 10]</sup>.

Max/Min Temp.		$\epsilon_{\text{eff}}$ <sup>[PPT-9]</sup>		$\phi_{\text{sun}}$	$\phi_{\text{albedo}}$	$P_{\text{sun}}$ per $\text{m}^2$	
50 °C	-50 °C	0.71	0.115	5°	90°	2.35 W	0 W
Ground Temp.		Power per $\text{m}^2$		$F_{\text{rad, ground}}$ <sup>[PPT-10]</sup>		$P_{\text{albedo}}$ per $\text{m}^2$	
250 K	50 K	0 W	2595 W	1.0	0.7	14.5 W	0 W

Where the red and blue cells in Table 5.13.3 correspond to the worst-case-hot and cold, respectively. The view factor between the radiator and the ground was calculated to be

approximately 0.7, by modeling the radiator and wheel as orthogonal flat plates with their corresponding approximate dimensions <sup>[PPT-10]</sup>. In order to calculate the minimum required area for a given motor efficiency under these circumstances, the following formula (Eq. 5.13.3) was used.

$$A_{rad} \left( F_{rad} \sigma \epsilon_{eff}^{open} [T_{max}^4 - T_{ground}^4] - \frac{P_{sun}}{A_{rad}} - \frac{P_{albedo}}{A_{rad}} \right) = P_{int} = \frac{P_{mech}}{\eta} (1 - \eta) \quad \text{Eq. (5.13.3)}$$

Where  $P_{sun}/A_{rad}$  and  $P_{albedo}/A_{rad}$  are tabulated in Table 5.13.3. Plotting radiator area (with an added 10% margin) vs. motor efficiency for 10, 15, and 20 cm/s yields the following curves (Fig. 5.13.6).

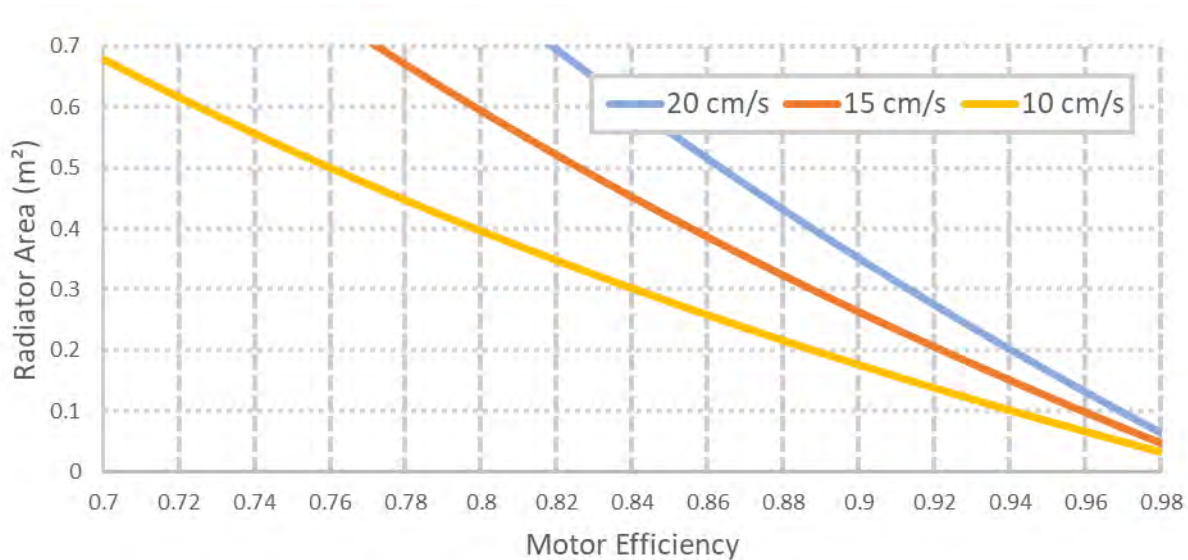


Figure 5.13.6: Minimum Motor Area vs. Motor Efficiency for Louver-Integrated Motors.

Immediately evident from this plot is that for a decreased motor efficiency, the required radiative area becomes quickly infeasible, given the limited space around the mobility modules. It was therefore necessary to use the most efficient possible motors and gearboxes, which through research we determined was about  $\eta = 0.9$ , corresponding to a motor and gearbox efficiency of 0.95 for each. Likewise, for a two-fold increase in vehicle speed (10 cm/s to 20 cm/s), there is approximately a two-fold increase in the required radiator area. From mission planning and analysis, we were able to determine that above around 10 cm/s, there are diminished returns on improved tasking ability, and so this was selected as our traversal speed under nominal (fully loaded) operation. This design point corresponds to an area of 0.18 m<sup>2</sup>, which was thus selected as our radiative area. A visual representation of this radiator, with a possible layout and configuration is pictured below (Fig. 5.13.7).

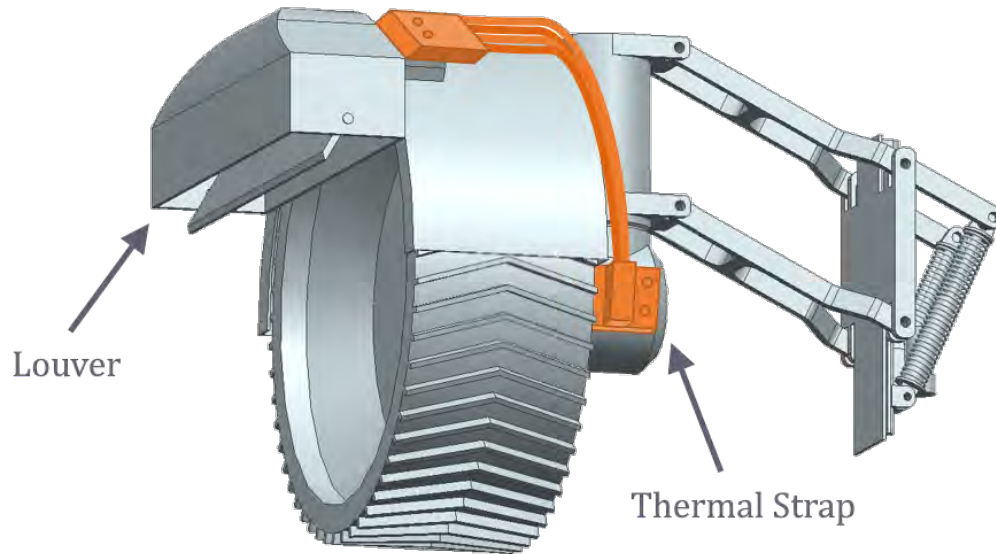


Figure 5.13.7: Motor Louvered Radiator (0.18 m<sup>2</sup>) Placement in Partially Opened Configuration.

In the cold case, radiative losses from the louvered radiator were considered, as for the other surfaces on the motor assembly, parasitic losses were calculated to be diminutive ( $\ll 1$  W), and conductive losses to the rover are not considered due to the fact that the rover body is maintained at a minimum temperature matching the motors (-50 °C). For the selected radiator area of 0.18 m<sup>2</sup>, this results in a net heating requirement of 2.90 W per motor, corresponding to 17.4 W of total heating. If similar lubricants are used to those in the MSL brushless motors (Braycote 600EF grease and Brayco 815Z oil in 2:1 ratio) [PPT-11], then the lower survival bound will be dictated by their respective freezing points (-80 °C and -72 °C) [PPT-12, 13]. Assuming a new minimum survival temperature of -70 °C, this results in a new net heating requirement of 1.99 W per motor, corresponding to 12.0 W of total heating. These results are summarized below in Table 5.13.4.

Table 5.13.4: Total Motor Heating Power by Minimum Control Temperature.

Total Heating Power for -50 °C	Total Heating Power for -70 °C
<b>17.4 W</b>	<b>12.0 W</b>

Generally, for an increased survival temperature interval, the radiator sizing and the heating required could be reduced as a function of the desired control temperatures, however for this first-pass analysis, the goal was to overestimate where reasonable so as to leave margin for when the design is refined. Therefore, for estimating power consumption by the motor thermal control subsystem, a nominal power of 17.4 W was assumed.

### 5.13.3 - Warm Electronics Box – Joshua Batstone

The warm electronics box (WEB) is a thermal control box which houses some of the most sensitive avionics in the vehicle, including the flight computers, storage devices, and communications equipment. It is therefore pertinent to carefully maintain its temperature to within tight temperature bands, corresponding to the most sensitive components present. For purposes of preliminary analysis, the flight computers, SSDs, IMU, and communications

transceiver are all assumed to be placed in the WEB, which have corresponding temperature intervals of (-55 to 125 °C) [PPT-1], (-40 to 85 °C) [PPT-2], (-54 to 71 °C) [PPT-4], and (-45 to 72 °C) [PPT-14], respectively. From this, our maximum design temperature interval was identified to be (-40 to 70 °C), and so add in some margin, we selected a maximum design temperature interval of (-30 to 50 °C), to account for the future addition of more temperature-sensitive components. Based on our power requirement analysis, at maximum operation these components will dissipate approximately 80 W in the form of heat, and so to account for other components located within the WEB, a dissipation allocation of 90 W was used to size the radiator.

In order to allow for high heat dissipation at nominal operation, while also conserving power during the lunar night, a louvered radiator was selected as the primary method of thermal control. Because of this, the WEB was placed underneath the spoiler, such that its radiator would have a relative unobstructed view to space, for maximum efficiency. This placement is represented visually in Fig. 5.13.8.

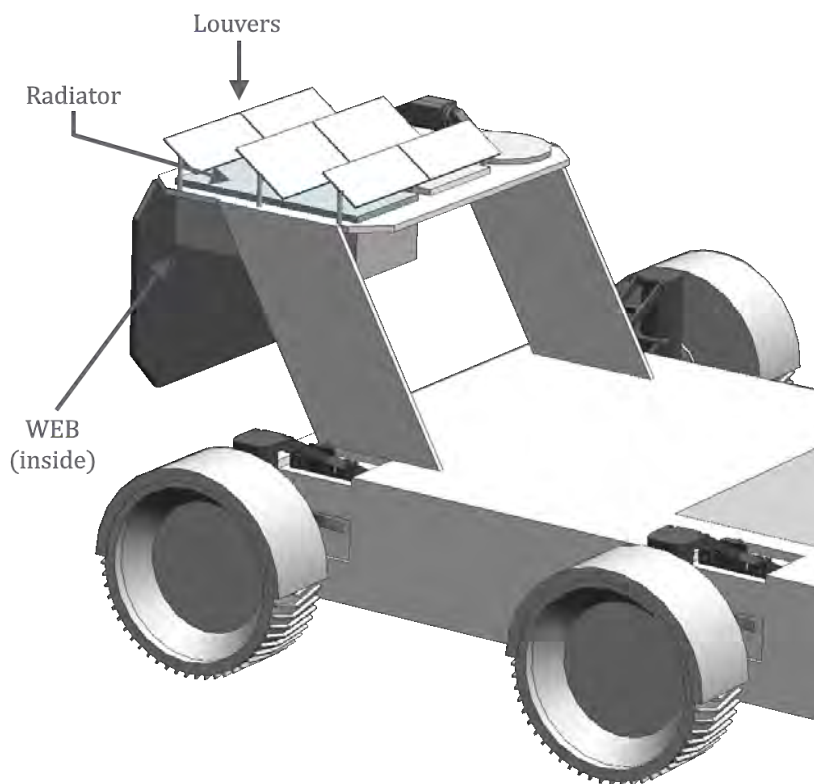


Figure 5.13.8: Warm Electronics Box and Radiator Placement on LLV.

To thermally isolate the WEB from the body of the rover, a combination of MLI and thermal standoffs (thermal breaks) were used. For the MLI a reference insulation consisting of 25 layers of double-side-aluminized mylar was used. For the thermal breaks, a thermal conductance of 0.2 W/m-K was assumed, which is representative of a number of commonly used insulators (such as PTFE) [PPT-15], with the total contact area between the breaks and WEB assumed to be approximately 15x15 cm, and the breaks assumed to be 5 cm long. Based on preliminary component selections, the WEB base area was estimated to be 50x50 cm, with a height of 20 cm.

In the worst-case-hot scenario, the direct sun angle to the radiator will be approximately 15°, and secondary sun effects are not considered due to the top-mounting of the panel. Additionally, under the highest loading case, the radiative view factor to the sky will be reduced by the presence of the habitat module. Modeling the radiator and habitat as orthogonal flat plates with a shared edge (sized accurately), results in an estimated view-factor to the sky of 0.65 [PPT-10], which should represent an overestimate. In the worst-case-cold scenario, both primary and secondary sun heating are assumed to be zero, and the view-factor to space is assumed to be 1.0. A diagram representing this thermal setup is pictured below in Fig. 5.13.9, and the conditions for the hot (red) and cold (blue) cases are tabulated below in Table 5.13.5.

Table 5.13.5: Worst Case Hot, Cold Conditions for Louver-Integrated WEB [PPT-9, 10].

Max/Min Temp.		$\epsilon_{\text{eff}}$ [PPT-9]		$F_{\text{rad, space}}$ [PPT-10]		Waste Power		$P_{\text{sun}}$ per $\text{m}^2$	
50 °C	-30 °C	0.71	0.115	0.65	1	90 W	0 W	34.9 W	0 W

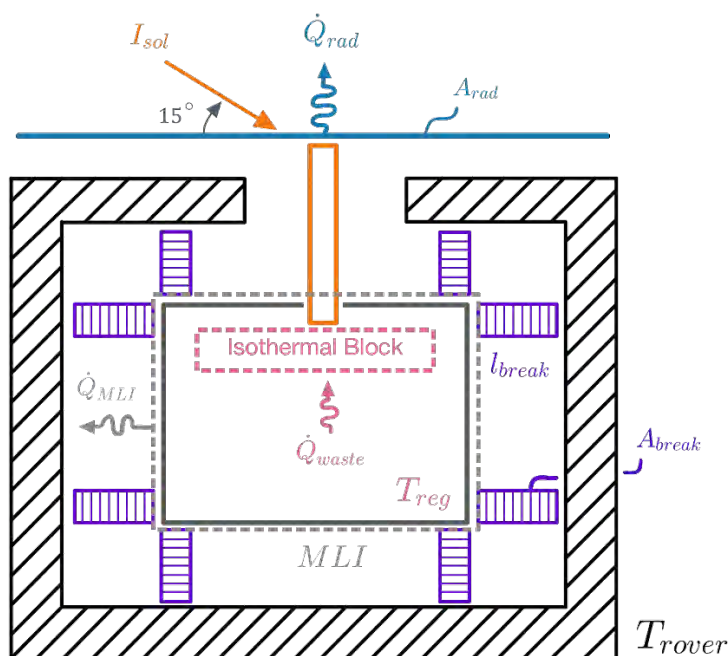


Figure 5.13.9: Hot Case Setup for Warm Electronics Box Thermal Analysis.

Performing a radiation balance on the system for the worst-case hot condition, the required radiator size was determined to be 0.37  $\text{m}^2$ . In the cold case, due to the lower temperature at which the rover is controlled to (-50 °C), power will be dissipated from the WEB to the rover body both radiatively through the MLI, and conductively through the thermal breaks. These losses were determined to be 0.78 W and 1.81 W, respectively. In addition to this, the dominant mode of heat loss in the cold case is through the louver blades themselves, accounting for 10.4 W of parasitic heat loss. Therefore, the total power required to maintain the minimum control temperature of the WEB was determined to be 13.0 W. These results are tabulated below (Table 5.13.6).

Table 5.13.6: Warm Electronics Box Radiator Area and Thermal Control Heating.

WEB Radiator Area	WEB Thermal Control Heating
0.37 m <sup>2</sup>	13.0 W

#### 5.13.4 - Battery Thermal Control – Adebayo Odusami

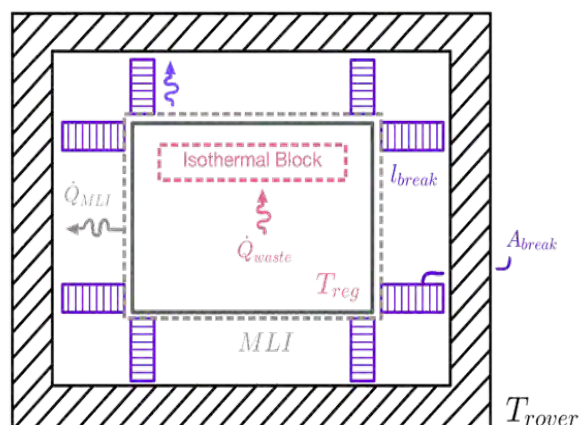


Figure 5.13.10: Setup for Warm Battery Box Thermal Analysis.

Our Warm Battery box was thermally isolated using Teflon thermal blocks to remove heat. We estimated the Teflon thermal break resistance to be about 0.1 W/-K and used 25 layers of MLI. We then calculated that the waste from the battery itself was about 2 Watts for our highest loading case. In our hottest case, the maximum operating temperature for the batteries is 313 Kelvin, and our maximum rover internal temperature is 300 Kelvin. In this case, we are generating around 2 Watts of waste heat, and the maximum internal heat that we can generate in the battery before the equilibrium temperature is greater than the maximum temperature is **7 watts**. Therefore, we have a margin of about 5 watts in our hot case. In our coldest case, our battery box minimum operating temperature is 253 Kelvin, and our minimum rover temperature is set at 223 Kelvin. This means that when the temperature inside the rover goes below 253

$$P_{rad} = \sigma \epsilon A (T_2^4 - T_1^4)$$

$$P_{cond} = \frac{KA(T_2 - T_1)}{L}$$

$$P_{total} = P_{rad} + P_{cond}$$

Kelvin, a certain amount of heat would be required to keep our internal battery box temperature at 253 Kelvin which is its minimum operating temperature. To do this, we calculated the heat lost to radiation and conduction for different temperature intervals from 253 to 223 kelvin using the **equations on the left**, and this would be the amount of heat we would need to provide to the battery box. Our calculations gave us a max heat power of

10W to be provided for the coldest case. The table below shows the parameters that were used for our thermal modeling calculations.

Table 5.13.6: Warm Battery Box Heat Calculation Parameters.

Area	Height	Waste Heat	Break Area	Break Length	Break K	No. MLI	MLI $\epsilon$ [PPT-8]
1.5 m <sup>2</sup>	0.4 m	2 W	0.1 m <sup>2</sup>	0.1 m	0.1 W/m-K	25	0.015

Table 5.13.7: Warm Battery Box Heat Calculation Summary.

<b>Battery Temp Interval</b>	253K – 313K
<b>Rover Temp Interval</b>	223K – 300K
<b>Max Power Draw</b>	3200 W
<b>Cell Resistance <sup>[PPT-17]</sup></b>	0.001 $\Omega$
<b>Current Per Cell</b>	2.4 A
<b>Waste Heat</b>	2 W
<b>Max. <math>P_{int}</math> (Hot Case)</b>	7.0 W
<b>Max Power Needed (Cold Case)</b>	10 W

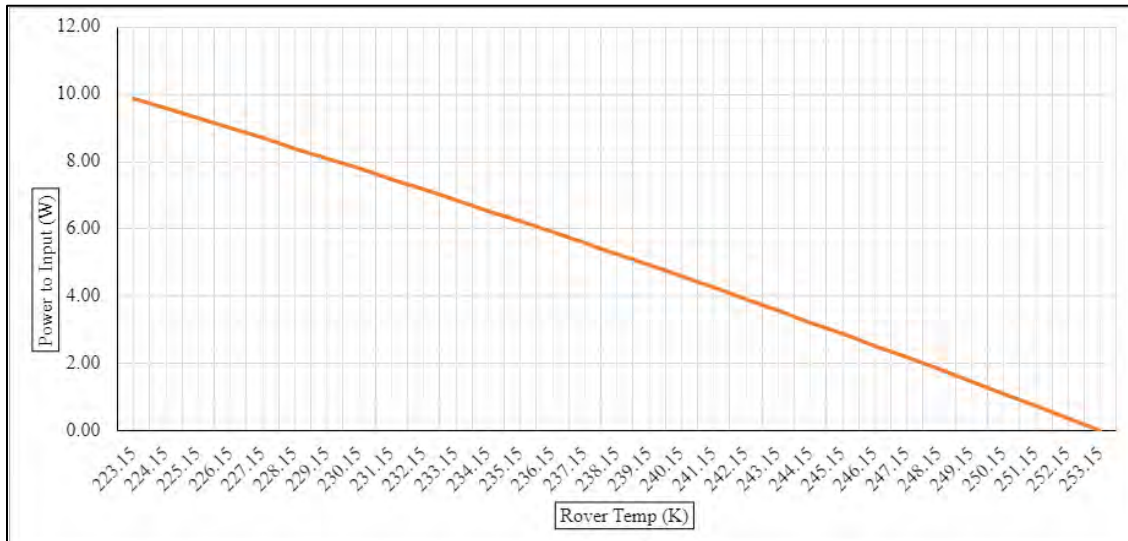


Figure 5.13.11: Power needed to keep WBB warm at different Temperatures.

#### 5.13.5 - Rover Body Thermal Control – Joshua Batstone

Maintaining the rover's body temperature is a central part of the thermal control system of the LLV, as it serves as the main conductive heat path for all other subsystems, while also housing thermally controlled components of its own. Perhaps the most critical of these is the 80 kW-hr lithium-ion battery, which must be maintained to within the relatively tight temperature band of (-20 to 40 °C). In order to allow the battery and other components integral to the power distribution system to dissipate their heat, the rover must be maintained at a lower temperature than the battery box. Based on this requirement, we set the upper control temperature of the rover body to be 25 °C. The lower control temperature was selected to be -50 °C, corresponding to the minimum design temperature of the motors, which should allow for relatively simple thermal control design for any internal actuators, cameras, and other electronics.

For this first-pass analysis, all surfaces are assumed to be covered by the same 25-layer MLI used in other analyses, with an effective emissivity of  $\epsilon_{eff} = 0.016$ , and an effective

absorptivity of  $\alpha_{eff} = 0.003$  [PPT-9]. It is worth noting that for the inner (working) surfaces of the rover (faces  $e$ ,  $b$  in Fig. 5.13.12), MLI is likely not a valid insulative option over the entire surface, due to pinching and compression concerns. Therefore, over these working surfaces (which will make direct contact with payloads via the standard payload interface, or SPI), a more durable insulative coating would be required.

In order to estimate the thermal equilibria of the rover body, we first simplified the geometric model by removing the wheels, latching extrusion, and other smaller features (see Fig. 5.13.12). The faces of the rover were then labeled and individually handled for both the hot and cold cases.

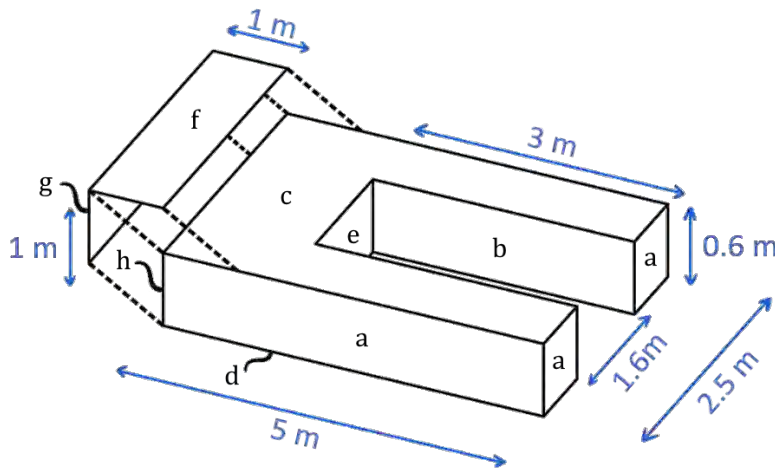


Figure 5.13.12: Simplified Rover Body Setup for Thermal Analysis.

From Fig. 5.13.12, faces  $g$  and  $f$ , corresponding to the solar array and radiator surfaces on the spoiler, are considered to be (for the most part) thermally isolated from the rest of the rover body, and so are not considered in either hot or cold analyses. Under nominal design conditions (habitat transportation), faces  $b$ ,  $c$ , and  $e$ , are considered fully occluded by the payload, meaning that in the hot case, they experience neither radiative absorption nor emission. In the cold case however, face  $c$  is assumed to have a clear view of the sky ( $F_{c,space} = 1$ ), faces  $b$  are calculated to have an approximate view-factor of 0.44 to both the sky and the ground ( $F_{b1,b2} \cong 0.12$ ) [PPT-10], and face  $e$  is calculated to have a view-factor of 0.43 to both the sky and the ground ( $F_{e,bs} \cong 0.14$ ) [PPT-10]. Faces  $a$  are assumed in both cases to have view-factors of 0.5 to both the sky and the ground, and face  $h$  is assumed to have a 0.5 view-factor to the ground, and a 0 view-factor to the sky (with the majority of upward pointing radiation assumed to hit the undersides of faces  $f$  and  $g$ ). Lastly, face  $d$  is assumed to have unobstructed visibility to the ground ( $F_{d,ground} = 1$ ). These view-factors, along with their respective areas, are tabulated below in Table 5.13.8.

Table 5.13.8: Rover Body Face View-Factors and Areas.

Face(s)	Area (m <sup>2</sup> )	Hot Case		Cold Case	
		$F_{view, space}$	$F_{view, ground}$	$F_{view, space}$	$F_{view, ground}$
<b>a</b>	<b>6.57</b>	<b>0.5</b>	<b>0.5</b>	<b>0.5</b>	<b>0.5</b>
<b>b</b>	<b>3.6</b>	<b>0</b>	<b>0</b>	<b>0.44</b>	<b>0.44</b>



<b>c</b>	<b>7.85</b>	<b>0</b>	<b>0</b>	<b>1</b>	<b>0</b>
<b>d</b>	<b>7.85</b>	<b>0</b>	<b>1</b>	<b>0</b>	<b>1</b>
<b>e</b>	<b>0.93</b>	<b>0</b>	<b>0</b>	<b>0.43</b>	<b>0.43</b>
<b>h</b>	<b>1.5</b>	<b>0</b>	<b>0.5</b>	<b>0</b>	<b>0.5</b>

In the worst-case hot condition, the radiation emitted from the rover will be dictated by the view-factors and areas in Table 5.13.8, assuming a ground temperature of 250 K. Both primary and secondary sun heating will occur on faces *a*, *h*, and *d*, with direct sunlight hitting faces *a* and *h* as shown in Fig. 5.13.13 and the bottom face *d* at an angle of 5°, and albedo effects depending on each face's view-factor to the ground. From this, the direct sun heating was calculated to be 16.4 W, and the net albedo heating was determined to be 4.31 W, assuming a surface albedo of 121 W/m<sup>2</sup>, as with previous analyses.

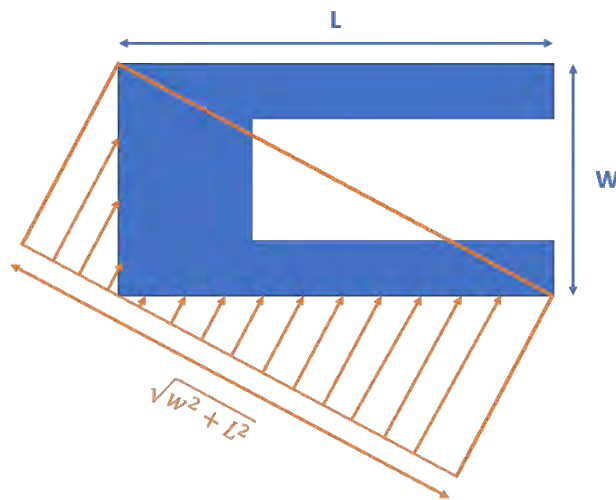


Figure 5.13.13: Worst Case Hot Direct Sunlight.

Under these worst-case hot conditions, the body temperature can be plotted as a function of internal power (internal waste heat), which yields the following graph (Fig. 5.13.14).

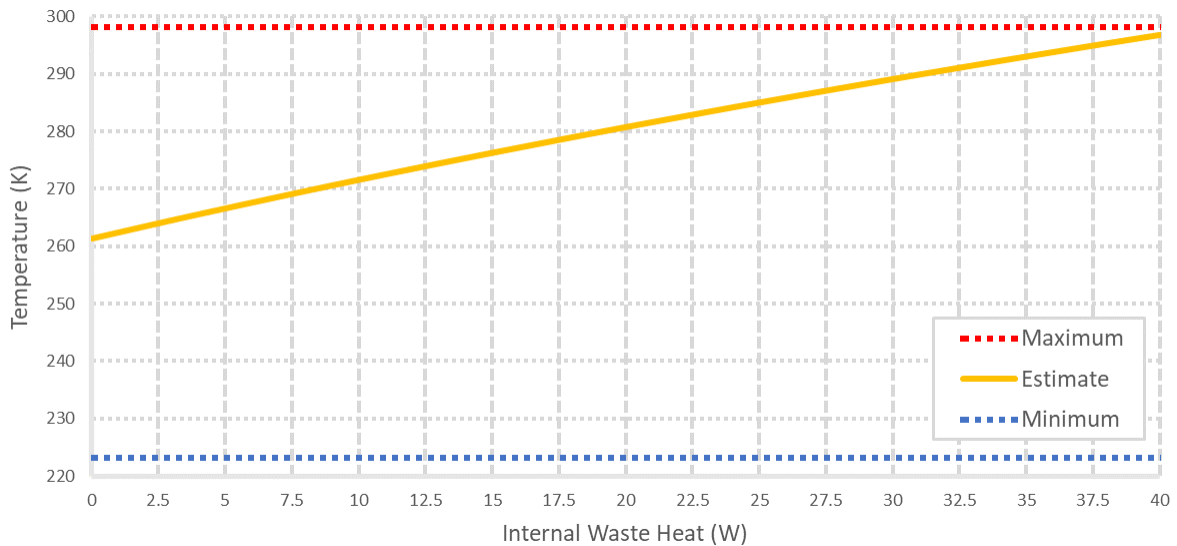


Figure 5.13.14: Estimated Maximum Body Temperature vs. Internal Waste Heat.

For a total internal waste heat of less than approximately 40 W, the rover is able to maintain its nominal temperature to below its maximum of 25 °C. For the cold-case analysis, the radiative view-factors and areas in Table 5.13.8 (cold case) were once again used, resulting in a minimum of 57 W to maintain a minimum temperature of -50 °C. Since all heat used to maintain the battery temperature is dissipated directly to the rover, we can subtract this amount (10 W), resulting in a net heating of 47 W. These results are tabulated below (Table 5.13.9).

Table 5.13.9: Rover Body Maximum Nominal Waste Heat and Heating Power.

Maximum Waste Heat	Rover Body Thermal Control Heating
40 W	47 W

### 5.13.6 - Solar Array Thermal Control – Nicholas Delafuente

During the lunar day and night, solar panels can only withstand a certain temperature before there is a major efficiency drop off or a potential break. To thermally regulate the solar cells, the environmental temperatures of the Moon must be known, as well as the ideal equilibrium temperatures of the solar cell. From the mission planning requirements, it is known that the coldest temperature the Moon will experience is -230 C and the hottest is -25 C. For solar panels to still be functional, the temperature band it can operate at is -80 C to 100 C [PPT-23]. However, to keep the entire rover thermally coupled as well as keep the efficiency of the solar panels at 34.2%, the ideal temperature bands were -50 C to 85 C.

Once the ideal equilibrium temperatures were established, there needed to be a way to thermally model the solar panels. The best method discovered was to do a two layer model where the top layer does all of the emitting and the bottom layer does all of the absorbing. Here, the top layer is a sheet of transparent glass with emissivity of 0.899, and the bottom layer as the solar panel with an effective absorptance of 0.578.

Since there is a hot and cold case, there must be two different thermal analyses. First, the hot case was considered. The highest angle of the Sun was 13 degrees, which effects the albedo. By setting in an equilibrium temperature of 85 C, it was discovered that it would take 260 W to radiate out all of the heat. In order to do this, a louvered radiator must be installed. By making it louvered, the heat is able to be released during the day and stowed during the night. Using the 260 W and a 20% buffer, the radiator size came out to be 0.44 m<sup>2</sup>.

For the cold case, after running the thermal analysis at -50 C for the equilibrium temperature, the results showed that it would take about 200 W to control. This is a potentially unachievable number, which means that the solar panels needed insulation during the night. To fix this, a door of multi-layer insulation (MLI) was installed to close over the solar panels. Since they are not charging at night, they do not need to be revealed. The MLI has an emissivity of 0.015 and an absorptance of 0.003. Using the new surface as well as the data from the radiator, the new power necessary to keep the equilibrium temperature at -50C came to less than 8 W. Attached below is an example of the setup for the hot and cold cases as well as the results.

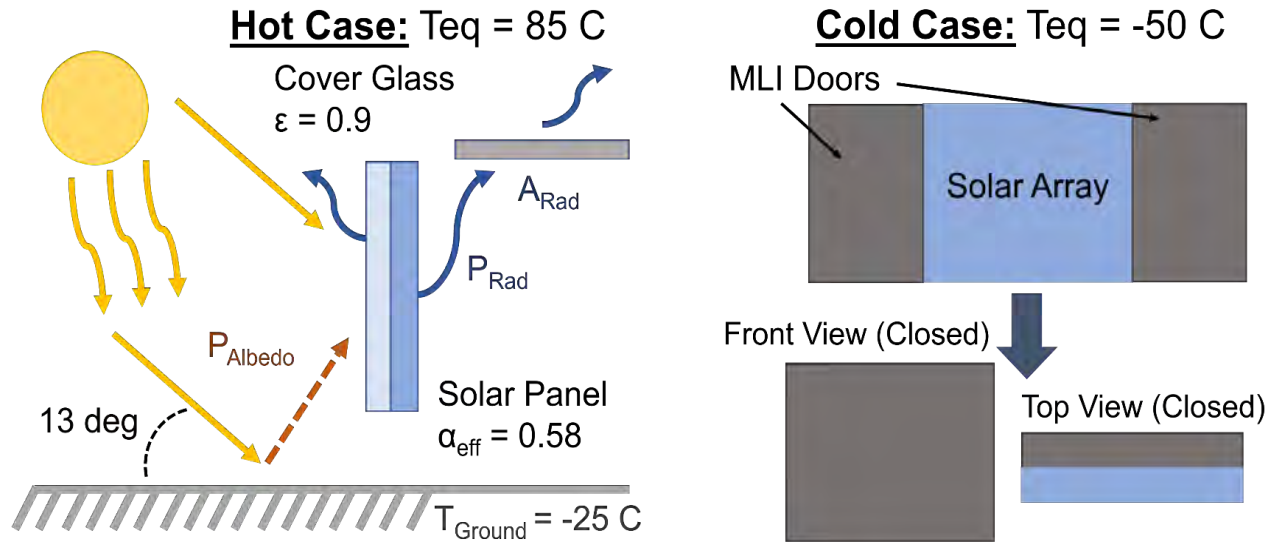


Figure 5.13.15

	Hot Case	Cold Case
Power Out (W)	$P_{rad} = 260$	$P_{cold} = 7.7$
Radiator Sizing ( $m^2$ )	0.44	

Table 5.13.10

## 5.14 - Dust Mitigation

### 5.14.1 - Dust Mitigation – Nicholas Delafuente

With solar cells and cameras, dust can be a major issue. Obviously dust sticking on the lens of a camera will reduce the visibility and make the tasks more difficult. With solar cells, dust reduces its efficiency. Since power generation is one of the most important aspects of SHELL, dust must be mitigated. There are two methods of approaching it: active and passive. With active methods, power will be required, whereas passive it will not. There are a lot of new technologies that are being developed, but below were the main considerations for active dust mitigation system.

Technology	Process
<b>Vibration using Piezo-Electric Actuators</b>	Vibration from actuators causes dust to fall off (demonstrated on Mars in 2007, 90% effective)
<b>Electrostatic and Dielectrophoretic Forces</b>	Send high voltage AC through parallel electrodes on surface
<b>Plasma Lofting Electron Beams</b>	On day side of the moon, surface nets positive (Sun radiation kicks off electrons). On dark side, surface nets negative (Sun plasma). Combine plasma coating with electron beaming to kick off charged dust particles
<b>Electrodynamic Dust Shield (EDS)</b>	Electrodes create a non-uniform electric field over the surface that needs protection, vibrating dust off

Table 5.13.11: Dust Mitigation Methods [PPT-24,25,26]

Taking a closer look at the dust mitigation techniques, it seemed there were only a few feasible options. Actuators and electrodynamic dust shield (EDS) are both over 90% effective, so those routes were explored further. As far as the piezo-electric actuators work, it is said that they need a high driving voltage and still the displacement is not as good as it should be [PPT-27]. Even without the setbacks of the piezo-electric actuators, after research, the electrodynamic dust shield was said to be over 98% effective [PPT-28,29]. From this discovery, the focus was on the EDS. As mentioned above, this uses electrodes to create an electric field, which ultimately causes dust to be vibrated off.

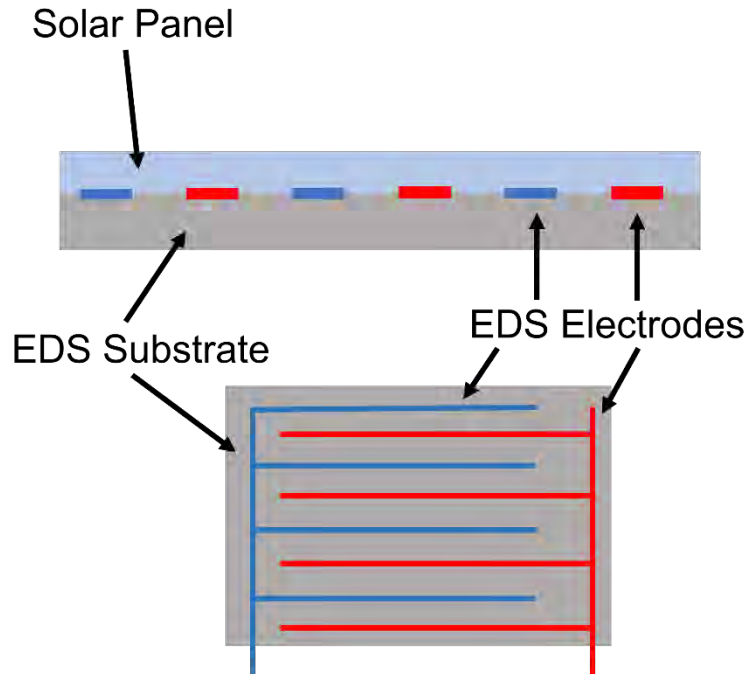


Figure 5.13.16

The diagram above is an example the setup of the electrodynamic dust shield with the solar cell. The substrate goes beneath the solar cell and the electrodes are between the substrate and the solar cell.

The second approach to dust mitigation is through passive methods. The most popular and efficient appeared to be a thin layer of titanium or titanium dioxide on top of the desired surface. This is a very hard and uniform layer which makes it difficult for dust to stick. For instance, a titanium dioxide coating of 40-80nm thick can remove 50% more dust than the bare glass surface of a solar cell [PPT-30]. The only potential issue of placing a coating on the surface of a solar panel is the emissivity changing, which would cause the thermal control system to be different than anticipated. However, the titanium dioxide coating is transparent, which means it has the same emissivity of the glass surface.

By being able to have a 98% efficiency from the electrodynamic dust shield, as well as an increased dust resistance from the surface of necessary components, dust mitigation should be very successful. Below is an example of the final design of the solar cell.

Figure 5.13.16

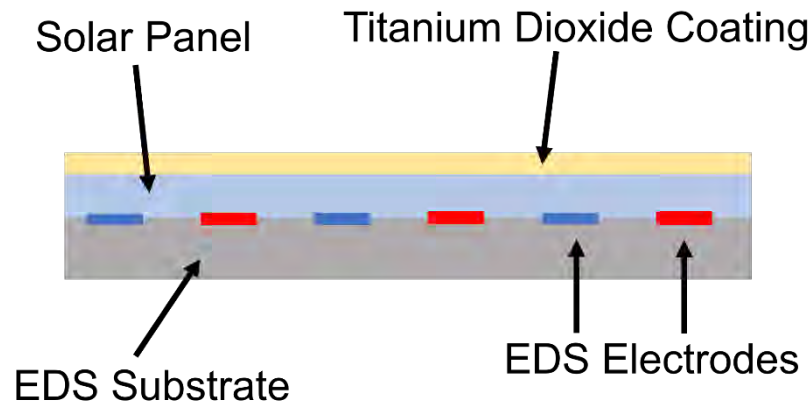


Figure 5.13.17

### 5.15 - Avionics Block Diagram – Matthew Visnich

Going into the avionics, communications, and management of the lunar logistics vehicle, categorizing different sections of components and their relations to others was one of the first things constructed. Green communication lines and red operating voltages between these sections, categorized as command and data handling, power management, communications and sensing, and motor systems are organized on the following block diagram. More specifically, a high-level display of the systems themselves, represented by different colored blocks, are shown on this diagram. It should be noted that the means of communication between each system is handled through a local area network connected via ethernet cables; while not the most modern communication method, the ethernet is still sufficient for data that is transmitted.

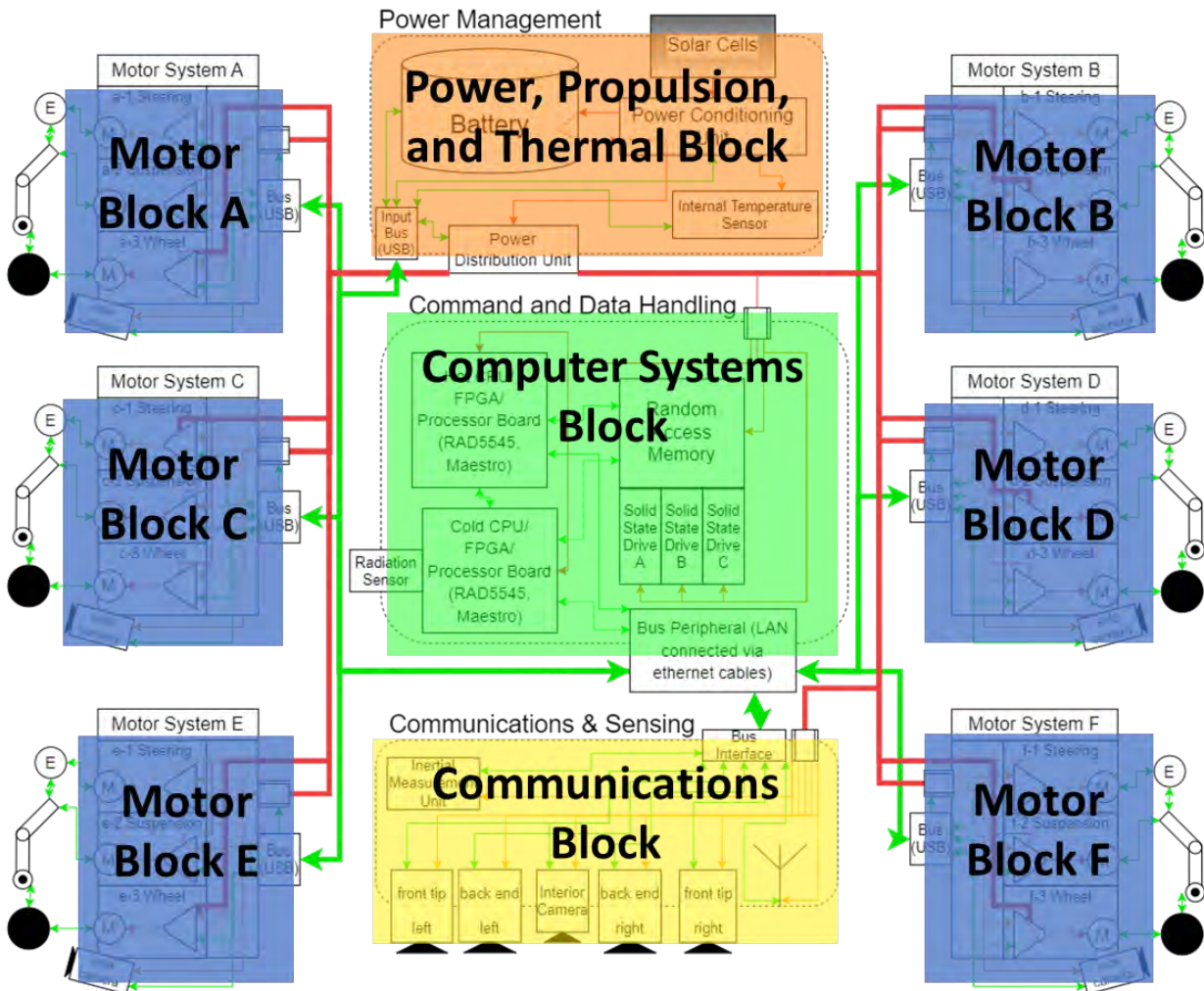


Figure 5.15.1: Avionics Block Diagram Overview

### 5.15.1 - Description of Various Blocks – Matthew Visnich

When reviewing the different sections of the avionics block diagram themselves, each block includes their own components that, although might not necessarily be embedded next to each other on the potential prototype of the vehicle, provide a function relevant to the block they have been placed in.

The “brains” of the lunar logistics vehicle lie in the computer systems/command and data handling block. Both processing units, hot and cold for radiation hardening purposes, are housed here along with random-access memory and three solid state drives for up to 192 gigabytes of memory management and storage. The units are interconnected to all other components within the vehicle through local area network ethernet lines from a large bus peripheral on the bottom. Some dashed lines run from the cold unit to the memory and peripheral; these are to indicate dormancy during normal operations and will only become active when the radiation environment overwhelms the hot central processing unit. Electricity is provided to the computers and memory

devices from power management in the form of red high (bus) voltage and orange regulated medium voltage from the voltage regulator in the top right of the block.

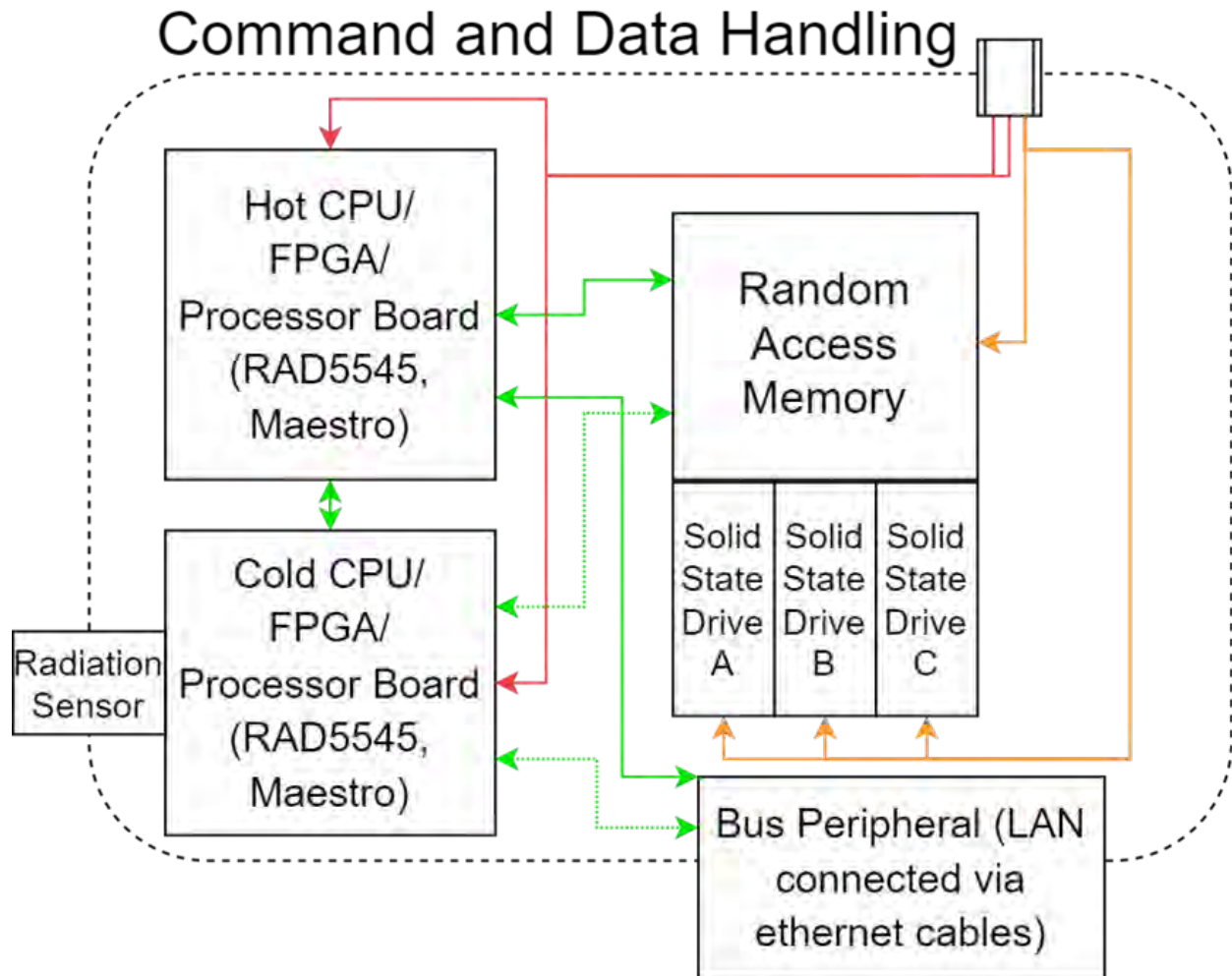


Figure 5.15.2: Command and Data Handling

Responsible for collecting, storing, and distributing power throughout the entire vehicle, the power management block provides the most important function second only to the computer systems block. Through the bus peripheral in the bottom left, the command and data handling unit has communication lines to each component within the block barring the solar cells which are not an avionics-based components themselves but feed power into the power conditioning unit which is both stored in the battery then distributed throughout the vehicle as high bus voltage. Additionally, an internal temperature sensor is housed in this block, as well as in our potential vehicle prototype, and is responsible for alerting the computer systems of any irregularities that may occur here.



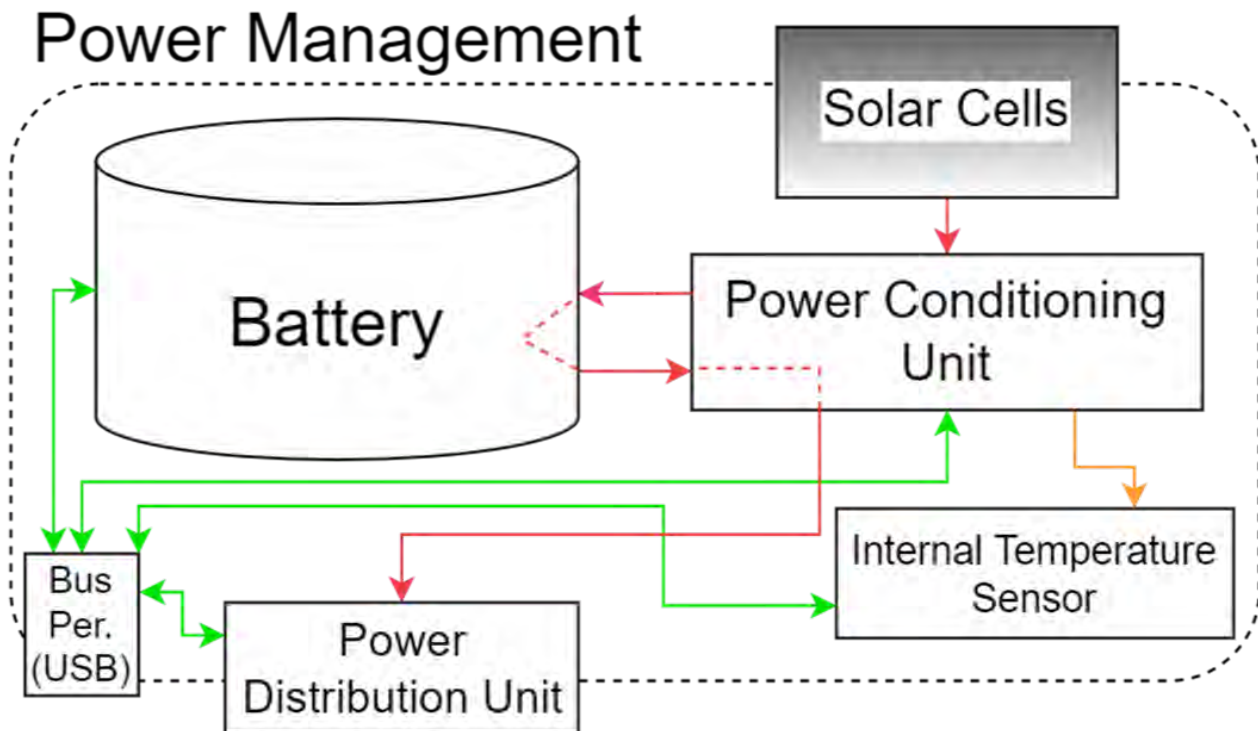


Figure 5.15.3: Power Management

Next is the Communications and Sensing block, encompassing all confirmed avionics components that help the vehicle sense its immediate surroundings and communicate as far away as an Earth ground station. The former function is accomplished with an inertial measurement unit and four optical cameras as well as a fifth camera placed in the center of the U-shape part of the vehicle to provide visuals to logistics items that are transported. The function of the latter is accomplished with a 26 gigahertz high gain antenna placed in the bottom right corner. Because the power requirements for communications were kept to a minimum, all the components have their power supplied through another voltage regulator placed in the top right corner. This power limit also prevented us from placing more advanced means of sensing in this section such as lidar, which was discussed as early as the preliminary stages but was ultimately cut.

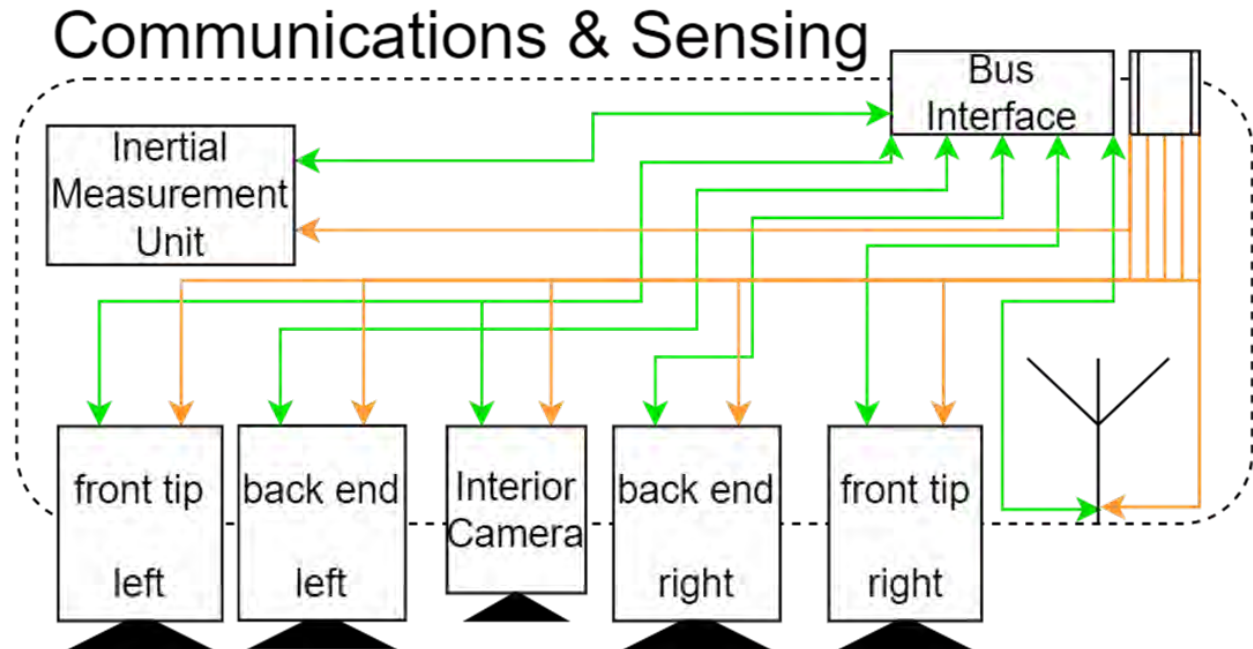


Figure 5.15.4: Communications and Sensing

The final blocks to discuss are the six sets of motors where, unsurprisingly, much of the high bus voltage is delegated to moving, steering, and suspending the desired logistical item, the latter of which must be at 0.95 m off the ground. The top left motor is shown below, containing the most indirectly labelled components of any block. Each set contains three motors which, going from bottom to top, control the speed of the wheel, movement of the active suspension, and steering of the wheel (aided by encoders). Each motor, barring the one handling steering, is the primary recipient of the high bus voltage from the power distribution unit, hence the red lines, and is activated by controllers that take in logic and input voltages from the computer represented by the green and orange arrows respectively. Each set of motors also has a camera mounted next to its wheel to view any potential obstructions and other hindrances that could affect the motion.

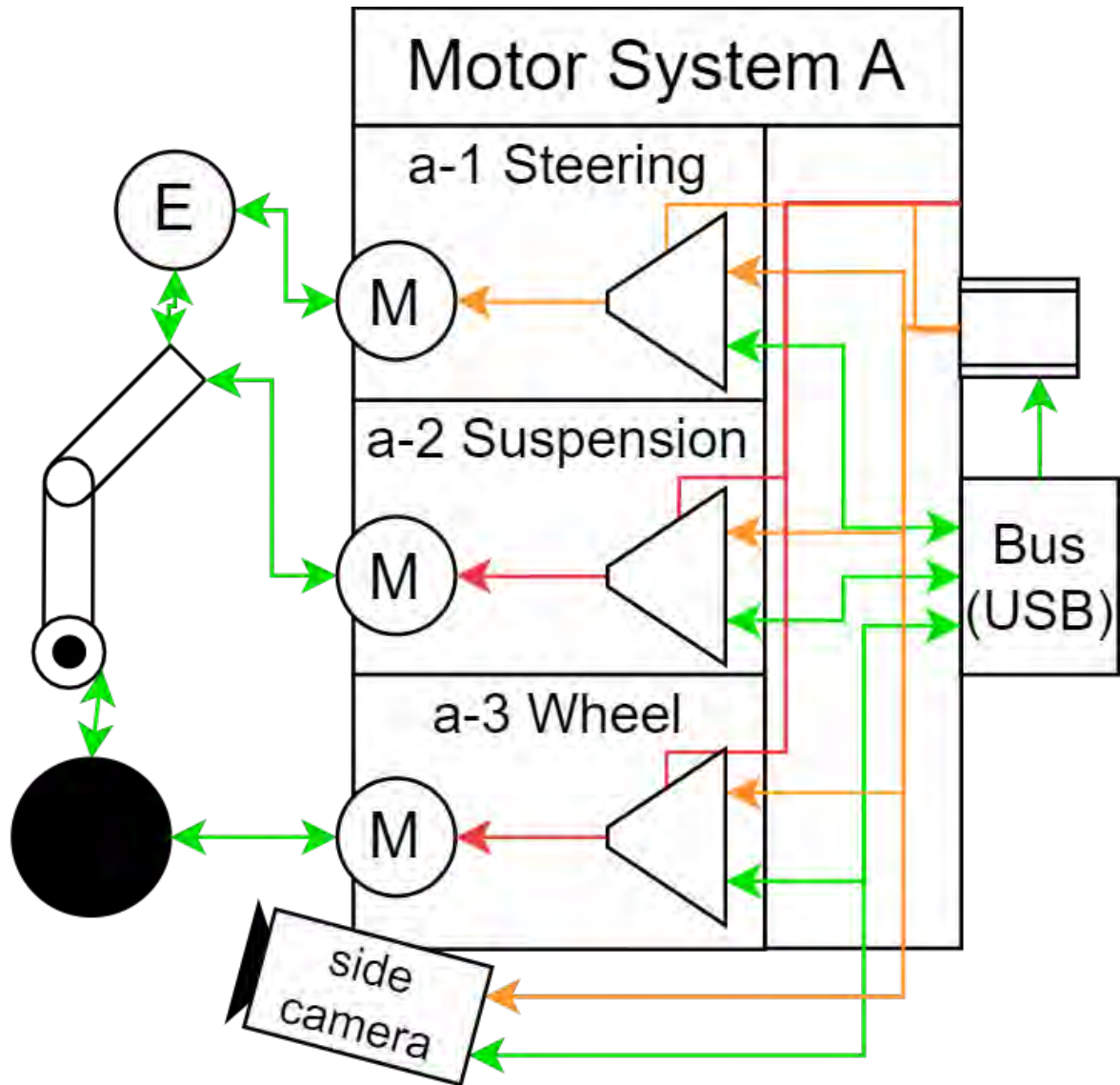


Figure 5.15.5: Motor System A

### 5.16 - Communications Architecture – Edwin Arevalo

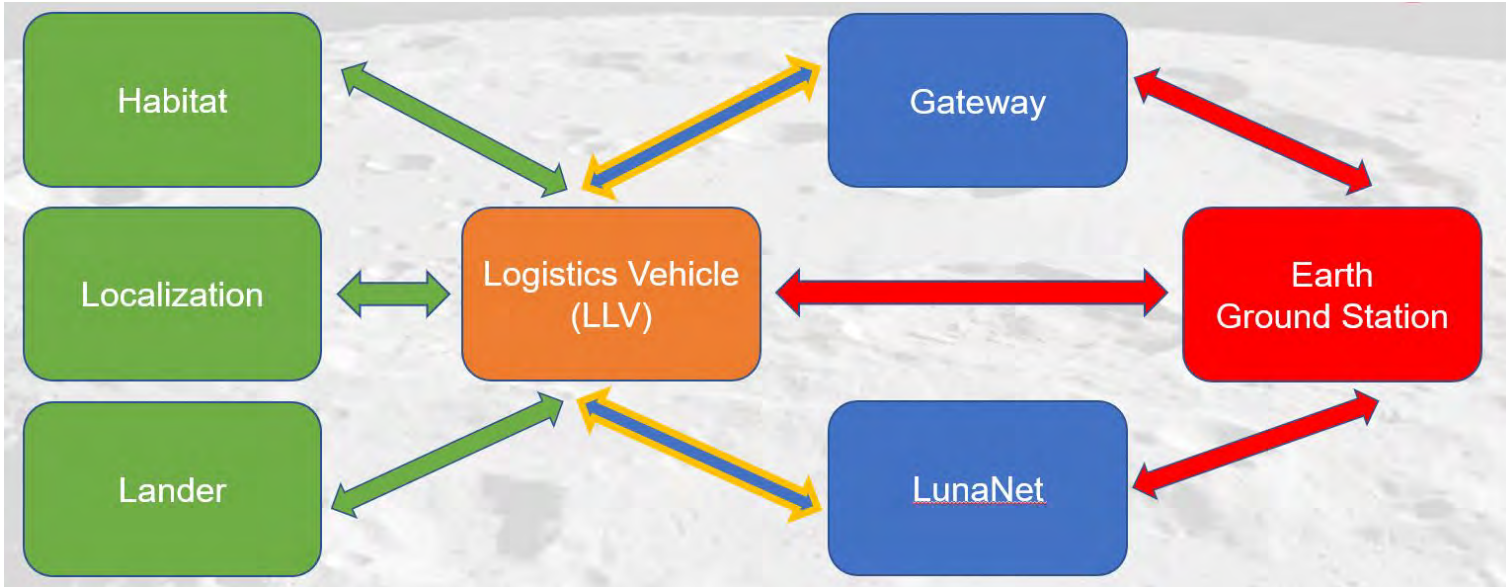


Figure 5.16.1: Communications Block Diagram

For the communications design of our vehicle, we wanted to have as much signal coverage as possible while on the lunar surface. Since our vehicle will not always have a direct line-of-sight to earth, relay satellites must be used to remain in communication with ground stations. As depicted in the diagram above our vehicle will also have the capability to communicate with various lunar assets such as a habitat, localization beacon, or lander. The three main relay satellites systems we looked into is Gateway and LunaNet, both of which made by NASA, and Lunar Pathfinder made by ESA. We conducted our trade study based on the following criteria:

Criteria	Reasoning
Coverage	How well the system provides coverage to the lunar surface -- important for consistent communication with earth.
Modularity	How well the system can be improved to increase coverage -- important for the longevity of the mission.
Reliability	How likely the system is to be up and running before the start date of our mission, takes into consideration current research and development states, and any available budget information.
Capacity	Roughly how used the system will be by other missions -- important to see how dedicated the system will be to our specific mission
Features	Does the system provide other capabilities such as Wi-Fi or a 5G network.

	Coverage	Modularity	Reliability	Capacity	Features	Total Score
--	----------	------------	-------------	----------	----------	-------------

Gateway	3	1	5	3	2	14
LunaNet	4	5	3	4	4	20
Lunar Pathfinder	3	2	4	4	3	16

Figure 5.16.2: Criteria + relay satellite trade study scores

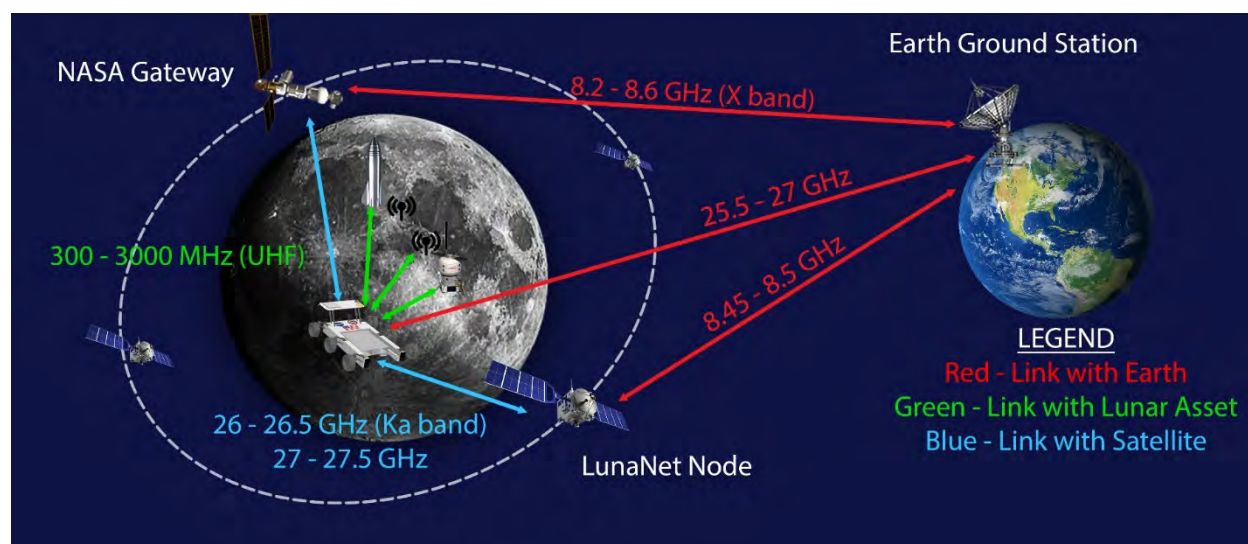


Figure 5.16.3: Communication breakdown

Although all relay satellite systems have a planned initial start date earlier than our 2028 planned start date and should in theory be up and running delays do happen and a reliability score was given based on how much available information there is to the public on the system. Based on the criteria stated above, an overall score was given to each relay system. Firstly, we took a look at NASA's Gateway which will be capable of communicating in both the S-band and Ka-band. Although NASA's Gateway currently looks like a great option to due to its very near launch date of late 2024 and plethora of supporting documents and information publicly available it was given a perfect score for reliability. However, Gateway is multi-purpose manned orbiting lunar outpost. It can conduct science research as well as help support other deep space missions [AFSS-7E]. With that being said, Gateway is not solely designed as a relay satellite and for that reason did not score well I other criteria. Further down the road Gateway is surely going to get occupied by other, possibly more pressing, lunar missions. For that reason, Gateway scored the lowest of the group. Next, we took a look the Lunar Pathfinder, the world's first dedicated lunar communications relay spacecraft that has a set launch date of 2024 [AFSS-1E]. Lunar Pathfinder is a single commercial satellite designed by Surrey Satellite Technology Ltd that is offering its services to the world and already has signed contracts with the European

Space Agency (ESA) to support its Moonlight initiative to bring communication and navigation services to the moon and NASA to support the Artemis program. However, the design for Lunar Pathfinder is only a single spacecraft at a time and each spacecraft can only operate in S-band and UHF; this may limit the amount of data that it is capable of relaying at high speeds. For that reason, Lunar Pathfinder received low scores in both coverage and modularity. Finally, we took a look at NASA's LunaNet program which is a modular relay satellite that initially consists of 3 spacecraft nodes for ample coverage and high connectivity times. Initial capabilities are focused on near continuous coverage of the south polar region [AFSS-12E]. Additionally, LunaNet has made it explicitly clear that they are designing for Network-to-Network Trunklinks that allow communications between two network infrastructure nodes with the end goal to have a constellation of satellites covering the lunar orbit [AFSS-6E]. This means that as time progresses, and more nodes are sent into orbit the network will only grow stronger. On the downside, we could not find a specific initial start dates for LunaNet but found multiple supporting documents that suggest LunaNet will support NASA's mission to have a sustainable presence on the lunar surface by 2028 [AFSS-6E]. For the reasons stated above LunaNet was given a low reliability score but nearly perfect marks in all other criteria. At the end of the trade study LunaNet was found to be the best solution to our communication crisis and a proposed communications architecture is seen in the figure below.

Initially we thought it necessary to have three separate antennas: a S-band to communicate with lunar relay satellites, Ka-band to communicate with earth, and a UHF antenna to communicate with lunar assets. However, based on our data requirements, available ground site operating frequencies, and LunaNet's extensive capabilities we were able to eliminate the need for an S-band antenna. Instead, we will rely on a single Ka-band antenna for both direct-to-earth transmission and communication to relay nodes while still maintaining the need for a UHF antenna to communicate with other lunar assets [AFSS-6E].

	Coverage	Modularity	Reliability	Capacity	Features	Total Score
Deep Space Network (DSN)	5	N/A	5	3	N/A	13
Lunar Exploration Ground Sites (LEGS)	5	N/A	4	5	N/A	14

Figure 5.16.1: Ground station trade study scores

A similar assessment was done for the available ground stations that our system would most likely be using. The two systems in question are Deep Space Network (DSN) and Lunar Exploration Ground Sites (LEGS). DSN is currently up and running, however, it is already being heavily used and therefore received a low capacity score. On the other hand, the construction for the LEGS is still yet to be completed but great progress has been made and, as the name suggests, these ground stations will solely support lunar mission therefore it received a high

capacity score. The available LEGS operating frequency's was also taken into account along with our data transmission requirement [AFSS-8E]. All-in-all, the LEGS was found to be the better of the two and we will most likely rely on it to service our communication needs.

### **5.17 - Data Budget -Brian Amaya**

The data budget was set by what would be needed to transfer data to the lunar that may be needed to operate the lunar logistics vehicle remotely and send data from the lunar logistic vehicle. To find the required bandwidth some factors need to be known. The most expensive operations in terms of bandwidth is the camera bandwidth.

The cameras that may be used while operating the car are the two front main cameras and the rear main cameras. These would be used to navigate the terrain. The combination of the front and rear cameras that are on the same side can be used to see the side of the vehicle, giving virtually a 360-degree view around the car with certain blind spots. This extended view allows for the operators to see around them and can be used by the vehicles computer to process images and find how far objects are and keep track of it to map obstacles in a local area and keep the vehicle from colliding into an obstacle.

The cameras are 1080p cameras that at 30 fps can be compressed to around 15-20 Mbps. They can be calculated by finding the bit depth of the cameras, the pixel numbers and the frames per second. They can be used to find the bits needed per second. This calculation turns to be the raw bit rate needed to process the video. This results in very high bit rates required that would need either a larger beamwidth or more power to transmit the raw video. Compressing the video can be done with standard compression methods. The one selected for this was x264. This is an open-source encoding scheme that allows for very efficient compression of video. Since the encoding ratio depends on the current situation and how much data the software needs to send to update the image. The bit rate may fluctuate. Using the values from a large streaming service [AFSS-3,4] we can assume the value for each 1080 p camera to be around 4.5 Mbps. There are better compression ratios that are available and open source that could be used. There are also other compression software or methods and other companies that use a different one that allow for higher compression ratio. The problem with some of the ratio compressions that are used by some companies is that they usually deal with prerecorded information so they can reference future frames to lower the data required to transfer. This is not possible with this system since the operators will want the most recent frames and not a stream of past events if they were to avoid obstacles and provide fast response time. The faster encoding schemes could be used but some of them need higher processing power than the systems computers can handle.

This encoding software could of course be traded but it would be difficult since the encoding ratio may be dependent on the scenario. If the image between two frames is drastically different, then more information will have to be sent. Since the system is moving slowly on the moon there may not be large differences between frames.

Using the value of 4.5 Mbps for each camera for 4 running simultaneously a bit rate of 18 Mbps. This accounts for the largest portion of the required bit rate. This can be assumed to be the max bit rate requirement for just the cameras for the lunar logistics vehicle. For docking the max camera usage may be 3 cameras. The rest of the bit rate budget will need to be for telemetry and

sending any other information to the ground station or the lunar habitat. The extra information that may be sent over will include things like local maps or extra information that can be processed by the operators. This can be information collected and then made a local map of the area and then can be sent to other systems. Looking at other systems like the James Webb space telescope [AFSS-9] a data rate of 200kbps were needed for telemetry. Since it cannot be found early into the development stage what extra information this rover might want to send an estimate of 2 Mbps were used for the telemetry and extra information. This allows for space in the bit rate budget for any of the additional information specified above. The system should also be capable of turning off cameras and just sending data at higher rates if it does need operator input or move at all.

Additional information may also be used for sending data from any cargo that is being transported. An example of this would be the pressurized logistic module. It may be useful to send information back to operators of the status of the module to allow them to know if anything may have happened to it during transport. This can be used for other systems too like future experiments that may want to use the lunar logistics vehicle for transport or as part of the experiment.

This brings a total bit rate requirement to 20 Mbps. This value was achievable with the communication and antenna architecture that is talked about in this paper. The additional bit rate for “additional information” accounts for a 10 percent margin.

Information Class	Bit Rate
Camera Streams	~18 Mbps
Telemetry	~200 Kbps
Margin	~1.8 Mbps
Total	20 Mbps

#### 5.17.1 - Antenna link budgets

Now that a data rate has been established the links can be determined. Since this system is being developed alongside the Artemis missions the system should comply with the communication systems that NASA plans to use for those said missions.

A few options were available to choose from, and the bandwidths had to be worked out a few times to see what the viable option was. The system that seemed to work best was a Ka-band frequency for communication with direct to earth communications and with relay satellites. This was useful as current and planned future systems will be in place that will have the same bandwidth available. For connectivity between lunar surface systems UHF was also specified as a possible solution. Since there has been no definitive habitat developed it can be needed that the habitat or lunar surface operators have access to UHF to be able to communicate and operate the lunar logistics vehicle. The habitat should also be able to communicate with the earth via either direct to earth or through a relay satellite at the required data rate we need. Requiring this should



be a large burden since it is expected these habitats will need to be in almost constant communication. If there are operators on the moon who have the time to operate the vehicle, then no video data has to be sent to earth.

The required power is a vital component when developing the system and calculating antenna specifications and link budgets. An important specification that had to be the system had to be developed around is the beamwidth angle. This parameter will let us know if we will be outputting the transmission power required for the signal to be decoded. The “baseline” beamwidth would be the angle needed so that the signal covers the entire earth. The beam width is a necessary parameter as this is a moving vehicle, it has to worry about the vehicle bouncing. This calculation can be done by calculating the max displacement that will occur to the vehicle over the max traversable bump height. This can then be used to find the speed the antenna needed to be able to steer to continue pointing at earth.

To get an estimate of how much the vehicle may move when traversing the lunar terrain, a simple model was made to see what the velocity of the vehicle would be if it went over a bump of the max height. The max height of 30 centimeters for obstacles that could be traversable was used, the speed of 20 centimeters per second was used as it was the case in most of all loading cases. The suspension and wheels were treated as rigid to get the maximum vertical speed that could happen. The wheel vehicle was modeled as driving at a constant speed and as it made contact with the rock there was no slip as slip would lower the vertical speed. It was assumed that as the wheel made contact it would grab be able to pull itself up. Assuming the momentum of the vehicle is much larger than the rock wheel interaction would dissipate the speed stayed constant through the initial impact. The height of the wheel was found by tracking the displacement. The displacement as found by assuming that after the contact and as it climbed over the obstacle, the wheel was also tangent and normal to the surface.

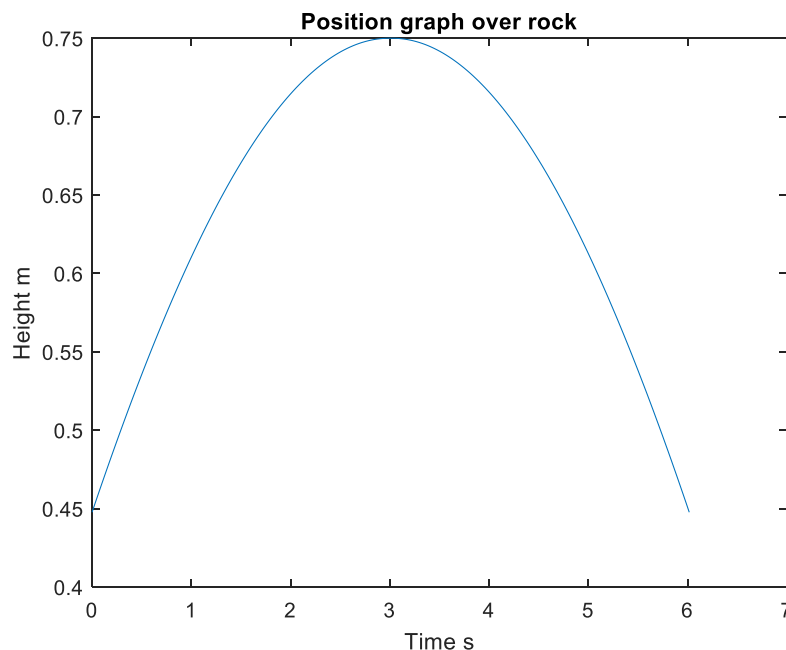


**Figure 5.17.1 showing the wheel displacement as it goes over rock**

The velocity can now be found on the graph showing. This is done by taking the assumption that velocity was constant and dividing the step size used for the x position to find the time step. This time step was then used to find the gradient of the vertical displacement.

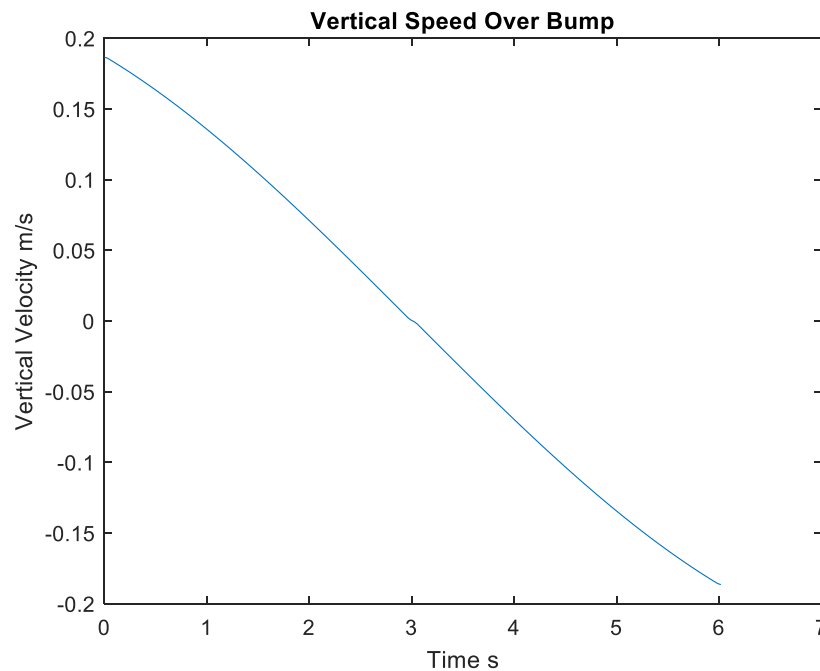


**Figure 5.17.2 Graph showing the velocity of the wheel going over a rock**

The vertical velocity can be found to be symmetrical with this model. The maximum velocity happens right at the beginning of the traversing over the obstacle. Using this the angular velocity of the body can be found. For the long axis of the vehicle this translates to an angular frequency of  $.046 \text{ s}^{-1}$ . The shorter side gives  $5 \text{ s}^{-1}$ . The antenna gimbaling system would need to be able to rotate  $.314 \text{ rad/s}$  to account for larger bumps like this. The small difference in the roll rate for the antenna in both directions means that an asymmetric parabolic dish could be used. This would allow for slightly less power usage. Since this is an approximation and the rates are very close to each other it does not seem feasible to design that specification.

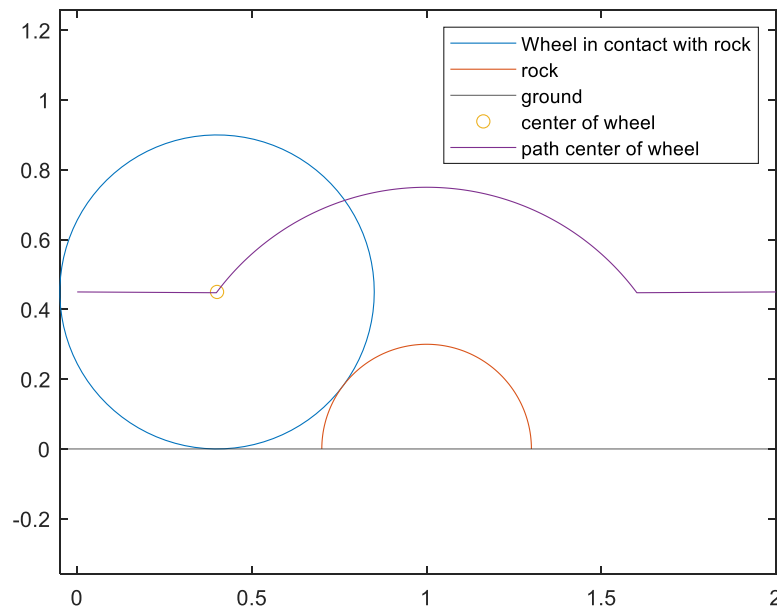


**Figure 5.17.3 showing the path the wheel would take over the rock**

The bandwidth that was used for preliminary calcs was around 4 degrees. This allowed for the earth to be covered in most scenarios. The habitat being a stable point on earth that is not moving will allow for a more stable connection.

To calculate link budgets sources for transmission losses, have to be used as well. Since this system has not been developed a lot of the losses come from sources for system design [AFSS-12 15 28] these are necessary as the losses make up most of the energy needed. Some losses accounted for include the free path loss, line loss, system temperature loss, lunar flux loss. Another factor is the data rate. A higher data rate will need higher transmission power.

The antenna being an integral part of the system has a major impact on the link budget. Parameters that can change include the antenna diameter, beamwidth, antenna gain and power. Usually when creating a link budget the antenna beam width will be calculated for and then be used for the system adjusting other parameters. Since this is a moving system, the beamwidth will be an important factor.

DNS	Rover		Freq GHZ	path length m	
	Power Provided	trans pwr DB	26	3.9E+08	
diamter	30	9.542425094	Losses	Antenna Gain DB	
	34 Efficiency		path loss	36.5512	
gain	0.3		-232.563		
	77 Trans Power W		TS		EIRP
Trans power dB	9		-28		45.5512
13.01029996	beamwidth perfect(deg)		RF loss Trans DB		
EBNO	2.440280639		-2		
16.48079837	Antenna Diameter		attenuation loss		
EBNO required	0.330983369		-1.7		
	10 data transfer bit/s		lunar flux loss fb		
	2.00E+07		-5		
			pointing losses		
Downlink Margin	6.48E+00		3		

**Figure 5.17.4. Direct to Earth Parameters and Specifications**

DNS	Rover		Freq GHZ	path lengt	
	Power Provic	trans pwr DB	26	70000000	
diamter	3	-0.457574906	Losses	Antenna G	
	1.25 Efficiency		path loss	36.5512	
gain	0.3		-217.643		
	48 Trans Power W		TS		
Trans power dB	0.9		-6.85714		
13.01029996	beamwidth perfect(deg)		RF loss Trans DB		
EBNO	2.44028064		-2		
16.24298685	Antenna Diameter		attenuation loss		
EBNO required	0.33098337		0		
	10 data transfer bit/s		lunar flux loss fb		
	2.00E+07		-5		
			pointing losses		
Downlink Margi	6.24E+00		2		

**Figure 5.17.5 Relay Satellite Parameters and Specifications**

UHF	Rover		Freq GHZ	path lengt	
	Power Provided	trans pwr DB	3	1500	
diamter	0.2	-12.2184875	Losses	Antenna G	
	1.25 Efficiency		path loss	3	
gain	0.3		-105.506		
	5 Trans Power W		TS		
Trans power dB	0.06		-22		
13.01029996	beamwidth perfect(deg)		RF loss Trans DB		
EBNO	2.440280639		-2		
2.49E+01	Antenna Diameter		attenuation loss		
EBNO required	0.1		0		
	10 data transfer bit/s		lunar flux loss fb		
	2.00E+07		-5		
			pointing losses		
Downlink Margin	1.49E+01		2		

### Figure 5.17.6 UHF Parameters and Specifications

#### 5.18 - Avionics Components – Justin DeVito / Matthew Visnich

The avionics components embedded in our lunar logistics vehicle are not the greatest in quantity but very specific in function. From our hot central processing unit responsible for the vehicle's normal operations to our antenna at a high gain frequency setting for communications between the lunar surface and our ground operations station, every component is based on a reliable counterpart, some commercial off the shelf, and has its power requirement under the allotted power limit for the avionics section.

##### 5.18.1 - Avionics Components Overview – Justin DeVito

Component	Quantity	Reference	Mass	Power Req.	Additional Specs.
Computer	2	<i>RAD5545</i>	2 kg	35 W	Single-board computer
SSD	3	<i>Greenliant</i>	0.5 kg	5-7 W	–
Navigation Camera	4	<i>Mars 2020 EECAM</i>	0.425 kg	< 10 W	≥ 1920 x 1080 resolution
Hazard Camera	8	–	–	–	–
IMU	2	<i>LN-200S</i>	0.748 kg	12 W	–
High-Gain Antenna	1	–	–	30 W	Parabolic, 26 GHz band, 0.33 m diameter

**Table 5.18.1: Avionics Components and Specifications [AFSS-1, 11, 25, 34]**

The vehicle will utilize a variety of avionics components for navigation, control, and communication. To determine specifications for these components for use in thermal, mass, and data budget calculations, we looked at flight proven hardware from similar missions.

##### 5.18.2 - Reference Processor Selection – Matthew Visnich

For the on-board computer, we sought out one that would provide useful power consumption and processing speed references. That computer came from this [paper](#) [AFSS-19] from the University of Florida that extracts data from and compares multiple space-graded processors: the BAE Systems RAD5545 quadcore central processing unit. Two of the benchmarks, representing performance and power efficiency from this processor, as well as two notable others, are plotted below on the graphs, measured in mega operations per second divided by a watt.

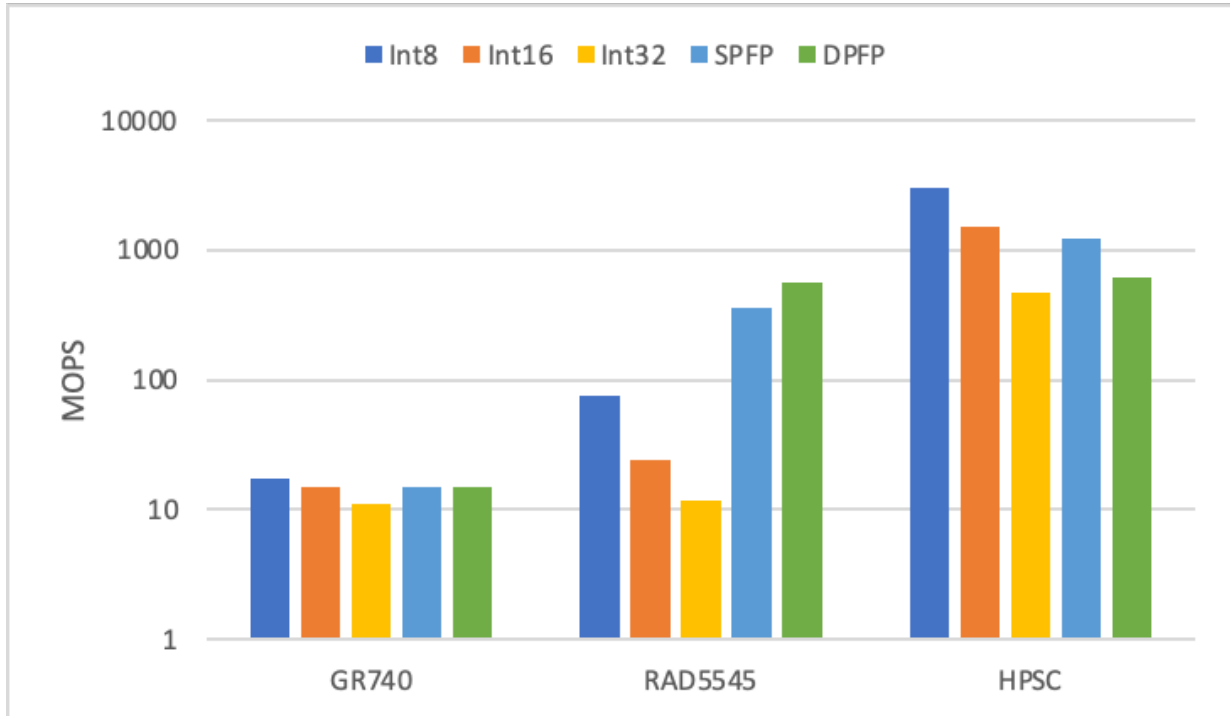


**Figure 5.18.1: Processor Performance**

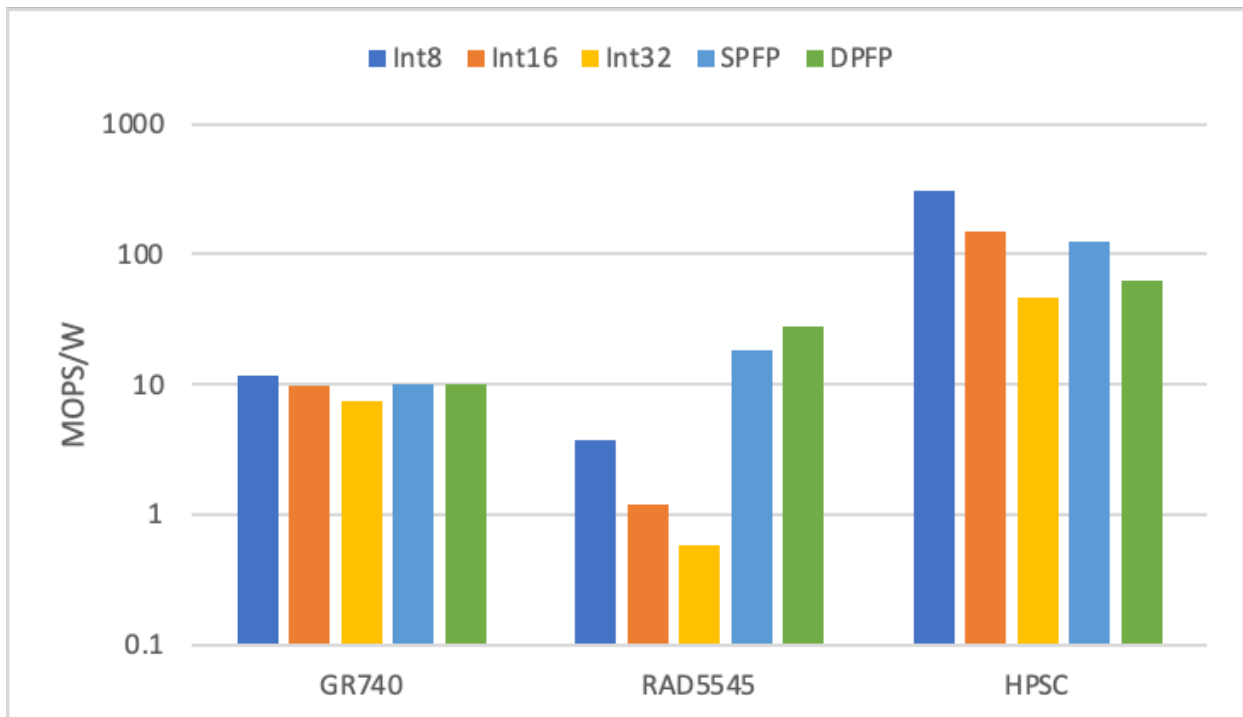


**Figure 5.18.2: Processor Power Efficiency**

Among the other processors are Cobham Gaisler's GR740 microprocessor and NASA's High Performance Spaceflight Computer, each with their own benefits. Based entirely on performance benchmarks, the HPSC seems to be the obvious choice to maximize power and efficiency based on its twelve-core architecture; however, it is not flight proven. The GR740 on the other hand, does not come close to the performance metrics of the two next to it, but does offer great, though not proportional, power efficiency compared to the others. Overall, for our final reference component that fits within our power and mass budget requirements, we thought it would be best to use a slightly outdated but flight proven part. Therefore, we went with the specifications of the RAD5545 from BAE Systems.

Some of the other reasons and considerations the RAD5545 was chosen included [transparent documentation](#) [AFSS-2], radiation hardened performance metrics (less than 50% processing power per watt dropped when exposed to high radiation environments) and having a viable commercial-off-the-shelf counterpart should we need one for testing purposes. Likewise, other reasons the GR740 and HPSC were not chosen were because of less efficient radiation hardened performance metrics and being only in a prototype stage as of now respectively.

### 5.18.3 - Acquisition Devices – Justin DeVito

For the cameras and IMUs, we looked at the current state of the art rovers on Mars. Our requirements for mass, size, power draw, and field of view of the navigation cameras were set based on the EECAMs on the Mars 2020 rover, and the mass, size, and power draw requirements for the IMU were set based on the Northrop Grumman LN-200S, also on board the Mars 2020 rover. These IMUs have 3 fiber optic gyroscopes and 3 silicon MEMS (Micro Electro-Mechanical Systems) accelerometers.

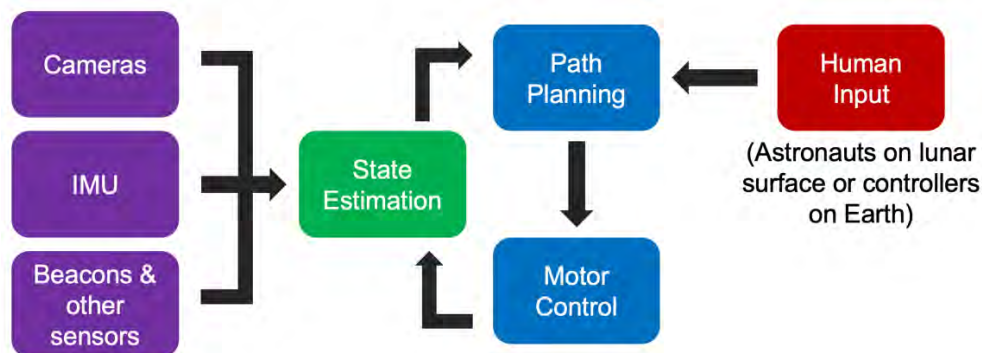


**Figure 5.18.3: Diagram of Mars 2020 EECAM Camera [AFSS-11]**



**Figure 5.18.4: Northrop Grumman LN200S IMU**

These sensors feed into the GNC system, shown below, which leaves room for remote operation by both astronauts on the lunar surface and controllers on Earth.



#### 5.18.4 - Redundancy – Justin DeVito

##### *5.18.4a - Computer redundancy*

We considered many solutions for computer redundancy. One idea was to have two computers, an “A-side” and a “B-side” with only one activate at any given time. Another option was to have three computers, one as the primary, one serving the role of a “watchdog,” and one as a cold spare. The last idea was to have three computers, were one was the primary but the other two were always active to be able to be used quickly.

Ultimately, we decided that the first choice with just two computers was sufficient for the slow-moving operation of our vehicle. This solution preserves mass and power when compared to the others, and is flight proven, as it was used on the MSL and Mars 2020 rovers.

##### *5.18.4b - Data redundancy*

The on-board data is stored redundantly on 3 drives. Initially, we looked at RAID as a widely used and flight proven technology for managing this data, but it was brought to our attention at our Preliminary Design Review that newer software-based approaches provide many advantages.

After looking into many different modern solutions, we found that erasure coding and object storage could be used as alternative to RAID and block storage that is much simpler, can use less storage capacity, and can reduce time and overhead for reconstructing data [AFSS-33].

#### 5.18.5 - Cameras – Justin DeVito

We determined that 4 navigation cameras would be a sufficient balance of power draw, complexity, and viewable area. These cameras will not need to operate at more than 15 FPS—at the top speed of 20 *cm/s*, this is 1.34 *cm/frame*. The cameras are used together to collect stereoscopic data for range calculations. These cameras will need a high dynamic range to be able to see the lunar surface even in bright sunlight.

We ultimately landed upon the blow configuration for the navigation cameras, as a way to maximize stereoscopic data in the front of the vehicle where it will be interfacing with payloads and docking with habitats, while still keeping the blind spots small enough. Even when



crab steering is used for payload alignment, we will want to use the front-facing cameras because those will be facing the payload.

Direction	Max Blind Spot Dist.
Front	0.91 meters
Rear	3.85 meters
Sides	3.70 meters

**Table 5.18.2: Navigation Camera Blind Spot Dimensions**

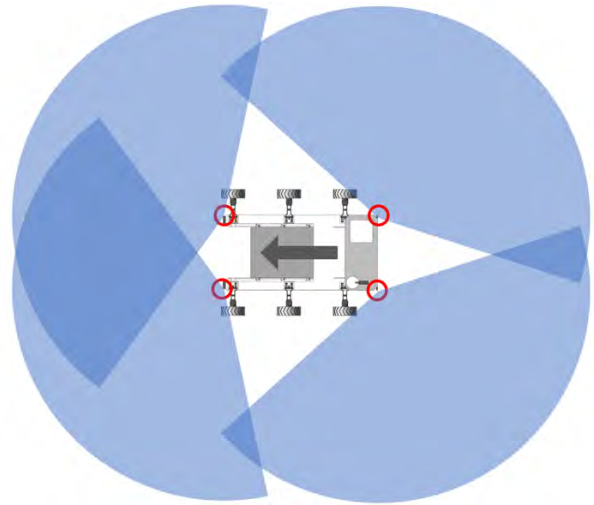


**Figure 5.18.6: Navigation Camera Placement on LLV**

However, issues arise with this configuration if anomalies occurred near the wheels or in one of the blind spots. Many flight-proved rovers provide small cameras for each wheel. For this reason, we will utilize 8 additional hazard cameras—one for each wheel, one for the front blind spot, and one for the rear blind spot.

#### 5.18.6 - Image Processing – Justin DeVito

To determine a minimum resolution for the navigation cameras, we set the requirement that a 30 cm obstacle must be able to be detected 1 meter before it reaches the furthest blind spot, because 30 cm is the minimum obstacle capability of the wheels.

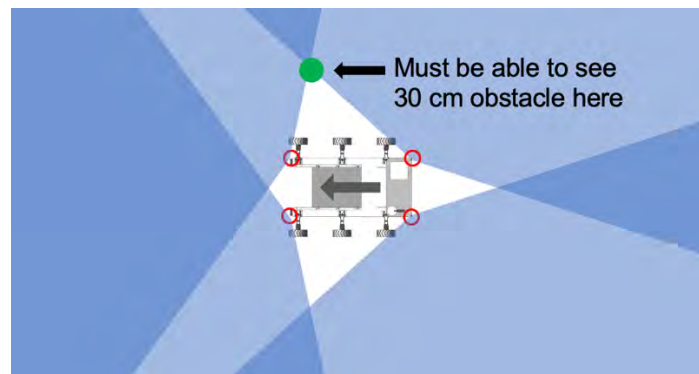


**Figure 5.18.7: Worst Case Location of Obstacle**

The minimum resolution to detect an object on the lunar surface was determined by using the Scale-Invariant Feature Transform (SIFT) algorithm for feature detection on an image from

the Chang'e 3 mission's PCAM. This algorithm is not specific to the lunar environment, and in practice we would likely use something that has knowledge of the structure of (features that make up) the obstacles we will encounter. Additionally, we could also use a machine learning model trained on images of the lunar surface where obstacles are known, such as in "Artificial Lunar Landscape Dataset" [AFSS-K]. The resolution of the image was varied and SIFT was used to see which obstacles can and cannot be detected at that resolution.



**Figure 5.18.8: Input Images [AFSS-K]**

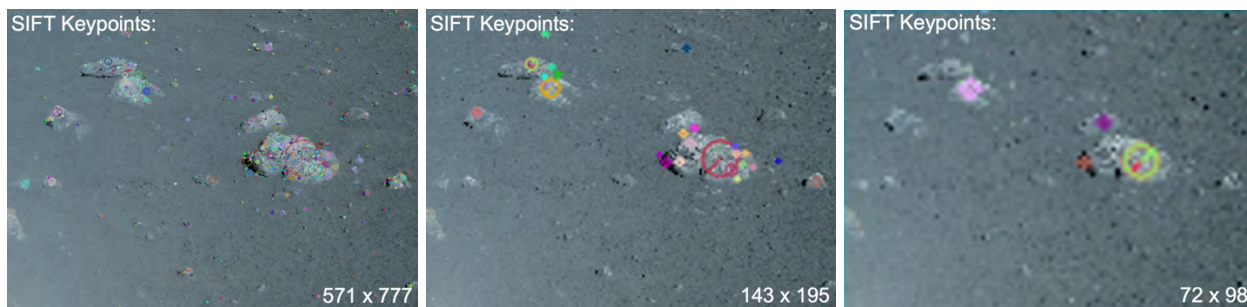


**Figure 5.18.9: Images with Sift Keypoints overlaid**

From this analysis, it was determined that the minimum amount of pixels needed to detect a lunar obstacle is approximately 20 pixels. Using that and simple geometry with the 156-degree field of view, it was determined that the minimum horizontal resolution to meet the requirements would be 1200 pixels. A sizeable margin was added to this due to the nature of this analysis not being entirely comprehensive, and we decided upon a standard 1920 x 1080 pixels resolution to be a good requirement for the navigation cameras. This corresponds to a 60% margin along the horizontal axis.

#### 5.18.7 - Navigation – Brian Amaya

Navigating will be a very important aspect of the design. Many previous rovers used multiple methods of navigation and positional tracking [AFSS-B4] to help keep its positional error low. Some of these systems would help "reset" or lower their error by using external measurements. Some of these systems would use orbiters to capture images of the system and then find its position. This could be done with this vehicle system but, it would mean a custom orbiter would

need to be built and then placed into orbit. This may not be viable. The use of previous orbiters may also not be the best option.

The use of a local resetting system could be useful. This could be using physical markers or fiducial markers to help reset positions. The physical markers could be something like reference spheres that can be processed by the cameras. If enough reference spheres are in the image a relative position could be found. What may be more useful could be fiducial markers which could provide more useful info. Fiducial markers are useful as one single marker can be used to find relative position using only one marker. The most common and known fiducial markers are April tags. They are black and white tags like QR codes that each can be processed and have a standard library attached to the image. The tag can be processed to give its physical size and the identification number attached to it. The tags have been used in robotics and other systems to locate themselves locally. The markers can be read at different angles and the image is processed to give the position and orientation that the marker is from the camera. This lets the vehicle find its position and orientation. The appendix shows sample code that was written for another project that can do the same. In that project the vehicle processes an image and is then able to find its heading. Now from here it can move to a wanted position relative to the tag. This is done by translating it and by controlling the vehicles' heading.

These tags provide very useful information and can be leveraged in many ways for this system. Placing these tags on a known stationary object with a well-known position like the habitat will allow the position to be reset when it gets close enough to these landmarks. The vehicle may leave the vicinity of the habitat, over time it's position error will accumulate. When it comes back it's error can be reset by seeing the tag and relating its position to said tag. This would work with these short-distance missions as it is only required to travel 1 km away from the habitat. If we take an error of 2.5-5% this would give a difference in 50-100 meters. The vehicle will be able to see the habitat or know a rough estimate of where the habitat will be and reset its location. This estimate for position error comes from other missions listed in the appendix. These errors came from longer missions, so the percents are taken as just worst-case scenarios.

The tags could also be placed on the payloads that the vehicle will have to transport. This will allow for alignment. A possible configuration for the tags is one on each of the long side and the side that interfaces with vehicle for power. Having this layout allows for the 3 cameras to have a view of a tag and find their own position relative to the payload. Having these redundancies would be helpful in case one of the tags is covered or damaged. Redundancy allows for a more accurate position.

Of course, standard April tag library may not be the best use. The Mars InSight lander uses its own sort of fiducial markers. These markers were used to localize the arm when it would complete operations with its arm.



**Figure 5.18.7 Left: Standard April tag Right: Mars Science Laboratory marker [AFSS-39]**

On the lunar surface the harsh solar sun may be harsh for regular black and white tags. There may be a specific color scheme or pattern that may work better. The scheme that would work better will have to be tested. The placement can also be twisted. The marker should be designed to be useful from all wide angles since that is where the cameras will view the tag.

## **6. Pressurized Logistics Module**

### **6.1 - Introduction – Adithya Arun**

The Pressurized Logistics Module (PLM) is used to resupply the habitat with logistics elements at regular intervals. For any sustained lunar settlement, there must be a steady resupply of crew needs from Earth—things such as atmosphere, water, food, hardware, and experiments. As such, the sizing of the PLM is tied to the expected crew volume, crew life support requirements, resource losses in the habitat, resupply cadence, and general expected hardware delivery.

Initial sizing of the PLM assumed a one-year cadence to minimize lunar vehicle logistics and planning. The higher the cadence, the more trips the launch vehicle, lander, and LLV must support and schedule. By maintaining a one-year cadence, we reduced the operational complexity, risk (due to failures during transport), and cost but in turn also reduced the number of viable launchers and landers. Additionally, the one-year PLM is also less flexible when it comes to emergency response for the lunar habitat should any supplies be in urgent need. When designing the initial PLM, much thought was put into crew life support requirements (water, atmosphere, and food), but cargo requirements were sidelined. Future iterations of the PLM had a more balanced look at the types of payloads in the PLM.

Due to an increased need for flexibility, a trade was created between cadence and PLM mass to find the optimal cadence that would correspond with a feasible PLM. From this trade, the PLM was resized for a nominal 45-day cadence. This PLM could fit within a wide range of launch vehicles and landers and was very close to ISS resupply rates, validating the flexibility of the module. However, an oversight in this design was the optimal launch cadence for lunar transfer which occurs in 28-day cycles.

The final redesign of the PLM changed the module sizing from a 45-day cadence to a 28-day cadence. A 56-day cadence was not chosen due to volume constraints as it would severely limit the types of launch vehicles available. A 28-day cadence is much more operationally intensive and higher cost (due to the number of launch vehicles and landers required) but offers the most flexibility in resupply as well and launch and lander vehicles. Alternatively, the 45-day cadence PLM design can be used as a baseline and launched every 28 days so that risk due to delays or incidents are mitigated through margin in the PLM resources.

### **6.2 - Initial Sizing – Joey Fluehr**

The primary factors in determining the necessary size of the PLM are the crew's metabolic, respiratory, and hygiene requirements. A standard crewmember's daily metabolic intake and output are summarized in Table 6.2.1 and the nominal crew hygiene requirements for the International Space Station (ISS) are summarized in Table 6.2.2 [LSM-12]. The ISS has a standard crew size of 6 while Artemis is slated to have a crew size of 4. Therefore, the hygiene requirements were scaled down accordingly when factoring them into the required PLM payload mass. Additionally, the lunar habitat's life support system was given equal capabilities of the ISS Environmental Control and Life Support System (ECLSS), namely production of oxygen

through electrolysis and overall oxygen and water reclamation efficiencies of 40% and 90%, respectively.

Metabolic Intake Mass (kg)		Metabolic Output Mass (kg)	
Oxygen	0.84	Carbon Dioxide	1.00
Food Solids	0.62	Respiration & Perspiration Water	2.28
Water in Food	1.15	Urine Water	1.50
Food Preparation Water	0.76	Feces Water	0.09
Drinking Water	1.62		
Water Subtotal	3.53	Water Subtotal	3.87
Total	4.99	Total	4.87

**Table 6.2.1: Standard Crewmember Daily Metabolic Intake & Output**

Requirement	Mass (kg)
Shower	2.73
Dishwash	5.45
Handwash	4.09
Urine Flush	0.5
Clothes Wash	12.5
Total	25.27

**Table 6.2.2: ISS Crew Hygiene Water Requirements**

Atmospheric losses were also considered when calculating the required PLM payload mass. For this iteration of the PLM, we defined the habitat atmospheric composition as being equal to that of the ISS: 20% oxygen and 80% nitrogen at 14.7 psi. This would change with later designs to decrease the payload mass required to service the habitat and to match NASA's stated habitat atmospheric design parameters for Artemis. The ISS has a standard leakage parameter of 0.23 kg per element per day, with a typical element having an internal volume of 106 m<sup>3</sup> and atmospheric mass of 125 kg [LSM-12]. This equates to 0.18% of the ISS atmospheric mass leaking per day. RASCAL has defined the lunar habitat as being no larger than 4.57 meters in diameter and 7.8 meters in height, giving it a maximum theoretical internal volume of 128 m<sup>3</sup>. Given that we defined the lunar habitat as having the same atmospheric composition as the ISS, and assuming the same leakage rate, a habitat with this volume would leak 0.28 kg of its atmosphere per day.

Similarly, the ISS was used as a model for calculating the atmospheric mass lost due to airlock cycling to accommodate extravehicular activities (EVAs) on the lunar surface. The ISS airlock has an internal volume of 26 m<sup>3</sup> and loses 10% of its atmospheric mass per cycle [LSM-12]. The same values were used to approximate atmospheric loss due to airlock cycling for the

lunar habitat, giving a loss of 1.6 kg per cycle. To extrapolate this loss over a period of time, EVA frequency was set to 1 EVA every 2 days with each EVA involving all 4 crewmembers, giving an average of 3.5 airlock cycles (5.6 kg mass loss) per week over the course of a mission. Additionally, 1 crewmember consumes an average of 0.63 kg of oxygen and 5.4 kg of water per EVA [LSM-12]. Table 6.2.3 is a summary of daily mass loss due to atmospheric leakage and metabolic, respiratory, and hygiene requirements for 4 crewmembers, with ECLSS reclamation efficiencies and hydrolysis considered. Table 6.2.4 is a summary of the yearly cargo mass required to replenish these losses.

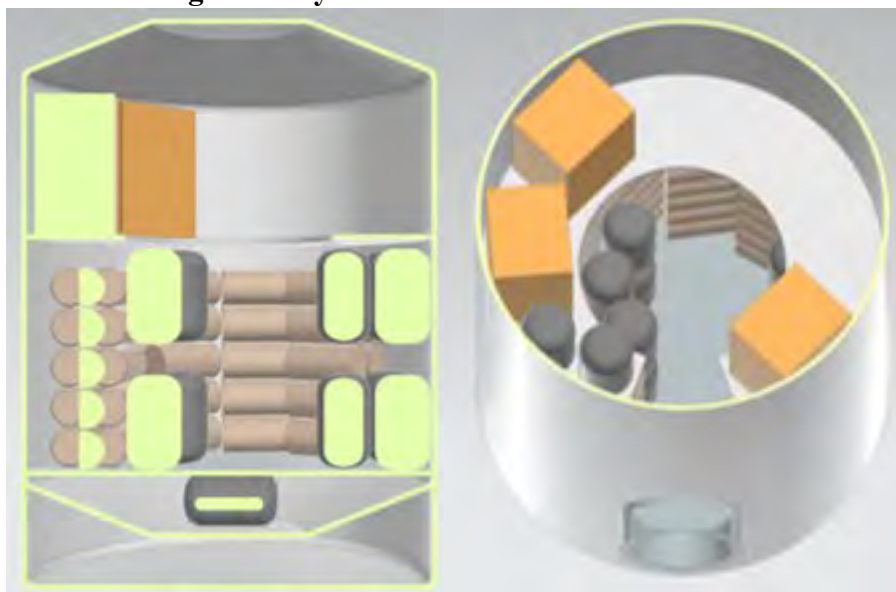
<b>Water</b>	<b>Mass (kg)</b>
Metabolic	1.6
Hygiene	1.7
EVAs	1.1
<b>Total Daily Water Loss</b>	<b>4.4</b>
<b>Food</b>	
Total Daily Food Consumption	2.5
<b>Atmospheric</b>	
Oxygen Consumed	2.0
Oxygen Consumed (EVAs)	0.8
<b>Oxygen Subtotal (ECLSS Inefficiency)</b>	<b>2.8</b>
Atmospheric Leakage	0.3
Air Lock Loss	1.6
<b>Total Daily Oxygen Loss</b>	<b>3.3</b>
<b>Total Daily Nitrogen Loss</b>	<b>1.4</b>

**Table 6.2.3: Daily Mass Loss**

<b>Cargo</b>	<b>Mass (kg)</b>
Food	906
Water	2752
Oxygen	115
Nitrogen	527
<b>Total</b>	<b>4300</b>

**Table 6.2.4: Yearly Resupply Requirements**

### 6.3 - Initial Internal Config – Adithya Arun



Figures 6.3.1a and 6.3.1b: Cross-sectional (left) and Isometric (right) Views of the One-Year Cadence PLM

The one-year cadence PLM is very large, with a diameter of 4 meters and a total height of 5.5 meters. The PLM can still be feasibly transported by the LLV as it is enveloped in volume and weight by the habitat, which the LLV must be able to transport as well. Shown in orange are the 189 food containers; in dark gray are the 25 atmosphere tanks; and in light brown are the 62 water containers. The PLM contains a pressurized main capsule with an unpressurized trunk in the bottom. The pressurized section has toroconical end caps and houses the food, atmosphere, water, and cargo. The unpressurized section holds things like batteries and environmental control plumbing. Also shown is a hatch modeled after the International Docking System Standard (IDSS) [LSM-33]. A member of the habitat would be expected to crawl through the hatch and up a ladder to transport the items on the top shelf back into the habitat.

Trades were conducted to choose the best containment method for atmosphere, water, food, and cargo.

For atmosphere containment, Nitrogen Oxygen Recharge System (NORS) tanks were chosen as the best method to transport atmosphere to the lunar habitat. This is because they presented the lowest mass option while maintaining high reliability and high technology readiness level. The NORS tanks store gas at around 6000 psi and can each carry either 60 lbs of nitrogen or 80 lbs of oxygen [LSM-36, 37, 38]. The tanks are Composite Overwrapped Pressure Vessels (COPVs) and have a dry mass of 122 lbs; they have been used to regularly service the International Space Station (ISS) Environmental Control and Life Support System (ECLSS) with atmosphere, which mirrors its usage in the PLM. They have very high reliability as they have never failed and are designed to leak before burst.

The other atmosphere containment system that was considered was the High-Pressure Gas Tank (HPGT). This is an older resupply system used for ISS ECLSS that stored oxygen and nitrogen at a typical operating pressure of 2400 psi. One HPGT can carry either 208 lbs of oxygen or 186 lbs of nitrogen. While HPGTs also have a high technology readiness level, their



gas-to-total mass ratio is much worse than NORS, hence why NORS was chosen as the baseline atmosphere containment system [LSM-40].

Tank Type	Gas-to-total mass ratio
Oxygen HPGT	0.15
Nitrogen HPGT	0.13
Oxygen NORS	0.41
Nitrogen NORS	0.34

Table 6.3.1: Atmosphere Containment Mass Ratios

Alternative storage methods were also considered and used in the baseline design. It was assumed that the lunar habitat would have some form of closed loop oxygen reclamation using water electrolysis, as is typical on the ISS for both American and Russian segments. Therefore, most of the oxygen (90%) is assumed to be transported as water due to safety, packaging, and mass considerations. Water can be much more efficiently stored, which will be discussed next, so the loss in transporting oxygen as water (88% mass ratio) is made up in the much higher mass ratios of water containment. With most of the oxygen being stored as water, there is much more nitrogen gas to transport to the habitat in both volume and mass. This drives the number of tanks for the one-year PLM. Other alternative nitrogen storage methods such as ammonia and hydrazine were considered to reduce the number of tanks transported. Both are liquid at room temperature and thus have a much higher density, allowing the volume of nitrogen transported to be much lower than with the NORS tanks. While hydrazine has a higher nitrogen weight ratio at 87.5%, it is an incredibly toxic and corrosive chemical. Ammonia is also toxic and has a lower nitrogen ratio, but there are multiple uses for ammonia as coolant and an existing, well documented process to convert ammonia to its constituent elements by reversing the Haber process. If it is assumed that the habitat has a machine capable of converting ammonia into nitrogen and hydrogen, then ammonia could be used in future PLM designs but ultimately due to toxicity and technology readiness concerns as well as the ability for the NORS system to conform to volume and mass constraints, this was not chosen as an atmosphere containment option.

The containment method for water storage was chosen to be Contingency Water Containers (CWCs) which are multipurpose cylindrical diaphragms that can store drinking water, liquid waste, and machine water. The dry mass is 1.36 kg, and each container can store 45 kg of water. Drinking water is typically iodinated to ensure no microbial growth, so there is an associated 0.041 kg/L of hardware for iodine removal, biocide, filters, syringe kits, and minerals. CWCs are the primary method of water transport to the ISS for the American segment and thus have a high technology readiness level [LSM-39].

The alternative storage method considered for the water was a Rodnik tank. These tanks are used during resupply with the Progress spacecraft to resupply the Russian segment on the ISS. The Rodnik tanks are much larger than CWCs and can contain 210 kg of water with a dry mass of 35.2 kg [LSM-41]. The tanks have a much higher mass ratio than the CWCs because they are pressurized to work in orbital conditions; since the habitat will exist in lunar gravity, it is reasonable to assume that a redesign of the Rodnik architecture for use in the lunar environment

could allow for mass savings. However, due to the need for redesign and the lower mass ratio, CWCs were chosen as the water containment method.

Container	Mass Ratio
Contingency Water Container	0.93
Rodnik Tank	0.86

Table 6.3.2: Water Containment Mass Ratio

Food is expected to be transported in U.S. Standard Non-Collapsible containers SEG48101834-301. This can hold 14.3 lbs with a bag tare of 3.75 lbs. Cargo is expected to be transported by Cargo Transfer Bags (CTBs). A single size CTB (SEG33111837/838) was the baselined transport bag of choice since it represents most of the cargo containment to the ISS [1]. The average single CTB contains about 10.26 kg of cargo, based on historical mass records to the ISS, with a bag tare of 1.81 kg. An international standard payload rack was also briefly considered due to its use on the ISS. However, due to the fact that the PLM is a temporary structure, it was found unnecessary to have a payload rack in the PLM and stacking and restraining CTBs was found as the better alternative option.

#### 6.4 - Initial Crew Assistance – Joey Fluehr

With this initial one-year cadence design, it became evident that some form of cargo offloading assistance would be beneficial to not overstrain the crewmembers in the process of transferring the estimated 4300 kg of cargo from the PLM into the habitat. A simple, cost-effective, and reliable solution of stowing a winch and collapsible cart in the habitat to use for offloading cargo from the PLM was theorized to remedy this. The winch would hook onto a mount point on the floor of the habitat and pull the loaded cart through the docking port, erasing the need for crewmembers to carry bulky cargo through the narrow passageway. A mounting point could also be included on the ceiling of the PLM to assist in lowering heavy cargo from the upper portion of the PLM. This idea is illustrated in Figure 6.4.1.

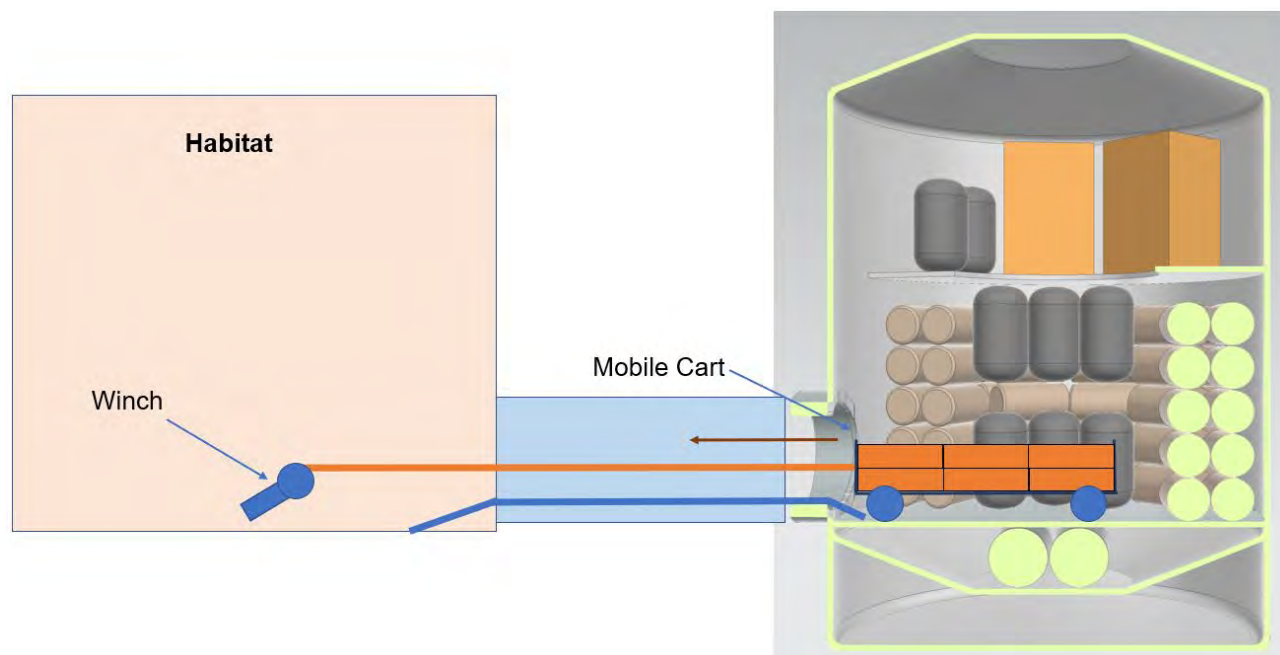


Figure 6.4.1: Cross-Section View of Offloading Concept

### 6.5 - Initial Offloading and Lander Selection – Adithya Arun

Since the one-year cadence PLM is so large, the only funded launch vehicle and lander that can feasibly transport the PLM is a cargo Starship variant. Cargo Starship or some vehicle equivalent must exist for long-term lunar bases to exist and fits within the Artemis architecture. According to SpaceX's Starship User's Guide, there will exist a Starship elevator to offload cargo; this was chosen as the primary method of offloading the habitat and since the habitat's volume and mass envelopes the PLM, it is assumed that the elevator will work for PLM as well.

### 6.6 - Initial Structural Analysis – Joey Fluehr

A launch load analysis and material trade study for this iteration of the PLM was conducted in order to achieve a first pass estimation of its structural mass. The Starship User's Guide was used as a reference to calculate the launch loads on the PLM. The PLM was modeled as a thin-walled canister with a tip mass consisting of the top structure. SS316, Al 6061-T6 & Al 7075-T73 were compared for the material trade study. The maximum load factors given by the Starship User's Guide are  $g_x = 6g$  and  $g_{lat} = 2g$ . The stress due to launch accelerations is given by Eqn. 6.6.1

$$\sigma_{LA} = \frac{Mr}{I} + \frac{m_{tip}}{A} g_x \quad (6.6.1)$$

The maximum pressurization load is given by the hoop stress shown in Eqn. 6.6.2.

$$\sigma_{hoop} = \frac{pr}{t} \quad (6.6.2)$$

The fundamental bending frequency for a cantilevered beam with a tip mass is given by Eqn. 6.6.3 [LSM-16].

$$f_1 = \frac{1.732}{2\pi} \sqrt{\frac{EIg}{m_{tip}l^3 + 0.236m_{canister}l^3}} \quad (6.6.3)$$

The fundamental frequencies of each material studied are given in Table 6.6.1.

Material	(Hz)
SS316	62
Al 6061-T6	49
Al 7075-T73	42

**Table 6.6.1: Fundamental Frequencies of Studied Materials**

Unfortunately, the Starship User's Manual does not provide information on the payload acoustic environment below 100 Hz, leaving this analysis partially incomplete with the hoop stress currently shown as the critical load applied to the PLM during launch, as shown in Table 6.6.2 with each material's respective structural mass shown in Table 6.6.3.

Load	SS316	Al 6061-T6	Al 7075-T73
$\sigma_{LA}$ (SF=1.4)	6.2%	10.2%	9.7%
$\sigma_{hoop}$ (SF=3)	0.9%	1.7%	1.5%

**Table 6.6.2: Launch Loads Margins of Safety for Studied Materials**

Material	Mass (kg)
SS316	3000
Al 6061-T6	1500
Al 7075-T73	1000

**Table 6.6.3: Structural Masses of Studied Materials**

## 6.7 - 45-Day Sizing – Joey Fluehr

A more comprehensive trade was done to evaluate the effect of different habitat atmospheric conditions on the payload mass required to service the lunar habitat, as well as more accurately account for other cargo besides that to support the crew's metabolic, respiratory, and hygiene requirements. Since differing atmospheres were considered, oxygen and nitrogen losses could not be approximated solely as a function of the differing volumes between the lunar habitat and a typical ISS element, as was done for the initial LSM iteration.

The ideal gas law, given by Eqn. 6.7.1, was used to calculate the oxygen and nitrogen mass fractions within the internal volumes of the lunar habitat and airlock.

$$p = \rho RT \quad (6.7.1)$$

Given  $M_{O_2} = 0.032 \frac{kg}{mol}$ ,  $M_{N_2} = 0.028 \frac{kg}{mol}$ ,  $R_{univ} = 8.314 \frac{J}{K \cdot mol}$ , and room temperature  $T = 298.15K$ , Table 6.7.1 shows the atmospheric mass fractions within these volumes as well as the average daily masses lost due to both atmospheric leakage and airlock cycling. Table 6.7.1 shows the yearly amount of nitrogen, oxygen, and water to service each atmosphere type, including food, which is unaffected by this consideration. The 8.2 psi, 34% O<sub>2</sub> atmosphere requires the least amount of payload mass to service the habitat of the three and was therefore used as the habitat atmosphere for this iteration of the PLM. This atmospheric condition is also stated by NASA as being a potential habitat operating condition for Artemis [LSM-13].

Atmosphere	Mass O <sub>2</sub> (kg)	Mass N <sub>2</sub> (kg)	Daily O <sub>2</sub> Loss (kg)	Daily N <sub>2</sub> Loss (kg)
14.7 psi, 21% O <sub>2</sub>	31.7	119	3.15	1.43
10.2 psi, 26.5% O <sub>2</sub>	28.0	77.6	3.11	0.93
8.2 psi, 34% O <sub>2</sub>	29.1	56.6	3.12	0.68

**Table 6.7.1: Daily Atmospheric Losses for Differing Atmospheric Conditions**

Atmosphere	Mass O <sub>2</sub> (kg)	Mass N <sub>2</sub> (kg)	Mass H <sub>2</sub> O (kg)	Total Mass (kg)
14.7 psi, 21% O <sub>2</sub>	115	522	2751	4293
10.2 psi, 26.5% O <sub>2</sub>	113	340	2734	4092
8.2 psi, 34% O <sub>2</sub>	114	248	2739	4006

**Table 6.7.2: Yearly Payload Masses Required for Differing Atmospheric Conditions**

To more accurately calculate the mass of other types of cargo, historical Class of Supply (COS) mass ratios of Progress M resupply missions to the ISS (shown in Table 6.7.3) [LSM-14] were used to estimate the mass of non-crew provisions that may be supplied by the PLM to the lunar habitat. COS 1 (propellants and fuels) were ignored for this as the lunar habitat does not require fuel for station-keeping, unlike the ISS.

COS 2 (Crew Provisions)	Other COS
0.38	0.41

**Table 6.7.3: Historical Progress M COS Mass Ratios**

Table 6.7.4 shows the total payload masses for differing resupply frequencies to the lunar habitat with an 8.2 psi & 34% O<sub>2</sub> atmosphere including the tare/dry weight of the necessary amount of NORS tanks, CWCs, CTBs & food containers. Table 6.7.5 shows this for a habitat with a 10.2 psi & 26.5% O<sub>2</sub> atmosphere, which NASA has stated as being the nominal operating atmosphere for the Artemis lunar habitat. These masses assume that all containers onboard the PLM are sent at full capacity, so there is a slight margin of extra supplies that could be stockpiled over time to help accommodate any emergencies that may arise in between resupplies. The 45-day resupply frequency was chosen because of its ability to quickly service the lunar habitat in the case of an emergency while providing enough of a margin to carry denser cargo or further structural changes that could increase its total mass while staying within the limits of 5000 kg class lunar landers.

Frequency (Days)	Food (kg)	Water (kg)	Atmosphere (kg)	Other Cargo (kg)	Total Payload (kg)
30	104	278	175	708	1265
45	156	371	257	996	1780
60	208	510	257	1239	2214
75	254	603	257	1415	2529
90	306	742	340	1761	3149

**Table 6.7.4: Resupply Payload Masses for Habitat at 8.2 psi & 34% O<sub>2</sub>**

Frequency (Days)	Food (kg)	Water (kg)	Atmosphere (kg)	Other Cargo (kg)	Total Payload (kg)
30	104	232	257	754	1347
45	156	371	257	996	1780
60	208	464	340	1286	2298
75	254	603	340	1519	2716
90	306	695	423	1808	3232

**Table 6.7.5: Resupply Payload Masses for Habitat at 10.2 psi & 26.5% O<sub>2</sub>**

As shown by Tables 6.7.4 and 6.7.5, at a 45-day launch cadence the PLM is able to service the lunar habitat operating at both atmospheric conditions while carrying the exact same amount of

cargo. This means a 45-day launch cadence would allow NASA to change between these environments at will without the need for any change in mission logistics. One such case could be comparing the physiological effects of living long-term in both of these atmospheres. Table 6.7.6 shows the number of each type of cargo container required to support a 45-day launch cadence for both atmospheres.

Container	Amount
CWCs	8
Food Containers	24
O <sub>2</sub> NORS Tanks	1
N <sub>2</sub> NORS Tanks	2
CTBs	83

**Table 6.7.6: 45-Day Launch Cadence Containers**

### 6.8 - 45-Day Internal Configuration – Adithya Arun

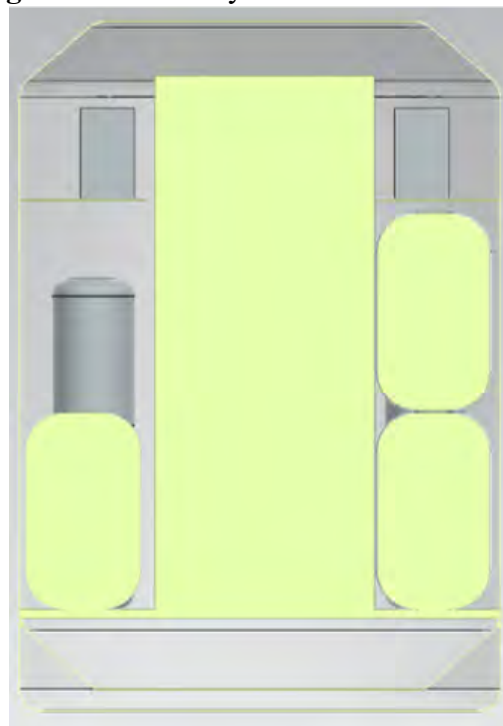


**Figure 6.8.1: Cross-sectional View of 45-Day Cadence PLM**

This second iteration of the PLM is much smaller than the initial one-year cadence PLM as it is designed for a 45-day resupply cadence. The PLM has a total height of 3.2 meters with a diameter of 2.2 meters. The overall architecture is the same as the initial PLM, with a pressurized section with toro-conical endcaps that contains the cargo in CTBs, nitrogen and oxygen NORS tanks, water in CWCs, and food in non-collapsible containers. There is an unpressurized trunk that holds batteries and piping for the positive and negative pressure relief system.

The cross-sectional image shows a large central rectangle which is a stack of CTBs and 24 food containers. The rectangles on the top shelf are also CTBs, bringing the total CTBs in the PLM to 83. There are 3 large green cylindrical tanks which represent the NORS tanks (2 nitrogen tanks and 1 oxygen tank). The smaller cylinders represent the 8 CWCs that are used for water transport.

Not pictured, there is a large central hatch that is used to interface with the habitat. Crew members are expected to walk through that hatch to retrieve logistics elements. At this point in time, trades were still being made for optimal hatch sizes and experiments were being designed to verify the best design, so an IDSS-type hatch was assumed for simplicity.

### 6.9 - 45-Day Structural Analysis – Adithya Arun

The critical loads on the PLM are expected to be launch loads rather than lunar transport loads, so those were the primary loads analyzed. Because of the size of the PLM, with a total mass coming out to 3300 kg, most heavy-class vehicles should be able to transport the PLM and associated lander to lunar transfer orbit. There is not much published data on launch vehicle payload mass to Lunar Transfer Orbit (LTO), but after a discussion with Dr. Akin, it was assumed that if the required mass was under 80% of the vehicle's payload mass to GTO, the vehicle could be assumed to be a feasible vehicle for transport. From this, the only currently operational vehicle that is still expected to be operational during the Artemis timeline is the Falcon Heavy. The Vulcan Centaur and New Glenn are also likely candidates but there isn't enough info about either to be sure of their capabilities and they are both not flight proven, so a Falcon Heavy was baselined as the launch vehicle of choice. This is important as the launch loads (vibrational and quasi-static) are derived from the Falcon User's Guide.

Also important is the structural quality of the PLM. A material trade was conducted to select the optimal material for the PLM. Stainless steel and aluminum were looked at as potential materials. The Multi-Purpose Logistics Module used an aluminum isogrid structure to support the capsule [LSM-42]. Due to a much higher strength-to-weight ratio and good thermal conductivity, Al 7075-T73 was chosen as the material of choice [LSM-19]. It is also good at resisting stress-corrosion cracking and is a space-proven material.

The wall thickness of this iteration of the PLM is 0.25 inches. Since the PLM is large and internally pressurized, hoop stress can be a potential concern. This iteration of the PLM had a baselined pressure of 8.2 psi. The hoop stress equation is shown by the following:

$$\sigma_{hoop} = \frac{pr}{t}$$

(6.9.1)

Based on the quasi-static load envelope in the Falcon User's Guide, the PLM will experience a maximum axial load of 6 g's and a maximum lateral load of 2 g's. Though not a part of the load envelope, the most conservative quasi-static loading case would be if these two conditions were to happen at the same time, which is what the quasi-static margin assumes. The moment due to lateral load is assumed to be at the center of the PLM to be conservative, even though the true center of gravity would likely be lower due to denser materials like the water tanks and NORS tanks at the bottom of the PLM. The following equations are taken from [LSM-16].



The total stress due to quasi-static acceleration is calculated using the following equation:

$$\sigma = \frac{Mc}{I} + \frac{mg_{axial}}{A_{cs}} \quad (6.9.2)$$

The vibrational environment can be derived from the power spectral density given in the payload handbook. Assuming the PLM is cantilevered at the base, the first fundamental frequency comes out to 236 Hz. This is given by the following equation:

$$f = \frac{1.732}{2\pi} \sqrt{\frac{EIg}{0.236Wl^3}} \quad (6.9.3)$$

Depending on the fundamental frequency, the damping ratio is given via the following table:

$f_n$	$\xi$
<150 Hz	.045
150-300 Hz	.020
>300 Hz	.005

(6.9.4)

Table 6.9.1: Damping Ratio Values for Varying Fundamental Frequencies

Given that the fundamental frequency is 236 Hz, the associated zeta value is 0.02. The associated power spectral density (PSD), given by a graph in the Falcon User's Guide, is 0.03 g<sup>2</sup>/Hz. Using Miles' Equation, the random load factor can be derived:

$$RLF = \sqrt{\frac{\pi f PSD}{4\xi}} \quad (6.9.5)$$

The random load factor from the previous equation comes out to 16.7 g's. This is applied to the quasi-static stress equation to derive an equivalent quasi-static stress due to random vibration loading.

The margins and safety factors are compiled on the following table:

Load Case	Margin	Safety Factor
Quasi-static Acceleration	1.4	26.4
Pressure	3	11.7
Random Vibration	3	0.95

Table 6.9.1: Structural Margins for the 45-Day Cadence PLM

Based on the results compiled in the margin table, the PLM clearly satisfies structural loading requirements as all margins are above 0. Notably, the critical loading case on the PLM is the random vibration loading during launch. The random load factor is heavily dependent on the fundamental frequency of the structure which is hard to predict accurately using only hand calculations assuming a cantilever beam type structure. While the beam calculations can give a rough order of magnitude, they are not fully representative of the expected structural modes. To grow design maturity, a structural Finite Element Analysis (FEA) should be conducted to verify the first mode of the structure and then derive the new structural margins, but that was

considered outside the scope of the project due to time constraints and issues with software licensing.

### 6.10 - 45-Day Cadence Launch and Lander Trade/Verification -- Adithya Arun

There are a few heavy class launch vehicles that can feasibly launch the PLM and lander, but a falcon heavy was baselined, with an expendable payload mass to GTO of 26700 kg. Assuming it can take 80% of this payload limit to LTO, that brings the payload mass to LTO to 21360 kg.

There are multiple NASA funded CLPS landers going to the moon—however the highest payload capacity lander through this program is the Astrobotic Griffin lander, which can bring 625 kg of payload with it to the poles [LSM-34]. Privately funded landers like Blue Origin’s Blue Moon Intuitive Machine’s NOVA-D are stated to hold up to 5000 kg of payload; Blue Moon is also supposed to be able to integrate with the New Glenn launch vehicle [LSM-35]. Starship is the only NASA funded lander that has enough capacity to fit a PLM and lander, however its 100 MT capacity is much higher than what is needed to transport the resupply elements frequently. Thus, since there is no NASA funded lander that is within the payload limits for the PLM, a feasibility study was conducted to estimate what a lander of the correct size might look like.

Sizing for a 5000 kg lander, similar to Blue Moon and NOVA-D, and assuming a Delta V from LTO to landing of 3250 m/s, the total mass of a LOX-LH2 lunar lander comes out to 9.8 MT. This makes the inert mass ratio for the lander 0.13. Using mass-estimating-relations (MERs) [LSM-17] to estimate the tank mass, insulation mass, avionics, harness, thrust structure, gimbal, and engine mass, the following inert mass table was created:

Inert Mass Summary		
LOX Tank	72.2	kg
LH2 Tank	144	kg
LOX Insulation	18.0	kg
LH2 Insulation	93.6	kg
Engine	105	kg
Thrust Structure	9.18	kg
Gimbals	2.33	kg
Avionics	320	kg
Wiring	210	kg
Structural mass	491	kg
Inert Mass	1470	kg
Mass Margin	31%	

Table 6.10.1: Final PLM Lander Inert Mass Summary

The lander was assumed to have one engine capable of 43 kN of thrust, which provides a thrust-to-weight-ratio of 1 at 50% throttle. This is very similar to Blue Moon’s single BE-7 engine, which has a thrust of 44.5 kN. To better estimate the size of the engine, which has effects on the envelope of the lander within the fairing, the Rocket Propulsion Analysis software was

used to nominally design the engine. Major assumptions were that the chamber pressure was 5 MPa, which is within the range used for LOX-LH2 engines, a nozzle expanded to a pressure of 0.05 atm, and a contour Rao nozzle. From this the following engine was sized using Rocket Propulsion Analysis (RPA) software:

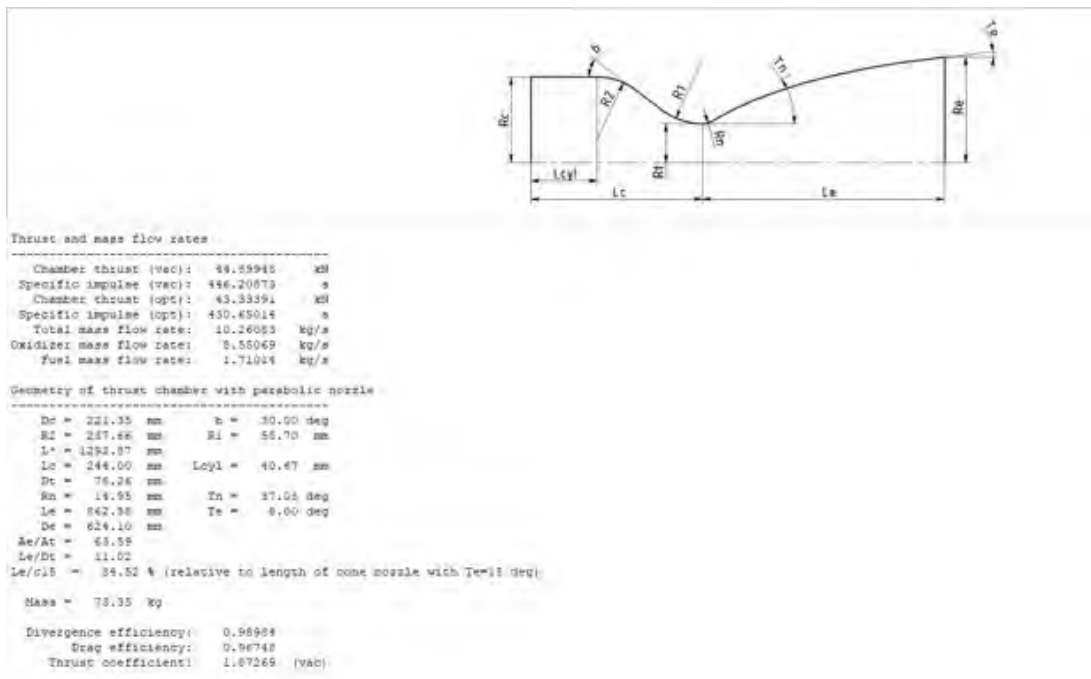


Figure 6.10.1: Engine Design

The lander CAD was created to understand the feasibility of the design and if both the PLM and lander can fit within the fairing dynamic envelope. The lander was based on the design of the released pictures of Blue Moon as that is the baselined lander for this iteration of the PLM. Thus, the lander has one large helium tank and a smaller oxygen tank within a hexagonal structure and a single large, highly throttleable central engine. There are also 4 large, actuated landing legs.

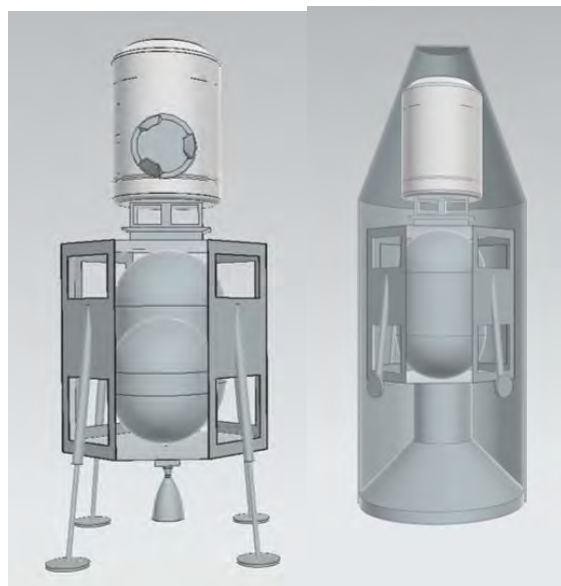


Figure 6.10.2a and 6.10.2b: PLM and Lander deployed (left), PLM and Lander Stowed (right)

As shown in the images above, the lander and PLM in stowed position can fit within the dynamic envelope of the Falcon Heavy fairing. The combined mass of the PLM and lander, both with 30% margin, is 13.1 MT which is far below the assumed 21.4 MT payload to orbit capability of a fully expendable falcon heavy. Therefore, a lander with a similar architecture to Blue Moon's is feasible for transporting the PLM.

### 6.11 - Final PLM Design Internal Configuration – Adithya Arun

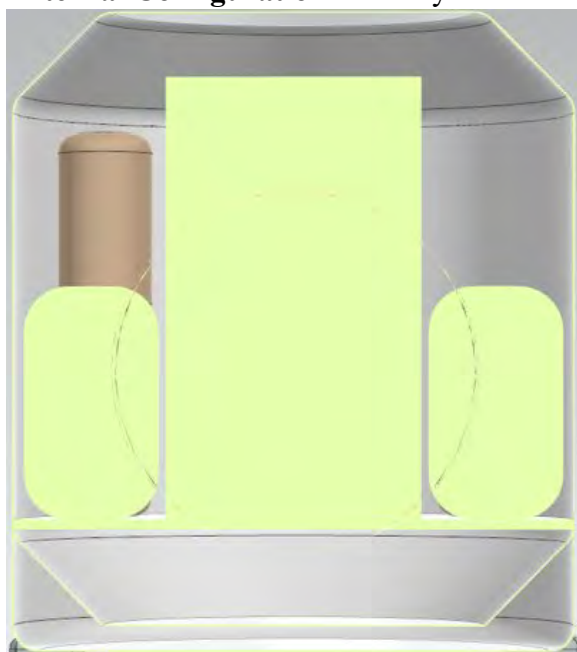


Figure 6.11.1: Cross-sectional View of 28-Day Cadence PLM

The final iteration of the PLM reduced the cadence from 45 days to 28 days due to resizing based on optimal launch windows to the moon, which occur in 28 day intervals. A 56 day cadence was considered as well, but the resized lander and PLM exceeded the payload envelope. Therefore, a 28-day cadence was chosen as the most optimal.

This new PLM is smaller than the 45-day cadence PLM and is 2.2 meters in diameter and 2.5 meters tall. This is very close to the size of the test article used to understand human factors when transporting logistics elements through the PLM hatch. From the data, a 40"x40" hatch was chosen as the preferred docking method and used for this PLM.

The PLM contains 5 CWCs, 15 Food containers, 1 oxygen NORS tank, 1 nitrogen NORS tank, and 53 CTBs. The total mass of the PLM comes out to about 1800 kg when including a 30% margin.

### 6.12 - Final PLM Structural Analysis – Adithya Arun

Similar to the 45-day cadence PLM, the PLM was modeled vertically cantilevered and fixed to the payload attachment. The primary loading conditions analyzed were launch and pressure loads. Due to the high margins from the previous PLM iteration and a decrease in vertical length, which leads to increased stiffness, the baselined wall thickness for the final PLM

was 0.125” (as opposed to the 0.25” wall thickness previously baselined). By reducing the wall thickness in half, the structural mass of the PLM greatly decreases, allowing for the PLM and lander to have higher mass and volumetric margins with respect to the launch vehicle’s capabilities. Again, Aluminum 7075-T73 was used as the structural material.

For the load environment, the quasi-static accelerations did not change from the previous iteration and were assumed to be 6 g’s in the vertical direction and 2 g’s in the lateral direction, applied at a center of gravity 1.3 meters above the base of the PLM. This center of gravity is conservative due to the density of objects below the center of the PLM. The pressurization of the PLM was kept the same as the previous iteration with an assumption of internal pressure equaling 8.2 psi.

The fundamental frequency had to be recalculated due to the new geometry of the structure, with thinner walls and a shorter height; the fundamental frequency is 350 Hz, which is much higher than the previous iteration and has an associated damping ratio value of 0.005. The new random load factor from this arrangement is 23.4 g’s.

Given the new loading conditions the margins and safety factors used for pressure loading, random vibration loading, and quasi-static loading are shown in Table 6.12.1.

Load Case	Margin	Safety Factor
Quasi-static Acceleration	35.6	1.4
Pressure	5.57	3
Random Vibration	0.64	3

Table 6.12.1: Structural Margins for 28-Day Cadence PLM

Given that all of the margins in the table are positive, at a preliminary level this PLM design should be able to survive launch and pressure loads. Similar to the last iteration, the calculation specifically for random vibration should be considered extremely preliminary as the fundamental frequency is very high for a primary structure. For a higher fidelity analysis, a structural FEA would need to be conducted to validate the first mode assumption to then derive a new random load factor. Again, this analysis was considered as outside the scope of the project due to time constraints and software license issues.

### 6.13 - Final PLM Launch and Lander Verification – Adithya Arun

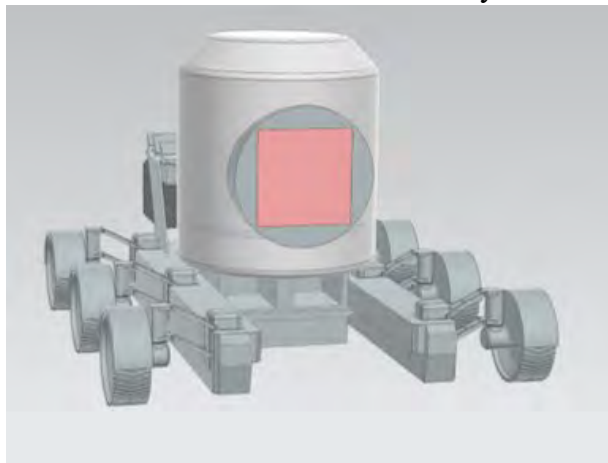


Figure 6.13.1: Final PLM With LLV

Assuming the Delta V from lunar transfer to landing is 3250 m/s, a LOX-LH2 lander should come out to a total mass of 3150 kg (including a 30% inert mass margin). Using mass estimating relations [LSM-#], the following inert mass table was created:

Inert Mass Summary		
LOX Tank	23	kg
LH2 Tank	45	kg
LOX Insulation	8.2	kg
LH2 Insulation	41	kg
Engine	68	kg
Thrust Structure	1.8	kg
Gimbals	0.5	kg
Avionics	210	kg
Wiring	120	kg
Structural mass	5.0	kg
Inert Mass	520	kg
Mass Margin	30%	

Table 6.13.1: 28-Day Cadence Lander Inert Mass Summary

Using the inert mass estimates to derive tank size for LH2 and LOX, the lander was created, modeled after Blue Moon. Though the PLM decreased in mass by almost half, there still exists no current NASA funded CLPS lander that can take the PLM to the moon. The largest CLPS lander, Astrobotic Peregrine, has a payload capacity of 625 kg to the poles of the moon. Therefore, deriving the feasibility of a lander is still valuable for this new PLM iteration.



Figure 6.13.2: PLM and Lander Within Falcon Heavy Fairing Envelope

Using the fairing envelope geometry as described in the Falcon User's Guide, a visual representation of the PLM and Lander within the fairing was created to check for interferences.

As expected, there were no interferences showing that the design for the lander and PLM are feasible.

#### **6.14 - Environmental Control System – Edwin Arevalo**

Our Environmental Control System (ECS) is a series of components that are designed to work together to monitor and control the environment within the Pressurized Logistics Module. Our ECS consists of pressure, thermal, humidity, and fire control. It is important to note that our ECS system will be controlled via an on-board computer of low voltage that can monitor the sensors in the system and control different aspects based on that information. The power required to run this computer was never calculated as that would depend on the specific make and model, however as it is not doing massive amounts of computations the power can be assumed low and its expenses covered within the built-in power margin designed. It is also important to note that the PLM is designed to be one-time-use and filled with trash and disregarded at the end of completing its mission to resupply a habitat. With this in mind, the system was designed to be relatively cost effective to allow for multiple PLM resupply missions.

##### 6.14.1 - Pressure

To determine the complexity of our pressure control system an analysis was run to determine how much pressure was expected to leak during an estimated maximum 7-day travel time. This 7-day travel time covers all the way from the time the PLM is sealed on Earth to the day it has reached its designated destination – in this case connected to a habitat on the lunar surface. This includes the estimated ~ 3-day transit time in orbit to the moon and overtimes of time for launch and landing and the actual transit time aboard the LLV from the lander to the habitat at a nominal speed of 10cm/s for an arbitrary overestimate of 4 km results in a travel time of about 5.56 hours. This estimation is talked about further in the mission planning section of this report. Using a report on overboard atmosphere leakage data provided by the International Space Station (ISS) [AFSS – 11E] that talks about the specification leakage and actual ground leakage of different modules aboard the ISS. The specification leakage takes into account the on-orbit leakage rates and the article interestingly found that this leakage is on average about 12-15 times higher than the actual ground leakage rate. This increase can be attributed to the faults caused by launch vibrations and additional interfaces when mating modules together, Cook et al. [AFSS-11E, p. 2]. The volume our PLM was modeled as a cylinder and two partial hemispherical endcaps and was found to be about 414 ft<sup>3</sup>. The atmosphere inside the PLM was modeled at 8.2 psi and 34% oxygen to provide the most accurate result based on advice from experts at NASA Marshall and was used to determine the molar mass and density inside of 29.28 g/mol and 0.0424 lbm/ft<sup>3</sup>. Finally, using that information the mass of the gas inside the PLM was found to be about 7.97 lbm. To accurately model our PLM, we used the data on the Russian DC-1 module which was of similar size, volume and mission purpose [AFSS-11E]. The specification leakage of 0.005 lbm/day because it is the limiting factor between the two estimates and since the PLM will spend most its time in microgravity. Importantly, after the 7-day period only 0.0035 lbm or ~ 0.02% of the pressure inside the PLM was lost and, assuming constant leakage, it would take about 35,130 days for total pressure loss. Therefore, no need for repressurizing tanks inside the PLM was found. Instead, our pressure control system is exclusively just 4 positive pressure relief valves

that can release and pressure build up inside the PLM possible caused by a NORS tank leak during transport. Four valves were chosen to provide zero net thrust during venting and to provide redundancy. Partial motivation for this model came from the relief valve design found aboard the Multi-Purpose Logistics Module and a guideline for devolving spacecraft aspects provided by NASA [AFSS-4E]. The valves must only be operated at very small vents as a larger and faster vent could cause an explosive decompression.

#### 6.14.2 - Thermal

An initial estimate for the PLM thermal calculations was done and we found that for the worst-case scenario where the PLM is in the hottest state with direct sunlight hitting it and solar

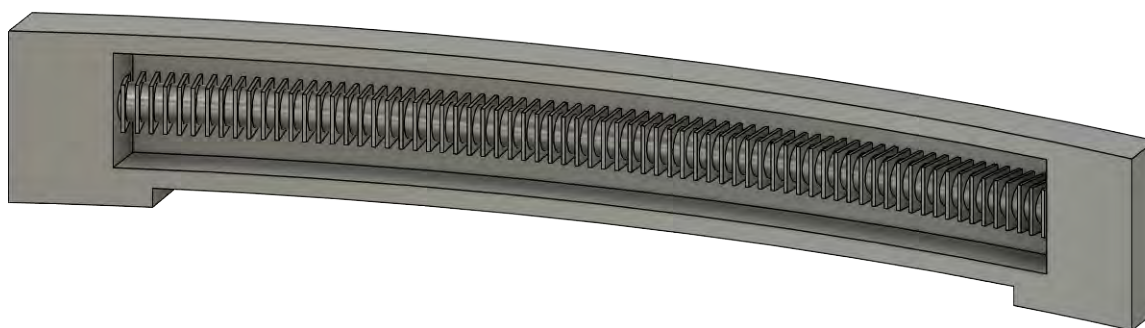


Figure 6.14.1: CAD design of the electric heater system. It is curved to match the shape inside the PLM and would likely be placed on along the top portion with vents redirecting the heat downwards.

reflections from the lunar surface; see *Initial PLM Thermal Calculations* in appendix. After speaking with experts from NASA Marshall this model was found to be unrealistic in practice and was handed down to the power, propulsion, and thermal team to refine upon it. For the actual design of the thermal control system it is comprised of a electric heater, multi-layered insulation primarily of mylar, and in-wall polyurethane spray foam. These components should give us the capability to control the emissivity and absorptivity of our system as well as control the temperature inside the PLM as long as the absorption was designed with the hottest case in mind and intent of never needing a cooling system as; as the design was done in prior calculations. The electric heater pictured in the figure below has an arc length of 48 inches, height of 8 inches and width of 4 inches.

Another important aspect of our thermal control are sensors placed strategically around the PLM to determine when the electric heater should be turned on. A main Lunar Outpost Canary-S sensor, or similar sensor, will be placed in the top ceiling of the PLM where it most exposed to the free volume. This sensor will help monitor not only the temperature but also the humidity, pressure, and present gases inside the PLM [AFSS-10E].

#### 6.14.3 - Humidity

Initially we determined that air ventilation would change power, weight, and heat requirements negatively and set out to find an alternative way to combat humidity. Additionally, a ventilation



system would add possible sources of failure for an electrical fire. We did not see a need for an expensive and dangerous air ventilation system, instead we settled on desiccants placed in modified Cargo Transfer Bags (CTB) to help regulate humidity as these can easily be thrown away with the PLM after its mission is complete. These desiccant packs are made of porous materials, most likely made from silica gel, that absorb moisture and help keep valuables around it, like electronics, dry and free from moisture related damages. Another important aspect of the humidity control was to require objects being stored inside the PLM to be checked for moisture content and sealed adequacy. This will further help regulate the moisture content inside the PLM and in turn the humidity.

It was later pointed out that without a ventilation system the temperature inside the PLM would not be homogenous as there would be cold spots throughout due to the uneven applications of the incoming thermal heat; this would in turn discombobulate our thermal management plan as different areas will be at different temperatures and a steady temperature could not be maintained throughout. Also, our fire detection system, mentioned further down in this report, would not function properly as there would be no flow to carry the fire elements to the detection device. Although a ventilation system would be costly to include it was found necessary to the successful operation of mission; to bring sensitive and valuable equipment remote parts of the lunar surface. This ventilation system would be comprised of ducting, electric ventilation fans, filters and vent covers. The input and output holes for the ducting will be placed along the top and bottom portions of the PLM along with the filters in the ducting to capture any contaminants in air. The filters would not need to be replaced as the PLM is disposable. The vent covers would also help ensure nothing serious enters the system that could cause a malfunction in the fans and possibly a fire. All in all, the design of the ventilation system is complicated and costly but necessary.

#### 6.14.4 - Fire Control

Our fire control system consists of three main aspects: prevention, detection, and suppression. Firstly, our prevention procedure relies heavily on how the PLM and its cargo are made. We will require Fault Detection, Isolation, and Recovery (FDIR) architecture and Electrical, Electronic, and Electromechanical (EEE) part selection be met on all electrical components inside PLM. The FDIR architecture ensures that the electrical components have some form of fault detection and shut down features. On the other hand, the EEE requirements ensure that proper safety and standards are met when putting components together, such as making sure all electrical cables are adequately shielded to prevent electrical sparks. Initially, another part of prevention relied on the lack of convection in microgravity and the absence of a ventilation system to cause small flames to self-extinguish. However, it is now found that a ventilation system is now indeed needed, and this no longer has any creditability.

For detection, initially we mainly relied on an optical beam smoke detector that in theory is good at monitoring a large volume by using lasers shot from a transmitter to a receiver to detect the presence of smoke based on how the light scatters. However, in practice smoke acts differently in microgravity. For example, normally on Earth smoke rises and thus smoke detectors are placed high up on ceilings, however, in microgravity smoke moves radially outwards from where the fire originated and is, for the most part, not guided in a singly direction.

Thus, we will use our ventilation system to guide the smoke to our smoke detectors by placing the detectors near the vents. This detector will not require any external receiver and only replies on the smoke entering the detector chamber much like a photoelectric or ionization detector. This will ensure the fastest and most reliable detection. Also, we can use the temperature sensors place around the PLM for the thermal control for dual purpose as we can also detect sudden increases in temperature which would indicate a fire.

Fire suppression consists of carbon dioxide suppressors. These were chosen because they leave no residue and are non-conductive, making them a perfect solution to use on sensitive electronics which they have been known for extinguishing [AFSS-24]. Carbon dioxide is toxic to humans but since the PLM is unoccupied during transport this is not a large concern. However, when the PLM is connected to the habitat at the final location the computer aboard the PLM must disable the carbon dioxide suppressors and the entire system must rely on the habitats fire suppression system which should include some form of handheld fire extinguisher. Additionally, if the carbon dioxide suppressors were to be used during transport, some air clean up would fall upon the air ventilation system however most of the cleanup would fall on the habitats filtration system as the PLM has no way to repressurize.

#### 6.14.5 - Thermal Control System – Joshua Batstone

In order to maintain the sensitive cargo onboard the pressurized logistics module, the PLM must be able to regulate itself to within a reasonably tight temperature interval. In order to accomplish this, a simple active thermal control system, comprised of resistive heating elements and multi-layer insulation, was developed. The design temperature interval used was 50 °F to 90 °F (10 °C to 32.3 °C), which is the same interval used on NASA's MPLM [PPT-16].

Since the system has no radiator, it must be capable of dissipating enough heat parasitically such that in the worst-case hot condition, the temperature does not exceed the maximum design temperature. All surfaces on the PLM are assumed to be covered by the same 25-layer MLI used in other analyses, with an effective emissivity of  $\epsilon_{eff} = 0.016$ , and an effective absorptivity of  $\alpha_{eff} = 0.003$  [PPT-9]. Similarly, a surface albedo of 121 W/m<sup>2</sup> was assumed, as with previous analyses. For the worst-case hot condition, the cylindrical side of the PLM (2.2 m diameter) is assumed to have a view-factor of 1.0 to the ground, resulting in both an overestimate of the albedo heating, and an underestimate of the radiative losses. Similarly, direct insolation is assumed to occur at 15° on the top surface, and normal to the cylindrical surface, as shown in Fig. 6.14.2 (another overestimate). These analyses resulted in an albedo heating of 7.64 W, and a direct sun heating of 26.3 W, totaling 33.9 W.

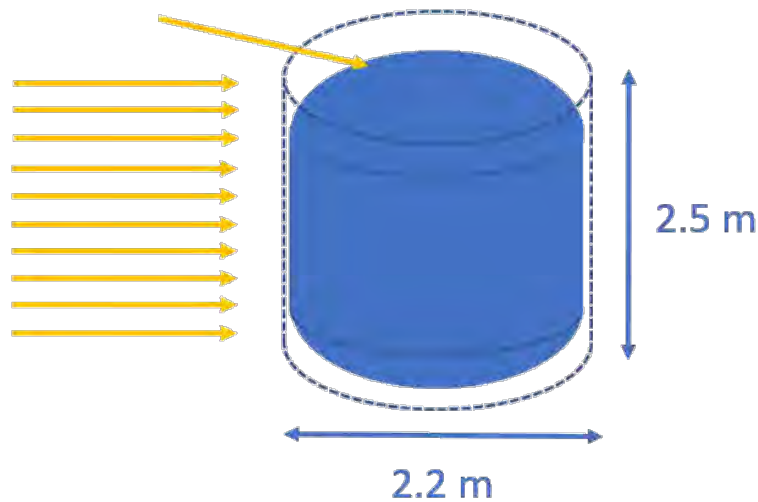


Figure 6.14.2: Worst Case Hot Setup for Pressurized Logistics Module.

For the worst-case cold condition, both primary and secondary sun heating are assumed to be zero, and the view-factor from the side-cylindrical face to the sky is assumed to be 1.0, resulting in an underestimate of the temperature. Plotting the heater power vs. the control temperature for both the hot and cold analyses results in the following graph (Fig. 6.14.3).

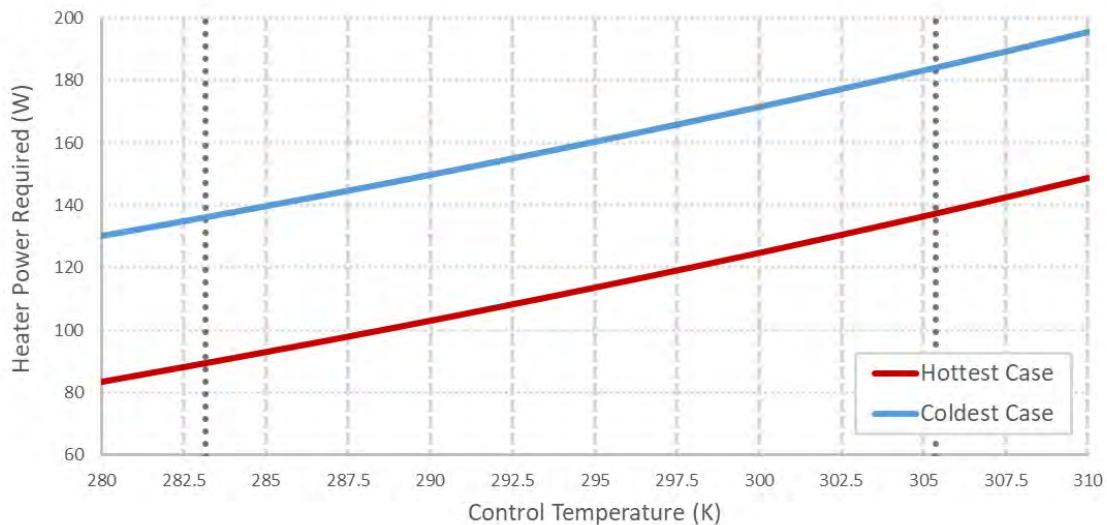


Figure 6.14.3: PLM Heater Power vs. Control Temperature.

Evident from Fig. 6.14.3 is that even for the worst-case hot condition, substantial heater power (approximately 90 W) is required just to keep the PLM at its minimum design temperature. This indicates that a radiator is indeed not required. For initial design purposes, we selected a nominal control temperature of 25 °C, and assumed the maximum heating power required, resulting in an estimate of 167 W. Assuming a mission duration of 7 days, and full thermal control over the entire mission duration, this results in an energy requirement of 28 kW-hr. These results are tabulated below in Table 6.14.1.

Table 6.14.1: Pressurized Logistics Module Thermal Control Power and Total Energy.

Thermal Control Heating	Total Energy (7-Day Mission)
167 W	28 kW-hr

#### 6.14.6 - PLM Battery – Adebayo Odusami

For our PLM battery we decided to go with a primary battery over a secondary battery mainly because of the short mission duration. Primary batteries are a better choice for short missions due to their high energy density. For our mission no recharging of the battery would be required because the mission would end before 0% DoD (Depth of Discharge). To meet the PLM power draw requirements of 28 KW-hr, we considered two types of cylindrical lithium-ion rechargeable cells; the Lithium Carbon Monofluoride (Li/CFx) cell, and the Lithium Thionyl Chloride cell (Li/SOCl<sub>2</sub>). Both cells had very similar specifications, so knowing that either cell chemistry would be a good choice, we made our final choice based on nominal voltage and temperature bands. Li/SOCl<sub>2</sub> which has a higher nominal voltage and wider temperature band, was the cell we decided to move forward with. The table below provides a summary of both cells' specifications.

	(Li/SOCl <sub>2</sub> )	(Li/CFx)
<b>Parameters</b>	<b>Value</b>	
Cell Nominal Voltage	3.6 V	2.6 V
Cell Nominal Capacity	19 Ah	19 Ah
Cell Mass	0.097 kg	0.072 kg
Cell Energy Density	705 W-hr/kg	690 W-hr/kg
Cell Operating Temperature	-55 to 85°C	-39 to 90°C
No. of cells needed	410	567
Total Cell Pack Mass	40kg	41kg
Total Battery Box Mass	73 kg	75kg

Table 6.14.2

The number of cells needed was calculated by dividing the total capacity by the capacity of each cell. The total cell pack mass was calculated by multiplying the number of cells needed by the mass of one cell. This gave us a total cell pack mass of 40kg. The next step was to find the mass of the housing and components. Taking the diameter of reference cell to be 3.4 cm, we multiplied this value by the number of cells which is 410, and by the height of a cell which is 10 cm (about 3.94 in) with a 30% margin. This gave us a number for the total volume of the box. We then offset these dimensions by 0.2 cm (about 0.08 in) for the sides and 0.3 cm (about 0.12 in) for the top and bottom to account for the thickness of the box. This gave us a battery box volume of 6000 cm<sup>3</sup>. Then using the density of CFRP which is about 2 g/cm<sup>3</sup>, we calculated the mass of the battery box housing to be 12 kg. This brings our total battery box mass to 52 kg,

and with a 40% margin to account for other components and possible human error, we have a final battery box mass of 73 kg.

### 6.15 - PLM Docking interface Jack Molter

Design of an error correcting active docking interface for the PLM to dock with an existing lunar habitat is required given the imperfect placement capability of the LLV. To begin the design process, I investigated existing docking like the ISS standard berthing mechanism and NASA Chariots, active-active ports [LSM-29, 30]. A trade was done between an active-active and an active-passive interface. The active-active has the advantage of having increased error correction thus requiring the rover to be less accurate in its PLM placement, with the downside being that the PLM mass, complexity, and cost increase. The active-passive dock was chosen as being the better alternative after it was determined by other LSM members that the rover's placement accuracy would be sufficient for only one side of the dock to be active.

Mimicking one half of the NASA Chariot design I began research into the Stewart platform for use as a 6 DOF manipulator. The Stewart platform allows for the docking interface to be moved to correspond to the port position of the PLM. Once docked, the hatch can be pressurized and opened to allow the astronauts to offload the cargo from the PLM. Control of the habitats active side of the dock could be done by an astronaut with line of site to the PLM, or autonomously if preferred.

At this point in the project the shape and size of the docking hatch was unknown but assumed to be rectangular. I started with a baseline of a 40 x 60-inch hatch and then following the nominal structure of the Stewart platform mapped the actuator locations around the port in a circular orientation. The basic design for how the active side would be constructed was complete and next the specifics were determined.

Finding the workspace envelope of a Stewart platform, and the singularity positions is non-trivial, for this simplified model I did not consider singularities. To determine this workspace model, I wrote a MATLAB script that took as input actuator base plate mounting position, actuator top plate mounting position, and desired translational and rotational movement [LSM-2, 28]. The script is brute force in that it outputs the lengths required of each leg to perform the desired movement, so that for a given stroke length it could be determined if a

position was possible. Using this Figure 6.15.1: CAD model of the docking approach  
for a set stroke length the maximum movements were determined. Along with the maximum movement possible in 6 DOF, the maximum movements in 5 DOF were also calculated under the assumption that the PLM hatch could be placed with high accuracy to the same height as the habitats hatch. This assumption was made because of the need to place the habitat on an even

level surface, and the proposed plan of lunar grading using our LLV. The CAD model of this design is shown in Figure 6.15.1.

The ratio of stroke length to base/top plate diameter determined the workspace envelope. At the time the required amount of correction for LLV placement inaccuracy was unknown making the final design measurements somewhat trivial. However, if the required correction had been found then the exact values needed could be determined from the model. The design I ended up using had actuators with 48-



inch stroke length. Although the base and top plate dimensions were never altered, a change from circular plates to rectangular would almost certainly have added capability to the design as the spacing between actuators would have decreased. With the diameter of the circle that connected the pivot points of the top and bottom plates set to 88 inches, (to fit the inscribed 40 x 60-inch port) the platform would be capable of  $\pm 3''$  of translational freedom in all directions, and  $\pm 4^\circ$  of rotational freedom. A not-to-scale model of the maximum capability of the platform is shown in Figure X, where the green plane is the nominal position of the docking plate, and the red plane is one case of the maximum movement of the platform. The blue circle shows the location of the base plate which would be the entry point into the habitat.

As a last-minute change to the design a new iteration of the PLM was done to work with the lunar cycle of 28 days. This reduced the size of the PLM and made the 40" x 60" port less practical. For this reason, on the final design a 40" x 40" port size is used. No analysis was done on this size port, in regard to the new capability of the active docking design. However, the smaller top and bottom platforms would only increase the ability of the platform to translate and rotate, leading to a greater degree of error correction.

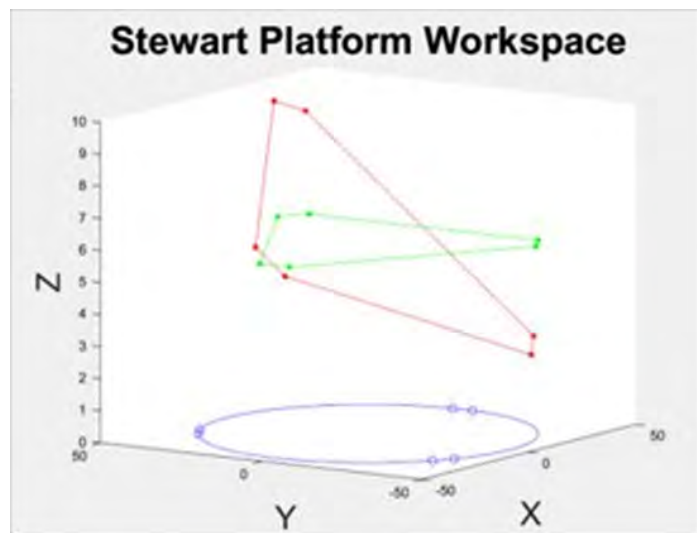


Figure 6.15.2: Maximum Movement of the Stewart Platform

### **6.16 - X-HAB Hardware Development Jack Molter**

An important part of the X-HAB portion of this project is the hardware development and testing. I oversaw hardware development for X-HAB from initial brainstorming to the building,

testing, and proceeding analysis of the test results. I began by discussing the most important things we could learn from hardware with other LSM members and some others from the team. Since the X-HAB project revolved around the PLM this is where most of the ideas naturally revolved around. Some of the first ideas that we had early on were building a docking mechanism, building a scaled PLM for testing, docking this PLM with a habitat, and offloading cargo from the PLM into the habitat for testing. The idea of using the SSL VERTEX rover to carry the mockup PLM was also discussed, including a possible habitat dock and offload while the PLM was being lifted by VERTEX. Because of our timeline these ideas were narrowed and refined as time went on to be more realistic.

At this point all of the testing or demonstrations that I wanted to do involved using some structure to simulate the PLM. At this point, little was known about what the final PLM would look like, but it was assumed that it would be cylindrical and at least large enough for a person to stand in, the orientation of the PLM relative to the habitat (vertical or horizontal) was not known yet. A circular structure, or something to act as a cylindrical boundary would be needed for all of the testing I had in mind. To try and best simulate this PLM I started researching spherical containers we could use and found that many water containers were the proper size of what we believed a rough estimate of the PLM would be, which was 6' in diameter and greater than 6' tall. By the final iteration of the PLM, the actual sizing was 6 feet in diameter and 6 feet tall, which was conveniently within margins of the water container that we used. It was at this point that we discovered that SSL had an old water container from an old project in the moon yard. After some painful work to uncover the container from its entrenched state we had a perfect 69" diameter 76" tall container to use as a PLM. The container had some existing holes from the past project, but these did not end up being an issue.

Before anything could be done with the container, it had to be pressure washed inside and out and the old scrap wood from past projects had to be removed. The current design for the PLM still did not have orientation determined but with limited time I made the decision to start designing for a horizontal orientation. The rationale behind this decision was primarily to preserve the strength of the water container. Since there were already large holes in either end it would be easy to use one of these ends as the port side and no additional holes would be required in the curved part of the cylinder.

With the orientation determined, how to facilitate this was the next step. Some of my initial ideas were using sandbags to create supports for the cylinder, building a wooden structure for raising and securing the structure, or using existing raised structure (for example a short wall) to raise the PLM. To use an existing structure, we would have to use something besides the SSL habitat to act as the docking structure, at this point in the design the other LSM members and myself had a strong desire to use the existing habitat if possible, so we ruled out this idea for now. Because of the large amount of useful wood, we already had at SSL to use I made the decision to design a wooden structure that we could use to suspend and secure the PLM to the habitat. I designed two possible builds using 2" x 4" and 4" x 4" wood that we had available at SSL. These designs are shown in Figure 6.15.2.

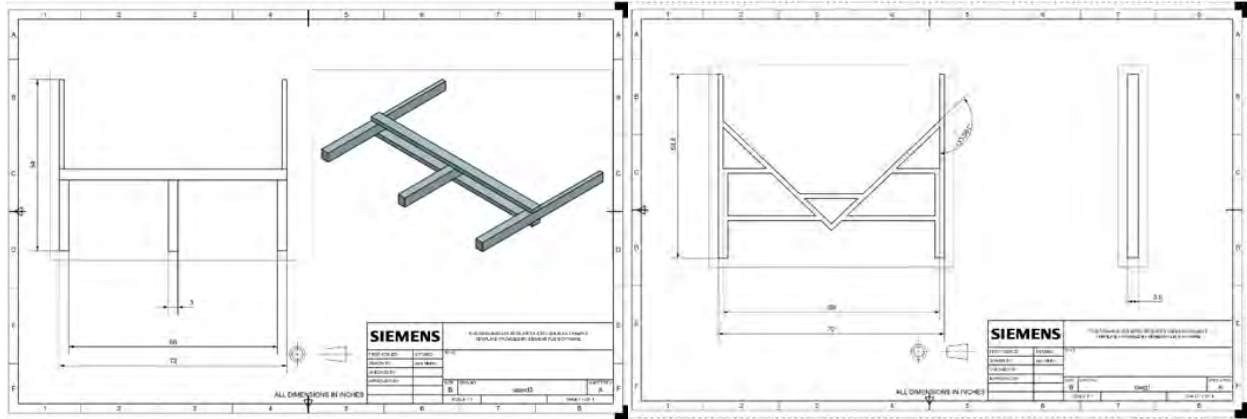


Figure 6.16.1: Proposed Stands for a Horizontally Oriented PLM

Shortly after these horizontal designs were finished it was determined by other members of LSM that the PLM would be designed for a vertical orientation for launch vehicle storage and ease of use for astronauts. With this new information I could either continue with the horizontal design or switch to a vertical design. To attempt to stay as true to our intended design as possible for more accurate testing a vertical design would become the path forward. The stands would not be needed for this orientation and were never constructed.

The original idea of designing and building an active docking mechanism was ambitious. For many reasons this idea was quickly narrowed to only include a scaled rendition of the main mechanism (the Stewart platform) for use as a concept showcase. Due to time constraints and having what I considered to be more important hardware to complete, the docking mechanism as part of the X-HAB hardware was not continued past an initial design and modeling phase as discussed in section 6.15. Moving forward, the testing and hardware development would focus on the human factors and port sizing, not the docking capabilities of effects on an offload.

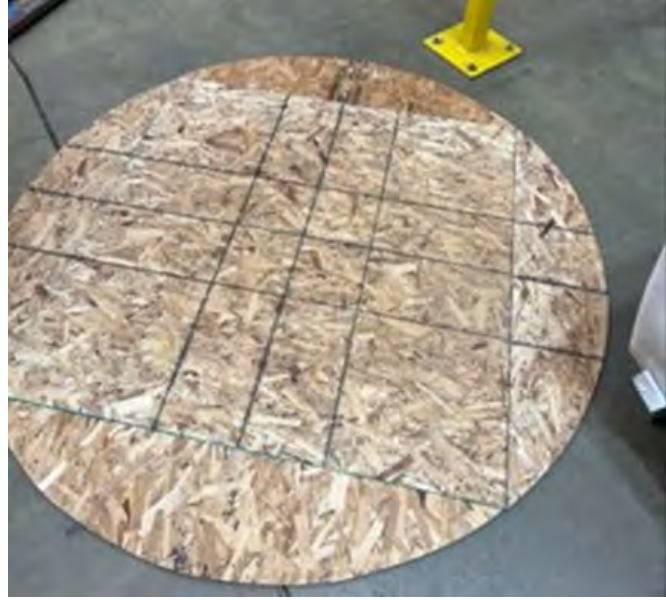
At this point in the project little had been done to work with VERTEX for carrying the PLM, this along with VERTEX being disassembled for most of the second half of the semester lead to this idea being killed. The scope was again further narrowed by the eventual shift from using the existing habitat to using a standard rack, which is a 20" x 40" x 80" structure made of aluminum 8020. This structure would act as a wall of a habitat, and we used to simulate the habitat's side of the dock. The updated hardware development plan was to use the mockup PLM for an offloading test to simulate cargo being offloaded into a habitat, from this we could experiment with different size ports, offloading techniques, storage strategies, and learn how these effected the astronauts.

With a more realistic goal for hardware, building began. First, I determined that we would need to build a floor for the PLM, with the new orientation there were uneven sections of the floor caused from the holes in the bottom side of the container. These holes caused sections of the plastic to be raised and posed both a safety issue and an unrealistic storage constraint. The floor was built by cutting a 4' x 8' sheet of plywood into a 68" diameter circle, split into 5 pieces, shown in Figure 6.16.2.

Next the port size and position were determined. The port hole was cut in the side of the PLM. The port hole was cut as a 40" x 40" square, raised 24" off the ground. The port hole was



not cut to the ground to determine the effects of a step over on astronauts doing offloading. The 40" x 40" dimensions were chosen to allow more than enough room for walk through and carry through testing. Building this to the largest size I intended to test allowed for the port to be easily shrunk to test smaller sizes. The decision to raise the port 24" from the ground was arbitrary, and looking back deeper thought into this part of the design could have been useful for more accurate testing.



Figure

#### 6.16.2: PLM Flooring

Once I had decided not to try and develop an active docking interface for testing a passive option was required to accurately interface the PLM with the standard rack. To build this I used 2" x 4" wood to cut wedges to create a plane tangent to the cylinder for the standard rack to touch up against. 4 of these pieces were cut for each of the corners of the port. The actual port was constructed out of plywood. Two C shape sections combined to create the port hole with a surrounding border. An image of the full testing setup can be seen in Figure 6.16.3.

Now that the required hardware had been constructed the next step was to create useful tests to perform on the PLM to improve our current design or validate the decisions we made. I planned to test how offloading under different conditions affected the ease of offload, and how the astronauts felt after completing an offloading. To act as the cargo 8 full size CTB's and 5 half size CTB's were used as cargo. This resulted in the PLM being only partially full, which is not consistent with how the true PLM would be stocked with over 80% packing ratio, however this inconsistency likely had little effect on the value gained from the testing. For these tests the CTBs were placed in a similar fashion for each test. Some of the CTB's had added weight to them and some were empty. After testing had been completed it was noted that looking into packing orientation and PLM storage techniques' effect on the offloading process would have been a good addition to the tests.

Testing would be split into solo offloading that required a walk through from PLM to habitat, and team testing that was done using a pass-through technique. For the team offloading the same subject was on the PLM side of the habitat side for every test, the person on each side did not enter the other section. We did not attempt to do a team offload where both subjects worked to offload cargo using the walk-through technique. Either 3 or 2 trials of each test were conducted.



Figure 6.16.3: X-HAB Testing Setup

The testing looked at the effects of decreasing the width of the port and how a single astronaut compared to a team of two astronauts. The data collected included the time it took to offload all the CTBs out of the PLM, 1.5 meters into the “habitat”, NASA TLX parameters, and the Cooper Harper Handling Qualities Scale (CH) were also collected. Less formal data was gathered by asking test subjects how they felt during parts of the test and documenting any interesting things that happened. Time was chosen as a means of assessing the degree of increase in offload difficulty when the port became more constrained. The TLX parameters were chosen as a useful tool for determining how the astronauts felt after the offload had been completed. And the CH scale was incorporated to add some additional value to the testing and add a different assessment of stress to the testing. The data and difference between the port sizes for each respective test is shown in Table 6.16.1 and Table 6.16.2. How the TLX and CH scales work can be found in [LSM -31, 32].

Solo Offload							
	Time (min)	Physical stress	Mental Stress	Effort	Performance	Frustration	CH rating
40 x 40 Port	1:58	5.7	1.7	3.7	9	3.7	4.7
40 x 30 Port	2:06	5.7	2.7	6	8	6.3	5.7
% difference	6.8	0	37.0	38.3	-12.5	41.3	17.5

Table 6.16.1: Solo Offloading Data

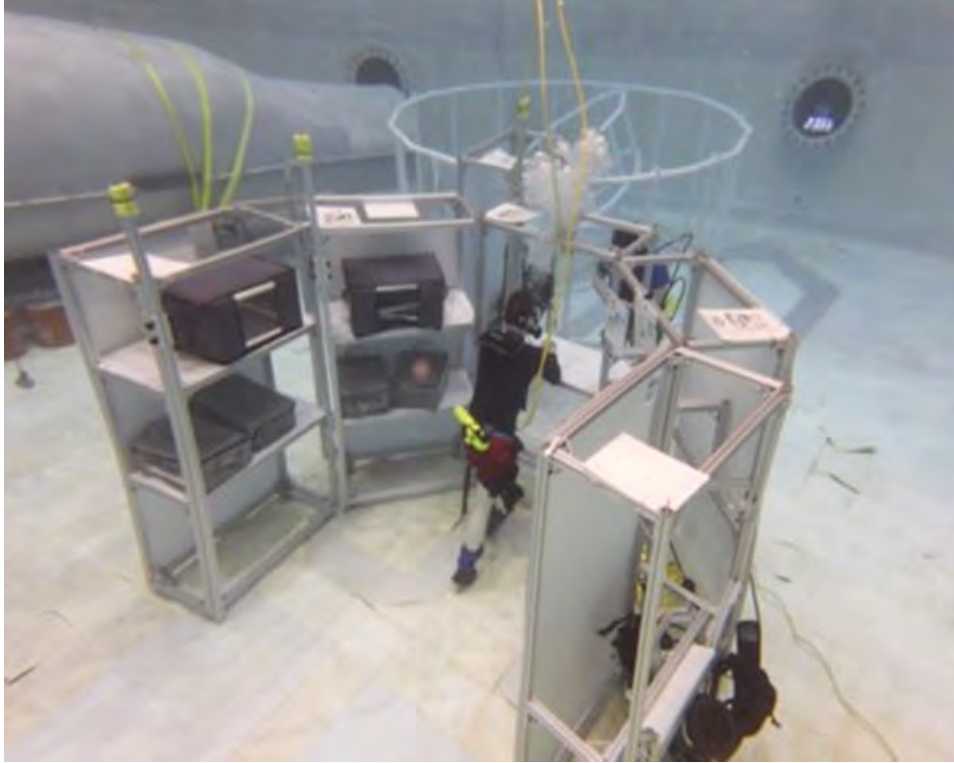
Team Offload							
	Time (min)	Physical stress	Mental Stress	Effort	Performance	Frustration	CH rating

40 x 40 Port	0:40	6	3.5	2.3	9.5	4.5	3.8
40 x 30 Port	0:41	6	3	1.8	10	4.5	3.5
% difference	2.5	0	-16.7	-28.6	-5.0	0.0	-7.1

Table 6.16.2: Team Offloading Data

Some of the data was not surprising, we knew going in that two people would be able to offload the cargo faster, and that a smaller port would likely cause an increase in time; however, the degrees to which these expectations were true was interesting. We found that a reduction in the port size had a moderate effect on the offload time for a single person but almost no change for the two-person offload. I believe that the important factor that affected this was the step over motion that was eliminated when using two people to do the offload via pass-through. The bottom of the port was raised 24 inches off the ground and was remarked as being the most difficult part of the offload. During testing we also had people drop CTBs and bump their head while stepping over. From these tests it was obvious that the stepover was not ideal if only a single astronaut would be offloading the PLM. A future test, with a 40" x 40" port on ground level would be the best way to verify this conclusion.

Some of the other data that we got was less conclusive. The TLX parameters may point to the smaller port increasing the difficulty of the offload, but this data is limited and overall, I did not find it to be as useful for analysis as I thought. If given the chance to redo these tests I believe that instead of asking for all this information after each trial, I would rely more on the subjects thoughts and actions during the tests. What's easy what's hard, as opposed to trying to put a number to a lot of different measures. I believe some of the TLX values may be misleading due to the lack of a baseline for the subjects to use. Some additional limitations to the test were that it was conducted under Earth gravity, the test subjects were wearing plain clothes not representative of the limitations of a spacesuit, and only two or three trials of each test occurred.



The results and conclusions from these tests have helped us to refine the PLM design and change the positioning and shape of our port. More analysis is still needed to determine the feasibility of designing a port the size we would like, to allow for a human to normally walk from a habitat into the PLM. If we find this is not feasible then further

testing into port size will be helpful.

Figure 6.16.4: Neutral Buoyancy Testing

Reflecting on these tests, I would have liked to run more trials and look at different variables. Now that it's clear the stepover is not practical experimenting with different port heights is the next logical step. We did not have the chance to test a circular port, and logic would suggest that unlike zero g, a circular port may not be ideal; however, the results of this test show that it may be better all together if the astronauts don't have to handle the cargo offload much at all. The addition of some apparatus to assist the astronauts in offloading would also be a useful next iteration of these tests. Another interesting idea would be a self-offloading PLM that is packed in such a way that an internal mechanism can offload the cargo into habitat storage without an astronaut in the loop.

In addition to the outdoor moon yard testing of the PLM, neutral buoyancy testing also took place thanks to the help of the divers at SSL. These tests looked into the benefits and drawbacks of different size ports and different styles of cargo offloading. The first tests were done with a 40" x 60" port hole and pass through as well as walk through testing. The 60" height made is so that the subjects could nearly walk through without having to bend over, and unlike the moon yard testing there was no step over present, the port was positioned at the base of the mockup PLM walls. After these tests this interface was replaced with a 40" x 80" port with a horizontal sheet in the center. Pass through testing above and below the center plane took place. The CTB's in this test were ballast to a variety of different weights, starting from 15 kgf and going as high as 68 kgf lunar weight.

Some interesting conclusions from these tests were that unlike the moon yard tests, just because the subjects were able to do an offload or refill faster, they didn't necessarily prefer that port or

way of offloading. For example, the test subjects remarked that they preferred using the 40" x 40" top port over the other ports, yet the offloads and refills with that port were the slowest of the three ports tested. This seems to be contributed to the ability to put the CTBs down on the sheet while the other person loads another CTB into the habitat. This action relieved stress on the muscles by allowing them to take a break. Another important thing that was found from this testing is that the heaviest CTB was difficult to handle in all the testing. It is likely that some sort of tool or mechanism would be needed to help astronauts deal with heavier cargo, especially considering that the CTB's are not planned to be the heaviest cargo in the PLM.

## **7. Cargo Manipulator**

### **7.1 - Mission Context – Matthew Thomas**

Thus far we have discussed how SHELL will be utilized for the transport of large pressurized lunar logistics, but sustaining a base on the moon will require more diverse payloads. For payloads which will be stored and used outside of the habitat, such as external radiation shielding, non-pressurized forms of transport would save considerable mass when compared with the PLM. By reducing mass and delivering these non-pressurized logistics on CLPS we can streamline SHELL into the existing NASA Artemis framework.

To achieve this model for non-pressurized logistics transport, a system must be developed to offload logistics from CLPS landers and pick logistics up from the lunar surface. The SHELL pressurized logistics transport system requires logistics be picked up from the lunar surface, but non-pressurized logistics will require more diverse capabilities given the wide variety of funded CLPS landers. The CLPS program will initially be funding systems with payload capacities of up to 500 kg, but the payload configurations are largely unspecified at this time [LSM-11]. To accommodate the widest array of CLPS landers, it will be critical that the developed offloading system be capable of manipulating the full range of payload capacities.

When manipulator development began, it was planned that the system would be used for both pressurized logistics and small non-pressurized payloads. This concept was sidelined because a manipulator capable of lifting and manipulating 15,000 kg habitats would be both difficult to stow and significantly over-sized for most use cases. After this realization, the manipulator was descoped and the large-scale manipulator concept was set aside in favor of the U-shape LLV concept. The large-scale pressurized transport was supported by the LLV and SPI interface, but the transport of small-scale non-pressurized logistics was still in need of a lunar transport concept.

For this purpose, a cargo manipulator was developed as an auxiliary payload for the LLV, which will provide the ability to lift and manipulate non-pressurized payloads up to 500 kg. The cargo manipulator will be attached to a loading bed which, like all other payloads, interfaces with the LLV using the SPI. In this way, the cargo manipulator will add additional functionality to the system without sacrificing the versatility of LLV's base structure. On the payload end of the manipulator, there will be a custom manipulator-payload interface to rigidly attach to logistics carriers. In addition to providing manipulation capabilities, the manipulator will also host a camera which can be used for inspecting objects of interest across the lunar surface.

### **7.2 - Concept of Operations – Matthew Thomas**

To provide a clear image of the purpose of this system, the concept of operations for our final manipulator design can be seen in fig. 7.2.1. A standard mission that will need to be completed by the cargo manipulator will be the transport of lunar logistics picked up from a CLPS lander or the surface of the moon. These cases drove the design approach and system trades, and ultimately led to our final design of the manipulator system which will be discussed throughout the upcoming sections.

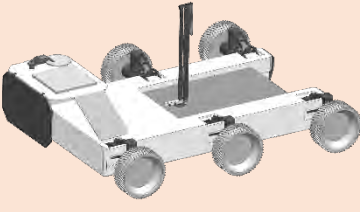
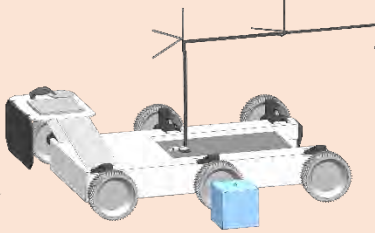
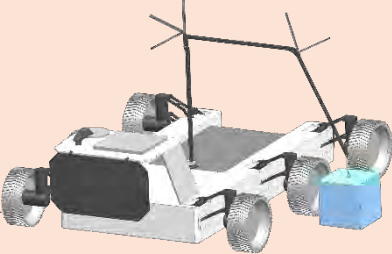
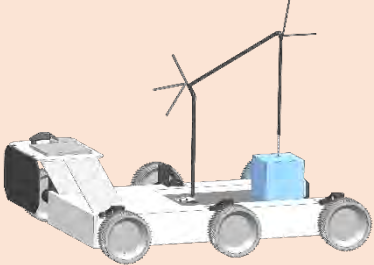
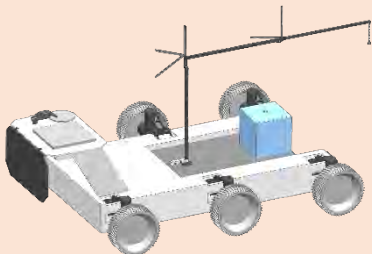
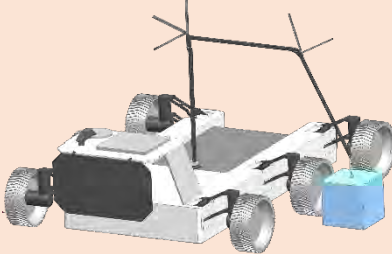
		
The manipulator will arrive on the lunar surface with the LLV in its stowed configuration	Once deployed, the LLV will position the manipulator adjacent to a logistics carrier	The manipulator will navigate to the logistics carrier and interface with the receptacle
		
The manipulator will lift the logistics carrier and position it on the loading bed	Once latched, the logistics carrier will be transported across the lunar surface by the LLV	The logistics carrier will be offloaded at the desired location

Figure 7.2.1: Cargo manipulator concept of operations

### 7.3 - Design Philosophy – Matthew Thomas

When designing the manipulator, several goals were set out for the final product. First, the system should be simple and robust. This meant minimizing the Degrees of Freedom (DOF) to only those necessary in an attempt to reduce opportunities for failure and complexity of the control system. The second goal was to minimize mass through intelligent materials selection and high mechanical advantage joints. Finally, it was desired that the system has a large reach envelope to ensure that logistics could be manipulated within the radius established in CME-5.

To achieve these goals, the design of the cargo manipulator went through several phases which will be discussed in upcoming sections. The process began by performing a literature review exploring existing manipulator technology being used by NASA and private organizations. From this research, a trade study was performed which examined crane-like manipulators and traditional robotic arms. This trade study resulted in the selection of the NASA Langley Lightweight Surface Manipulator System (LSMS), which leverages crane technology for space applications [LSM-11]. After selecting LSMS, a static force model was created to determine various load configurations and size the cross-sections for SHELL's manipulator. To ensure the viability of the manipulator, further investigations into deployment, stability, thermal management, and payload interfacing were performed.

#### **7.4 - Arm vs. Crane Trade – Yida Shen**

In the realm of lunar surface transportation, the comparison between the Arm vs. Crane tradeoffs plays a crucial role in the design and functionality of the Lunar Logistics Vehicle (LLV). The Arm, a robotic manipulator system, offers unparalleled versatility and precision in manipulating objects, allowing for efficient material handling and assembly tasks. Its multi-jointed structure and advanced gripping mechanisms enable it to handle diverse payloads, including delicate scientific instruments and heavy construction materials. On the other hand, the Crane offers an alternative approach with its towering mechanical arm, capable of lifting and relocating bulkier payloads over longer distances. The Crane's extended reach and robust lifting capacity make it an excellent choice for scenarios that require rapid movement of large-scale equipment, such as habitat modules or regolith mining machinery. Ultimately, the choice between the Arm and Crane in the LLV design depends on the specific mission objectives and payload requirements, with each system bringing unique advantages to lunar surface operations.

In the context of a Lunar Logistics Vehicle (LLV) with a funding limitation for systems with payload capacities of up to 500 kg, the implementation of a robotic arm brings several advantages. The robotic arm's versatility and precision make it a valuable tool for handling and manipulating payloads within this weight range. Its articulated structure and precise control mechanisms allow for intricate movements and delicate operations required for scientific experiments, equipment maintenance, or assembly tasks. With a payload capacity of up to 500 kg, the robotic arm can efficiently handle a wide range of objects, including scientific instruments, tools, and smaller equipment components. Additionally, the arm's dexterity and adaptability enable it to perform intricate tasks with high accuracy, ensuring the safety and integrity of the payload during transport and deployment on the lunar surface. By integrating a robotic arm into the LLV system, we can leverage its capabilities to effectively manage payloads within the specified weight range, providing enhanced operational flexibility and efficiency for lunar surface missions.

#### **7.5 - LSMS Overview – Matthew Thomas**

The LSMS concept was originally designed in 2007 but has since gone through years of development and testing at NASA Langley. The system leverages known crane concepts to provide high stiffness and mechanical advantage, and by doing this reduces the overall mass of the system. NASA designed the system to be scalable so that it could be applied for a variety of load cases from 300-3000 kg [LSM-11]. LSMS can be broken down into four major linkage types: primary links, spreaders, tension rods, and cables.



The primary links, denoted by the letter “B” in fig. 7.5.1, support the main compressive loads of the payload and act as the main body of the manipulator during actuation. The spreaders, denoted by the letter “S”, distribute the compressive loads from the primary links to the tension rods and provide the necessary mechanical advantage for the actuation system. The tension rods, denoted by the letter “T” in later sections, support the tension loads between each of the spreaders and carry the force required to actuate the primary links. Finally, the cables, denoted by the letter “C”, attach the tension rods to the motors which will provide the energy required for actuation of the whole system. Through these linkages, LSMS can provide 3 DOF manipulation of any objects within it’s given envelope [LSM-11].

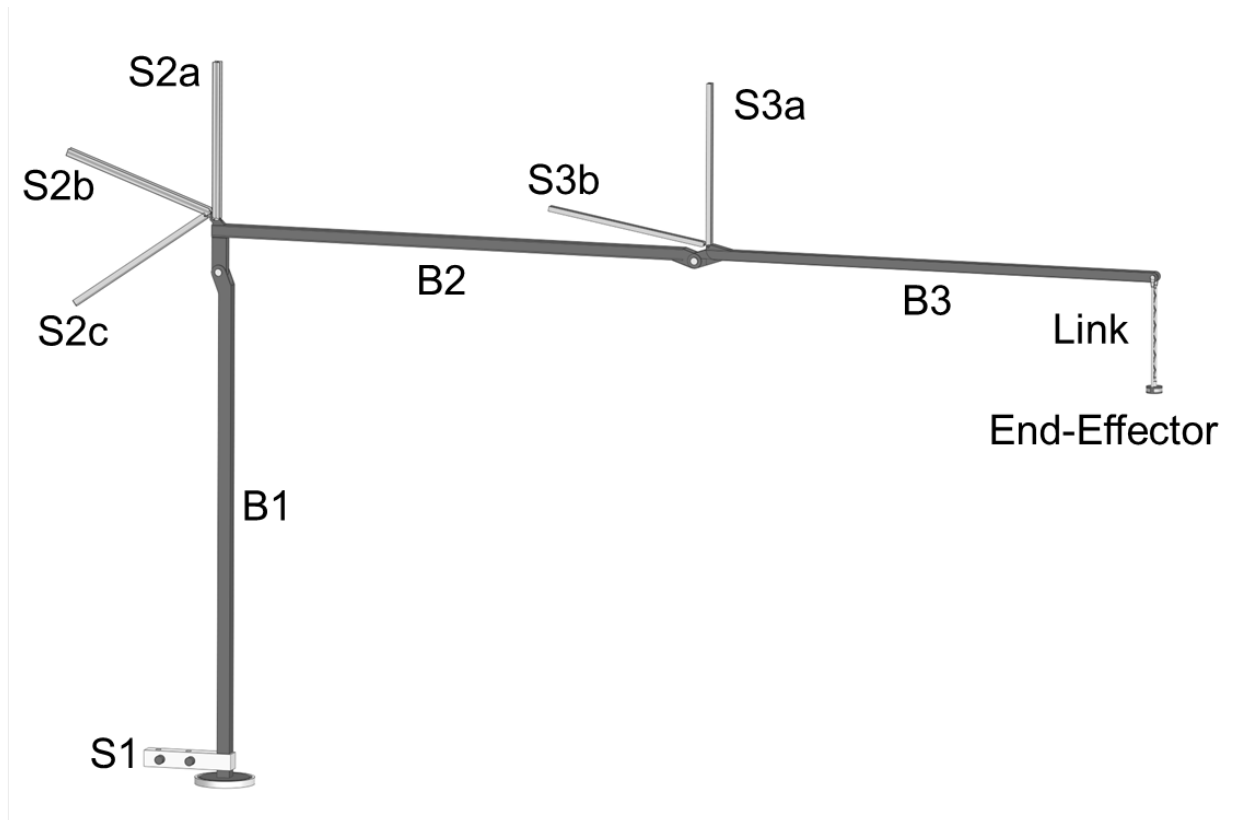


Figure 7.5.1: LSMS primary link and spreader diagram

### 7.6 - Static Force Model – Matthew Thomas

To support in the design of SHELL’s cargo manipulator and size LSMS to our 500 kg payload application, a static force model was created in Excel. The model utilizes joint analysis to solve for the forces in each linkage of the assembly throughout the entire operational envelope. While moving through the envelope, there are conditional contact relationships between certain linkages which are accounted for in the calculations and can even be visualized by the model. For inputs, the model first requires the configuration of the manipulator to be established with linkage lengths, relative linkage angles, and payload mass. After this, cable lengths are input to establish the current orientation of the manipulator. From this information, the model will output the forces in each linkage. To explore how the forces change throughout the operational envelope, one can cycle through a variety of cable length inputs for a single configuration. In addition to force calculations, the model also plots the position vectors of each

linkage on a graph to visualize the system and show the current configuration and orientation of LSMS.

Using these features, the team cycled through a variety of scaled versions of the original LSMS linkage dimensions to find the configuration that best suited CMX-2 and CME-5. In addition, the graph was utilized to verify that the manipulator would be capable of orientations for manipulating logistics carriers on landers and the lunar surface. Through this process, the lengths shown in Table 7.6.1 were selected for each linkage in SHELL's cargo manipulator. After selecting the lengths for each linkage, the force outputs were used to examine the wide variety of load configurations that needed to be considered during cross-section design and sizing.

Linkage	Length (m)
B1	2.00
B2	2.00
B3	2.00
S1	0.25
S2a	0.63
S2b	0.63
S2c	0.68
S3a	0.63
S3b	0.63
T1	2.02
T2a	2.10
T2b	0.72
T2c	0.60
T3a	2.10
T3b	0.80

Table 7.6.1: SHELL LSMS linkage lengths

### 7.7 - Load Configurations – Matthew Thomas

In preparation for cross-section selection and sizing, a wide variety of load configurations were examined by cycling through cable lengths in the force model to see how linkage forces shifted throughout the movement. Through this process, the team was able to identify several key load configurations which correlated with the maximum expected forces for certain linkages. Identifying the maximum expected force for each linkage was crucially in sizing the cross-sections in the next section.

The first configuration to be discussed is the extended configuration, shown in fig. 7.7.1 with the expected forces for each linkage. This configuration shows the manipulator at its full 4-meter range while sustaining the 500 kg payload at the end of the B3 linkage. This was a configuration of concern due the significant amount of torque applied at the B1-B2 joint due to the moment arm created by full extension. As a result, this configuration was closely tied to the maximum expected force for the T2 tension rods.



Figure 7.7.1: Extended configuration plot and expected forces

The second configuration of concern was the peak load configuration, shown in fig. 7.7.2 with expected forces for each linkage. When moving the payload inward toward the base of the manipulator, the forces in the B1 linkage begin increasing dramatically. While the peak load configuration varies for each linkage, this configuration is considered the general peak load because it features some of the greatest forces seen throughout movement of the manipulator, particularly at the base.

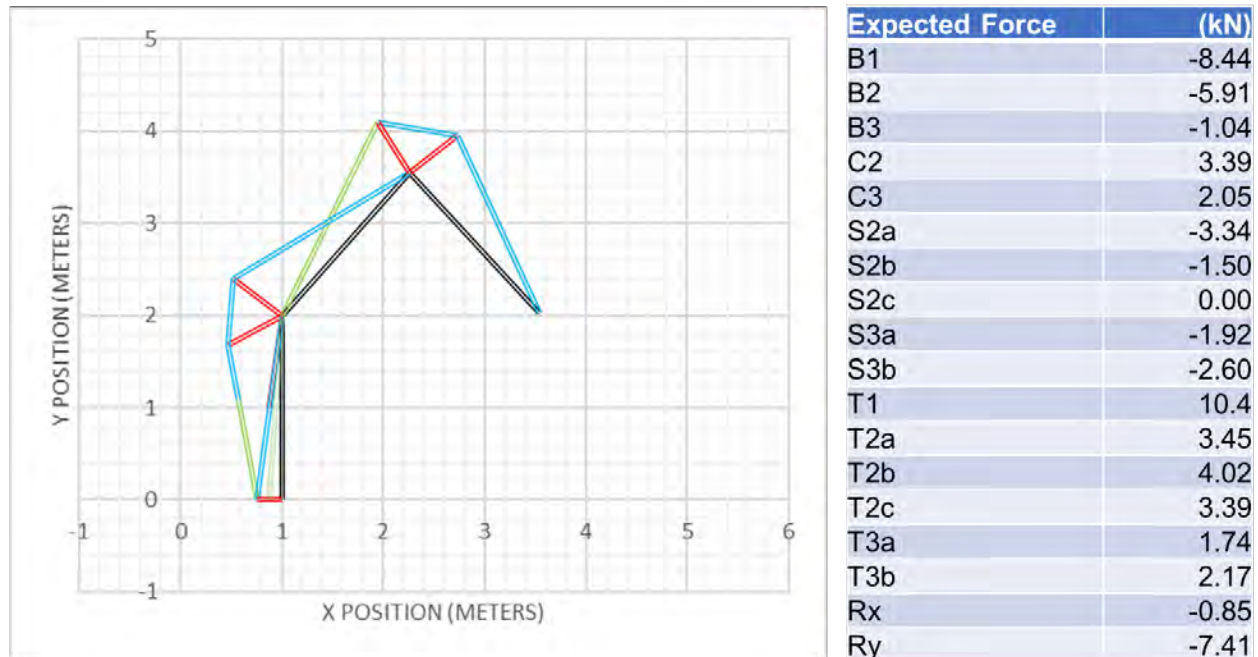


Figure 7.7.2: Peak load configuration plot and forces

After considering the above configurations among many others within the operational envelope, the highest expected force for each linkage were tabulated for cross-section sizing. The max expected force for each linkage can be seen in Table 7.7.1. For linkages around the same joint with similar max expected forces, such as T2a, T2b, and T2c, they were unified under a single label to simplify cross-section sizing.

Linkage	Max Force (kN)
B1	12.0
B2	8.00
B3	2.80
S2a/b	6.00
S2c	6.00
S3a/b	3.20
C2	5.80
C3	3.00
T1	14.5
T2a/b/c	6.50
T3a/b	3.50

Table 7.7.1: Max expected forces in each linkage

## 7.8 - Cross-section Design – Matthew Thomas

### 7.8.1 - Material Selection

To perform cross-section design, the first step was the selection of materials for each linkage in the manipulator assembly. While material selection was open to change as more

failure modes were integrated into the analysis, the initial selections were required to examine failure cases, size cross-sections, and calculate margins. Key properties that were sought after during the materials search were high yield strength and high specific stiffness. By maximizing these properties, the assembly would be more resistant to buckling and bending failure, which were the primary failure modes. In addition, high specific stiffness is a mass-efficient way to reduce deflection which would make the system difficult to control. Table 7.8.1 shows several candidate materials and their associated high-importance properties.

Alloy	Density [kg/m <sup>3</sup> ]	Yield Strength [MPa]	Specific Stiffness [MN-m/kg]	Young's Modulus [GPa]
Al 7075	2.83e03	530	27.2	76
Al 2024	2.78e03	381	27.4	75.7
Ti-6AL-4V	4.43e03	1.08e3	26.9	119
AISI 304	8.06e3	310	25.6	203

Table 7.8.1: Candidate materials and key properties [LSM-19]

From the preliminary materials research, both aluminum alloys stood out for their high specific stiffness, improving their resistance to buckling failure. Al-7075 was ultimately selected as the best candidate material due to its high yield strength and low density, which will make it a lightweight solution for preventing bending failure. Al-7075 was used for the cross-section sizing of the primary links, spreaders, and tension rods. For the cables, AISI 304 was utilized for sizing due to its prevalence among cables properly configured for our application [LSM-20]

### 7.8.2 - Shape Selection

Before sizing the cross-sections, the cross-section shape had to be determined for each of the linkages. For the primary linkages a box cross-section was selected due to its strength-to-weight and performance under torsion, which will be important for the main structure. While a hollow cylinder would perform better under torsion, the box cross-section was selected because it would be easier to mount flanges and nest the linkages while stowed.

For the spreaders, a combination of I-beam and C-channel cross-sections were selected. I-beams were utilized due to their high strength-to-weight under axial compression, and the C-channels were selected to make the system easier to stow. When in the stowed configuration, the C-channel cross-sections can be easily nested within the I-beams [LSM-11].

For the tension components the selections of cross-sections were more straightforward as their expected failure mode is normal stress. The cables will be made up of several wire strands twisted together. The tension rods use a simple circular cross-section.

### 7.8.3 - Sizing

To size each of the linkage cross-sections, the primary failure mode was identified and then used to solve for acceptable cross-sections with suitable margin. For all compression linkages, which includes primary links and spreaders, buckling was considered the primary failure mode, and a safety of 1.25 was used as specified by NASA-STD-5001 [LSM-21]. To be

conservative the fixed-free configuration was assumed for each linkage in compression. Manipulating the Euler Buckling Criterion, eq. 7.8.1 was created to calculate the minimum moment of inertia required to have a critical buckling load equal to the max expected force in the linkage [LSM-22].

$$MOI = \frac{SF*F_E(2L)^2}{\pi^2 E} \quad (7.8.1)$$

After calculating the minimum moment of inertia, the cross-sections were sized to exceed their minimum cross-section. The cross-section sizes can be found in Table 7.8.2.

S2a/b		S3a/b		B2	
X-section Type	I-beam	X-section Type	I-beam	X-section Type	Box
Height	35 mm	Height	30 mm	Height	48 mm
Width	30 mm	Width	20 mm	Width	48 mm
Shelf	5 mm	Shelf	8 mm	Height Inner	37 mm
Web	5 mm	Web	8 mm	Width Inner	37 mm

S2c		B1		B3	
X-section Type	C-Channel	X-section Type	Box	X-section Type	Box
Height	25 mm	Height	52 mm	Height	40 mm
Width	27 mm	Width	52 mm	Width	40 mm
Shelf	5 mm	Height Inner	39 mm	Height Inner	34 mm
Wall	5 mm	Width Inner	39 mm	Width Inner	34 mm

Table 7.8.2: Cross-section dimensions for each compression linkage

Using the selected dimensions, the actual moment of inertia for each cross-section was calculated and the critical buckling load was determined using the traditional Euler Buckling Criterion, eq. 7.8.2.

$$P_{cr} = \frac{\pi^2 EI}{(2L)^2} \quad (7.8.2)$$

After determining critical buckling load for each linkage, the margin of safety was calculated using the calculated critical buckling load and the max expected force for the compression linkages. The margin of safety for each linkage can be seen in Table 7.8.3 at the end of the section.

$$MoS = \frac{CriticalBuckling}{MaxExpected*SF} - 1 \quad (7.8.3)$$

For the circular cross-sections of the tension rods the process was simpler. The primary failure mode for the tension rods was assumed to be normal stress. Using the max expected force in each tension rod, yield strength, and a safety factor of 1.25, the minimum cross-sectional area was determined with eq. 7.8.4.

$$A_{min} = \frac{SF*F_E}{S_y} \quad (7.8.4)$$

The diameter dimensions of T1, T2, T3 were calculated as 7.57mm, 5.05mm, and 3.75mm respectively. After determining the minimum cross-sectional area, a sufficient area was selected for the actual cross-section, and the MoS was calculated using eq. 7.8.5.

$$MoS = \frac{S_y}{\frac{F_E * SF}{A}} - 1 \quad (7.8.5)$$

The cross-sectional dimensions and capacity for the cables were retrieved from options available online. C2 had a diameter of 3/8" and a maximum capacity of 2,300 lbs. C3 had a diameter of 1/4" and a maximum capacity of 1,000 lbs [LSM-20]. To calculate the MoS for the cables, shown in Table 7.8.3, eq. 7.8.6 was utilized.

$$MoS = \frac{Capacity}{MaxExpected * SF} - 1 \quad (7.8.6)$$

Linkage	Margin of Safety
B1	0.30
B2	0.34
B3	0.37
S3	0.35
S2	0.25
S2c	0.30
C2	0.41
C3	0.19
T3	0.33
T2	0.30
T1	0.32

Table 7.8.3: Margin of Safety for each linkage in the manipulator assembly

Using the linkage volumes obtained throughout the sizing process in conjunction with the generally accepted material densities, the mass of each linkage was also calculated [LSM-19]. To obtain a mass estimate for the actuation system, EMRAX electric motors with suitable torque characteristics for the cables were utilized. The motors used were EMRAX 188, EMRAX 228, and EMRAX 268 [LSM-23]. It should be noted that these motors are not the selected motors for the system, nor are they space-rated. These motors were utilized exclusively for rough mass estimates of electric motors with the necessary torque characteristics for the manipulator system. Combining the motor and linkage mass estimates, the estimated system mass is 66.7 kg.

## 7.9 - Stability – Matthew Thomas

When lifting significant masses outside of the footprint of the rover, tipping is a legitimate concern. To verify the stability of the LLV throughout the pick-up process, tipping calculations were performed to confirm that the LLV would not tip in the riskiest configuration, the extended configuration. The extended configuration places the 500 kg mass 4-meters from the center post, causing the center of mass of the LLV-Manipulator body to shift outward. To

ensure that this new center of gravity remains within the footprint of the rover, eq. 7.9.1 was used to find its position.

$$X_{cm} = \frac{m_{LLV}x_{LLV} + m_{B1}x_{B1} + m_{B2}x_{B2} + m_{B3}x_{B3} + m_{PL}x_{PL}}{m_{LLV} + m_{B1} + m_{B2} + m_{B3} + m_{PL}} \quad (7.9.1)$$

The calculations assumed consistent gravity across each body, a rigid configuration, and static loading conditions. The static assumption was made because the manipulator is expected to move at low speeds, making the system quasi-static. With the dimensions shown in fig. 7.9.1, the above calculation was performed and resulted in a new center of gravity 0.6-meters from the center of the LLV footprint. This result is within the 2.2-meter footprint of the LLV by a significant margin, eliminating any concerns around static tipping.

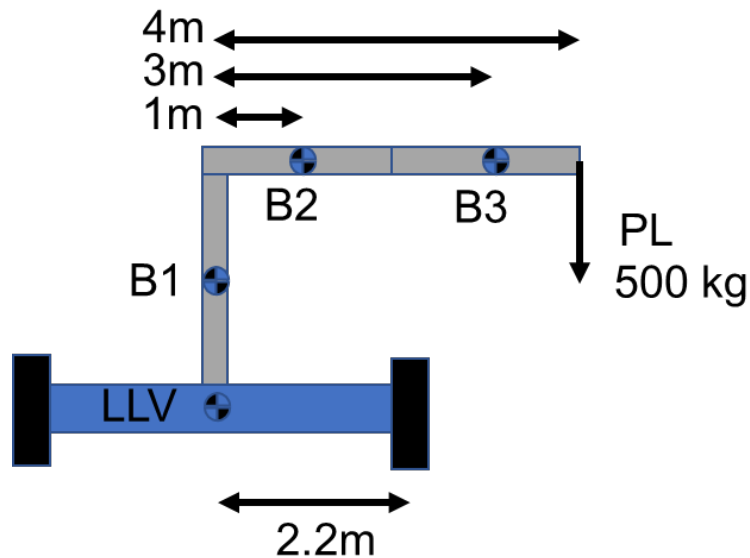


Figure 7.9.1: LLV-Manipulator diagram with dimensions



### 7.10 - Offloading & Deployment – Matthew Thomas

The cargo manipulator will be integrated with the LLV throughout transport to the surface of the moon. Once Blue Moon lands, the LLV will be offloaded with the cargo manipulator attached in its stowed configuration, shown in fig. 7.10.1. While the primary con ops intend for the LLV and manipulator to arrive integrated, the low mass of the cargo manipulator system would allow for a delayed delivery on a CLPS lander with a payload capacity of 500 kg.

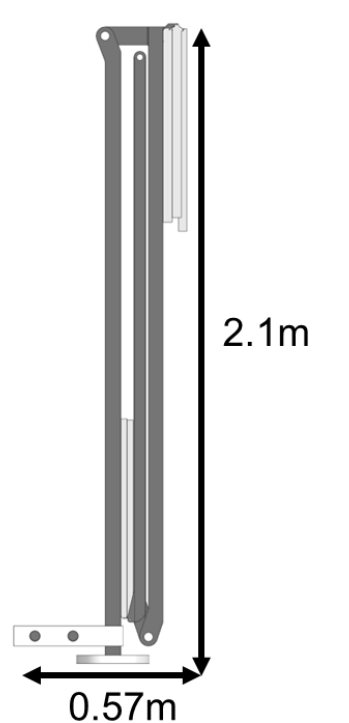


Figure 7.10.1: Cargo manipulator stowed configuration with dimensions

Once offloaded, the cargo manipulator will be deployed and prepared for moving logistics carriers. While development of the deployment system is still in progress, it has been determined that the manipulator will use a one-time deployment system. This means that once it is deployed, it cannot be returned to its stowed configuration. One-time deployment was selected because it would reduce the complexity of a deployment system with over 10 moving linkages. While this does mean the manipulator will be deployed during transit, the high specific stiffness of Al-7075 will reduce vibrations, and the proportionally low mass of the manipulator will not be capable of tipping the LLV at low accelerations. For one-time deployment, stored energy methods would be preferred due to their simplicity. The deployment systems could include frangibolts or paraffin wax actuators paired with a spring-damper system, but more research and analysis is necessary to confirm the final configuration for the manipulator's complex deployment system.

### 7.11 - Payload-Manipulator Interface – Matthew Thomas

To constrain the logistics carriers to the cargo manipulator throughout the lifting process, a payload-manipulator interface concept was developed. The interface has two major sections: the end-effector and the receptacle. The receptacle will be a simple circular opening on the

logistics carrier with an overhanging edge. The end-effector will feature a circular puck with an extendable outer surface. The surface will be extended using an internal cam to catch the overhanging edge of the receptacle and prevent the end-effector from exiting the receptacle. The system will use springs return the outer surface inwards when the lifting process is complete. The payload-manipulator concept can be seen most clearly in fig. 7.11.1.

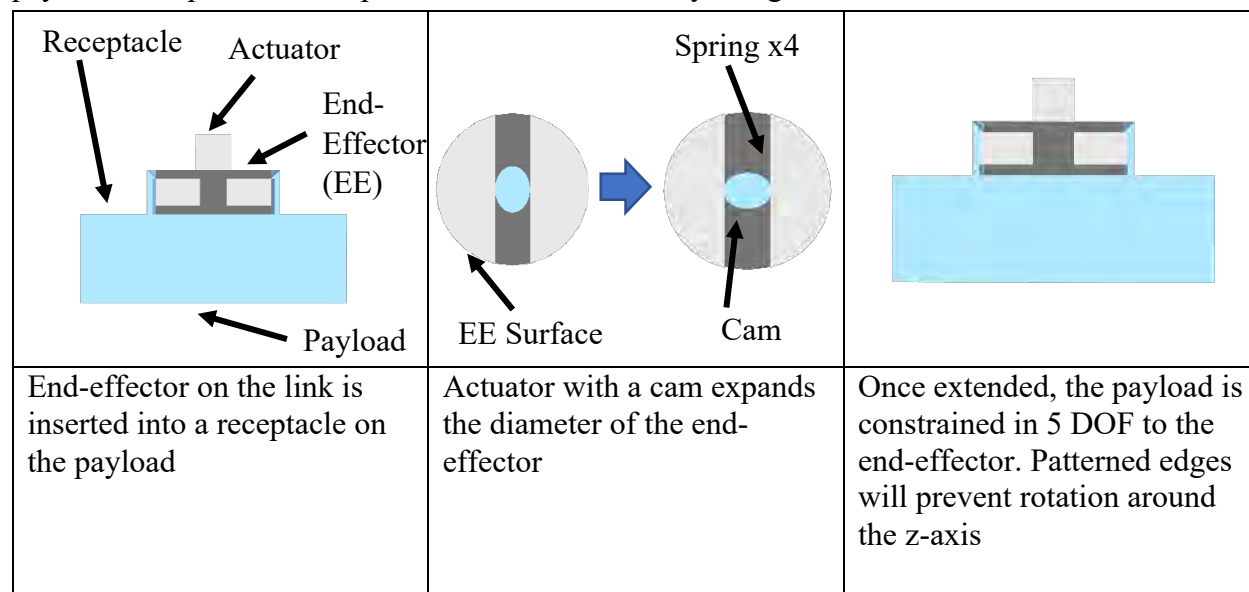


Figure 7.11.1: Payload-manipulator interface concept

The dimensioning and motor sizing for the payload-manipulator interface is still in progress. This concept represents the current direction of the interface's design but will be subject to change throughout development given the immense challenge of the peg-in-hole problem in autonomous space robotics.

## 7.12 - Thermal Management

### *7.12.1 - Cargo Manipulator Thermal Control – Nicholas Delafuente*

#### *7.12.1a - Passive and Active Design Using Radioisotope Heater Units and Resistive Heating Elements*

For the thermal control of the cargo manipulator, the hottest temperature it will experience is -50 C and the coldest temperature is -230 C. The cargo manipulator will contain two motors at the base of the arm, as well as a camera at the end of the arm. In order to find out what the equilibrium temperatures should be for the hot and cold case, the operational temperatures of the motors and camera must be known. The motors can operate from -50 C to 50 C and the camera can operate from -55 C to 50 C. This means that the equilibrium temperatures will take the temperature bands of the motor (>-50 C, <50 C).

To actually model the cargo manipulator, the surface area of the arm was calculated to figure out how many square meters were going to have to be thermally controlled. Since the arm will be folded together and extended, the best way was to take the entire area and equally distribute the thermal regulation. The cargo manipulator was also completely wrapped in multi-layer insulation to make heating it significantly easier.

First the cold case must be considered. By setting in an equilibrium temperature of -40 C for a buffer, the power necessary to heat the motors and camera came to 5 W. There are two

ways of heating the cargo manipulator: passive and active regulation. The first and less complicated is passive control. A radioisotope heater unit (RHU) generates heat from the natural decay of plutonium dioxide [PPT – 31]. One RHU will generate one Watt of heat power, so acquiring five of them and evenly spacing them out will thermally regulate the cargo manipulator [PPT - 31]. However, RHUs can be extremely difficult to come by since they are created by the Department of Energy (DOE). They can be very expensive since it takes a lot of time away from the government to allow a company/organization to acquire them. Due to the difficulty or acquiring RHUs, an active heating solution was generated for the cargo manipulator.

Since only 5 W are needed to thermally regulate the cargo manipulator, to actively do this, it will be a simple design: solar panels on the cargo manipulator arms, a battery connected to the motors, and 1 W electric heaters that will heat motors/camera when necessary. For sizing, we know that we can only charge for a total of 144 hours over the lunar day, and need to generate a total of 2100 W-hrs per lunar day. Using the same triple junction cells as before, we know that it generates 445 W/m<sup>2</sup>. This brings us to sizing of about .032 m<sup>2</sup>, or 0.5 kg. Using the past knowledge from thermal analyses, the solar panels must be covered in MLI doors during the lunar night. After completing the thermal analysis for this size solar panel during the lunar day, the size of the radiator with a 20% buffer must be 0.11 m<sup>2</sup>.

For the hottest temperature case for the cargo manipulator, there were more factors to consider. Since there is sunlight, the Sun and albedo need to be considered. As the motors turn, there is also heat given off, which is known as internal power generated. For this case, adjusting the angular velocity that the motors moved at would produce a different equilibrium temperature. Using the known torques, assuming 90% motor efficiency, and adjusting the angular velocities, the ideal equilibrium temperature could be set to less than 50 C.

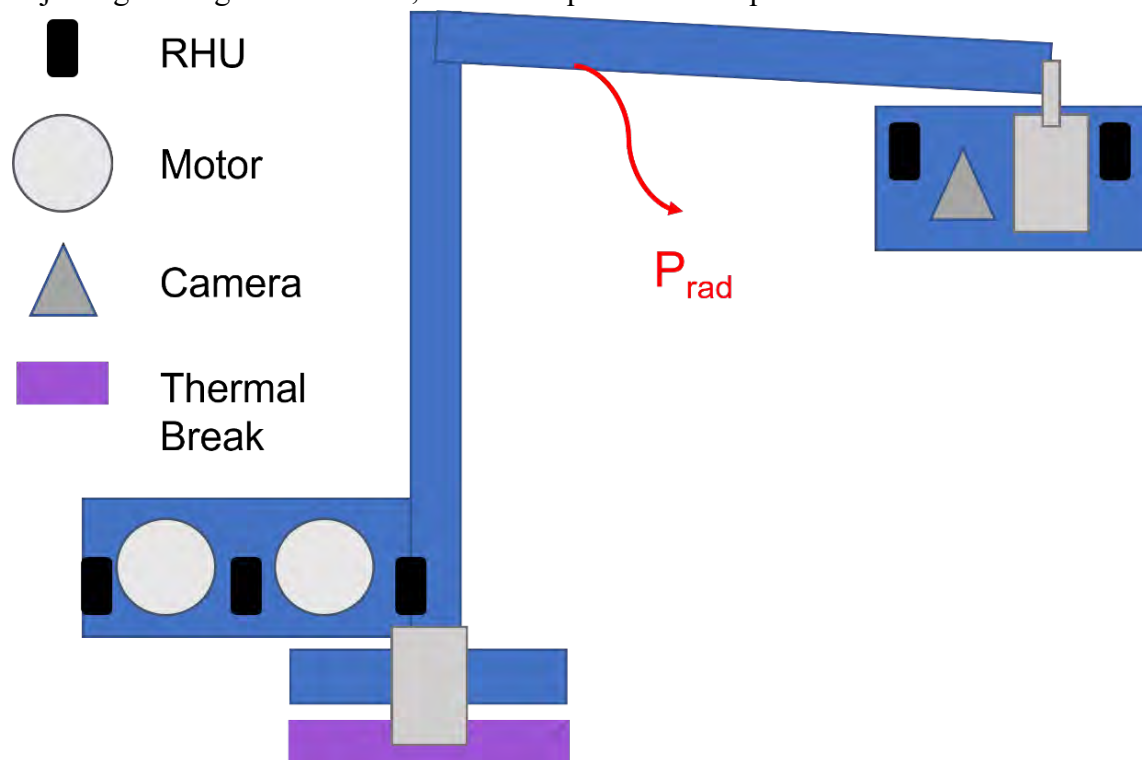


Figure 7.12.1: Diagram of Cargo Manipulator Thermal Control

The figure above shows an example of the layout of the cargo manipulator heated passively. The motors are at the base of the cargo manipulator with the camera at the tip of it. Below are the results of the thermal analysis, showing the power required to heat, equilibrium temperatures, and motor performance.

	Cold Case	Hot Case
Sunlight Angle (deg.)	0	13
Ground Temperature (C)	-230	-50
Formula	$P_{\text{rad}} = P_{\text{RHU}}$	$P_{\text{rad}} = P_{\text{sun}} + P_{\text{albedo}} + P_{\text{int}} + P_{\text{RHU}}$
Equilibrium Temperature (C)	-40	47
RHUs Necessary	5	

Table 7.12.1: Thermal Values for Cargo Manipulator

Motor Efficiency	$\omega 1$ (rpm)	$\omega 2$ (rpm)	Total Motor Power (W)
90%	0.67	0.19	52

Table 7.12.2: Motor Values for Cargo Manipulator

## 7.13 - Power System

### 7.13.1 - Umbilical Power – Nicholas Delafuente

Since the cargo manipulator has the ability for passive and active thermal control, it will have a power system on board. This will consist of a battery, solar panel, and electric heaters. However, this power system is not the one that will power the cargo manipulator. The motors and camera will receive power from the rover, which means that there will be umbilical power. When the cargo manipulator is attached to the rover, the umbilical power cord will be attached to the main battery configuration that is also on the rover.

## 8. Budgeting

### 8.1 - Initial Cost Estimations- Ayush Varaiya

To estimate the cost of the total mission, we researched prior missions and saw their cost breakdowns for uncrewed and crewed missions. We planned to base our cost estimation on the recent Artemis mission since the cost breakdown will be in terms of 2022 and we will be landing on the Artemis landing sites as well. When going through the Artemis handbook, we saw that the cost was split into two phases. The first phase included the launch cost using the Space Launch Systems, landing system, logistics, and the technologies needed on the moon. The second phase included future research and development for the mission.

The cost breakdown started with the past research and development from 2012 to 2020 which cost 40 billion dollars. After, the first phase had a total cost of 5.6 billion dollars per year while the mission is in commission. For the next phase, Artemis estimates 25 billion dollars.

Once all these values were added up, the total cost for the whole mission was 93 billion dollars which is about 7 billion dollars per year from start to finish (MPA-14).

To estimate the initial cost of the mission, we divided the mission into vehicle costs and launch costs. To calculate the cost for the vehicle, we used the Spacecraft/Vehicle Level Cost Model (MPA-5) which helps estimate the total cost for a research vehicle from initial stage to final stage. This cost also included the major components of the vehicle such as avionics, structure, and thermal systems. In addition, the model included labor costs, mission operations, and mission control.

Given the vehicle mass of 2000 kilograms, we used the cost model for a scientific instrument and put it into the equation  $C(M) = a[m(\text{inert}[kg])]^b$  where  $a$  had a value of 2.76 and  $b$  had a value of 0.5. (MPA-5) Since these multiples were given in terms of 2018, to get a better estimate, we transferred the multiples to 2028 terms which was the estimated launch year (MPA-12). We multiplied these values by a factor of 1.34 and got a nonrecurring cost of 600 million dollars. After, we calculated the first production value for the mission which had an  $a$  value of 0.52 and a  $b$  value of 0.94 after changing into terms of 2028. Applying these numbers to the equation, the recurring costs 650 million dollars. Since we wanted the cost for each kilogram of mass, we totaled the amount for one production and the estimated amount was about 620,000 dollars.

We also estimated the launch costs if we launched the vehicle on Starship. Since there is no information on how much Starship will cost NASA, we decided to use Falcon 9 for the basis of our calculations. First, we found the dry mass of Falcon 9 which was 45,600 kilograms and the cost for one launch was about 1.3 billion dollars for NASA which came out to be 28,000 dollars per kilogram of payload. From previous missions, we calculated a factor of 0.6 for NASA estimates to actual SpaceX costs. Also, these estimates were given in 2010 so we had to change it into terms of 2028 as well. Using the development cost for each launch vehicle, we were able to calculate the launch cost of SpaceX Falcon 9 which has a development cost of 390 million dollars and a launch cost of 67 million dollars and 22,000 dollars per kilogram (MPA-8). Based on this estimate, we used the development cost of SpaceX Starship which was 1 billion dollars and gave us a launch cost of 150 million dollars with 25,000 dollars per kilogram. Adding the launch cost as well as a 2000-kilogram vehicle as a payload, the total cost per launch on Starship would be 200 million dollars. The initial estimate for the whole mission including one launch and development of the vehicle was about 2.1 billion dollars.

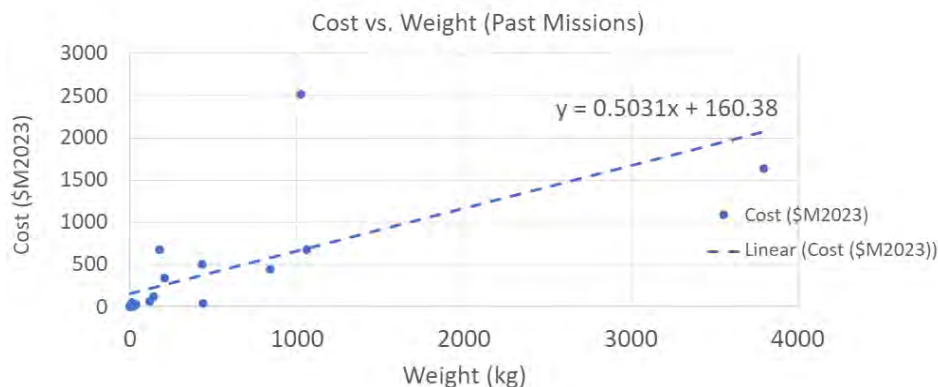


**Figure MPA-12. Cost of Mission vs Weight of Rover**

Upon reviewing this estimate, it seemed impractical, so we tried to create a better estimate with a different method. To refine the cost of vehicle development, we decided to use past missions with the same parameters as our mission. I created a list of missions from around the world and recorded the weight of their rover and the cost for the mission. We collected data from 1971-2023 and received data for 19 rovers. Since all the costs we researched were based on the year of the mission, we used the NASA handbook to find the factors and convert all the costs into terms for 2023 (MPA-15). After, we created a graph, as shown above, that plotted each of the costs vs. the weight of the vehicle. Upon creating the line of best fit, we got an equation of  $y = 0.5031x + 160.38$  where  $x$  is the weight of the vehicle and  $y$  is the cost of the mission in millions. Based on this model, the total cost for the mission is estimated to be 1.2 billion dollars.

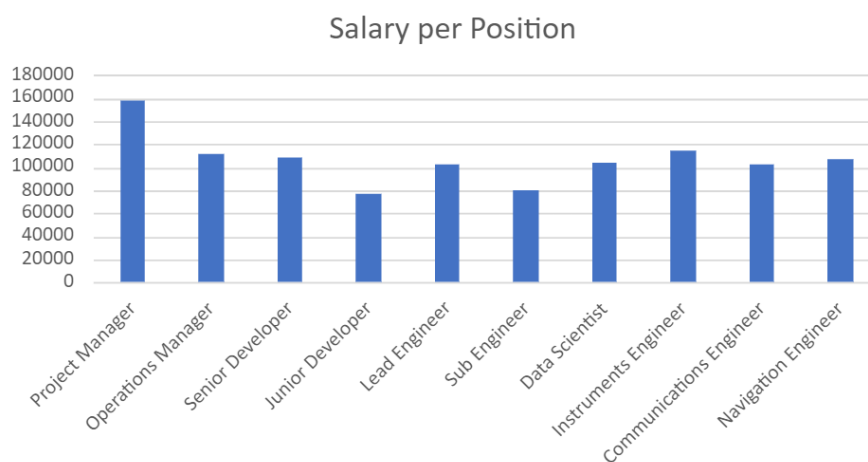


**Figure MPA-13. Graph of Salary**

Once development and research costs were calculated, we had to calculate personnel costs for the mission. We based our personnel needs using the team breakdown for the Mars rovers and found average salaries online as well. We planned to have one project manager, one operations manager, one senior developer, two junior developers, one lead engineer, four sub engineers, two data scientists, two instruments' engineers, two communication engineers, and two navigation engineers. The junior developer would help with operations development and making the vehicle more autonomous, and the sub engineer would help with vehicle operations to ensure the vehicle is operating at nominal parameters. This would be the bare minimum we would need to run this mission over the 5 years. As shown in the chart above, these are the average salaries per job title for NASA. Each of the salaries are in terms of 2023 as well (MPA-9). After totaling the amount of employees needed and adding their yearly salary together, the total cost per year would be about 1.8 million dollars. For the whole duration of the mission, the total cost would be about 9 million dollars. This does not include any emergency procedures which could bring more people on the team and the model estimates each person is working only 40 hours per week.

## 8.2 - Refined Cost Estimations – Cameron Storey

Once we had an initial estimate for the cost of our mission, or at least for the logistics vehicle, we set about determining a more detailed cost estimation and breakdown for the entire

mission, including the logistics vehicle, all the pressurized logistics modules, and the cargo manipulator. To do this we used NASA's Project Cost Estimating Capability, or PCEC, which was recommended on RASC-AL's website.

PCEC draws on past mission costs to determine the cost per pound for a vast array of different types of systems, subsystems, and components. To begin with we found the masses of each of the different parts of the system. These masses were largely sourced from the work done by the other sub teams. These masses were converted into weights, and then fed into PCEC to determine a price estimate for each part.

By far the most complex system for this process was the logistics vehicle. With ten different subsystems/components spread across LSM, AFSS, and PPT, there was quite a bit to figure out. Most of the masses were sourced from LSM's mass breakdown for the logistics vehicle, although their bulk allocation for avionics was further broken down into the computer, the cameras, the comms dish, and then bulk avionics mass for overall wiring, harnessing and specific components which PCEC did not have specific cost estimating relations (CERs) for. For the vast majority of the LLV, a first pound cost CER was used to determine the cost of subsystems/components. One notable exception to this was the onboard cameras which are used for obstacle avoidance. Because the camera CER was mainly for cameras like the ones found on telescopes, I did not believe that it would be an accurate CER for our rover. Instead, a CER for body mounted instruments was used, which found a cost estimate based on both mass and max wattage, both of which we knew.

Aside from the camera, all the CERs used were based on weight, and drew analogies to already existing spacecraft. For the logistics vehicle, the analogous spacecraft of choice was Mars Pathfinder, as that was the primary rover that PCEC had in its database. However, where other rovers were additionally available, they too were used on top of Mars Pathfinder. There are two exceptions to this, which are the camera, which was previously discussed, and the rover mobility system. PCEC had a dedicated CER for estimating mobility systems based on the Apollo lunar rover, which was used in this case.

The cargo manipulator's CER's were very similar to the ones for the logistics vehicle. Mars Pathfinder was used for the reference for most of the CERs. The exception is once again the camera, which is once again an externally mounted instrument. The pressurized logistics module on the other hand differs from the LLV and the CM in that it does not use Mars Pathfinder or other rovers as references for its CERs. Instead, it uses a cumulative reference of all the various crewed capsules that PCEC has in its database, as the pressurized logistics module is effectively a crewed attachment to a habitat.

For design and development costs, along with testing costs, PCEC helpfully provides all those costs in all of its CERs, although with one notable exception, once again being the camera. For the camera, it only provides the material cost, so for the design and testing for the camera, we took an average of the cost of design and testing per unit mass of the other subsystems and components, and then applied that to the camera, and it seemed reasonable.

With CERs for all the subsystems/components, we simply fed in the mass to acquire cost estimations, which are laid out below along with the mass used for the subsystem/ component. It is worth noting that All of the CERs provided costs in 2015 dollars (except for the camera once

again which was in 2004 dollars). These were all converted to 2023 via PCEC's inflation calculator. What is listed below is the converted 2023 costs. The next three tables serve as not only our overall cost breakdown for SHELL, but also as the overall mass breakdowns.

### 8.2.1 – LLV – Cameron Storey

LLV	Total Mass (kg)	Material Cost (\$M)	D&D Cost (\$M)	Testing Cost (\$M)
<b>LSM</b>				
<b>Chassis</b>	700			
Mobility	450			
Mechanical	150			
<b>AFSS</b>				
<b>Computer</b>	4			
Avionics	141.3			
Camera	1.7			
Antenna	3			
<b>PPT</b>				
<b>Solar Panels</b>	30			
Batteries	650			
Thermal Management	60			
<b>Totals</b>				
<b>Total w/o Margin</b>	2190			
With 30% Margin	2847			

### 8.2.2 – PLM – Cameron Storey

PLM	Total Mass (kg)	Material Cost (\$M)	D&D Cost (\$M)	Testing Cost (\$M)
<b>LSM</b>				
<b>Structure</b>	173.00			
<b>AFSS</b>				
<b>ECS</b>	25.00			
<b>PPT</b>				
<b>Batteries</b>	73.00			
<b>OTHER</b>				
<b>Cargo</b>	1145.00			
<b>Totals</b>				
<b>Total w/o Margin</b>	1416.00			
With 30% Margin	1840.80			

### 8.2.3 – CM – Cameron Storey

CM	Total Mass (kg)	Material Cost (\$M)	D&D Cost (\$M)	Testing Cost (\$M)
----	-----------------	---------------------	----------------	--------------------



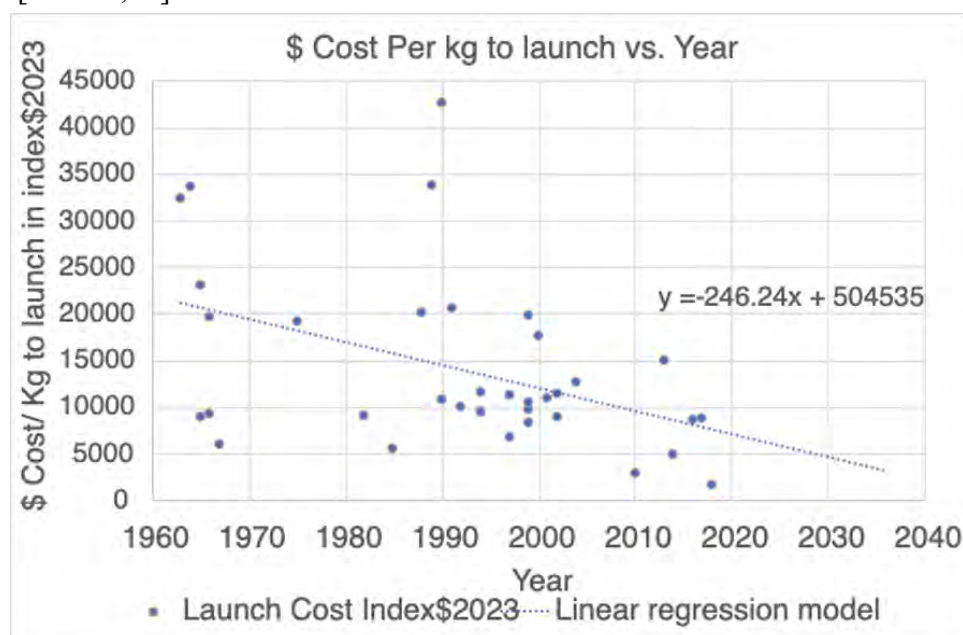
<b>LSM</b>				
<b>Structure</b>	24.80			
Mechanical	41.90			
<b>PPT</b>				
<b>Thermal Management</b>	0.10			
Battery	14.00			
Solar Panels	0.50			
<b>AFSS</b>				
<b>Camera</b>	0.43			
<b>Totals</b>				
<b>Total w/o Margin</b>	81.73			
With 30% Margin	106.24			

#### 8.2.4 - Launch Costs – Jeet Patel, Cameron Storey

Lunar Lander	Year (YYYY)	\$Cost for launch (per Kg) 2021	Cost \$2023
Atlas centaur	1963	29500	32450
Titan II	1964	30600	33660
Titan III+	1965	21000	23100
Soyuz	1966	17900	19690
R-36/cyclone	1966	8400	9240
Long March 2A	1975	17500	19250
Long March 2C	1982	8300	9130
Zenit 2	1985	5100	5610
Ariane 44	1988	18300	20130
Long March 2E	1990	9900	10890
Delta II	1990	38800	42680
Atlas II	1991	18700	20570
Long March 2D	1992	9100	10010
H-II	1994	10500	11550
Long March 3A	1994	8700	9570
PSLV	1994	8500	9350
Long March 3B	1997	6200	6820
Long March 4B	1999	7600	8360
Zenit 3SL	1999	8900	9790
Dnepr	1999	9600	10560
Delta III	1999	18000	19800
Atlas III	2000	16000	17600
GSLV	2001	10000	11000

Delta IV	2002	10400	11440
Atlas V	2002	8100	8910
Falcon 9	2010	2600	2860
Anteras	2013	13600	14960
LVM3	2017	8000	8800
Proton	1965	8200	9020
Saturn V	1967	5400	5940
Titan IV	1989	30800	33880
Ariane 5G	1997	10200	11220
Delta IV Heavy	2004	11600	12760
Angara	2014	4500	4950
Long March 5	2016	7900	8690
Falcon Heavy	2018	1500	1650

[SI – 21,23]



To calculate the cost of launching the lunar lander, we utilized data from previous launches to low Earth orbit (LEO). By examining the historical launches, we established a regression equation that relates the launch year (x) to the cost per kilogram of launch systems (y), represented as " $y = -246.24 * x + 504,535$ ". Based on the regression model, we estimated the cost/kg to launch to LEO in 2028 as \$5,160.28/kg. However, since our objective is to launch to the lunar surface, we need to consider the additional complexities involved. To account for these factors, we adjusted the cost ratio to be 16 times [DR AKIN 2023] that of launch cost/kg to LEO, suggesting on average, it would require approximately 16 times more cost to launch a kilogram of payload to the lunar surface compared to LEO. Multiplying the LEO cost/kg by a factor of 16, resulted in a cost of \$82,564.48/kg to launch to the lunar surface in 2028.

Considering the weight of our lunar logistics vehicle (LLV) at 2190 kilograms, the estimated cost to launch the LLV to the lunar surface in 2028 would amount to approximately \$180.8 million, before factoring in any cost margin. Considering a 30% cost margin to accommodate unforeseen expenses, the total cost of launching the LLV would be approximately \$235.0 million.

Doing the same for the Cargo Manipulator at 81.7kg, the estimated cost to launch the CM to the lunar surface in 2028 would amount to approximately \$6.7 million, before factoring in any cost margin. Considering a 30%, the total cost of launching the CM would be approximately \$8.7 million.

Finally, looking at the cost\$/kg to launch the PLM with 1416 kg to the lunar surface in 2028 would amount to approximately \$116.9 million, before factoring in any cost margin. Considering a 30%, the total cost of launching the PLM once would be approximately \$151.9 million. However, since we are launching PLMs with a cadence of 28 days over a 5 year period, this means we are actually launching 65 PLMs. With a learning curve of 85%, The total launch cost for the PLMs is \$3.66 billion, which with a 30% margin comes out to \$4.76 billion.

Therefore, the total cost of launching this entire mission to the moon in the year 2028 would be about \$3.85 billion without margin, and \$5 billion with a 30% margin.

#### 8.2.5 – Overall – Cameron Storey

Below you can see our overall costs for the entire SHELL mission. The recurring and non-recurring costs of our three different systems are those of which that are described in section 8.2, and laid out in 8.2.1-3, and the launch costs are those which are described above in section 8.2.4. The learning curve for the 65 PLMs is the same as for the 65 PLM launches, which is 85%. Additionally it is worth noting that the total cost for the design, development, testing, and construction of the LLV is about \$billion, which is similar to the \$billion estimated above in section 8.1. The grand total mission cost for SHELL comes out to \$billion dollars, which with a 30% margin, is billion dollars.

Overall	Recurring (\$M)	Non Recurring (\$M)
LLV		
PLM x 65		
CM		
<b>Launch Costs</b>		
LLV + CM		
PLM x 65		
<b>Grand Total</b>		
<b>Total w/o Margin</b>		
<b>With 30% Margin</b>		

## **9. Risk Analysis**

### **9.1 - S3001 Risk Breakdown and Analysis – Pranav**

For the risk analysis conducted for SHELL, we used [SI-4] NASA S3001: Guidelines for Risk Management. This document contained all the necessary information for our team to identify and assess risks for our system. As this document was created with the purpose of minimizing risk and increasing cost effectiveness within NASA programs, we believed it would be essential to use it as the basis for our own risk analysis for SHELL

We utilized the majority of the same methods and metrics used in NASA S3001. The major change we made in our analysis was with the consequence criteria. NASA S3001 has a metric for Human Safety, as shown in Figure [X]. However, since SHELL is intended to be operated remotely without human interaction, we decided to disregard that human safety consequence criteria. We also utilized the likelihood criteria provided by NASA S3001, since it was mainly a quantitative approach to risk, shown in Table [X].

*Figure X*

*Table X*

The combination of the above two metrics, including our changes, creates a 5x5 risk matrix, which indicates the priority of the different risks we have identified. This is shown in Figure [X].

*Figure X*

Using NASA S3001 allowed the team to determine where to prioritize redundancy and reinforcement within SHELL. Every system and subsystem

### **9.2 - Fault Tolerance Stories - Darian**

We have identified 27 serious potential sources of unmitigated risk within our system, encompassing the Lunar Logistics Vehicle, Pressurized Logistics Module, and Cargo Manipulator. These potential sources or risk vary in terms of probability of occurrence and negative outcome severity; however, they all result in a high enough priority score from our 5x5 risk matrix to warrant creating/utilizing mitigation strategies or technologies, and contingency strategies. These mitigation strategies or technologies aim to reduce the likelihood or severity of a corresponding failure method. The contingency strategy is the plan that will take place if such failure occurs. Both the mitigation and contingency strategies aim to decrease the likelihood, severity, or both of a potential failure method. These 27 potential sources of unmitigated risk are broken down by major systems (LLV, PLM, and CM) and discussed further below.

#### **9.2.1 - LLV – Darian, Cameron**

Of the 27 potential sources of unmitigated risk, 15 pertain to the Lunar Logistics Vehicle. These 15 failure methods, descriptions, unmitigated likelihood and probability, mitigation technology/method, and mitigated likelihood and probability are shown below in Table .2.1

Table 9.2.1: LLV Fault Tolerance Stories

Subsystem	Event	What components are affected?	Impact to the Mission	Unmitigated	
				Prob	Severity

LLV	Drive Motors fail	Most other components related to mobility rendered useless but shouldn't be harmed	LLV can't move making delivery of payloads impossible	2	5
LLV	Steer Motors fail	Drive system will still be operational, but less precise and efficient	Limited maneuverability, but LLV should still be able to move and skid steer	2	3
LLV	Suspension Motors fail	LLV cannot level itself properly or pickup/drop payloads	Loss of active suspension makes the squatting stance for loading/unloading payloads impossible	2	4
LLV	Primary computer failure	Almost every other electronic component will be inoperable	Without primary computer LLV can't move, sense, etc.	3	5
LLV	Cameras Fail	No damage to other components - possible damage if rover collides with obstacle	Without sensing, LLV can't approach payloads or avoid obstacles	3	5
LLV	Dust Accumulation on Camera	No damage to other components - possible damage if rover collides with obstacle	Without sensing, LLV can't approach payloads or avoid obstacles	4	4
LLV	Dust Accumulation on Solar Panels	Loss of power generation prevents use of electronics; potential damage to components if there's not enough power for thermal regulation	Limits power generation, eventually leading to loss of power	5	4
LLV	Solar Panel Physical Failure	Loss of power generation prevents use of electronics; potential damage to components if there's not enough power for thermal regulation	Halts power generation leading to loss of power	2	5

LLV	Battery Failing to Store Charge	No physical damage to other components; thermal regulation concerns	Battery Failure will lead to loss of power storage capabilities	2	5
LLV	Battery Structural Damage	Possible damage to nearby components depending on the type and location of the physical damage	Loss of power storage capabilities and possibly loss of power supply to parts depending on how batteries are wired (ask PPT)	2	5
LLV	Antenna Failure	No direct damage to other components - possible damage if rover collides with obstacle	Unable to communicate with LLV making it impossible to give new instructions	2	5
LLV	Loss of Signal Due to Obstruction	No direct damage to other components - possible damage if rover collides with obstacle	Unable to communicate with LLV making it impossible to give new instructions	2	5
LLV	SSD Failure	No damage to other components but loss of memory inhibits use of electronics	Unable to store instructions/data	2	5
LLV	IMU - Inertial measurement unit	No damage to other components unless LLV collides with obstacle	Exact position/orientation of LLV is unknown, making picking up payloads more difficult	2	4
LLV	PSU - Power supply unit	Potential damage to electronics if voltage supplied is unstable	Loss of use of electronic components	2	4

Note that many of the mitigated severity ratings are a three, which is higher than we would have hoped. This is in accordance with the S3001 guidelines. According to the S3001 guidelines consequence (severity) rating table, if the asset is damaged but fully repairable the failure method has a severity rating of three. In many cases, with our mitigation and contingency strategies the LLV will be able to continue operations fully and for an extended period of time without requiring repairs, or the required repairs are very simple, quick, and small; however, since repairs are required nonetheless, the severity rating remains a three.

### 9.2.2 - PLM – Jeet Patel

Seven potential unmitigated risk events are associated with the Pressurized Logistics Module (PLM). These include failures of the docking mechanism, Environment Control Unit (ECU), batteries, storage shelves, latching mechanism, supplies catching fire, or crew lighting turning off. Failure to manage or repair any of these events in a timely manner could critically impact the mission's success. The following table 9.2.2 again (Like LLV) presents these events, their components, impact on the mission, unmitigated probability/severity ratings, mitigation methods, and mitigated probability/severity ratings. The S3001 guidelines were used again to assess unmitigated and mitigated probability/severity ratings, with most of the mitigated PLM severity ratings being 3 or below, indicating that the damaged parts are repairable, and the PLM can continue operations on auxiliary or redundant parts until repairs are completed.

Table 9.2.2: PLM Fault Tolerance Stories

Subsystem	Event	What components are affected?	Impact to the Mission	Unmitigated	
				Prob	Severity
PLM	PLM Docking mechanism / Airlock hatch failure	Could depressurize the habitat along with the PLM	Affects the docking ability of the PLM with the habitat, potentially depressurizing both of them, endangering the crew and the cargo.	2	5
PLM	ECU Failure	Potential damage to the Air revitalization, oxygen generation, temp and humidity control systems. Also hazardous to the crew and cargo	Affects the ability of PLM and the habitat to monitor their internal atmosphere and maintain safe air quality for the crew and live cargo.	3	5
PLM	Battery damage	Would stop power supply to ECS systems	PLM could lose temperature and pressure controls	2	5

PLM	Internal Logistics Manipulation/Storage shelves breaks	Potential damage to the cargo	The storage shelf breaks resulting in potential damage to the cargo.	1	3
PLM	Over-center latching mechanism with the Cup-Cone Interface of the LLV	Potential damage to the PLM, LLV, Manipulator or the habitat.	Could result in the PLM being detached unintentionally while between transport	2	4
PLM	Components or supplies catch fire	Damage to the PLM internal systems or fire hazard	Might result in damage to all of internal PLM systems or fire hazard resulting in catastrophic mission failure	2	5
PLM	Internal lighting for the crew turns off	Potential damage to the cargo or injury to the crew.	Loss of PLM internal lighting would result in crew not being able to locate essential supplies and cargo, and can also result in an injury.	2	2

### 9.2.3 - CM – Pranav

Table 9.2.3: CM Fault Tolerance Stories

Subsystem	Event	What components are affected?	Impact to the Mission	Unmitigated	
				Prob	Severity
CM	One or more cables snap	Potential damage to the pulley system, motors, and payload if cable snaps under load.	CM would no longer be able to be mission viable, as the cables used for manipulation are needed for any payload.	1	5



CM	Umbilical power system is not attached accurately and precisely.	All components of the CM.	Loss of power would result in an inability to manipulate the CM, resulting in no function.	3	5
CM	Tension rods buckle/snap	Cable and pulley systems	Loss of functionality to manipulate payloads	1	5
CM	Motors fail	Any components that require motors to be used.	Loss of functionality to manipulate payloads	2	5
CM	Umbilical power system is disconnected during manipulation.	All components of the cargo manipulator, as well as the payload if CM is in the middle of manipulation.	CM loss of power would result in loss of tension in the cables, dropping the payload to the lunar surface and loss of control of the CM.	3	5

### 9.3 - Mitigation Strategies – Pranav, Darian, Cameron, Jeet

After identifying potential sources of unmitigated risk that are significant enough to potentially lead to mission interruptions/failure, we developed mitigation technologies/methods to reduce the likelihood or severity of each failure method and a contingency plan that will take place in the event failure does occur. Each mitigation technology/method and contingency is listed in Table x below. Table x also highlights how each mitigation strategy attempts to solve the failure method and the new mitigated probability and severity.

Table 9.3.1: Mitigation Strategies

Subsystem	Event	Mitigation Technology/ Method	How does it solve the issue	Contingency	Mitigated	
					Prob	Severity
LLV	Drive Motors fail	Redundant drive motors	If one fails. the other 5 will still allow full maneuverability	Operate with redundant motors until repairs can be made	2	3
LLV	Steer Motors fail	Redundant steer motors	If one fails. the other 5 will still allow full maneuverability	Operate with redundant motors until repairs can be made	2	3
LLV	Suspension Motors fail	Redundant suspension motors	If one fails. the other 5 will still allow full maneuverability	Operate with redundant motors until repairs can be made	2	3
LLV	Primary computer failure	Redundant computer	If the primary computer fails. the auxiliary will be able to take over	Operate with auxiliary computer until primary can be replaced	3	3
LLV	Cameras Fail	Stop operations and replace camera	Creates a situation where the rover stops itself from	Pause of mission tasking	3	3

			conducting any tasks and prevent any risk from camera failure.			
LLV	Dust Accumulation on Camera	Electrodynamic Dust Shield	Actively clears dust off of the camera lens.	Continued normal operations	1	4
LLV	Dust Accumulation on Solar Panels	Electrodynamic Dust Shield	Actively clears dust off of the camera lens.	Continued normal operations	1	4
LLV	Solar Panel Physical Failure	Extra Solar Panel Area	Remaining Solar Panel Area will be able to Power Rover	Operate with extra area until repairs can be made	2	3
LLV	Battery Failing to Store Charge	Batteries wired in Parallel	Remaining Battery Cells will still work	Operate with remaining batteries until repairs can be made	2	3
LLV	Battery Structural Damage	Batteries wired in Parallel	Remaining Battery Cells will still work	Operate with remaining batteries until repaired can be made	2	3
LLV	Antenna Failure	Short range antenna to relay with the HAB	Auxiliary Antenna will take over	Operate with auxiliary antenna until repairs can be made	2	3
LLV	Loss of Signal Due to Obstruction	If loss of signal, return to last location with signal	Wait for Reacquisition of Signal	Halt Operations until Signal is Reacquired	2	1

LLV	SSD Failure	Two Redundant SSD's	Auxiliary SSD will take over/store a backup of any data	Operate with auxiliary SSD until repairs can be made	2	3
LLV	IMU - Inertial measurement unit	Redundant IMU	Auxiliary IMU will take over	Operate with auxiliary IMU until repairs can be made	2	3
LLV	PSU - Power supply unit	Stop operations and replace damaged components	Minor repairs allow for continued use of LLV	Halt operations until repairs are completed	2	3
PLM	PLM Docking mechanism / Airlock hatch failure	Redundant supplies/actuators	If one actuator fails, others would still be able to keep a airlock seal, until astronaut can replace the damaged part	Redundant actuators would keep the seal intact until repairs can be made	2	5
PLM	ECU Failure	Backup ECU	Auxiliary ECU will take over	Operate with auxiliary ECU until repairs can be made	3	3
PLM	Battery damage	Auxiliary Battery	Auxiliary PSU will take over	Operate with auxiliary battery until repairs can be made	2	3
PLM	Internal Logistics Manipulation/ Storage shelves breaks	Redundant shelves with cargo evenly spread when loading	Minimal weight on shelves helps prevent failure	Salvage cargo and repair damaged shelves	1	1

PLM	Over-center latching mechanism with the Cup-Cone Interface of the LLV	Redundant 4 interfaces on each side of the chassis	If one interface fails, 3 more latches would still work	Payload interface would still work with the redundant latches until parts can be replaced.	2	3
PLM	Components or supplies catch fire	ECU fire prevention extinguishes fire	Prevents fire from occurring in the first place, or extinguishes existing fire to prevent further damage	Allow ECU fire suppression to extinguish fire	2	2
PLM	Internal lighting for the crew turns off	Redundant LEDs	If some of the lighting fails, redundant lighting still provides enough light	Operate with redundant lighting until repairs can be made	4	2
CM	One or more cables snap	Design not to Fail	High safety factors will help ensure there is no failure	Halt CM operations until repairs can be made	1	5
CM	Umbilical power system is not attached accurately and precisely.	Detach and reattach	Reattaching ensures proper connection and supply of power	Continue attempting to reattach until proper connection maintained	3	2
CM	Tension rods buckle/snap	Design not to fail	High safety factors will help ensure there is no failure	Halt CM operations until repairs can be made	1	5
CM	Motors fail	Replace if fail	Allows CM to continue operations	Halt CM operations until repairs can be made	2	3

CM	Umbilical power system is disconnected during manipulation.	Reattach if not broken & design power attachment out of the way of manipulation	Prevents disconnection from occurring; allows work to resume after disconnecting	Reattach and continue work if repairs not needed	2	3
----	---	---	--	--	---	---

#### 9.4 - FMECA - Pranav

*Probably getting moved to appendix*

### **10. Technology Readiness Levels (TRL) Analysis – Jeet, Pranav, Darian, Cameron**

Technology Readiness Levels (TRLs) play a crucial role in the aerospace and overall engineering industry by providing a standardized framework for assessing the maturity and readiness of technologies. TRLs serve as a valuable tool to evaluate the progression of technologies from their early conceptual stages to their eventual deployment. In aerospace, where safety and reliability are crucial, TRLs help us evaluate if a technology is ready for use in space or aircraft systems. There are nine TRL levels, with level 1 being the earliest stage and level 9 indicating full maturity and successful use in real-world situations. As a technology moves up the TRL scale, it goes through testing, prototyping, and demonstration to make sure it works well and is ready to be used. TRLs also help engineers and project managers make good decisions about technologies, hence we decided to assess our project and its chosen components for their TRL analysis. The following tables represent three parts of our project (LLV, PLM and CM) and the TRL breakdown of their components.

Table 10.1: Technology Readiness Levels

TRL Level	Description
9	Actual system "flight proven" through successful mission operations
8	Actual system completed and "flight qualified" through test and demonstration (ground or space)
7	System prototype demonstration in a space environment
6	System/subsystem model or prototype demonstration in a relevant environment (ground or space)
5	Component and/or breadboard validation in relevant environment
4	Component and/or breadboard validation in laboratory environment
3	Analytical and experimental critical function and/or characteristic proof-of concept

2	Technology concept and/or application formulated
1	Basic principles observed and reported

[SI-2]

### 10.1 - LLV TRL Analysis – Jeet Patel

Table 10.1.1: LLV TRL Analysis

Teams	Component Type	Component	TRL Rating	Reasoning
Actuation	Wheels	6 wheels with chevron angled grousers	9	Successful mission on Earth and Mars
	Suspension	Low-bandwidth active suspension	6	Prototype demonstration on Earth
	Standard Payload Interface	Cup-cone interface and over-center latching mechanism	3	Proof of Concept / before testing
	Drive motors	In-wheel hub actuator	9	Successful mission on Earth and Mars
	Steering	Active Steering	6	Prototype demonstration on Earth
Avionics	Primary/aux computer	RAD5545 SBC from BAE Systems	9	Successful mission on Earth and in space
	Camera	Standard commercial surveillance cameras	9	Successful mission on Earth and Mars
	SSD	Greenliant	9	Popular SSD for use in variable temperatures
	IMU	LN-200S	9	Successful mission on Earth and in space
	Antenna	High-Gain Antenna	9	Successful mission on Earth and in space
Power Mgmt.	Solar Panels	III-junction	9	Successful mission on Earth and in space
	Batteries	NCA Batteries	9	Successful mission on Earth and in space
	Dust Mitigation Tech (Passive/active)	Electrodynamic dust shield	8	Test and demonstration on ground and space
	Resistive Heater	Kapon Flexible Heaters	9	Successful mission on Earth and in space

	Temperature Sensor	Internal Temperature Sensor	9	Successful mission on Earth and in space
Mission Planning	Launch Vehicle	Blue Origin, Blue Moon	3	Prototype/Proof of Concept on Earth

[SI – 2,6,7,8,9,10,11,12,13,15,24]

The Lunar Logistics Vehicle “LLV” incorporates a wide range of complex technologies, each with its own unique TRL rating. The components of LLV are divided into several categories, each responsible for a specific set of components. The actuation category, for example, is responsible for the LLV's wheels, suspension, pallet, trunnion system, drive motors, and steering. The avionics category, on the other hand, is responsible for the LLV's primary and auxiliary computer systems, cameras, solid-state drives (SSD), inertial measurement units (IMU), and antennas. The power management category is responsible for the LLV's solar panels, batteries, dust mitigation technology, resistive heater, and temperature sensor.

As shown in the LLV TRL rating table, most of the LLV's components have a TRL rating of 9, indicating that they have been successfully tested on Earth and in space. This is particularly important for critical components such as the LLV's wheels, drive motors, and solar panels, which must operate reliably in the harsh environment of the lunar surface. Other components, such as the LLV's suspension system and avionics, have a TRL rating of 6, indicating that they have undergone a prototype demonstration on Earth and are still in the testing phase. While, the LLV's Standard Payload Interface has a TRL rating of 3, which indicates that it is still in the proof-of-concept stage and have not yet undergone testing. While the BlueOrigin’s BlueMoon lander is also rated at the TRL of 3 due to only having a prototype demonstration to NASA by Blue Origin. While the launch vehicle itself would not directly affect LLV’s development, it is a crucial factor in enabling the deployment of the LLV, PLM and CM systems. These components are critical to the LLV's functionality and must be rigorously tested before they can be considered for use in a lunar mission.

In conclusion, the LLV's TRL rating provides valuable insights into the level of development and readiness of the LLV's various components. It highlights the significant progress that has been made in the development of the components onboard LLV and also identifies areas where further research and testing are required. By carefully assessing the TRL ratings of each component, we can report that majority of the components onboard LLV could have the TRL rating of 9. Thus, engineers and scientists can make informed decisions about the suitability of the LLV for its logistics use in a lunar mission, ensuring that it operates safely and reliably in the challenging lunar environment.

## 10.2 - PLM TRL Analysis – Jeet Patel

Table 10.2.1: PLM TRL Analysis

Category	Component Type	Component	TRL Rating	Reasoning
----------	----------------	-----------	------------	-----------



Actuation	Internal Logistics Manipulation/Storage	Storage shelves	9	Successful missions in MPLM space shuttle program
	Airlock Docking / Hatch	Stewart platform design	3	Proof of Concept MGAAMA by NASA / no testing
Avionics	Fire Detection	line-of-sight radiometer	3	Proof of Concept / before testing
	ECU Sensor (Temp, Humidity, Pressure, gases)	Lunar Outpost Canary-S sensor	9	Successful on Earth and in space (ISS)
	Primary/aux computer/ECU	RAD5545 SBC from BAE Systems	9	Successful on multiple satellites in space
	Camera	Standard surveillance cameras	9	Successful on ISS in space
	SSD	Greenliant	9	Popular SSD for use in variable temperatures
Power Mgmt.	Internal Lighting	Standard LED's	9	Successful on ISS in space
	Batteries	Li/SOCl <sub>2</sub> Batteries	9	Multiple Successful uses in space (ex-deep impact)
	Fire Suppression	carbon dioxide fire suppressor	9	Currently on ISS in space
	Resistive Heater	Kapon Flexible Heaters	9	Multiple Successful missions on space probes
	Space heater	Standard internal space heaters	9	Successful on ISS in space
	Multi-Layer Insulation (MYLAR)	10 MYLAR layers	9	Successful use on multiple spacecrafts including ISS
Mission Planning	Launch Vehicle	Starship	6	Prototype demonstration on Earth

[SI-2,8,10,14,16]

As with any space mission, the components of the PLM must undergo rigorous testing and analysis to ensure they are ready for use in space by maintaining a pressurized system for the crew and cargo. The TRL analysis table for the PLM again provides a detailed overview of each component and its readiness to handle internal pressurized environment in the vacuum of space. The table is divided into similar categories as the LLV table: Actuation, Avionics, Power Management, and Mission Planning.

As shown in the PLM TRL rating table, most of the PLM's components have a TRL rating of 9, indicating their advanced stage of development and successful implementation on Earth and in space. Among the components with a TRL rating of 9, we find the Storage shelves, ECU Sensor (Temp, Humidity, Pressure, gases), Primary/aux computer/ECU, Camera, SSD, Internal Lighting, Batteries, Fire Suppression, Resistive Heater, Space Heater, and Multi-Layer Insulation (MYLAR). These components have demonstrated their reliability and readiness in previous missions, including on the International Space Station (ISS), the space shuttle and multiple space probes, making them well-suited for providing a pressurized environment for the crew and ensuring the safe transportation of essential supplies/cargo to the moon. Further, the Mission Planning category includes the Launch Vehicle (SpaceX Star Ship), which has a TRL rating of 6, meaning it is still in the prototype demonstration stage and has not fully demonstrated its capabilities beyond earth. Finally, it is crucial to carefully evaluate components that are still in the early stages of development with a TRL rating of 3. The Airlock Docking/Hatch with the Stewart platform design and Fire Detection using a line-of-sight radiometer fall into this category. Although they are considered proof of concept with limited testing, further development and evaluation are necessary to ensure their suitability and compatibility with the pressurized environment of the PLM.

Overall, from the TRL analysis table for the PLM, it is evident that many of the components have successfully completed missions in space and have a high TRL rating. However, some components are still in the proof of concept or prototype stage and require further testing before they can be used in space.

### 10.3 - CM TRL Analysis - Jeet Patel

Table 10.3.1: CM TRL Analysis

Category	Component Type	Component	TRL Rating	Reasoning
Actuation	Cables	Wire Strands	6	Successful demonstration by NASA LSMS
	Material	Al 7075-T6	6	Widely used in aerospace industry for its yield strength
	Motors	Linear and Rotary actuators	6	Successful demonstration by NASA LSMS
Avionics	Rotation sensor	Rotary encoder	6	Successful demonstration by NASA LSMS
	IMU/Tilt Sensor	LN-200S	9	Successful missions in multiple space probes
	Primary/aux computer/ECU	RAD5545 SBC from BAE Systems	9	Successful on multiple satellites in space

	Camera	Mars 2020 EECAM	9	Successful perseverance mission on Mars
	SSD	Greenliant	9	Popular SSD for use in variable temperatures
Power Mgmt	Dust control	Dust protection cover	6	Successful demonstration by NASA LSMS
	Resistive Heater/Thermal Control	Kapon Flexible Heaters	9	Multiple Successful missions on space probes
	Multi-Layer Insulation (MYLAR)	MYLAR Insulation layers	9	Successful use on multiple spacecrafts including ISS
Mission Planning	Launch Vehicle	Blue Moon	3	Prototype/Proof of Concept on Earth

[SI-2,6,8,10,11,18,19]

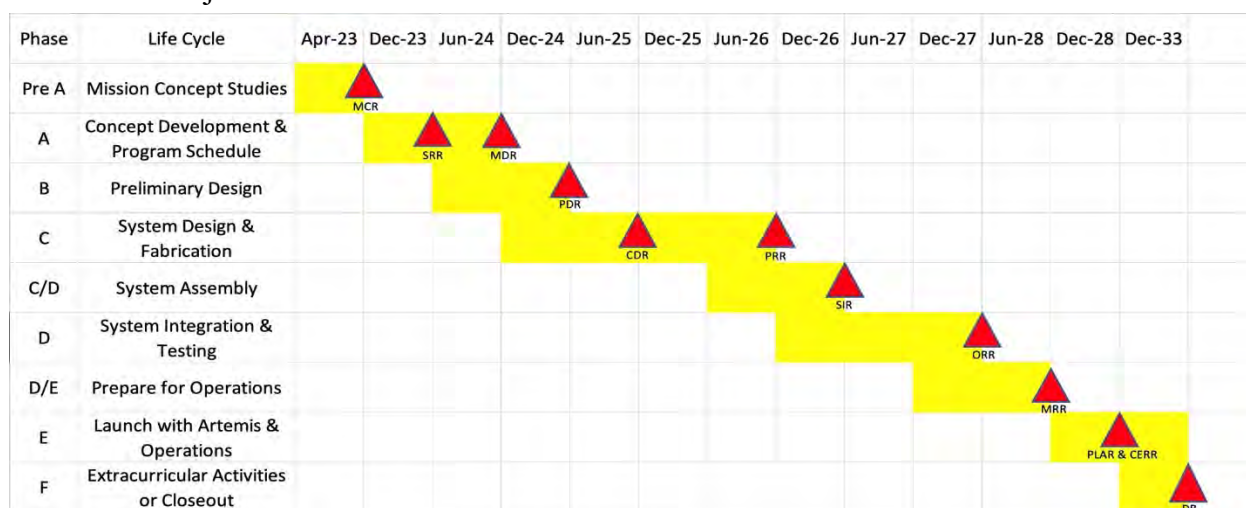
The Cargo Manipulator “CM” is mounted on top of the LLV and is responsible for handling cargo and payloads during transportation. Therefore, it is essential to ensure the reliability and effectiveness of the CM. This analysis assesses the maturity and readiness of each component of the CM based on the previous testing and performance data. The TRL table is again divided into the same four categories. Each category includes several sub-components, such as cables, materials, motors, rotation sensors, IMU sensors, computers, cameras, SSDs, dust control mechanisms, thermal control, insulation layers, and launch vehicles.

Again, from the CM TRL rating table, it is evident that most of the CM’s components have a TRL rating of 9. Among these components, we find the LN-200S IMU/Tilt Sensor, known for its successful deployments in multiple space probes, can provide accurate motion and orientation data for cargo handling operations. The Primary/Auxiliary Computer/ECU from BAE Systems, with its track record of reliability on multiple satellites, ensures efficient control and coordination of the CM during cargo transportation. The Mars 2020 EECAM camera, which successfully operated on the perseverance mission on Mars, offers visual feedback for precise cargo positioning. The Greenliant SSD, widely recognized for its performance in varying temperature conditions, provides reliable storage for critical data related to cargo management. Moving to TRL 6, we find components that are specifically designed for cargo manipulation by NASA LSMS (Lunar Surface Manipulation Systems) team. The Cargo Manipulator (CM) by SHELL incorporates various elements that have undergone successful demonstrations by NASA LSMS. These include Cables with Wire Strands, enabling reliable and flexible connections for cargo handling. Additionally, Motors equipped with Linear and Rotary actuators provide the necessary actuation for precise cargo movement. The Dust Control system, equipped with a Dust Protection Cover, ensures the efficient and safe operation of the CM in lunar surface environments. Finally, the component still in preliminary development stages with a TRL rating of 3 includes the Launch Vehicle, Blue Moon, which as discussed before is currently in the prototype or proof-of-concept stage by Blue Origin.

Overall, this TRL analysis table shows that most of the components in the logistics module have a TRL rating of 6 or 9, indicating that they have been successfully demonstrated in previous space missions or on earth. This suggests that the module has a high level of readiness and is likely to perform well on its intended mission. However, the lower TRL rating of the launch vehicle indicates that there may be some uncertainty around its performance and reliability, and additional testing and development may be necessary to ensure its success.

## 11. Project Timeline – jeet

Chart 11.1: Project Timeline



[SI-5]

The chart presented above outlines a generic NASA project timeline designed by SHELL to incorporate our proposed project, detailing the different phases and the review stages of a typical project. NASA's projects are usually quite complex, and they go through several stages before completion. The table lists the phases in order, from Pre-A to F, and each phase has specific project review timestamps associated with it.

The Pre-A phase is the first stage of the project, where the initial concepts are studied and defined. During this stage, NASA identifies the project's goals and determines the mission's feasibility. The Concept Development & Program Schedule stage (A) follows, where the project's details are further developed, and the program schedule is created. The next stage is the Preliminary Design phase (B), where NASA creates the initial design and architecture for the project. Following this, the System Design & Fabrication stage (C) involves building the subsystems required for the mission. Once the subsystems are built, the C/D stage involves their assembly. The System Integration & Testing phase (D) is a crucial part of the project, where all the subsystems are brought together, integrated, and tested. The next phase, D/E, involves preparing the mission for operations, which is a vital part of the project since it ensures that everything is in place for the mission's success. The final two stages, E and F, involve the launch of the mission with Artemis, NASA's lunar exploration program, and the Extracurricular

Activities or Closeout. The timeline listed in the table provides an estimated schedule for the completion of each life cycle stage and their subsequent reviews from April 2023 through December 2033. The table of various project reviews and their acronyms is listed below.

Table 11.2: Project Reviews and their Acronyms

Acronyms	Expansion
MCR	Mission Concept Review
SRR	System Requirements Review
MDR	Mission Definition Review
PDR	Preliminary Design Review
CDR	Critical Design Review
PRR	Production Readiness Review
SIR	System Integration Review
ORR	Operational Readiness Review
MRR	Mission Readiness Review
PLAR	Post-Launch Assessment Review
CERR	Critical Events Readiness Review
DR	Decommissioning Review

[SI-5]

It is important to note that this timeline is tentative and subject to change, as various factors such as funding, resource availability, and technical challenges can impact the timeline. However, the timeline provided in the table is an excellent starting point for understanding the various stages that a NASA project typically goes through and the approximate timeline for each stage.

## **12. Appendix**

### **12.1 - Spoiler Deployment – Matthew Thomas**

An alternative LLV design utilized a deployable spoiler to reduce vibration concerns throughout launch. The concept utilized a rotary actuation system at the base of the spoiler arms to move the spoiler from its forward stowed position to its deployed position. For actuation, this design considered both re-deployable concepts with electric motors and single-deployment concepts, such as frangibolts with torsion springs. The single deployment appeared favorable as it would simplify the system and require less active control. Before a final decision was made, the spoiler deployment concept was sidelined to provide more space on the chassis for electronics. The stowed configuration and deployed configuration can be seen in fig. 12.1.1 and fig. 12.1.2 respectively.

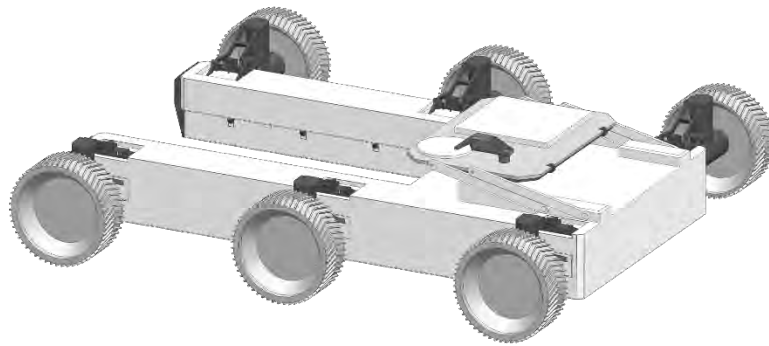


Figure 12.1.1: LLV stowed configuration

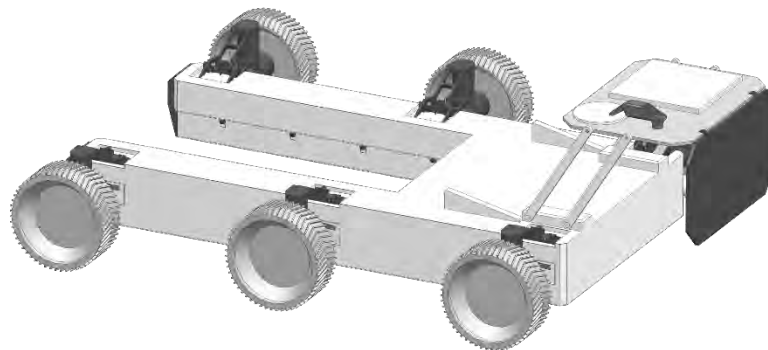


Figure 12.1.2: LLV deployed configuration

In the stowed configuration above, the spoiler arms rest on ramps where they are latched to the top of the LLV chassis. Additionally, by stowing the spoiler, the envelope is reduced from 6.05x4.54x1.96 meters to 5.24x4.54x1.22 meters, which is nearly a 25 cubic meter reduction in volume. Both changes serve to reduce the vibrations of the spoiler throughout the launch sequence and decrease the volume occupied within the fairing of the launch vehicle.

## 12.2 - Radiation Hardening Assurance Research – Matthew Visnich

We've been considering how to protect our electronic components from different types of radiation present on the lunar surface ranging from solar protons to galactic cosmic rays, both of which can cause semiconductor degradation and other harmful effects if left unmitigated. In [our research](#), we found two mitigation strategies: external shielding and processor reconfigurability. The former solution installs outer layers of materials with proven tolerance on the vehicle, such as titanium, or places the onboard computers into areas of the vehicle that have much of the existing structure around them (the center of our U-shape). The latter solution encompasses equipping the lunar logistics vehicle with extra electronic components so that in the event a primary component malfunctions, the secondary component activates, at least for a time, to keep normal functions performing.

As indicated on the final version of the block diagram, our solution for this ever-persistent issue came from equipping our vehicle with cold central processing unit that is not online during normal operation; hence why its communication lines to the memory and peripheral are dashed lines in the representation above. This secondary computer only activates when radiation effects overwhelm the hot processing unit or when the attached radiation sensor detects an unsafe radiation environment. For an extra layer of precaution, the cold processing unit would be placed in an area of the vehicle most insulated from the environment due to the sheer number of structures and components around it.

## 12.3 - Phase Change Materials – Nicholas Delafuente

When looking for methods to thermally regulate each system on SHELL, phase change materials (PCMs) seemed to be a promising idea. PCMs are substances that release and absorb energy at their phase transition to provide heating and cooling. The most common type of phase change materials are solid to liquid/liquid to solid (absorb/release heat). There were three main types of PCMs considered: inorganic, organic, and eutectic. The data for inorganic and organic PCMs is placed below.

Inorganics	Melting Point (C)	Latent Heat Capacity (kJ/kg)	Thermal Conductivity (W/cm*C)
Salt Hydrates	0 to 100	60 to 300	.006 to .01
Metallics	150 to 800	25 to 100	.12 to 4.3

Table 12.3.1

Organics	Melting Point (C)	Latent Heat Capacity (kJ/kg)	Thermal Conductivity (W/cm*C)
Paraffin	-20 to 100	200 to 280	.002
Nonparaffin	5 to 120	90 to 250	~.002

Table 12.3.1 [PPT-32,33]

When choosing an appropriate PCM to fit a system, the temperature bands must be considered. For example, motors must be regulated between -50 C to 50 C. This means that a PCM with similar temperature bands should be chosen, like paraffin. Although phase change materials were never chosen, the next goal was to determine how much heat would need to be absorbed/released at certain temperatures and then determine the mass of the PCM based off of latent heat capacity.

### 12.4 - Regolith Heating – Joshua Batstone

In order to determine whether pointing the motor radiators towards the regolith would result in significant heating, a finite element model was developed in NX Space Systems Thermal solver, implementing a two-layer regolith model as used in [PPT-6]. This model was first run to steady-state, and then a restart was performed to determine the transient behavior over a duration of 1 hour, with 40 W nominal heating in the IR spectrum. The before and after FEM mesh is shown in Fig. 12.4.1, and the temperature plot for a node located on the top of the regolith is shown in Fig. Fig. 12.4.2.

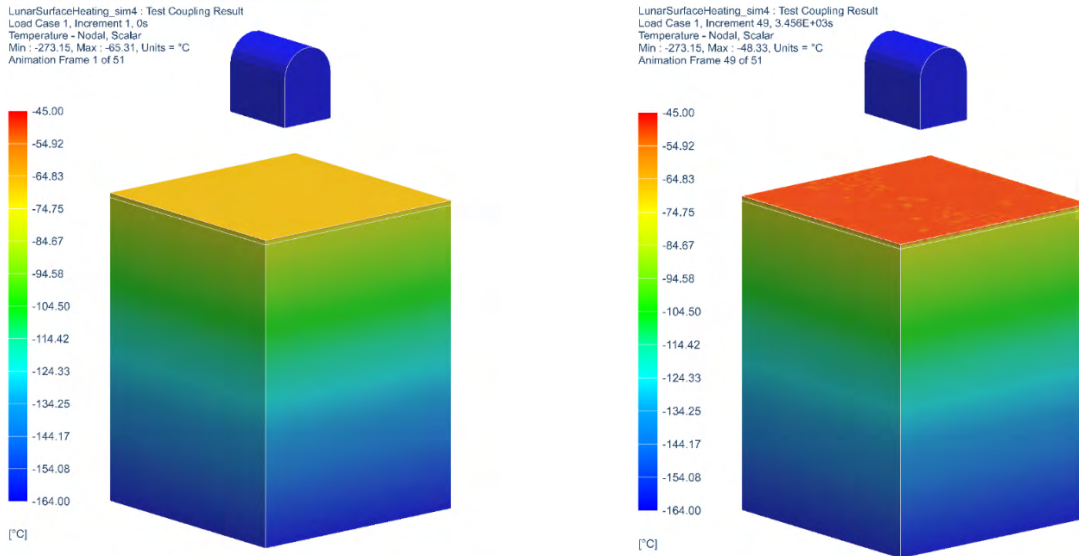


Figure Fig. 12.4.1: Before (left) and After (right) of Regolith After 1 hour.

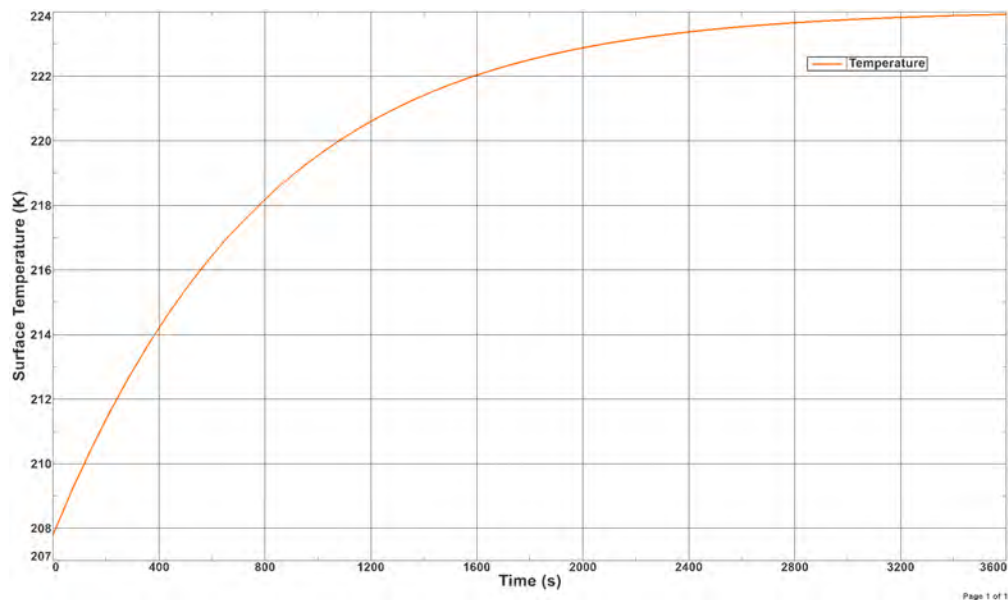




Figure Fig. 12.4.2: Transient Temperature vs. Time for Lunar Surface.

From this analysis, it was determined that the temperature change due to regolith heating was reasonably small over short heating durations. Additionally, in steady-state conditions, the increased ground temperature remained significantly less than the 250 K we used for design purposes, and so it was determined that regolith heating would not appreciably impact the effectiveness of the motor radiators.

### 12.5 - Azimuthal Sun Tracking – Joshua Batstone

For power generation, different charging regimes were considered, including azimuthal solar tracking, and stationary orientation/crab steering for both one and three-sided array mountings. On a lunar-day basis, assuming 40% sun visibility and 33% cell conversion efficiency, these different regimes produce energy according to the following distributions (Figure 12.5.1).

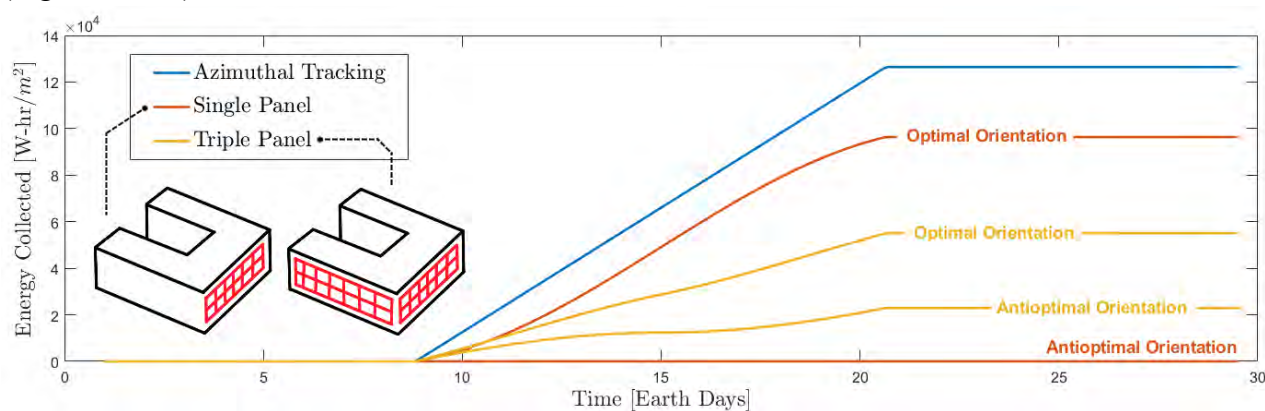


Figure 12.5.1: Solar Power Generated Over Lunar Day for Different Charging Regimes.

Three-sided arrays were deemed infeasible due to LLV wheel sizing and placement, and so a front-mounted solar array was selected. If the system tracks the sun azimuthally, during periods of sunlight the system will generate approximately 445 W/m<sup>2</sup>, allowing the battery to fully charge in 180 hr for 1 m<sup>2</sup> of area (corresponding to 25% of the lunar day). For initial solar array sizing, we have selected a panel area of 2 m<sup>2</sup> which will allow the battery to fully charge in approximately 90 hr.

### 12.6 - Ideal Charging Zones – Seth Gussow

One of the considerations when initially going about site selection was finding charging zones within these sites to sit our LLV. As we are mainly relying on solar power it was an important step to find locations where we could rest our LLV and let it charge for an extended period. As discovered, we needed upwards of 80 hours to charge if we depleted the battery to our 80% depth of discharge line, meaning that we would need that much constant sunlight. In planning our mission, we wanted to see if it was possible to understand where areas would be safe for us to charge based on terrain and sunlight height.

As discussed previously, we could determine the sunlight height as visible from an observer on the lunar surface using NASA JPL's Horizon tool to map the path of the sun over

time. This was useful to determine the actual height of the sun in degrees of elevation which we could use to map where it was versus the terrain. Getting the terrain height was much more difficult as we needed to set a point and attempt to see the impeding terrain in a full 360-degree scope. While we could find slope data for the lunar surface using the QuickMap tool from ASU, it was difficult to determine the max slope in any direction [MPA-1].

In consultation with Ernest Wright of NASA Goddard Space Flight Center and Dr. Mark Shirley of NASA Ames Research Center we were pointed towards the raw gridded data reports (GDR) from the Lunar Reconnaissance Orbiter's database to view the slope information independently. This proved to be massively difficult as specific software such as QGIS (an open-source graphic information system) to view data and require subroutines that were not publicly available. While it was possible to view the data, it did not provide the sunlight mapping that could be created and does exist with the help of Wright [MPA-4]. Dr. Shirley, being the head of NASA's VIPER lunar mission, indicated that while it was possible to find the data using GDRs that it was likely illogical to proceed down this path for the scope of our project.

Therefore, we were left with the preliminary work that we had completed which consisted of pairing sunlight information that was propagated with the Horizons tool in addition to Earth visibility data that was equally created using Horizons. We were interested in the Earth visibility over the five-year period of our LLV operation as at the time we felt we would need constant visibility to operate. This left the slope in a 360-degree view of our terrain and required an attempt to lay it against the elevation of the sun.

Using ASU's QuickMap we were able to loosely create the terrain in a 360-degree view by laying points on the lunar surface equidistant from a midpoint. We chose to use a 500-meter radius circle as we felt this would accommodate most obstacles in our way. By laying down connecting lines, we could measure the slope along these lines and create a 360-degree map of our slope at 500-meter radius. A downside to this method is that we could not physically set a center point of these connecting lines and required us to convert the selenocentric coordinates of the endpoints of the lines to an azimuth based on a center point.

By setting the center point (using its own selenocentric coordinate) we could measure the azimuth based on the radius and the exterior circle created by the connecting lines. This left us with a usable excel file that could be plotted against the generated text files from the JPL Horizons tools. It is important to note that we also had to calculate the elevation in degrees of the slope based once again on the terrain height of the center point versus the terrain height of

**Figure MPA-X: Sunlight and Earth Visibility  
with Terrain Elevation**

outlining circle. This gave us a very rough version of the terrain slope in degrees instead of a raw meter's value and allowed us to directly compare the two numbers.

Now that we had values for Sun elevation over 5 years, Earth elevation over 5 years, and terrain elevation, we could map all three values together and estimate the best area to charge in during sunlight hours. This is seen in figure MPA-A1, displaying the optimal Azimuth which promoted prominent sunlight availability. While this

map is a rough estimate, we felt that it indicated positive sunlight versus terrain elevation during our daytime hours as well as positive Earth visibility.

The shortcoming of this analysis stems mainly from the limitations in software prompts that could have more accurately mapped the terrain in a circle. Additionally, the positive of this analysis did not promote enough for our charging availability that we felt further exploration was needed. As pointed out by Dr. Shirley, there were other items that existed that could essentially provide us with similar answers to what we required. For example, QuickMap by ASU shows the average sunlight availability over approximately a 20-year period. While this does not show the exact timing of sunlight and where we could expect it to be coming from, a simple location paired with LLV sun tracking would essentially give us the same information. As such, we chose to explore these other options instead of using the created MATLAB subroutines that would pair this data together.

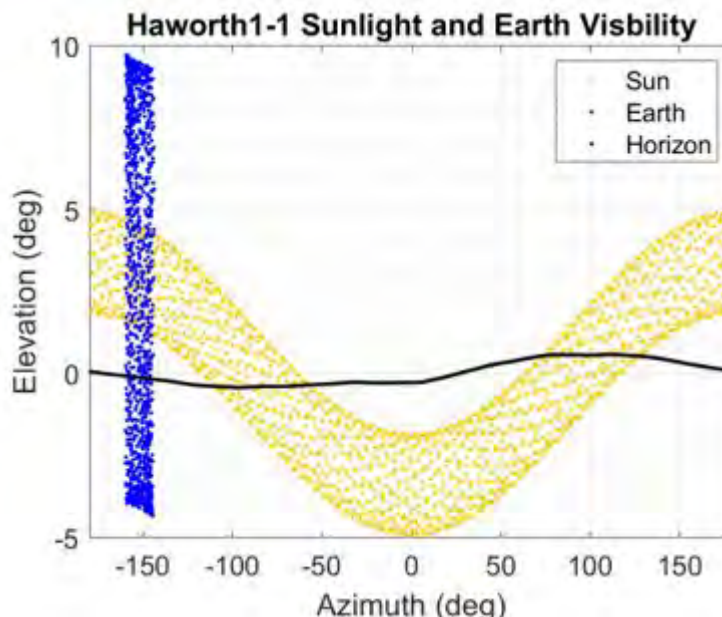


**Figure MPA-A1: Experimental Sunlight and Earth Visibility Plot in Relation to the Lunar Horizon Line**

### 12.7 - Site Selection Decision Matrix – Seth Gussow

Sites	Sunlight Max (Days)	Area (km <sup>2</sup> )	Roughness	Earth Vis	Weighted Total
Haworth1-1	10	39.648	0.9386	37	20.69
Haworth1-2	10	7.47	0.94215	37	11.04
Haworth 2	10	36.968	1.06521	51.8	21.38
Haworth 3	10	18.77	1.17159	57.9	16.54
Haworth 5	9	14.29	0.880812	26.6	11.54
Haworth 6	10	2.47	1.08565	54.2	11.27
Leibnitz 2	13	2.31	0.774423	75	14.77
Leibnitz 3	12	2.4	1.097	65.3	13.36
LN 2	12	5.26	0.885813	52.1	12.88
LN 3	12	2.77	0.972415	45.8	11.51
Massif 1	11	2.45	1.19714	76.8	14.03
Massif 4	11	16	0.941	72.7	17.66
Massif 5	11	16	1.192	64.2	16.84
NR1-1	13	1.52	0.870875	48.7	11.91
NR1-2	13	4.84	1.02111	65.2	14.57
NR1-3	12	2.36	0.971907	58.1	12.62

<b>Weight (100%)</b>	<b>100.00%</b>
Sun	50.00%
Area	30.00%
Rough	10.00%
Earth Vis Avg	10.00%

### 12.7 - Initial PLM Thermal Calculations – Edwin Arevalo

Three cases of PLM heat loads were looked at.

Case #1: Direct sunlight + reflections from the lunar surface

Case #2: NO direct sunlight + reflections from the lunar surface

Case #3: NO direct sunlight + NO reflections from the lunar surface

Using an emissivity of mylar  $\varepsilon_{mylar} \approx 0.03$  the effective emissivity was then calculated using the following formula:

$$\varepsilon_{eff} = \frac{\varepsilon_{mylar}}{(N - 1)(2 - \varepsilon_{mylar})}$$

Where  $N$  is the number of layers. In the case of about 6 layers the effective emissivity was found to be  $\epsilon_{eff} = 0.003046$  which was later found to be unrealistic and inconsistent with what is found in practice. However, at the time that emissivity was used to determine a desired absorptivity ( $\alpha$ ) and internal power requirements. Again, here the PLM was modeled as a cylinder with two partial hemispherical endcaps. At the time, the volume and surface area was found to be  $62.57 \text{ m}^3$  and  $84.4 \text{ m}^2$  respectively. Here the assumption that heat radiated equally from all faces of the PLM was made and case #1 was used as the limiting case to find a desired absorptivity. Case #1 was used because it represents when the PLM will be the hottest and we didn't want to design our system where we also needed a cooling system. In our case it is easier to heat the PLM than to cool it so by using case #1 we can determine an absorptivity that will allow the PLM to only always need heating assuming a max temperature at our landing location of about 260 Kelvin; this stems from research done by our mission planning team and data found on lunar surface temperatures provided by NASA [AFSS-9E]. The following equation was used to solve for the internal power requirement of a electric heater based on the radiative heat at varying values of absorptivity:

$$I_s \alpha A_s = \epsilon_{eff} \sigma A_{rad} (T^4 - T_{env}^4)$$

Where  $I_s = 1394 \text{ W m}^{-2}$  insolation constant at 1AU,  $A_s$  is the surface area being hit by the sun,  $\sigma$  is the Stefan Boltzmann constant,  $A_{rad}$  is the area where heat is being radiated from,  $T$  is the temperature inside the PLM and  $T_{env}$  is the temperature of the environment. Using this model a desired absorptivity of  $\alpha = 0.00155$  was found; see figure below.

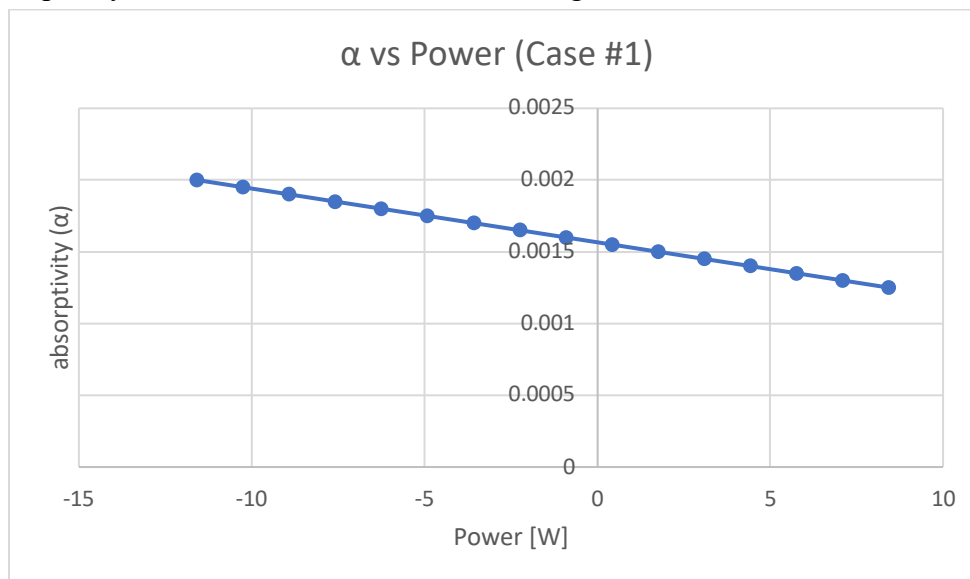


Figure X: absorptivity vs. Power for case #1 where the PLM is being heated by direct sunlight and reflection off the lunar surface. Used to calculate a desired absorptivity that minimizes power.

It was later found that both the effective emissivity and absorptivity of 0.003 and 0.0016 were found to be unrealistic in practice as lunar dust can cover the mylar layering, changing both its emissivity and absorption.

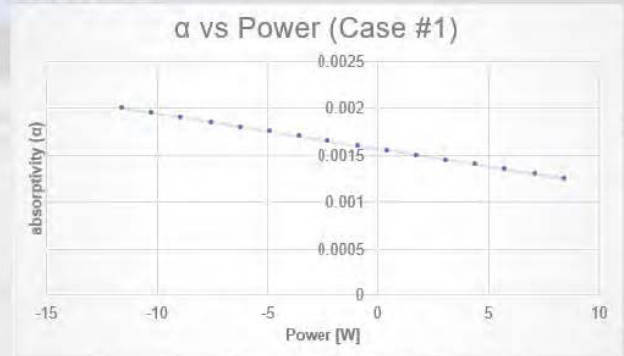
## Power Requirement for Heater

$\epsilon$  of mylar  $\approx 0.03$

→ 6 sheets of mylar  $\epsilon_{eff} = 0.0030$

→ calculated  $\alpha \approx 0.00155$

$$I_s \alpha A_s + P_{int} = \epsilon \sigma A_{rad} (T^4 - T_{env}^4)$$



CASE:	absorp ( $\alpha$ )	emm ( $\epsilon$ )	Sun Effects [W]	T body	T env (K)	P int [W]
Sun + Moon reflection	0.00155	0.0030	41.36	293	260	0.4258
No Sun + Moon Reflection	0.00155	0.0030	0	293	140	104.2
No Sun + No Moon Reflection	0.00155	0.0030	0	293	40	109.9

X-HAB Progress Report  
ENAE 484 – Space Systems Design

21

A. JAMES CLARK  
SCHOOL OF ENGINEERING

### 12.8 - Possibility of Solar Panels to Provide Additional Capabilities to PLM – Edwin Arevalo



*Solar panel concept on PLM*

Although we plan on throwing each and every PLM away after its first use, we can however decide to create PLM's that are modular and add onto existing habitats. In this concept we added solar panels to a mock PLM to allow it to have a greater standalone capability. CAD of

this concept is shown in the figure above that was made with the assistance of Brian Amaya. Rechargeable batteries can be added in the unpressurized section of the PLM to replace expensive RTG's and, once the PLM is connected to the habitat, it can also give power to a habitat once connected via its solar panels, increasing the power capacity of the habitat and promoting further base building. The solar panels will need to be protected and have other dust mitigation capabilities such as a piezoelectric vibrating mechanism to ensure longevity and efficiency.

### 12.9 - Making The Video That Got Us Into RASC-AL – Edwin Arevalo

An important part of the 2023 RASC-AL competition submission was a video outlining what makes our project stand out from the rest and showcasing different components that are easier to display as animations rather than in a PDF. In order to make this possible we needed to make a script first explaining the con ops then some unique features; these were assisted by Pranav Ampani. Next, we created different animations showcasing the capabilities of our steering, latching mechanism, and suspension; these were done by Matthew Thomas. Finally, numerous videos and slides were put together and a voice over was done using a rented professional grade microphone to create a single coherent video submission to be presented to RASC-AL judges. The video was made in Adobe Premiere Pro. Unique animations were created at the end to seamlessly tie everything together and help promote the SHELL project. Additionally, copyright-free music was found and used to help set the pace of the video and retain the viewers' attention. Link to Video:

<https://www.youtube.com/watch?v=D8AVLZO9A4c>

The script for the video was the following:

#### Start:

Hello! We are SHELL, the System for Heavy-Lift, End-to-End Lunar Logistics, from the University of Maryland.

#### Why?:

SHELL will help by creating a logistics system that will support base-building and logistics transportation on the Lunar surface.

#### Conops page:

This is a Con Ops breakdown for a Payload Transportation Mission

Starting off our vehicle will align itself with the payloads Standardized Payload Interface, which we named SPI for short.

Once aligned, our vehicle will lower down using its active suspension to match the height of the payload and latch to the payloads corresponding SPI system.

The suspension system will then raise itself up and proceed to the delivery location.

Where upon arrival it will lower the payload onto the lunar surface and release

#### PLM

Payloads vary from mission to mission, this is our concept for a pressurized logistics module to transport delicate good across the harsh lunar surface.

#### Cargo Manipulator

Next is our Cargo Manipulator, this can be used to unload landers and help transport non-pressurized logistics.

#### Small Cargo

Smaller non-pressurized logistics would then be placed on a separate interface and transported.

#### Paver

Our paver concept can be used to move large obstructions and build highways for transportation from site to site.

**Suspension demo:**

Here, you will see a demonstration of our active suspension system. The suspension enables the functionality of our PMI system and will also help the vehicle navigate the rough lunar landscape. In order to reduce our suspension requirements, we adapted an above latching technique which saves us from having to go lower to pickup our payload

Above latching also allows us to pick up payload that may have sunken a bit into the lunar soil.

**SUIT demo:**

Above latching also allows us to connect to payloads that may have sunken into the lunar soil.

Our latching system is comprised of two types of the SUIT mechanisms, a plug, or male, SUIT located on the payloads and a receptacle, or female, SUIT located on the Vehicle.

The SUIT system also provided temporary power to our payloads.

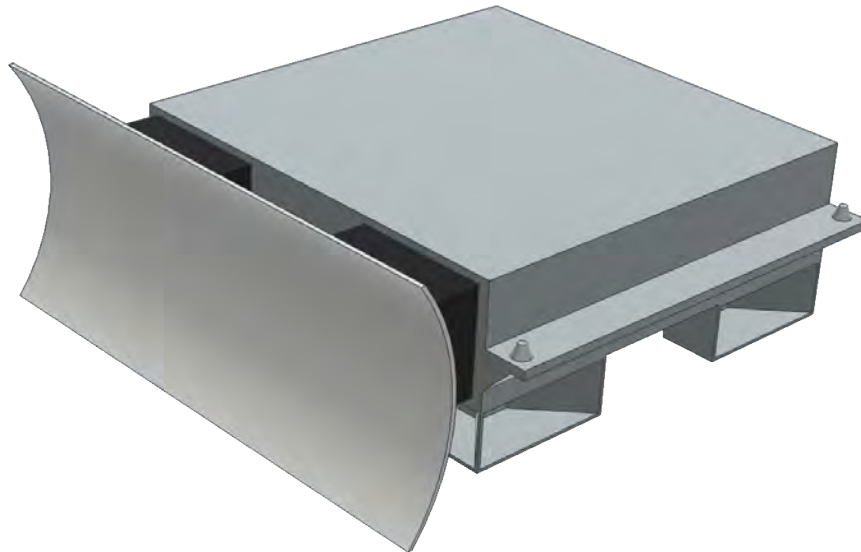
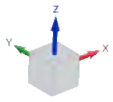
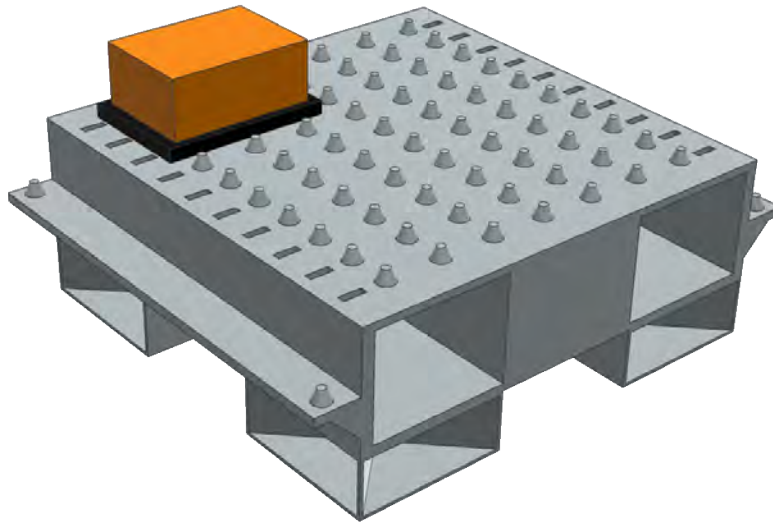
**Full demo:**

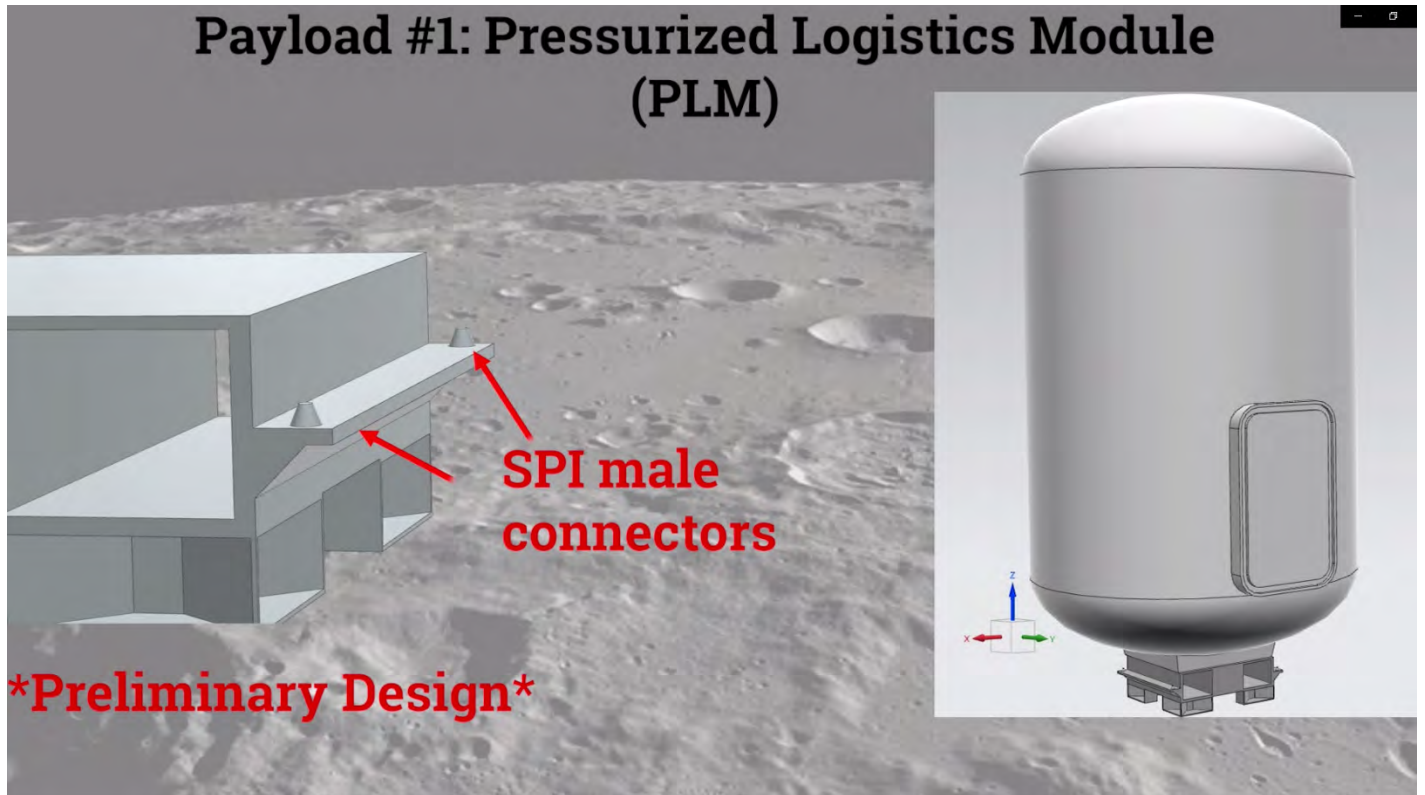
SHELL will be able to transport many different types of payloads, utilizing it's active suspension to adjust for any height. This will enable smoother operations on the Lunar surface for habitat building and scientific missions requiring large equipment.

**Ending:**

That's it from us for now. We hope you enjoy what we have so far, we still have a lot of work ahead of us.



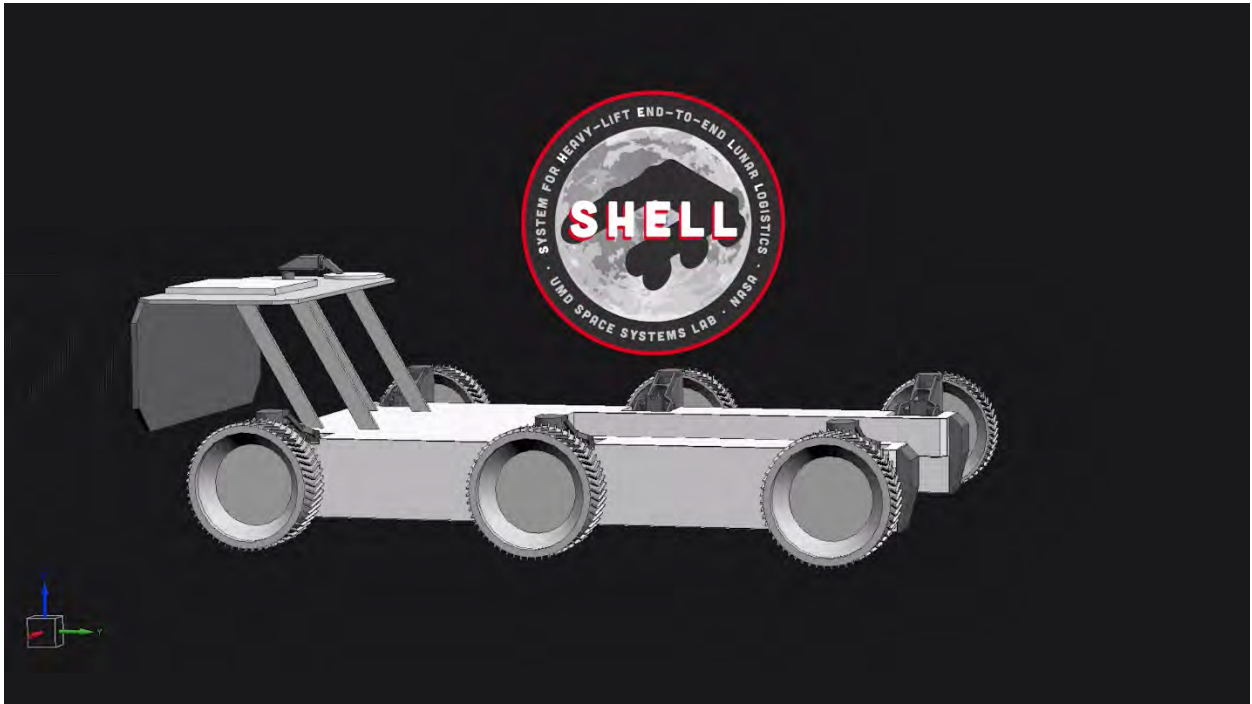
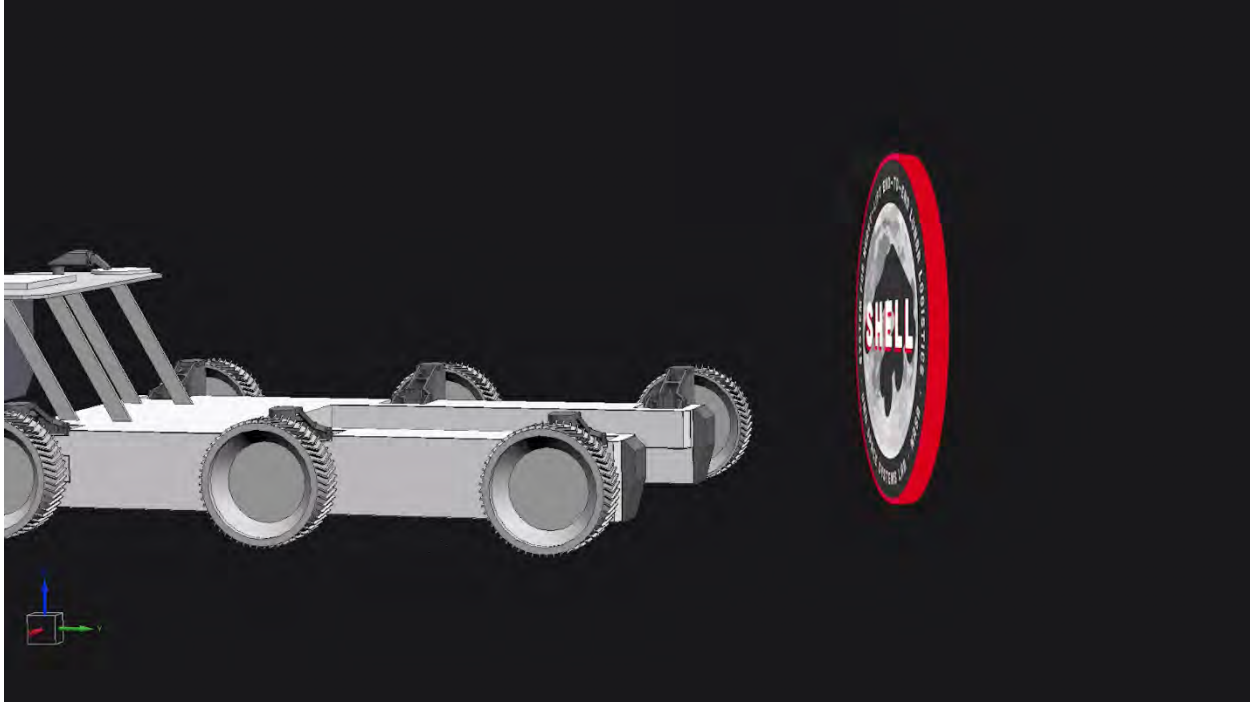




Various unique payload design features that were created and displayed in the video are seen above.



The 2D static SHELL Logo created by Justin DeVito was then transformed into a rotating and translating 3D object in Adobe After Effects and made into an animation along with the vehicle entering the screen. Other slides presented in the video include:



## Concept of Operations - Payload Transportation Mission:

- 1) The Lunar Logistics Vehicle (LLV) will approach the payload, maintaining its body above the payload's attached Standardized Payload Interface (SPI).
- 2) Once aligned, suspension system will drop down and interlock the payload's SPI system with the LLV onboard interface and provide temporary power to the payload.
- 3) Then suspension system will rise up to operating height. The LLV will proceed to the pre-determined end location for payload delivery.
- 4) The LLV will then lower its suspension, release the SPI system, and unload the transported payload onto the lunar surface.

### 12.10 - Flexible User Radio – Edwin Arevalo

The Flexible User Radio allows us to design without committing to a specific relay satellite system by supporting a wide range of frequencies. The Flexible Radio has near-real time adaptation to different relay satellites by using a phased array antenna to scan the sky for available networks. A similar device called the Wideband User Terminal was found to support 17.7 - 23.55 GHz receiving and 25.25 - 31 GHz transmitting; much of this capability is directly applicable to the Flexible Radio. The Flexible radio works by changing different aspects such as the antenna polarization, transmit/receive power levels, modulation, framing format, packetization and network protocols [AFSS-2E]. It is being initially designed to work across the Ka-band supporting 25.5 – 27.5 GHz transmitting and 22.55 – 23.55 GHz receiving. Research has been done to prove that this concept may work, however the actual design is still in development with a TRL of 4. All-in-all the concept is still too early in development to rely on it and we decided to abandon it.

## 12.11 - References

### 12.11.1 - AFSS

- [AFSS-1] BAE Systems, Radiation-hardened electronics product guide. Available:  
www.baesystems.com
- [AFSS-2] “BAE Systems RAD5545TM SpaceVPX Single-Board Computer.” Virginia, Mar. 2017.
- [AFSS-3] “Broadcasting Guidelines,” Customer support Available:  
[https://help.twitch.tv/s/article/broadcasting-guidelines?language=en\\_US](https://help.twitch.tv/s/article/broadcasting-guidelines?language=en_US).
- [AFSS-4] “Choose live encoder settings, bitrates, and resolutions - youtube help,” Google Available:  
<https://support.google.com/youtube/answer/2853702?hl=en#zippy=%2Cp%2Cp-fps>.
- [AFSS-5] Communications,” Mars 2020 Mission Perseverance Rover Available:  
<https://mars.nasa.gov/mars2020/spacecraft/rover/communications/>
- [AFSS-6] Deep Space Network - NASA Jet Propulsion Laboratory,” NASA JPL DSN Available:  
[https://deepspace.jpl.nasa.gov/files/DSN\\_Radio\\_Astronomy\\_Users\\_Guide.pdf](https://deepspace.jpl.nasa.gov/files/DSN_Radio_Astronomy_Users_Guide.pdf)
- [AFSS-7] Dendy, R., Mortensen, D., Zeleznikar, D., and Booth, S., “Flexible user radio for lunar missions - ntrs.nasa.gov” Available:  
[https://ntrs.nasa.gov/api/citations/20220014991/downloads/FLR\\_BigSky\\_2022%20submitted%20version.pdf?attachment=true](https://ntrs.nasa.gov/api/citations/20220014991/downloads/FLR_BigSky_2022%20submitted%20version.pdf?attachment=true).
- [AFSS-8] Descanso - Book Series,” NASA Available:  
<https://descanso.jpl.nasa.gov/monograph/mono.html>
- [AFSS-9] Destevez, “Decoding James Webb Space Telescope,” Daniel Estvez Available:  
<https://destevez.net/2021/12/decoding-james-webb-space-telescope/>.
- [AFSS-10] Earth png transparent image download, size: 1789x1787px” Available:  
<https://pngimg.com/image/25344>
- [AFSS-11] ENHANCED ENGINEERING CAMERAS (EECAMs) FOR THE MARS 2020 ROVER” Available: <https://www.hou.usra.edu/meetings/ipm2016/pdf/4132.pdf>
- [AFSS-12] Fortescue, P. W., Stark, J., & Swinerd, G. (2011). Spacecraft Systems Engineering. Wiley.
- [AFSS-13] Gateway – Transparent Background Alternative View,” ESA Available:  
[https://www.esa.int/ESA\\_Multimedia/Images/2019/05/Gateway\\_transparent\\_background\\_alternative\\_view](https://www.esa.int/ESA_Multimedia/Images/2019/05/Gateway_transparent_background_alternative_view)
- [AFSS-14]  
[https://www.nasa.gov/sites/default/files/atoms/files/lunanet\\_overview\\_to\\_nesc\\_lunar\\_science\\_workshop\\_2022-6-7.pdf](https://www.nasa.gov/sites/default/files/atoms/files/lunanet_overview_to_nesc_lunar_science_workshop_2022-6-7.pdf)
- [AFSS-15] Israel, D. (2022). ENAE694 Spacecraft Communications Introduction and Course Overview. Lecture.
- [AFSS-16] Jamal, H., “Localization for Lunar Micro-Rovers”, Carnegie Mellon University, 2021

- [AFSS-17] James Schier, Chief Architect, “LunaNet Overview.” Presentation ”Available: [https://www.nasa.gov/sites/default/files/atoms/files/lunanet\\_overview\\_to\\_nesc\\_lunar\\_science\\_workshop\\_2022-6-7.pdf](https://www.nasa.gov/sites/default/files/atoms/files/lunanet_overview_to_nesc_lunar_science_workshop_2022-6-7.pdf)”
- [AFSS-18] John, K., and Fritz, A., “Survive the night dust - ntrs.nasa.gov” Available: <https://ntrs.nasa.gov/api/citations/20220018433/downloads/Survive%20the%20Night%20Dust%20Presentation%20-dec2022%20-%20v4.pdf?attachment=true>.
- [AFSS-19] Keys, Andrew S, et al. “International Planetary Probes Workshop - 5.” NASA, *The Vision for Space Exploration*, 2007. *NASA Technical Reports Server*, <https://ntrs.nasa.gov/api/citations/20070032045/downloads/20070032045.pdf>.
- [AFSS-20] Kurth, D., thesis, “Range-Only Robot Localization and SLAM with Radio”, The Robotics Institute Carnegie Mellon University, 2004
- [AFSS-21] Larson, W. J., and Wertz, J. R., “Chapter 7 & 13,” *Space mission analysis and design*, Dordrecht: Kluwer Academic Publishers, 2005
- [AFSS-22] Lazio, J. (2021). (publication). *The Deep Space Network Radio Astronomy User Guide*.
- [AFSS-23] Lee, W.-J., Cho, K.-K., Yoon, D.-W., and Hyun, K.-M., “Design and performance analysis of downlink in Space Communications System for Lunar Exploration,” *Journal of Astronomy and Space Sciences*, vol. 27, 2010, pp. 11–20
- [AFSS-24] Lewis, J., Barido, R., and Tuan, G., “Crew exploration vehicle environmental control and life support fire ...” Available: <https://ntrs.nasa.gov/api/citations/20070021223/downloads/20070021223.pdf>.
- [AFSS-25] LN-200s Inertial Measurement Unit (IMU) - northrop grumman” Available: <https://www.northropgrumman.com/wp-content/uploads/LN-200S-Inertial-Measurement-Unit-IMU-datasheet.pdf>
- [AFSS-26] Lovelly, Tyler M. “COMPARATIVE ANALYSIS OF SPACE-GRADE PROCESSORS.” *University of Florida*, University of Florida, 2017, pp. 4–67.
- [AFSS-27] Moon png transparent image download, size: 348x368px - pngimg.com” Available: <https://pngimg.com/image/25382>
- [AFSS-28] Roddy, D., *Satellite Communications*, New York: McGraw-Hill, 2001
- [AFSS-29] Rover Brains,” NASA Available: <https://mars.nasa.gov/mars2020/spacecraft/rover/brains/>.
- [AFSS-30] Satellite PNG transparent image download, size: 2560x1621px” Available: <https://pngimg.com/image/106146>
- [AFSS-31] Schaezler, R., Cook, A., Leonard, D., and Ghariani, A., “Trending of overboard leakage of ISS cabin atmosphere - NASA” Available: <https://ntrs.nasa.gov/api/citations/20110012997/downloads/20110012997.pdf>.
- [AFSS-32] Schier, J., “LunaNet Overview” Available:
- [AFSS-33] Sheldon, R., “Why object storage is becoming an alternative to raid: TechTarget,” *Storage Available*: <https://www.techtarget.com/searchstorage/tip/Why-object-storage-is-becoming-an-alternative-to-RAID>.

- [AFSS-34] Solid State Storage ,” Greenliant Available:  
<https://www.greenliant.com/products/removable-ssds.dot#interface=msata>
- [AFSS-35] Yin Li, Jian Sun, S. B. Kang and Heung-Yeung Shum, "Symmetric stereo matching for occlusion handling," 2005 IEEE Computer Society Conference on Computer Vision and Pattern Recognition (CVPR'05), San Diego, CA, USA, 2005, pp. 399-406 vol. 2, doi: 10.1109/CVPR.2005.337.
- [AFSS-36] Burner, L., “Velocity Control for Mobile Robots,” *CMSC477*, Mar. 2023.
- [AFSS-37] Singh, C. D., “Visual Odometry for Navigation,” *CMSC477*, Apr. 2023.
- [AFSS-38] Singh, C. D., “Correlation and Convolution,” *CMSC477*, Apr. 2023.
- [AFSS-39] P. Bailey et al., "Deployed Instrument Monocular Localization on the InSight Mars Lander," 2020 IEEE Aerospace Conference, Big Sky, MT, USA, 2020, pp. 1-13, doi: 10.1109/AERO47225.2020.9172343.
- [AFSS-K] “Artificial Lunar Landscape Dataset” Available:  
<https://www.kaggle.com/datasets/romainpessia/artificial-lunar-rocky-landscape-dataset>.
- [AFSS-1E] Agency, U. S., “Lunar Pathfinder Case Study,” GOV.UK Available:  
<https://www.gov.uk/government/case-studies/lunar-pathfinder>
- [AFSS-2E] Dendy, R., Mortensen, D., Zeleznikar, D., and Booth, S., “Flexible User Radio for Lunar Missions ,” NASA Available:  
[https://ntrs.nasa.gov/api/citations/20220014991/downloads/FLR\\_BigSky\\_2022%20submitted%20version.pdf?attachment=true](https://ntrs.nasa.gov/api/citations/20220014991/downloads/FLR_BigSky_2022%20submitted%20version.pdf?attachment=true)
- [AFSS-3E] Dendy, R., Zeleznikar, D. J., and Zemba, M. J., NASA Lunar Exploration Gateway’s power and propulsion element ... Available:  
[https://ntrs.nasa.gov/api/citations/20210019019/downloads/ICSSC\\_2021%20Gateway%20PPE%20Comm%20Links.pdf](https://ntrs.nasa.gov/api/citations/20210019019/downloads/ICSSC_2021%20Gateway%20PPE%20Comm%20Links.pdf)
- [AFSS – 4E] Holladay, J., Day, G., and Gill, L., Guidelines for Developing Spacecraft Structural Requirements; A Thermal and Environmental Perspective Available:  
<https://ntrs.nasa.gov/api/citations/20040085957/downloads/20040085957.pdf>
- [AFSS-5E] Israel, D. J., and Babu, N., “Draft LUNANET interoperability specification,” NASA Available: <https://ntrs.nasa.gov/citations/20220010998>
- [AFSS-6E] Israel, D. J., Mauldin, K., Roberts, C., Mitchell, J., Pulkkinen, A., Cooper, L. V., Johnson, M., Christe, S., and Gramling, C., “LunaNet: A flexible and Extensible Lunar Exploration Communications and ...,” NASA Available:  
<https://ntrs.nasa.gov/api/citations/20200001555/downloads/20200001555.pdf>
- [AFSS-7E] Johnson, S. K., Mortensen, D. J., Chavez, M. A., and Woodland, C. L., Gateway – a communications platform for Lunar exploration Available:  
[https://ntrs.nasa.gov/api/citations/20210018935/downloads/GW\\_Comm\\_ICSSC\\_Paper.pdf?attachment=true](https://ntrs.nasa.gov/api/citations/20210018935/downloads/GW_Comm_ICSSC_Paper.pdf?attachment=true)
- [AFSS-8E] Lunar exploration ground sites (legs) - explorers.larc.nasa.gov Available:  
[https://explorers.larc.nasa.gov/2023APPROBE/pdf\\_files/Prog05d.%20LEGS%20Brochure%20r20.pdf](https://explorers.larc.nasa.gov/2023APPROBE/pdf_files/Prog05d.%20LEGS%20Brochure%20r20.pdf)

- [AFSS-9E] “Moon: Surface temperature,” Science On a Sphere Available: <https://sos.noaa.gov/catalog/datasets/moon-surface-temperature/>
- [AFSS-10E] “Sensor Detail,” Lunar Outpost Canary-S Available: <https://www.aqmd.gov/aq-spec/sensordetail/lunar-outpost-canary-s>.
- [AFSS – 11E] Schaezler, R., Cook, A., Leonard, D., and Ghariani, A., “Trending of overboard leakage of ISS cabin atmosphere - NASA” Available: <https://ntrs.nasa.gov/api/citations/20110012997/downloads/20110012997.pdf>.
- [AFSS-12E] Schier, J., LunaNet Overview Available: [https://www.nasa.gov/sites/default/files/atoms/files/lunanet\\_overview\\_to\\_nesc\\_lunar\\_science\\_workshop\\_2022-6-7.pdf](https://www.nasa.gov/sites/default/files/atoms/files/lunanet_overview_to_nesc_lunar_science_workshop_2022-6-7.pdf)

### 12.11.2 - LSM

- [LSM-1] Skonieczny, K., Moreland, S. J., and Wettergreen, D. S. “A Grouser Spacing Equation for Determining Appropriate Geometry of Planetary Rover Wheels.” 2012 IEEE/RSJ International Conference on Intelligent Robots and Systems, 2012. <https://doi.org/10.1109/iroso.2012.6386203>.
- [LSM-2] Heverly, M., Matthews, J., Lin, J., Fuller, D., Maimone, M., Biesiadecki, J., and Leichty, J. “Traverse Performance Characterization for the Mars Science Laboratory Rover.” Journal of Field Robotics, Vol. 30, No. 6, 2013, pp. 835–846. <https://doi.org/10.1002/rob.21481>.
- [LSM-3] D. Akin, “Terramechanics 1.” Accessed: Apr. 24, 2023. [Online]. Available: [https://spacecraft.ssl.umd.edu/academics/788XF22/788XF22L06.terramechanics1\\_r1x.pdf](https://spacecraft.ssl.umd.edu/academics/788XF22/788XF22L06.terramechanics1_r1x.pdf)
- [LSM-4] D. Akin, “Steering Forces/Slopes and Static Stability .” Accessed: Apr. 24, 2023. [Online]. Available: <https://spacecraft.ssl.umd.edu/academics/788XF22/788XF22L10.steering-slopesx.pdf>
- [LSM-5] D. Akin, “Steering Forces/Flexible Wheels .” Accessed: Apr. 24, 2023. [Online]. Available: [https://spacecraft.ssl.umd.edu/academics/788XF22/788XF22L18.flexible\\_wheelsx.pdf](https://spacecraft.ssl.umd.edu/academics/788XF22/788XF22L18.flexible_wheelsx.pdf)
- [LSM-6] Budynas, R., Nisbett, J. and Shigley, J., 2011. *Shigley's mechanical engineering design*. 9th ed. New York: McGraw-Hill, p.422-433.
- [LSM-7] Cup and Pancake Component Gearsets. *Harmonic Drive*. [https://www.harmonicdrive.net/\\_hd/content/LegacyLit/HDCEnglishComponents.pdf](https://www.harmonicdrive.net/_hd/content/LegacyLit/HDCEnglishComponents.pdf). Accessed Apr. 24, 2023.
- [LSM-8] “Planetary Gearbox with DC Motor: How Does It Works?,” *ASSUN MOTOR TECHNICAL BLOG*, Mar. 22, 2023. <https://assunmotor.com/blog/planetary-gearbox/> (accessed Apr. 24, 2023).
- [LSM-9] Akin, D. Suspension Systems. <https://spacecraft.ssl.umd.edu/academics/788XF22/788XF22L14.suspensionx.pdf>. Accessed Apr. 24, 2023.
- [LSM-10] Herman, J., Sadick, S., Maksymuk, M., Chu, P., and Carlson, L., “Dust-Tolerant Connector Development for Lunar Surface Systems.” Honeybee Robotics, SPACE, 2009.



- [LSM-11] Jones, C., Thomas, “A Protoflight Lightweight Surface Manipulation System to Enable High-Load, Long-Reach Lunar Surface Operations.” NASA Langley Research Center, ASCEND, 2021.
- [LSM-12] Jones, H., “Design Rules for Life Support Systems.” NASA Ames Research Center, 2002. Available: <https://ntrs.nasa.gov/api/citations/20040012725/downloads/20040012725.pdf>
- [LSM-13] Kessler, Paul, et al. “Artemis Deep Space Habitation: Enabling a Sustained Human Presence on the Moon and beyond - NASA Technical Reports Server (NTRS).” *NASA*, NASA, 19 Jan. 2022, <https://ntrs.nasa.gov/citations/20220000245>.
- [LSM-14] Siddiqi, Afreen, et al. “Matrix Modeling Methods for Space IGHM Campaign Logistics Analysis.” *Matrix Modeling Methods for Spaceflight Campaign Logistics Analysis*, MIT, 11 Jan. 2009, [http://strategic.mit.edu/docs/2\\_29\\_JSR\\_46\\_5\\_1037\\_M-Matrix-Sep-2009.pdf](http://strategic.mit.edu/docs/2_29_JSR_46_5_1037_M-Matrix-Sep-2009.pdf).
- [LSM-15] Budynas.R , Nisbett.K . (2008) . Shigley's Mechanical Engineering Design . 8th edition. McGraw-Hill
- [LSM-16] D. Akin, “Structural Design and Analysis.” Accessed: Apr. 24, 2023. [Online]. Available: [https://spacecraft.ssl.umd.edu/academics/483F22/483F22L22.struct\\_design/483F22L22.struc\\_design.pdf](https://spacecraft.ssl.umd.edu/academics/483F22/483F22L22.struct_design/483F22L22.struc_design.pdf)
- [LSM-17] D. Akin, "Mass Estimating Relations.” Accessed: Apr. 24, 2023. [Online]. Available: <https://spacecraft.ssl.umd.edu/academics/483F22/483F22L08.MERs/483F22L08.MERs.pdf>
- [LSM-18] Hertzian contact stress calculator. Hertzian Contact Stress Calculator. (n.d.). Retrieved April 24, 2023, from <https://amesweb.info/HertzianContact/HertzianContact.aspx>
- [LSM-19] “Ansys GRANTA EduPack software, ANSYS, Inc., Cambridge, UK, YEAR ([www.ansys.com/materials](http://www.ansys.com/materials)).”
- [LSM-20] McMaster-Carr. *Mcmaster.com*. <https://www.mcmaster.com/products/wire-rope/material~stainless-steel/application~for-lifting/ultra-flexible-corrosion-resistant-wire-rope-for-lifting/>. Accessed May 19, 2023.
- [LSM-21] *NASA-STD-5001 STRUCTURAL DESIGN and TEST FACTORS of SAFETY for SPACEFLIGHT HARDWARE NASA TECHNICAL STANDARD NOT MEASUREMENT SENSITIVE*. 1996.
- [LSM-22] J. Smith, Engineers’ Practical Databook, 1<sup>st</sup> edition.
- [LSM-23] E-MOTORS - EMRAX. *EMRAX*. <https://emrax.com/e-motors/>. Accessed May 19, 2023.
- [LSM-24] Carrier, W.D., Olhoeft, G.R., Mendell, W., 1991. Physical Properties of the Lunar Surface. In: Heiken, G.H., Vaniman, D.T., French, B.M., eds. Lunar Sourcebook. Cambridge University Press.
- [LSM-25] Hertz, H., 1882. On the contact of elastic solids and on hardness. In: Miscellaneous Papers, pp. 146-183. Macmillan
- [LSM-26] Baglioni, P., Hovland, S., & Cappellari, F. “Lunar Rover Technologies and SEV as a Testbed for Future Human Missions.” *Earth and Space 2012: Engineering, Science, Construction, and Operations in Challenging Environments*, 2012.

- [LSM-27] Richter, L., Coste, P., & Gromov, V. "The Challenges of Designing Wheels for Lunar Rovers." 8th ESA Workshop on Advanced Space Technologies for Robotics and Automation, 2005.
- [LSM-28] Wang, J., "Workspace evaluation and kinematic calibration of Stewart platform ..." Available: <https://www.proquest.com/openview/c584f85286f43df7fcfd752dddbc44a2/1?pq-origsite=gscholar&cbl=18750&diss=y>.
- [LSM-29] "International Docking System Standard." International Docking System Standard (IDSS), July 2022, [www.internationaldockingstandard.com/download/IDSS\\_IDD\\_Revision\\_F.pdf](http://www.internationaldockingstandard.com/download/IDSS_IDD_Revision_F.pdf).
- [LSM-30] NASA. "Space Exploration Vehicle Fact Sheet - NASA." *Space Exploration Vehicle Fact Sheet*, [www.nasa.gov/pdf/464826main\\_SEV\\_FactSheet\\_508.pdf](http://www.nasa.gov/pdf/464826main_SEV_FactSheet_508.pdf). Accessed 19 May 2023.
- [LSM-31] NASA. "NASA Task Load Index." *NASA Task Load Index | Digital Healthcare Research*, [digital.ahrq.gov/health-it-tools-and-resources/evaluation-resources/workflow-assessment-health-it-toolkit/all-workflow-tools/nasa-task-load-index](http://digital.ahrq.gov/health-it-tools-and-resources/evaluation-resources/workflow-assessment-health-it-toolkit/all-workflow-tools/nasa-task-load-index). Accessed 19 May 2023.
- [LSM-32] *Cooper-Harper Experience Report for Spacecraft Handling Qualities*, [ntrs.nasa.gov/api/citations/20090025299/downloads/20090025299.pdf?attachment=true](http://ntrs.nasa.gov/api/citations/20090025299/downloads/20090025299.pdf?attachment=true). Accessed 19 May 2023.
- [LSM-33] *International Docking System Standard (IDSS) Interface Definition Document (IDD) Revision F Cleared by NASA for Public Release*. (2022). Retrieved from [https://www.internationaldockingstandard.com/download/IDSS\\_IDD\\_Revision\\_F.pdf](https://www.internationaldockingstandard.com/download/IDSS_IDD_Revision_F.pdf)
- [LSM-34] Wikipedia Contributors. (2023, March 15). Commercial Lunar Payload Services. Retrieved May 19, 2023, from Wikipedia website: [https://en.wikipedia.org/wiki/Commercial\\_Lunar\\_Payload\\_Services#:~:text=Missions%20contracted,-No&text=Will%20carry%2028%20payloads%2C%20including,mass%20up%20to%20256%20kg](https://en.wikipedia.org/wiki/Commercial_Lunar_Payload_Services#:~:text=Missions%20contracted,-No&text=Will%20carry%2028%20payloads%2C%20including,mass%20up%20to%20256%20kg).
- [LSM-35] Wikipedia Contributors. (2023, May 19). Blue Moon (spacecraft). Retrieved May 19, 2023, from Wikipedia website: [https://en.wikipedia.org/wiki/Blue\\_Moon\\_\(spacecraft\)](https://en.wikipedia.org/wiki/Blue_Moon_(spacecraft))
- [LSM-36] Schaezler, R., and Cook, A. *Report on ISS O2 Production, Gas Supply & Partial Pressure Management*. 2015.
- [LSM-37] Air Supply: High Pressure Tanks Ready for Space Station. NASA. <https://www.nasa.gov/content/air-supply-high-pressure-tanks-ready-for-space-station>.
- [LSM-38] Dick, B. *Current Status of the Nitrogen Oxygen Recharge System*.
- [LSM-39] Carter, L., Brown, C., and Orozco, N. *Status of ISS Water Management and Recovery*.
- [LSM-40] Jones, H. *Oxygen Storage Tanks Are Feasible for Mars Transit*. 2017.
- [LSM-41] Andreychuk, P., Romanov, S., Zeleznyakov, A., Bobe, L., Kochetkov, A., Arakcheev, D., Niichimmash, Russia, M., and Sinyak. *The Water Management on the Russian Segment of the International Space Station and Prospective Space Stations*.

[LSM-42] Bergin, C. MPLM Reberthed into Discovery's Payload Bay ahead of Undocking. *NASASpaceFlight.com*. <https://www.nasaspaceflight.com/2009/09/mplm-reberthed-into-discoverys-payload-bay-ahead-of-undocking/>. Accessed Mar. 6, 2023.

### *12.11.3 - MPA*

- [MPA-1] ACT. (2023). LROC Quickmap. QuickMap. Retrieved March 4, 2023, from <https://quickmap.lroc.asu.edu/>
- [MPA-2] Arney, D., & Wilhite, A. (2012). *Rapid cost estimation for space exploration systems*. AIAA space forum. Retrieved March 4, 2023, from <https://arc.aiaa.org/doi/10.2514/6.2012-5183>
- [MPA-3] Baird, D. (2021, October 5). *LunaNet: Empowering Artemis with Comm and Nav Interoperability*. NASA. <https://www.nasa.gov/feature/goddard/2021/lunanet-empowering-artermis-with-communications-and-navigation-interoperability>
- [MPA-4] Chen, R. (2021, January 27). *Viper's mission operations*. NASA. <https://www.nasa.gov/viper/lunar-operations>
- [MPA-5] D.L. Akin (n.d.) "Orbital Mechanics". *UMD*. <https://spacecraft.ssl.umd.edu/academics/483F22/483F22L04.orbmech/483F22L04.orbmech.pdf>
- [MPA-6] Duggleby, W. (2020, July 10). *Cost estimating handbook*. NASA. <https://www.nasa.gov/content/cost-estimating-handbook#2.2.2>
- [MPA-7] Gaier, J. (n.d.). *Evaluation of brushing as a lunar dust mitigation strategy for thermal*. Evaluation of Brushing as a Lunar Dust Mitigation Strategy for Thermal Control Surfaces. <https://ntrs.nasa.gov/api/citations/20120000070/downloads/20120000070.pdf>
- [MPA-8] Gersten, E. (2010, August). *Falcon 9 vehicle NAFCOM estimates*. NASA. Retrieved March 4, 2023, from [https://www.nasa.gov/pdf/586023main\\_8-3-11\\_NAFCOM.pdf](https://www.nasa.gov/pdf/586023main_8-3-11_NAFCOM.pdf)
- [MPA-9] *Headquarters, NASA salaries of 2021*. FederalPay. (n.d.). <https://www.federalpay.org/employees/headquarters-nasa>
- [MPA-10] Hille, K. (2022, December 16). *Steering by landmarks – on the moon*. NASA. <https://www.nasa.gov/feature/steering-by-landmarks-on-the-moon>
- [MPA-11] Hurler, K. (2023, March 1). *Experiments with Barbie dolls reveal a surprising way to keep spacesuits clean on the Moon*. Gizmodo. <https://gizmodo.com/liquid-nitrogen-moon-suits-free-lunar-dust-1850172542>
- [MPA-12] Keeter, B. (2016, May 20). *Sid Publications*. NASA. <https://www.nasa.gov/offices/ocfo/sid/publications>

- [MPA-13] Musk, E. (2020, March). "Starship User Guide." *SpaceX*. Retrieved March 5, 2023, from [https://www.spacex.com/media/starship\\_users\\_guide\\_v1.pdf](https://www.spacex.com/media/starship_users_guide_v1.pdf)
- [MPA-14] NASA. (2021, November 15). *NASA'S MANAGEMENT OF THE ARTEMIS MISSIONS*. Report No. IG-22-003. Retrieved March 4, 2023, from <https://oig.nasa.gov/docs/IG-22-003.pdf>
- [MPA-15] NASA. (n.d.). *NASA TechPort*. NASA. <https://techport.nasa.gov/view/93240>
- [MPA-16] NASA. (n.d.-a). *How perseverance drives on mars – NASA mars exploration*. NASA. <https://mars.nasa.gov/resources/26660/how-perseverance-drives-on-mars/>
- [MPA-17] Thesheetztweetz. (2021, August 4). *Bezos' Blue Origin calls Musk's starship "immensely complex & high risk" for NASA Moon Missions*. CNBC. <https://www.cnn.com/2021/08/04/bezos-blue-origin-musks-spacex-starship-complex-high-risk.html>
- [MPA-18] Weitering, H. (2019, May 10). *Blue Moon: Here's how Blue Origin's new Lunar lander works*. Space.com. <https://www.space.com/blue-origin-blue-moon-lander-explained.html>
- [MPA-19] Wells, I. (n.d.). *Liquid nitrogen removal of lunar regolith simulant from ... - iopscience*. Liquid nitrogen removal of lunar regolith simulant from spacesuit simulants. <https://iopscience.iop.org/article/10.1088/1757-899X/1240/1/012003>

#### 12.11.4 - PPT

- [PPT-1] "RAD5545™ spacevpx single-Board Computer - BAE Systems" Available: <https://www.baesystems.com/en-media/uploadFile/20210404061759/1434594567983.pdf>.
- [PPT-2] GLS87CR064G3 / 128G3 / 256G3 / 512G3 PX Series Industrial Temp SATA M.2 ... July 2022, <https://www.greenliant.com/dotAsset/57547.pdf>.
- [PPT-3] Maki, J. N., Bell, J. F., Herkenhoff, K. E., Squyres, S. W., Kiely, A., Klimesh, M., Schwochert, M., Litwin, T., Willson, R., Johnson, A., Maimone, M., Baumgartner, E., Collins, A., Wadsworth, M., Elliot, S. T., Dingizian, A., Brown, D., Hagerott, E. C., Scherr, L., Deen, R., Alexander, D., and Lorre, J., "Mars Exploration Rover Engineering Cameras," *Journal of Geophysical Research: Planets*, vol. 108, 2003.
- [PPT-4] LN-200s Inertial Measurement Unit (IMU) - Northrop Grumman. <https://www.northropgrumman.com/wp-content/uploads/LN-200S-Inertial-Measurement-Unit-IMU-datasheet.pdf>.
- [PPT-5] ACT. (2023). LROC Quickmap. QuickMap. Retrieved May 13, 2023, <https://quickmap.lroc.asu.edu/>
- [PPT-6] Bosch, A., Modelling and control of the Life Support System of a lunar habitat Available: [https://www.research-collection.ethz.ch/bitstream/handle/20.500.11850/487923/MA\\_report\\_Boesch.pdf?sequence=1](https://www.research-collection.ethz.ch/bitstream/handle/20.500.11850/487923/MA_report_Boesch.pdf?sequence=1).

- [PPT-7] Nikolov, N., and Zeller, K., On the average temperature of airless spherical bodies and the ... Available:  
[https://www.researchgate.net/publication/277600023\\_On\\_the\\_average\\_temperature\\_of\\_airless\\_spherical\\_bodies\\_and\\_the\\_magnitude\\_of\\_Earth's\\_atmospheric\\_thermal\\_effect](https://www.researchgate.net/publication/277600023_On_the_average_temperature_of_airless_spherical_bodies_and_the_magnitude_of_Earth's_atmospheric_thermal_effect).
- [PPT-8] da Silva, D. F., and Garcia, E. C., Experimental determination of the effective thermal properties of a multi-layer insulation blanket Available:  
<https://abcm.org.br/anais/cobem/2013/PDF/1126.pdf>.
- [PPT-9] Gilmore, D. G., and Bello, M., Satellite Thermal Control Handbook, El Segundo, Ca.: The Aerospace Corporation Press, 1994, pp. 4–108.
- [PPT-10] Howell, J. R., A catalog of radiation heat transfer configuration factors Available:  
<http://www.thermalradiation.net/calc/index.html>.
- [PPT-11] Suffern, D., Mobley, J., and Smith, S., Mars 2020 Motor Bearing Failure, investigation and response Available: <https://esmats.eu/amspapers/pastpapers/pdfs/2020/suffern.pdf>.
- [PPT-12] “Braycote 600EF high vacuum grease,” Z05107 | SPI Supplies Available:  
<https://www.2spi.com/item/z05107/>.
- [PPT-13] “Brayco 815Z PFPE base oil,” Z05088 | SPI Supplies Available:  
<https://www.2spi.com/item/z05088/>.
- [PPT-14] “Mars UHF Transceiver (C/TT-510) Electra-Lite,” Mars UHF Transceiver Available:  
[https://www.l3harris.com/sites/default/files/2020-07/ims\\_eo\\_datasheet\\_UHF\\_Mars\\_Transmitter.pdf](https://www.l3harris.com/sites/default/files/2020-07/ims_eo_datasheet_UHF_Mars_Transmitter.pdf).
- [PPT-15] “Space materials database. materials details,” SPACEMATDB Available:  
<https://www.spacematdb.com/spacemat/datasearch.php?name=PTFE>.
- [PPT-16] Programmable thermostats for MPLM shell heater control Available:  
<https://ntrs.nasa.gov/api/citations/20090033636/downloads/20090033636.pdf>.
- [PPT-17] “Current State of the Electrodynamic Dust Shield for Mitigation ... - USRA.” *Lunar Dust 2020*, 2020, [www.hou.usra.edu/meetings/lunardust2020/pdf/5027.pdf](http://www.hou.usra.edu/meetings/lunardust2020/pdf/5027.pdf).
- [PPT-18] Masterson, Victoria. “Why Don’t Solar Panels Work as Well in Heatwaves?” *World Economic Forum*, [www.weforum.org/agenda/2022/08/heatwaves-can-hamper-solar-panels/#:~:text=Solar%20cells%20%E2%80%93%20the%20electronic%20devices,%C2%B0F\)%2C%20EnergySage%20says](http://www.weforum.org/agenda/2022/08/heatwaves-can-hamper-solar-panels/#:~:text=Solar%20cells%20%E2%80%93%20the%20electronic%20devices,%C2%B0F)%2C%20EnergySage%20says).
- [PPT-19] Jude, Tamara. “8 Most Efficient Solar Panels (2023 Guide).” *Architectural Digest*, 7 Apr. 2023, [www.architecturaldigest.com/reviews/home-improvement/most-efficient-solar-panels/#:~:text=Monocrystalline%20solar%20panels%20are%20the,15%25%20to%2022%25%20efficiency](http://www.architecturaldigest.com/reviews/home-improvement/most-efficient-solar-panels/#:~:text=Monocrystalline%20solar%20panels%20are%20the,15%25%20to%2022%25%20efficiency).

- [PPT-20] Theristis, Marios. “Electrical-Thermal Analysis of III–V Triple-Junction Solar Cells under Variable Spectra and Ambient Temperatures.” *Solar Energy*, 23 June 2015, [www.sciencedirect.com/science/article/pii/S0038092X15003059](http://www.sciencedirect.com/science/article/pii/S0038092X15003059).
- [PPT-21] Greentumble. “Effect of Temperature on Solar Panel Efficiency.” *Greentumble*, 22 Apr. 2023, <https://greentumble.com/effect-of-temperature-on-solar-panel-efficiency>.
- [PPT-22] Aiken, D.J., et al. “Triple-Junction Solar Cells with 39.5% Terrestrial and 34.2% Space Efficiency Enabled by Thick Quantum Well Superlattices.” *Joule*, Cell Press, 18 May 2022, <https://www.sciencedirect.com/science/article/abs/pii/S254243512200191X#:~:text=Article-Triple%2Djunction%20solar%20cells%20with%2039.5%25%20terrestrial%20and%2034.2%25,by%20thick%20quantum%20well%20superlattices>.
- [PPT-23] Theristis, Marios. “Electrical-Thermal Analysis of III–V Triple-Junction Solar Cells under Variable Spectra and Ambient Temperatures.” *Solar Energy*, 23 June 2015, [www.sciencedirect.com/science/article/pii/S0038092X15003059](http://www.sciencedirect.com/science/article/pii/S0038092X15003059).
- [PPT-24] Zeitlin, Nancy. *Electrodynamic Dust Shield for Lunar/ISS Experiment Project*. 2016, <https://ntrs.nasa.gov/api/citations/20150016160/downloads/20150016160.pdf>.
- [PPT-25] Agui, J. H., Hambourger, P., Wirfs-Brock, J., Griffin, J. M., Hindall, J. T., and Morgan, A. G., “Durable coating technology for lunar dust protection and mitigation,” *SAE Technical Paper* Available: <https://trid.trb.org/view/1808608>.
- [PPT-26] Jenner, L., “NASA's coating technology could help resolve Lunar Dust Challenge,” *NASA* Available: <https://www.nasa.gov/feature/goddard/2019/nasa-s-coating-technology-couldhelp-resolve-lunar-dust-challenge/>.
- [PPT-27] Fu, Y.Q. “Piezoelectric Actuator.” *Piezoelectric Actuator - an Overview | ScienceDirect Topics*, 2012, [www.sciencedirect.com/topics/engineering/piezoelectric-actuator](http://www.sciencedirect.com/topics/engineering/piezoelectric-actuator).
- [PPT-28] Granath, Bob. “Scientists Developing Dust Mitigation for Exploration.” *NASA*, 24 Feb. 2015, [www.nasa.gov/content/scientists-developing-ways-to-mitigate-dust-problem-for-explorers](http://www.nasa.gov/content/scientists-developing-ways-to-mitigate-dust-problem-for-explorers).
- [PPT-29] “NASA” Available: [https://trs.jpl.nasa.gov/bitstream/handle/2014/44299/13-3547\\_A1b.pdf?sequence=1](https://trs.jpl.nasa.gov/bitstream/handle/2014/44299/13-3547_A1b.pdf?sequence=1)
- [PPT-30] Isaifan, Rima J, et al. “Improved Self-Cleaning Properties of an Efficient and Easy to Scale up Tio<sub>2</sub> Thin Films Prepared by Adsorptive Self-Assembly.” *Scientific Reports*, 25 Aug. 2017, [www.ncbi.nlm.nih.gov/pmc/articles/PMC5573374/](http://www.ncbi.nlm.nih.gov/pmc/articles/PMC5573374/).

[PPT-31] “Radioisotope Heater Units - NASA RPS: Radioisotope Power Systems.” *NASA Facts*, 26 May 2016, [rps.nasa.gov/system/downloadable\\_items/31\\_Final\\_RHU\\_Fact\\_Sheet\\_2016\\_5-26-16.pdf](https://rps.nasa.gov/system/downloadable_items/31_Final_RHU_Fact_Sheet_2016_5-26-16.pdf).

[PPT-32] “Home.” *Advance Cooling Technologies*, [www.1-act.com/products/pcm-heat-sinks/pcmselection/](http://www.1-act.com/products/pcm-heat-sinks/pcmselection/).

[PPT-33] “Metals, Metallic Elements and Alloys - Thermal Conductivities.” *Engineering ToolBox*, [www.engineeringtoolbox.com/thermal-conductivity-metals-d\\_858.html](http://www.engineeringtoolbox.com/thermal-conductivity-metals-d_858.html).

### 12.11.5 - SI

[SI-1] Akin, D. (n.d.). *Enae 483/788d - Fall, 2022 lecture #02 Space systems engineering*. Lecture #02 - ENAE 483/788D - Fall, 2022 - University of Maryland. Retrieved March 6, 2023, from <https://spacecraft.ssl.umd.edu/academics/483F22/483F22L02.systems/483F22L02.html>

[SI-2] Technology Readiness Level. *NASA*. [https://www.nasa.gov/directorates/heo/scan/engineering/technology/technology\\_readiness\\_level](https://www.nasa.gov/directorates/heo/scan/engineering/technology/technology_readiness_level). Accessed Mar. 6, 2023.

[SI-3] Prince, A., Alford, B., Boswell, B., Pitlyk, M., and Pedigo, M., “Project Cost Estimating Capability,” *PCEC – Project Cost Estimating Capability*, May 2014.

[SI-4] NASA. (2017). NASA Procedural Requirements (NPR) 8000.4A: Agency Risk Management Procedural Requirements (Version G). Retrieved from [https://www.nasa.gov/sites/default/files/atoms/files/s3001\\_guidelines\\_for\\_risk\\_management\\_-\\_ver\\_g\\_-\\_10-25-2017.pdf](https://www.nasa.gov/sites/default/files/atoms/files/s3001_guidelines_for_risk_management_-_ver_g_-_10-25-2017.pdf)

[SI-5] NASA. (2007, March 26). *NPR 7123.1A - Chapter5*. NASA. Retrieved April 24, 2023, from [https://nodis3.gsfc.nasa.gov/displayCA.cfm?Internal\\_ID=N\\_PR\\_7123\\_001A\\_&page\\_name=Chapter5](https://nodis3.gsfc.nasa.gov/displayCA.cfm?Internal_ID=N_PR_7123_001A_&page_name=Chapter5)

[SI-6] J. N. Maki, C. M. McKinney, R. G. Sellar, R. G., Willson, D. S. Copley-Woods, D. C. Gruel, D. L. Nuding, D. L. Nuding, T. Goodsall, J. McGuire, J. Kempenaar, & T. E. Litwin. (2016). *3rd International Workshop on Instrumentation for Planetary Missions (2016)*. Retrieved April 24, 2023, from <https://www.hou.usra.edu/meetings/ipm2016/pdf/4132.pdf>

[SI-7] Dunbar, B. (2008, February 27). *NASA's newest concept vehicles take off-roading out of This World*. NASA. Retrieved April 24, 2023, from [https://www.nasa.gov/mission\\_pages/constellation/main/lunar\\_truck.html](https://www.nasa.gov/mission_pages/constellation/main/lunar_truck.html)

[SI-8] Greenliant. (n.d.). EnduroSLC Industrial Grade 2.5" SATA SSD. Retrieved from <https://www.greenliant.com/products/?inode=54466>

[SI-9] C. R. Buhler<sup>1</sup>, M. Johansen<sup>1</sup>, M. Dupuis<sup>1</sup>, M. Hogue<sup>1</sup>, J. Phillips<sup>1</sup>, J. Malissa<sup>1</sup>, J. Wang<sup>1</sup> and C.I. Calle<sup>1</sup>. (2020). *Current state of the electrodynamic dust shield for mitigation ... - USRA*. CURRENT STATE OF THE ELECTRODYNAMIC DUST SHIELD FOR

MITIGATION. Retrieved April 24, 2023, from <https://www.hou.usra.edu/meetings/lunardust2020/pdf/5027.pdf>

[SI-10] Staff Writers. (2019, May 15). *BAE Systems Radiation-hardened electronics in orbit a total of 10,000 years*. Space Daily. Retrieved April 24, 2023, from [https://www.spacedaily.com/reports/BAE\\_Systems\\_Radiation\\_hardened\\_Electronics\\_in\\_Orbit\\_a\\_Total\\_of\\_10000\\_Years\\_999.html](https://www.spacedaily.com/reports/BAE_Systems_Radiation_hardened_Electronics_in_Orbit_a_Total_of_10000_Years_999.html)

[SI-11] Northrop Grumman. (2022, December 7). *LN-200s Inertial Measurement Unit*. LN-200S Inertial Measurement Unit. Retrieved April 24, 2023, from <https://www.northropgrumman.com/what-we-do/ln-200s-inertial-measurement-unit/>

[SI-12] NASA. (n.d.). *Antennas*. MARS Reconnaissance Orbiter Mission. Retrieved April 24, 2023, from <https://mars.nasa.gov/mro/mission/spacecraft/parts/antennas/>

[SI-13] NASA. (2019, November 20). *NASA*. 2019 NASA Aerospace Battery Workshop. Retrieved April 24, 2023, from [https://www.nasa.gov/sites/default/files/atoms/files/eas\\_batteries\\_presentation\\_nasa\\_battery\\_workshop\\_-\\_2019\\_11\\_20\\_v2.1\\_small.pdf](https://www.nasa.gov/sites/default/files/atoms/files/eas_batteries_presentation_nasa_battery_workshop_-_2019_11_20_v2.1_small.pdf)

[SI-14] Robert L. Howard, Jr. (n.d.). *A multi-gravity docking and utilities transfer system for a Common Habitat Architecture*. Retrieved April 24, 2023, from <https://ntrs.nasa.gov/api/citations/20210020833/downloads/A%20Multi-Gravity%20Docking%20and%20Utilities%20Transfer%20System%20for%20a%20Common%20Habitat%20Architecture.pdf?attachment=true>

[SI-15] Hall, L. (2021, May 26). *Measuring moon dust to fight Air Pollution*. NASA. Retrieved April 24, 2023, from [https://www.nasa.gov/directorates/spacetech/spinoff/Measuring\\_Moon\\_Dust\\_to\\_Fight\\_Air\\_Pollution](https://www.nasa.gov/directorates/spacetech/spinoff/Measuring_Moon_Dust_to_Fight_Air_Pollution)

[SI-16] Rao Surampudi, John Elliott, Julian Blosiu, Kumar Bugga, Patricia Beauchamp and James Cutts. (2018, February 23). *Advanced Energy Storage Technologies for Future NASA Planetary Science Mission Concepts*. Retrieved April 24, 2023, from <https://www.lpi.usra.edu/opag/meetings/feb2018/presentations/Surampudi.pdf>

[SI-17] Dunbar, B. (2004, January 4). *Fire prevention in space*. NASA. Retrieved April 24, 2023, from [https://www.nasa.gov/missions/shuttle/f\\_fireprevention.html](https://www.nasa.gov/missions/shuttle/f_fireprevention.html)

[SI-18] Team, G. (2021, March 19). *7075 aluminum: Get to know its properties and uses*. Gabrian. Retrieved April 24, 2023, from <https://www.gabrian.com/7075-aluminum-properties/>

[SI-19] Jones, T. C. (2021). *A protoflight lightweight surface manipulation system to enable high load, long-reach lunar surface operations*. ASCEND 2021. <https://doi.org/10.2514/6.2021-4167>

[SI-20] Elkins-Tanton, L. (2018, April 9). *Margins*. Medium. Retrieved March 12, 2023, from <https://medium.com/the-nasa-psyche-mission-journey-to-a-metal-world/margins-e19f3dce28b6>

[SI-21] Duggleby, W. (2020, July 10). *Cost estimating handbook*. NASA. Retrieved March 12, 2023, from <https://www.nasa.gov/content/cost-estimating-handbook#2.2.2>



[SI-22] Keeter, B. (2016, May 20). *Sid Publications*. NASA. Retrieved March 12, 2023, from <https://www.nasa.gov/offices/ocfo/sid/publications>

[SI-23] Roberts, T. G., & Kaplan, S. (2022, September 1). *Cost for space launch to low Earth Orbit- Aerospace Security Project*. Aerospace Security. Retrieved March 12, 2023, from <https://aerospace.csis.org/data/space-launch-to-low-earth-orbit-how-much-does-it-cost/>

[SI-24] Rohinton P. Billimoria. (n.d.). *DESIGN OF MECHANISMS TO LOCK/LATCH SYSTEMS UNDER ROTATIONAL OR TRANSLATIONAL MOTION*. NASA.gov. <https://ntrs.nasa.gov/api/citations/19760021194/downloads/19760021194.pdf>